HAL open science

boltzmann-ginzburg-landau approach to simple models of active matter

Anton Peshkov

▶ To cite this version:

Anton Peshkov. boltzmann-ginzburg-landau approach to simple models of active matter. Other [cond-mat.other]. Université Pierre et Marie Curie - Paris VI, 2013. English. NNT : . tel-00921017

HAL Id: tel-00921017

https://theses.hal.science/tel-00921017v1

Submitted on 19 Dec 2013

HAL is a multi-disciplinary open access archive for the deposit and dissemination of scientific research documents, whether they are published or not. The documents may come from teaching and research institutions in France or abroad, or from public or private research centers.

L'archive ouverte pluridisciplinaire **HAL**, est destinée au dépôt et à la diffusion de documents scientifiques de niveau recherche, publiés ou non, émanant des établissements d'enseignement et de recherche français ou étrangers, des laboratoires publics ou privés.

THÈSE DE DOCTORAT
DE L'UNIVERSITÉ PIERRE ET MARIE CURIE

Spécialité :Physique

École doctorale : La Physique de la Particule à la Matière Condensée

réalisée au

LABORATOIRE SPHYNX, SPEC, CEA SACLAY

et au

LABORATOIRE DE PHYSIQUE THÉORIQUE DE LA MATIÈRE CONDENSÉE

présentée par

PESHKOV ANTON

pour obtenir le grade de :

DOCTEUR DE L'UNIVERSITÉ PIERRE ET MARIE CURIE

BOLTZMANN-GINZBURG-LANDAU APPROACH TO SIMPLE MODELS OF ACTIVE MATTER

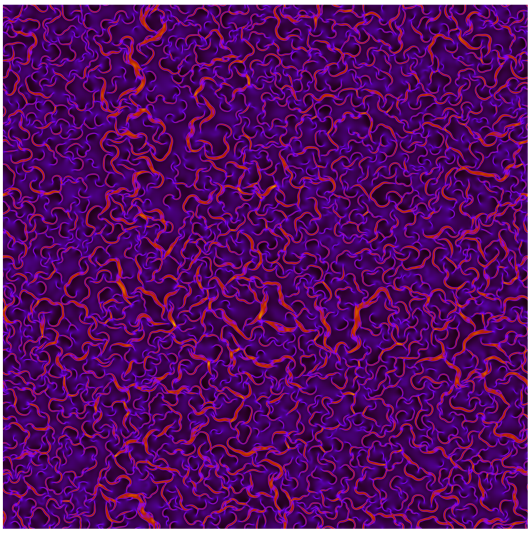

soutenue le

24 SEPTEMBRE 2013

devant le jury composé de :

M. BARTOLO Denis	Examinateur
M. CHATÉ Hugues	Co-Directeur de thèse
M. JOANNY Jean-Francois	Examinateur
M. TAILLEUR Julien	Examinateur
M. TRIZAC Emmanuel	Rapporteur

On the cover: Spatio-temporal chaos in simulation of hydrodynamic equations of active-nematic.

Peshkov Anton: *Boltzmann-Ginzburg-Landau approach to simple models of active matter,* , © soutenue le 24 september 2013

II ne faut pas laisser les intellectuels jouer avec les allumettes

Parce que Messieurs quand on le laisse seul

Le monde mental Messssieurs

N'est pas du tout brillant

Et sitôt qu'il est seul

Travaille arbitrairement

S'érigeant pour soi-même

Et soi-disant généreusement en l'honneur

des travailleurs du bâtiment

Un auto-monument

Répétons-le Messieurs

Quand on le laisse seul

Le monde mental

Ment

Monumentalement.

–Jacques Prévert, Paroles, Il ne faut pas...

ABSTRACT

Collective motion is observed in many different biological systems like bird flocks or fish schools. In these systems, collective motion may arise without any leader or external force, and is only due to the interactions among individuals and the out of equilibrium nature of the whole system.

We study simple models of such collective motion situations in order to establish universality classes of "dry" active matter, i.e. when the fluid medium in which individuals evolve is neglected. Many of such systems have already been studied at the "microscopic", particle-based, level. In this thesis, we obtain coarse-grained hydrodynamic equations of such models which we compare to the microscopic level results. Their analysis also reveals new collective properties. We introduce the "Boltzmann-Ginzburg-Landau approach" to derive our equations in a controlled manner.

The equations are derived for four different Vicsek-type models. The simple polar model (original Vicsek model), a mixed case of polar particles with nematic interactions, a model of nematic particles with nematic interactions and finally a model for polar particles with metric free interactions. In each case, the obtained equations are studied analytically and numerically. We find that our equations reproduce faithfully the qualitative properties of the underlying microscopic models, such as the different observed phases and the nature of the phase transitions between them. Some new phases not previously observed in microscopic models are found. Their existence was confirmed a posteriori in further simulations of the microscopic models.

RÉSUMÉ

Le phénomène de mouvement collectif est présent parmi beaucoup de systèmes biologiques comme dans les volées d'oiseaux ou des bancs de poissons. Dans ces systèmes, le mouvement collectif apparait sans aucun leader ni force extérieure et est exclusivement dû à l'interaction parmi les individus et à la nature hors-équilibre de tout le système. Nous voulons étudier des modèles simples de mouvement collectif afin d'établir des classes d'universalité parmi la matière active sèche, c'est-à-dire des individus interagissant sans l'aide d'un fluide. Beaucoup de ces systèmes ont déjà été étudiés microscopiquement.

Nous voulons obtenir des équations hydrodynamiques de ces systèmes pour confirmer les résultats microscopiques et pour prédire des

propriétés nouvelles. Nous effectuons une dérivation d'équations hydrodynamiques en utilisant l'approche Boltzmann-Ginzburg-Landau introduit dans cette thèse.

Quatre modèles de type Vicsek sont considérés. Un modèle polaire simple identique au modèle de Vicsek, un modèle mixte avec des particules polaires avec interactions nématiques, un modèle avec des particules polaires et interactions nématiques et finalement un modèle avec des particules polaires avec des interactions non-métriques. Dans chaque cas les équations obtenues sont étudiées de façon analytique et numérique. Nous trouvons que les équations obtenues reproduisent de façon fidèles les propriétés qualitatives des modèles microscopiques considérées, comme les différentes phases observées et la nature de transition entre ces phases. Dans certains cas des phases nouvelles sont trouvées, qui n'ont pas été reportées auparavant dans les modèles microscopiques. Beaucoup d'entre elles ont été confirmées a posteriori dans les simulations numériques de ces modèles.

ACKNOWLEDGMENTS

I want to thanks my thesis advisors Hugues Chaté and Bertrand Delamotte for their support during my thesis.

I also acknowledge my collaborators Eric Bertin, Franchesco Ginelli, Guillaume Grégoire and Sriram Ramaswamy.

I am especially thankful to Igor Aronson for his collaboration and for receiving me on two occasion in his laboratory at ANL, USA.

Finally I want to acknowledge the Max Planck Institute for the Physics of Complex Systems and the director of Biophysics group Frank Jülicher for receiving me at the advanced study group "Statistical Physics of Collective Motion" where a big part of this work was done.

CONTENTS

i GENERALITIES ON COLLECTIVE MOTION 1

1 INTRODUCTION 3
- 1.1 Collective motion 3
- 1.2 The Vicsek model 4
- 1.3 The Toner and Tu approach to collective motion 5
- 1.4 New insight on the Vicsek model 8
- 1.5 Overview of approaches for hydrodynamic equations of collective motion 9
  - 1.5.1 Bertin-Droz-Grégoire approach 9
  - 1.5.2 Thomas Ihle approach 9
  - 1.5.3 Marchetti and coworkers approach 10
  - 1.5.4 Other approaches 11
- 1.6 Organization of the thesis 11

ii THE BOLTZMANN-GINZBURG-LANDAU METHOD 17

2 COARSE-GRAINING OF VICSEK-LIKE MODELS 19
- 2.1 Generalities on the Vicsek like models 19
- 2.2 The Boltzmann approach 21
- 2.3 Derivation of hydrodynamic equations 23
- 2.4 The closure approximation 24
- 2.5 Limit of the validity of the scaling ansatz. 25
- 2.6 Langevin equations 26

iii METRIC MODELS 31

3 THE POLAR MODEL 33
- 3.1 The Vicsek polar model 33
- 3.2 Derivation of hydrodynamic equations 36
  - 3.2.1 Boltzmann equation 36
  - 3.2.2 Hydrodynamic equations 38
  - 3.2.3 Expansion and closure 41
- 3.3 Homogeneous solutions and their stability analysis 43
  - 3.3.1 Homogenous solution 43
  - 3.3.2 Stability to inhomogeneous perturbations 45
  - 3.3.3 Going beyond the third order truncation 48
- 3.4 Numerical simulations 54
  - 3.4.1 Simulation of 1D solution 54
  - 3.4.2 2D simulations 57
- 3.5 Solutions of the ODE equation 58
  - 3.5.1 Shooting of the ODE 59
  - 3.5.2 Analytic front solution 68
- 3.6 Conclusion 69

4 MIXED POLAR-NEMATIC MODEL 75

4.1 The microscopic model 75
4.2 Derivation of hydrodynamic equations 77
4.3 Numerical simulations 83
4.4 Stability of the band solution 84
4.4.1 Analytical investigation 84
4.5 Conclusion 94
5 ACTIVE-NEMATIC MODEL 99
5.1 Introduction to the microscopic model 99
5.2 Derivation of hydrodynamic equations 100
5.3 Numerical simulations 129
5.3.1 Band solution 129
5.3.2 Nematic defects 129
5.4 Stability of the band solution 130
5.4.1 Analytical investigation 130
5.4.2 Numerical analysis 134
5.5 Conclusions 136

IV METRIC-FREE MODEL 145
6 THE POLAR METRIC-FREE MODEL 147
6.1 Introduction to the microscopic model 147
6.2 Derivation of hydrodynamic equations 148
6.3 Conclusion 155

V CONCLUSIONS 161
7 SUMMARY 163
8 PERSPECTIVES 165
8.1 Further studies of the current equations 165
8.2 Derivation of the Langevin equations 165

BIBLIOGRAPHY 167

Figure 1 Various results for the Vicsek model. (a) Values of the order parameter v_a as a function of noise amplitude η for various system sizes. (b,c,d) Various phases initially reported for the Vicsek model. (b) Disordered phase at high noise. (c) Clustered phase at low density and low noise. (d) Homogenous ordered phase at high density and low noise. 6

Figure 2 (a) High density bands of particles in the Vicsek model. (b) Traversal cutoff of a band showing the density profile. Images from ref[**?**]. 8

Figure 3 (a) Time averaged mean order parameter $\langle P \rangle_t$ as a function of noise amplitude η for different system sizes. (b) Time averaged Binder cummulant $\langle B \rangle_t$ as a function of noise amplitude η. Images from ref[**?**]. 34

Figure 4 (a) The phase diagram of the microscopic Vicsek model. (b) The hysteresis of the order parameter as a function of angular noise. Images from ref[**?**]. 35

Figure 5 Amplitude of $\left|\vec{P}\right| = |f_1|/\rho$ as a function of density, for $\sigma = \sigma_t\,(\rho = 1)$. The red line correspond to the case of a density dependance of the ξ term, the blue line in the absence of such dependance. 44

Figure 6 Stability diagram in the case of a pure third order truncation. The color code indicates the direction, in radians, in which the eigenvalue is the most unstable, as compared to the direction of the homogeneous solution. The line σ_t corresponds to the transition to collective motion solution. This solution is unstable up to the restabilisation line σ_s. Completely longitudinal instabilities exist only above line $\sigma_{\|}$. Another, probably spurious, instability appears after the line σ_u. Completely transversal instabilities exist below the line $\sigma_{\perp}$. 49

Figure 7 Stability diagram in the case of density dependance of the ξ term. The color code indicates the direction, in radians, in which the eigenvalue is the most unstable, as compared to the direction of the homogeneous solution. The line σ_t corresponds to the transition to collective motion solution. This solution is unstable up to the restabilisation line σ_s. Completely longitudinal instabilities exist only above line $\sigma_{\|}$. Another, probably spurious, instability appears after the line σ_u. Completely transversal instabilities exist below the line $\sigma_{\perp}$. 50

Figure 8 Modulus of largest eigenvalues in the case of a pure third order truncation (a) and if keeping the rho dependance of ξ (b). 51

Figure 9 Homogeneous solutions to the equation truncated at fifth order. The lines represent the homogeneous solutions f_n, with n decreasing from top to bottom. In red approximate analytical solutions, in green exact numerical ones. 53

Figure 10 Homogenous solutions to the equation truncated at seventh order. The lines represent the homogeneous solutions f_n, with n decreasing from top to bottom. In red approximate analytical solutions, in green exact numerical ones. 54

Figure 11 Final state of the density field at time $T = 2.5 \times 10^7$ in a box of size $L = 1000$ with no density dependance of the ν term starting from random initial conditions. The simulation was done with a spatial stepping of $\Delta x = 0.25$ and a time steping of $\Delta t = 0.01$. The mean density in the system is $\rho_0 = 1$ and the noise value is $\sigma = 0.64$. 55

Figure 12 Final state of the density field at time $T = 4 \times 10^7$ in a box of size $L = 1000$ with density dependance of the ν term starting from random initial conditions. The simulation was done with a spatial stepping of $\Delta x = 0.25$ and a time steping of $\Delta t = 0.01$. The mean density in the system is $\rho_0 = 1$ and the noise value is $\sigma = 0.64$. 56

Figure 13 Final state of the density field at time $T = 1.1 \times 10^7$ in a box of size $L = 1000$ with density dependance of the ξ term only starting from random initial conditions. The simulation was done with a spatial stepping of $\Delta x = 0.25$ and a time steping of $\Delta t = 0.01$. The mean density in the system is $\rho_0 = 1$ and the noise value is $\sigma = 0.64$. 56

Figure 14 Band solution in a 2d simulation box. The orientation of the bands in the system correspond to the initial orientation of a periodic perturbation on density and polar order. 57

Figure 15 The asymptotic density ρ_{gas} versus the speed c. Values obtained at $\sigma = 0.1$. 61

Figure 16 The height, the width at half-height and the mass of the soliton versus speed c. Results obtained at $\sigma = 0.1$. 62

Figure 17 The $^{height}/_{width}$ parameter as a function of speed c. Values obtained at a noise $\sigma = 0.1$. 63

Figure 18 Exponents $k_{\pm}$ and the symmetry coefficient $\varsigma(c)$ as a function of speed. Measured for $\sigma = 0.1$. 63

Figure 19 Profiles of the solitons for speed values near c_{min}, ρ_{gas}^{min} and c_{max}. The exact values of speed are $c = 0.708$, $c = 0.854$ and $c = 0.877$. The noise value is $\sigma = 0.1$. 64

Figure 20 The speed of solitons as a function of noise σ. 65

Figure 21 Values of ρ_{gas} as a function of noise σ. Note that the values for c_{max} and ρ_{gas}^{min} are indistinguishable on this graph, those the latter is not ploted. The restabilisation noies σ_s is given for reference. 65

Figure 22 Height of the solitons as a function of noise σ. 66

Figure 23 The width at half-height and the mass of the soliton for the case ρ_{gas}^{min} as a function of noise σ. 67

Figure 24 Rules of nematic collision for polar particles. In the case of a head-tail collision, the particles align polarly. In the case of a head-head collision, they align nematicaly. Note that the finite size of the particles is only for representation purpose, the particles in the model are point-like. Image from ref[19]. 75

Figure 25 The four different phases observed in microscopic mixed polar-nematic model. (a) At low noise, a long-range nematic order exist. (b,c) At a higher noise, a disordered band appear which grow with increase of noise. (d) At a critical noise parameter this band destabilise, leading to a chaotic phase. The transition between phase II and III mark the order-disorder transition. (e) At even higher noise, the system become completely disordere. Figure from ref[19]. 76

Figure 26 The four different phases observed in simulation of hydrodynamic equations. Compare this image with Fig 25 on page 76. Obtained for $L = 200 \times 200$, $\rho_0 = 1$ and different noise values. 84

Figure 27 Density field comparison of two chaotic solutions in the mixed case. Both are obtained for $L = 4000 \times 500$ and $\rho_0 = 1$ from a perturbed band solution. On the left a completely chaotic solution obtained for $\sigma^2 = 0.278$ at time $T = 6E5$. On the right, while the border are chaotic, the band solution survives, for $\sigma^2 = 0.26$ at time $T = 1.2E6$. 85

Figure 28 Study of the time series of $\langle \Delta\rho \rangle_\tau$ at $L = 400 \times 400$. The difference is recorded at time intervals $\tau = 40$. At high values of noise ($\sigma = (0.282, 0.28)$) the solution converges to a completely chaotic one. At a lower noise values ($\sigma = (0.282, 0.275)$) a band persists, but its borders are unstable. Initially, the instability of the borders is oscillating, but at later times it becomes chaotic. The inset shows the transformation from a periodic to a chaotic instability of the border at $\sigma = 0.275$. Finally at low noise values ($\sigma = (0.26, 0.25)$) the solution decays to a homogeneous ordered solution. Note that at the value of noise $\sigma = 0.278$ the solution decayed to an isotropic disordered one, because this value of noise is bigger than $\sigma_t \approx 0.277$. 86

Figure 29 Study of the time series of $\langle \Delta\rho \rangle_\tau$ at $L = 1000 \times 1000$. The difference is recorded at time intervals $\tau = 100$. At high values of noise ($\sigma = (0.282, 0.28)$) the solution converges to a completely chaotic one. At a lower noise values ($\sigma = (0.278, 0.275)$) a band with oscillating borders exists initially, but transforms into a completely chaotic one after some time. Note that at $\sigma = 0.275$ the simulation explodes during this transformation, due to the numerical stiffness of our equations. At a lower noise values ($\sigma = (0.27, 0.26)$) a band persists, but its borders are unstable. The inset shows the transformation from a periodic to a chaotic instability of the border at $\sigma = 0.27$. Finally at low noise value $\sigma = 0.25$ the solution decays to a homogeneous ordered solution. 87

Figure 30 Study of the time series of $\langle \Delta\rho \rangle_\tau$ at $L = 2000 \times 2000$. The difference between the means is recorded at time interval $\tau = 100$. We see that both at a noise above and below the transition noise $\sigma_t \approx 0.277$ the final obtained solution is the completely chaotic one. 88

Figure 31 Density field of a simulation at $\sigma = 0.04$ and $L = 1600 \times 1600$. A collision of nematic defects can be seen in the center of the figure, which lead to the explosion of the simulation code. 130

Figure 32 Values of the function $g(a)$ on the domain $]0:1[$. We see that the function is strictly positive, thus the band solution is unstable. 135

Figure 33 Fit of the order parameter as a function of system size, for different noise values. From top to bottom the noise values are $\sigma = 0.275$, $\sigma = 0.2775$ and $\sigma = 0.28$. 137

Figure 34 Temporal auto-correlation function of the mean nematic order parameter for different system sizes at $\sigma = 0.28$. 138

Figure 35 2D Spatial auto-correlation function of the density for $L = 6400$ and $\sigma = 0.28$. 138

Figure 36 1D Density spatial auto-correlation function. From top to bottom the noise values are $\sigma = 0.275$, $\sigma = 0.2775$ and $\sigma = 0.28$. 139

LIST OF TABLES

Table 1 Coefficients of the integrals(39,40) 93

LISTINGS

ACRONYMS

Part I

GENERALITIES ON COLLECTIVE MOTION

1 INTRODUCTION

1.1 COLLECTIVE MOTION

The study of collective motion in general consists in studying the auto-organization and coherent movement of a large number of moving individuals. The type of individuals involved in this kind of motion is extremely diverse. In biological systems it ranges from bacteria[33] and microfilaments[32] on micro-scale, numerous insects[12] and small water organisms on larger scales going up to fish[17], bird[13] and quadruped flocks on scales of tens or hundreds of meters, as well as human crowds. But collective motion can also be observed in man-made systems, like shaken rods, colloids, specially designed small robots[38] or large complicated robotic systems[4]. What is common to all these systems is the fact that collective motion emerges without any leadership from a particular individual or external force, and is only due to interactions among individuals and to the non-equilibrium nature of the whole system. The non-equilibrium state of these systems come from the self-production of energy by each individual.

Collective motion can be studied from many different points of view. Biologists are generally interested in the precise nature of interactions that exist among individuals in the complex behavior heuristics that drive the collective motion for example in the case of pedestrian motion[29]. For physicists the main interest are the mechanisms that produce collective motion independently of the type of individual entities involved, i.e they are interested in finding universality classes that exist among different types of collective motion.

The first simple minimal model of collective motion was produced by computer animator Craig Reynolds in 1986 in a program called "Boids"(an abbreviation from "birdoid") to simulate a bird flock. In this program the boids followed three simple rules:

1. Align with each other;
2. Try to follow each other ;
3. Avoid collisions

These three simple rules allowed to produce realistic bird or fish flocks for computer animation, where the "Boids" program is still in use.

In 1995 Vicsek et al.[39] inspired by this model, proposed a minimal model for collective motion, where they have kept only one rule from

Reynolds program, align with each other. This rule alone, as will be explained later, is capable of producing a long range order in a two dimensional system.

Based on the original Vicsek model, many other minimal models of collective motion were proposed[**?** 19, 18]. All these models share some basic common principles. They consist of self-propelled particles (spp) that are not subjected to any external forces, but extract their energy from the surrounding medium. The speed of these particles is generally considered as constant, they can have a polar or a nematic symmetry. They interact with each other through metric or topological interaction rules with various symmetries.

Another common point of all these systems is an absence of interaction through the medium, this is why they are generally called "dry active matter". However at microscopic scales, for example for bacteria, the interaction with the medium is certainly not negligible and lead to a new class of materials generally referred to as "active fluids" or "active gels". These materials consist of particles suspended in a liquid medium. Interaction with the medium can be extremely strong, the above mentioned bacteria[33, 34] can have collective speeds than increase by a factor of six compared to a speed of an individual bacterium. This is due to the creation of a flow by collectively moving bacteria. These materials have many other striking properties; diminishing viscosity when the concentration of self-propelled particles[22, 33] increase or turbulence at low Reynolds numbers[15, 34]. However these materials as of today still lack any universal theoretical description. I do not deal with them in my thesis and will not mention them anymore. All spp's mentioned in this thesis will have exclusively direct interactions between them.

The goal of my thesis is to study coarse-grained equations of different type of minimal models of collective motion, derived from the Vicsek-style models. This with the aim of establishing some universality classes that exist behind different types of dry active matter. In the next sections I will make a brief overview of what had already been done in the study of minimal models of collective motion.

1.2 THE VICSEK MODEL

The Vicsek model[39] consists of self-propelled particles with identical speed moving off-lattice in a 2d space with periodic boundary conditions. The dynamics of these particles is ruled by the following streaming and collision rules

$$\begin{aligned} x_i^{t+1} &= x_i^t + v_0 \mathrm{e}\left(\theta_i^{t+1}\right)\Delta t \\ \theta_i^{t+1} &= \bar{\theta}_i + \xi_i \end{aligned}$$

Where $\bar{\theta}_i = \arg\left(\sum_{j\in R_i} e^{i\theta_j}\right)$ is the mean angle of all particles in the disk R_i around the particle i, $\xi_i \in [-\eta\pi : \eta\pi]$ is an uncorrelated white noise with an amplitude $\eta \in [0:1]$, e is a unit vector with direction θ and v_0 is the speed of particles. This model is actually a dynamic analog to the well known XY spin model. To study the collective motion in the system we can introduce the mean polar order parameter $P = \frac{1}{Nv_0}\left|\sum_{i=1}^{N} \vec{v}_i\right|$ which can vary from 0, corresponding to a completely disordered system, to 1 corresponding to all particles moving in the same direction.

Starting from random initial conditions, Vicsek et al. studied the final value of the order parameter as a function of noise amplitude η. As seen on Fig(1a) the author have found a continuous transition to an ordered state when the noise amplitude is decreased. They have observed three different phases as shown on Fig(1b,c,d). At high noise the particles are completely disordered, Fig(1b). At low noise and low density the particles form clusters that moves coherently, Fig(1c). If we keep the noise low but increase the density, all the particles in the system become aligned, Fig(1d). Given the coherent movement of all particles in the system the authors suspected the presence of effective long range interactions. It was latter proven by Toner and Tu[35] that this system really exhibits long range order at low density. Note that long range order is impossible in 2d systems at equilibrium due to the Mermin-Wagner theorem[27], this prove once again that the Vicsek model is an out of equilibrium one.

1.3 THE TONER AND TU APPROACH TO COLLECTIVE MOTION

In 1995 Toner and Tu[35] proposed a continuous description of minimal models of collective motion, which notably includes the Vicsek model. Based exclusively on symmetry principles they proposed the following set of two equations for the local density ρ and velocity $\vec{v}$ fields for polar particles:

$$\begin{aligned}
\frac{\partial \rho}{\partial t} &= -\nabla\cdot(\vec{v}\rho) \\
\partial_t \vec{v} + \lambda\left(\vec{v}\cdot\nabla\right)\vec{v} &= \left(\alpha - \beta\left|\vec{v}\right|^2\right)\vec{v} - \nabla P + D_L \nabla\left(\nabla\cdot\vec{v}\right) \\
&\quad + D_1\nabla^2\vec{v} + D_2\left(\vec{v}\cdot\nabla\right)^2\vec{v} + \vec{f}
\end{aligned}$$

The first equation is just the continuity equation representing the conservation of the number of particles. In the second equation we have on the l.h.s an advection term represented by the term λ. The value of λ will be one in the case of a system that conserves momentum. In that case we can get rid of this term by placing ourselves in the Lagrangian reference frame. However the Vicsek model does not conserve momentum, thus in this case λ will be different from one. On the r.h.s we have the Ginzburg-Landau like terms that will help

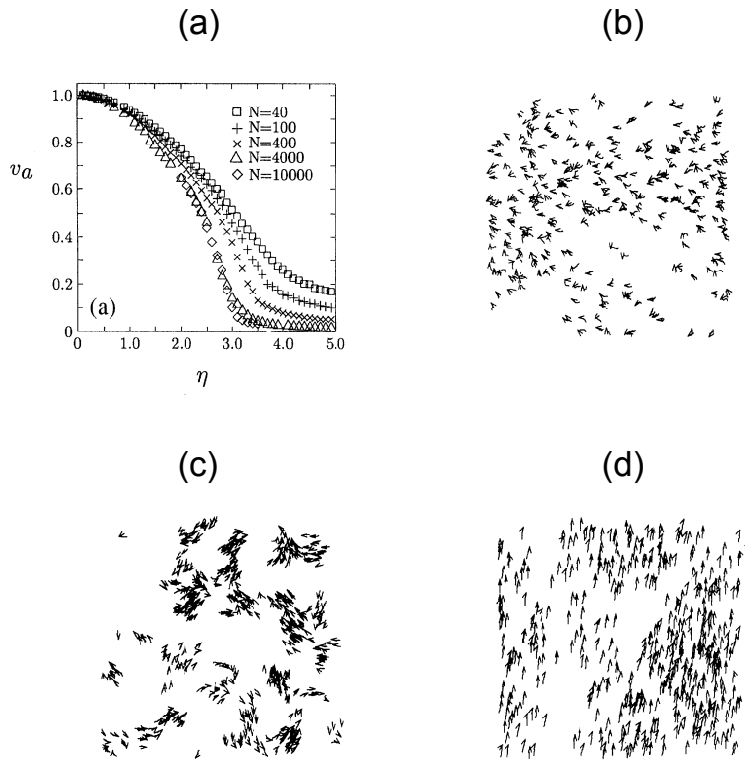

Figure 1: Various results for the Vicsek model. (a) Values of the order parameter v_a as a function of noise amplitude η for various system sizes. (b,c,d) Various phases initially reported for the Vicsek model. (b) Disordered phase at high noise. (c) Clustered phase at low density and low noise. (d) Homogenous ordered phase at high density and low noise.

to maintain the order at a non-zero level $\vec{v} = \sqrt{\alpha/\beta}$ when $\alpha > 0$. The pressure term is given by $P(\rho) = \sum_{n=1}^{\infty} \sigma_n (\rho - \rho_0)^n$, where ρ_0 is the mean density in the system and σ_n are the coefficients of the pressure expansion. Then we have three diffusion terms given by coefficients $D_{L,1,2}$ and finally an additive Gaussian white noise $\vec{f}$.

As all these terms are obtained exclusively from the symmetries of the underlying microscopic models, the dependence of coefficients on different parameters of the model is totally unknown. For example as we have seen in the previous section, the transition from disorder to order in the Vicsek model depends on density and angular noise, thus α should depend somehow on these parameters.

Studying this system by the renormalisation group approach the authors have come to the following results:

1. For dimensions less than four, the system has non-mean-field exponents;

2. For $d \geq 2$, this system will exhibit long-range order;

3. Some of the scaling exponents in the case d=2 can be computed if some approximations are admitted, for which no justification exists as so far(Toner 2012)

In a latter publication[37] Toner and Tu checked if their results were consistent with microscopic simulations. To that end they used a microscopic model similar to the Vicsek one, differing only in the addition of a repulsion and attraction term, to prevent the formation of clusters in the ordered regime.

The authors have found good agreement of the scaling coefficients between the hydrodynamic equations and the microscopic model. Most of the scaling parameters in this model are anisotropic, being different in the direction of collective motion and perpendicular to it. For example the density auto-correlation function scale as $q_{\parallel}^{-2}$ in the direction parallel to collective motion and as $q_{\perp}^{-6/5}$ for direction perpendicular to it. Most important are however the sound propagating speeds. Not only they differ in different directions, but in each direction there are actually two such speeds, one that the authors call v_s, the other is then given by λv_s. Where λ is the advection coefficient that we have defined previously. For systems that conserve momentum the value of λ will be one and thus only one speed will be present like in classical fluids. However as we have already pointed out the Vicsek model does not conserve the momentum because of the fixed value of the speed of particles, thus λ will be different from one and thus the system will have two different sound speeds. In their model the authors have measured a value $\lambda = 0.75$. However we will show in this thesis that for the Vicsek model this value is not fixed and vary as a function of angular noise and density.

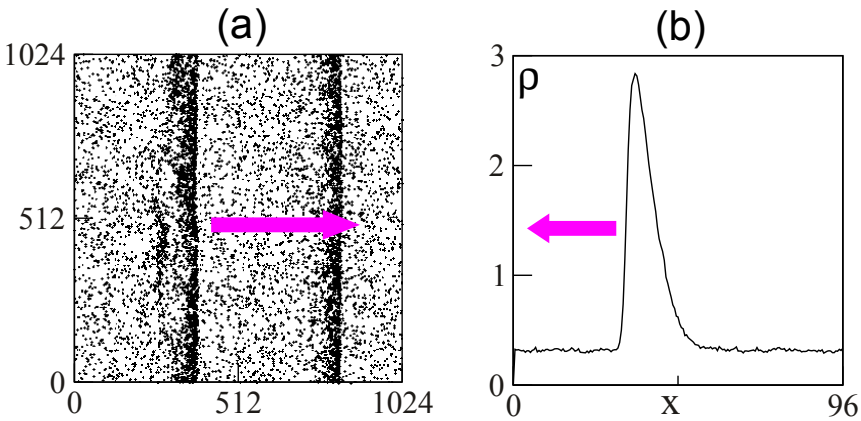

Figure 2: (a) High density bands of particles in the Vicsek model. (b) Traversal cutoff of a band showing the density profile. Images from ref[?].

1.4 NEW INSIGHT ON THE VICSEK MODEL

But in 2004 Guillaume Grégoire and Hugues Chaté[?] studied the Vicsek system with much larger system sizes than those used by Vicsek et al. They have discovered that at larger system sizes, the transition from the ordered to the disordered phase becomes discontinuous. A third state appears between the disordered and the globally ordered homogenous phases. This state is characterized by high density, high-order, bands traveling in the direction of the order parameter in a disordered sea. As seen on Fig(2a) these bands span across the whole system, and are oriented perpendicular to the borders(as a consequence of the periodic boundary conditions). They are asymmetric if seen from a cut across as on Fig(2b), approaching a shock-vawe configuration on the front, and having a much more gentle slope on the back. The number and the size of these bands vary as a function of many parameters and will be discussed later in the thesis.

To produce such non homogeneous solutions, the continuous equations must have coefficients depending on density. But using the symmetries approach of Toner and Tu it is impossible to know the value of the coefficients of different terms in equations. Thus other approaches must be used to derive hydrodynamic equations of collective motion, that will account for such structures. A brief summary of such approaches will be given next.

Latter the authors confirmed [?] another striking properties of the Vicsek model, the giant density fluctuations. The fluctuation ΔN of particles as a function of number of particles $\langle N \rangle$ is not decreasing with a power law of $1/2$, as this is the case for equilibrium systems, but as a power of 0.8 . This properties was predicted earlier by Toner and coworkers[36].

In its original form the Vicsek model studied only polar particles, however later works studied many other types of particles and interactions[? 19, 18]. I will explain more precisely each model in the following chapters.

1.5 OVERVIEW OF APPROACHES FOR HYDRODYNAMIC EQUATIONS OF COLLECTIVE MOTION

1.5.1 *Bertin-Droz-Grégoire approach*

There are several approaches to derive coarse-grained equations of collective motion. First we can just postulate equations based on symmetry principles like it was done by Toner and Tu[35] or by Ramaswamy and coworkers[36].

The second approach consists in starting from a precise microscopical model and obtaining equations by coarse-graining. The first authors to use such an approach were Eric Bertin, Michel Droz and Guillaume Grégoire[8, 9], therefore we will in the next parts of this thesis refer to this approach as the BDG approach. Starting from a Boltzmann equation for the particles dynamics, they performed a Fourier expansion of this equation around the transition point to obtain closed equations for density and polar order, with explicit form of coefficients. As this is the simplest approach which gave plausible results, this is the approach that was retained for my thesis for deriving coarse grained equations of different types of microscopic models. A detailed review of this approach will be given in the next part of the thesis. I will extend this approach to a more precise formalism that we call the "Boltzmann-Ginzburg-Landau" (BGL) approach to collective motion.

1.5.2 *Thomas Ihle approach*

As will be described in this thesis, the BDG approach can qualitatively describe the global dynamics seen in different microscopic models. However as the main point of the Boltzmann approach is the supposition of the molecular chaos and hence a binary collision dynamics, we can argue that BDG equations can not faithfully reproduce the high density structures in the microscopic models. Thus an alternative method to derive coarse grained equations was proposed by Thomas Ihle[23], that treats a full multi-particle collisions. However this method has a major drawback: the multi-particle collision integrals can not be solved analytically in most cases. Thus all the values of coefficients of different terms of the equations are known only numerically. Given the local density dependence of these coefficients, in a simulation they must be reevaluated or approximated at each time step, which is extremely costly in terms of computing resources. In

his first publication, Thomas Ihle was not able to obtain any bands like structures in his simulations, probably pointing to a problem in his method of truncating his equations.

Lately the author submitted another article[24] in which he used another truncation technique. Notably limiting the collision integrals, to a binary collision, and making a fifth order Fourier truncation of his equation. Thus transforming his approach in some analog of the BDG approach presented previously. In this case the author was able to obtain bands structure in a 1D simulation of his equations. However more insights are needed to determine if this approach gives any new results as opposed to the BDG approach.

1.5.3 *Marchetti and coworkers approach*

An alternative way of deriving hydrodynamic equations in the case of binary collisions was proposed by Cristina Marchetti and coworkers in a series of papers[6, 28, 21]. The main difference from the previous approaches, as explained by the authors, is the use of 'real' physical model as a starting point for their equations. This is as opposed to the 'rule based' models like the Vicsek one. The considered physics is the non-zero size of the particles, with a volume exclusion interaction between them. This precise physical model was first used in the article by Baskaran and Marchetti[6]. In that article they considered polar self-propelled rods and derived density, polar-order and nematic order fields equations from a Smoluchowski equation.

However using such an approach the authors were not able to obtain a saturating third order Ginzburg-Landau term, i.e such equations will explode if simulated. The authors pretend that this is due to the underlying physical model. Thus the author where obliged to introduce such a term by hand as a phenomenological parameter. Such an approach where also used in all they latter publications.

Thus even if the equations derived by Marchetti et al., and used in all they latter articles, come from a coarse-graining of a precise microscopical model, some terms and all coefficients have values introduced phenomenologically. However this allows the authors to study a large phase diagram of many different parameters showing the existence of phases not seen in our equations, because our equations have precise set of coefficients. For example, in the case of polar particles they were able to find a phase with polar asters[21]. This phase exists only with high values of the λ parameter of advection, as defined previously for the Toner and Tu equations. Of course our λ parameter is fixed, so we were never able to see such a phase. We will try to compare our results with those obtained by Marchetti et al. in this thesis when this will be relevant.

1.5.4 *Other approaches*

We first must mention a series of papers by Aranson and Tsimring[1, 2, 3]. In these papers the authors derived coarse-grained equations for real experimental systems; for shaken rods in one case[1] and for microtubules and motors[2, 3] in the other. In the first case the authors introduced phenomenological equations for the density based on a Cahn-Hilliard approach and a phenomenological equation for the order parameter based on the Ginzburg-Landau equation. As for the case of microtubules and motors the authors derived their equations from a phenomenological probability equation based on Maxwell interaction rules. In both cases the authors used a precise Ginzburg-Landau like approach to truncate their equations. I will explain this method in the next chapter, as I kept it to truncate the equations obtained with the BDG approach.

They are also different approaches, for the case when the microscopic models are more complicated and differ strongly from the Vicsek model. For example in the case of variable particle speed, an approach based on coarse-graining of Fokker-Planck equations was developed by Romanczuk and coworkers[31].

We will not deal with such kind of approaches in this thesis, where only Vicsek like models will be studied.

1.6 ORGANIZATION OF THE THESIS

This thesis is organized in the following way. In Part II, a full introduction to the Boltzmann-Ginzburg-Landau method of deriving coarse-grained equations of Vicsek like-models will be given.

In Part III, three chapters coming after will each deal with a specific type of Vicsek like model with metric interactions and in Part IV a case with topological interactions will be presented. In these two parts, each chapter will start with an introduction to the microscopic model behind the equations, continued with the corresponding article with hydrodynamic-equations derivation. It will be followed by additional investigations that did not yet made their way into a separate article and finished with some conclusions. The only exception will be the chapter dealing with the case of the simplest Vicsek polar case. While the derivation of equations for this case was already done by Bertin et al., an article with further investigations is still in elaboration at the time of writing this thesis. Thus the article in this chapter will be replaced by the current state of investigation on this model with details of the work already done by Bertin et al.

BIBLIOGRAPHY

[1] I.S. Aranson and L.S. Tsimring. Model of coarsening and vortex formation in vibrated granular rods. *PRE*, 67(2):021305, 2003. (Cited on page 11.)

[2] I.S. Aranson and L.S. Tsimring. Pattern formation of microtubules and motors: Inelastic interaction of polar rods. *Physical Review E*, 71(5 AR 050901), 2005. (Cited on page 11.)

[3] I.S. Aranson and L.S. Tsimring. Theory of self-assembly of microtubules and motors. *PRE*, 74(3):031915, 2006. (Cited on page 11.)

[4] T. Balch and R.C. Arkin. Behavior-based formation control for multirobot teams. *Ieee Transactions on Robotics and Automation*, 14(6):926–939, 1998. (Cited on page 3.)

[5] M. Ballerini, N. Cabibbo, R. Candelier, A. Cavagna, E. Cisbani, I. Giardina, V. Lecomte, A. Orlandi, G. Parisi, A. Procaccini, M. Viale, and V. Zdravkovic. Interaction ruling animal collective behavior depends on topological rather than metric distance: Evidence from a field study. *Proceedings of the National Academy of Sciences*, 105(4):1232–1237, 2008. (Cited on page 147.)

[6] A. Baskaran and M.C. Marchetti. Hydrodynamics of self-propelled hard rods. *PRE*, 77(1):011920, 2008. (Cited on pages 10 and 24.)

[7] A. Baskaran and M.C. Marchetti. Self-regulation in self-propelled nematic fluids. *European Physical Journal E*, 35(9):95, 2012. (Cited on page 136.)

[8] E. Bertin, M. Droz, and G. Grégoire. Boltzmann and hydrodynamic description for self-propelled particles. *Physical Review E*, 74(2 AR 022101), 2006. (Cited on pages 9 and 36.)

[9] E. Bertin, M. Droz, and G. Grégoire. Hydrodynamic equations for self-propelled particles: microscopic derivation and stability analysis. *Journal of Physics A-mathematical and Theoretical*, 42(44):445001, 2009. (Cited on pages 9, 43, and 48.)

[10] D.L. Blair, T. Neicu, and A. Kudrolli. Vortices in vibrated granular rods. *PRE*, 67(3):031303, 2003. (Cited on page 130.)

[11] J.P. Boyd. *Chebyshev and Fourier spectral methods*. Dover Publications, 2001. (Cited on page 57.)

[12] J. Buhl, D. Sumpter, I.D. Couzin, J.J. Hale, E. Despland, E.R. Miller, and S.J. Simpson. From disorder to order in marching locusts. *Science*, 312(5778):1402–1406, 2006. (Cited on page 3.)

[13] A. Cavagna, A. Cimarelli, I. Giardina, G. Parisi, R. Santagati, F. Stefanini, and M. Viale. Scale-free correlations in starling flocks. *Proceedings of the National Academy of Sciences of the United States of America*, 107(26):11865–11870, 2010. (Cited on page 3.)

[14] L.-Y. Chen, N. Goldenfeld, and Y. Oono. Renormalization group and singular perturbations: Multiple scales, boundary layers, and reductive perturbation theory. *Physical Review E*, 54(1):376–394, 1996. (Cited on page 54.)

[15] L.H. Cisneros, R. Cortez, C. Dombrowski, R.E. Goldstein, and J.O. Kessler. Fluid dynamics of self-propelled microorganisms, from individuals to concentrated populations. *Experiments in Fluids*, 43(5):737–753, 2007. (Cited on page 4.)

[16] D.S. Dean. Langevin equation for the density of a system of interacting langevin processes. *Journal of Physics A-mathematical and General*, 29(24):L613–L617, 1996. (Cited on page 26.)

[17] J. Gautrais, C. Jost, M. Soria, A. Campo, S. Motsch, R. Fournier, S. Blanco, and G. Theraulaz. Analyzing fish movement as a persistent turning walker. *Journal of Mathematical Biology*, 58(3):429–445, 2009. (Cited on page 3.)

[18] F. Ginelli and H. Chaté. Relevance of metric-free interactions in flocking phenomena. *Physical Review Letters*, 105(16):168103, 2010. (Cited on pages 4, 9, 20, and 147.)

[19] F. Ginelli, F. Peruani, M. Bar, and H. Chaté. Large-scale collective properties of self-propelled rods. *Physical Review Letters*, 104(18):184502, 2010. (Cited on pages xiii, xiv, 4, 9, 20, 75, and 76.)

[20] L. Giomi, M.J. Bowick, X. Ma, and M.C. Marchetti. Defect annihilation and proliferation in active nematics. *PRL*, 110(22):228101, 2013. (Cited on page 130.)

[21] A. Gopinath, M.F. Hagan, M.C. Marchetti, and A. Baskaran. Dynamical self-regulation in self-propelled particle flows. *Physical Review E*, 85(6 AR 061903), 2012. (Cited on page 10.)

[22] Y. Hatwalne, S. Ramaswamy, M. Rao, and R.A. Simha. Rheology of active-particle suspensions. *Physical Review Letters*, 92(11):118101, 2004. (Cited on page 4.)

[23] T. Ihle. Kinetic theory of flocking: Derivation of hydrodynamic equations. *Physical Review E*, 83(3 AR 030901), 2011. (Cited on page 9.)

[24] T. Ihle. Invasion-wave induced first-order phase transition in systems of active particles. *eprint arXiv:1304.0149*, 2013. (Cited on page 10.)

[25] C. Lanczos. *Linear differential operators*. Van Nostrand, 1961. (Cited on pages 91 and 133.)

[26] L.D. Landau. *Collected papers of L.D. Landau. Edited and with an introduction by D. ter Haar*. Oxford, New York, Pergamon Press, 1965. (Cited on pages 24 and 25.)

[27] N.D. Mermin and H. Wagner. Absence of ferromagnetism or antiferromagnetism in one- or two-dimensional isotropic heisenberg models. *PRL*, 17(22):1133–1136, 1966. (Cited on page 5.)

[28] S. Mishra, A. Baskaran, and M.C. Marchetti. Fluctuations and pattern formation in self-propelled particles. *PRE*, 81(6):061916, 2010. (Cited on page 10.)

[29] M. Moussaid, D. Helbing, and G. Theraulaz. How simple rules determine pedestrian behavior and crowd disasters. *Proceedings of the National Academy of Sciences of the United States of America*, 108(17):6884–6888, 2011. (Cited on page 3.)

[30] S. Ramaswamy, R.A. Simha, and J. Toner. Active nematics on a substrate: Giant number fluctuations and long-time tails. *Europhysics Letters*, 62(2):196–202, 2003. (Cited on page 99.)

[31] P. Romanczuk and L. Schimansky-Geier. Mean-field theory of collective motion due to velocity alignment. *Ecological Complexity*, 10:83–92, 2012. (Cited on page 11.)

[32] V. Schaller, C. Weber, C. Semmrich, E. Frey, and A.R. Bausch. Polar patterns of driven filaments. *Nature*, 467(7311):73–77, 2010. (Cited on pages 3 and 35.)

[33] A. Sokolov and I.S. Aranson. Reduction of viscosity in suspension of swimming bacteria. *Physical Review Letters*, 103(14):148101, 2009. (Cited on pages 3 and 4.)

[34] A. Sokolov, R.E. Goldstein, F.I. Feldchtein, and I.S. Aranson. Enhanced mixing and spatial instability in concentrated bacterial suspensions. *Physical Review E*, 80(3):031903, 2009. (Cited on page 4.)

[35] J. Toner and Y.H. Tu. Long-range order in a 2-dimensional dynamical xy model - how birds fly together. *Physical Review Letters*, 75(23):4326–4329, 1995. (Cited on pages 5, 9, and 26.)

[36] J. Toner, Y.H. Tu, and S. Ramaswamy. Hydrodynamics and phases of flocks. *Annals of Physics*, 318(1):170–244, 2005. (Cited on pages 8, 9, and 75.)

[37] Y. Tu, J. Toner, and M. Ulm. Sound waves and the absence of galilean invariance in flocks. *PRL*, 80(21):4819–4822, 1998. (Cited on pages 7 and 35.)

[38] A.E. Turgut, H. Celikkanat, F. Gokce, and E. Sahin. Self-organized flocking in mobile robot swarms. *Swarm Intelligence*, 2(2-4):97–120, 2008. (Cited on page 3.)

[39] T. Vicsek, A. Czirok, E. Benjacob, I. Cohen, and O. Shochet. Novel type of phase-transition in a system of self-driven particles. *Physical Review Letters*, 75(6):1226–1229, 1995. (Cited on pages 3, 4, and 33.)

Part II

THE BOLTZMANN-GINZBURG-LANDAU METHOD

2 COARSE-GRAINING OF VICSEK-LIKE MODELS

2.1 GENERALITIES ON THE VICSEK LIKE MODELS

In this chapter I give a general description of the BDG method to derive coarse-grained equations of Vicsek-like models of collective motion. We can start by recalling the principal properties of these microscopic models. These models consist of self-propelled point particles that evolve off lattice in a n-dimensional space. All the particles have the same speed v_0, and differ only by their direction which is indicated by an angle θ_i that the particle i has with the general reference frame. We can first note that this system does not conserve momentum(the momentum of the system is actually proportional to the global polar order parameter) nor does it have Galilean invariance, both remarks are due to the fixed speed. Thus the same must apply to the hydrodynamic equations that we will obtain from this microscopic model, which is in contrast to the case of Navier-Stocks equation of fluid motion. While the initial Vicsek model dealt only with polarly oriented particles, we can also use nematic particles as in ref[**?**]. In this case the particles randomly choose to move in the forward or backward direction at each time step. A detailed description of this model will be given in the corresponding chapter.

This ballistic motion of particles is subjected to stochastic events, which corresponds to a change $\theta_i^{t+1} = \theta_i^t + \xi$ of the angle of motion at each time step, where ξ is a random angle of distribution $P(\xi)$. This change in angle prevents the system from having a trivially organized collective motion due just to ballistic motion. $P(\xi)$ is a general noise distribution function defined on the support $[-\eta\pi : \eta\pi]$. In the following we consider a generalized wrapped normal distribution

$$P(\xi;\eta,\sigma) = \begin{cases} \frac{1}{\sqrt{2\pi}\sigma} \sum_{k=-\infty}^{\infty} e^{-\frac{(\xi-2\pi\eta k)^2}{2\sigma^2}} & \xi \in [-\eta\pi : \eta\pi] \\ 0 & elsewhere \end{cases}$$

If we set $\sigma = \infty$ we recover the uniform distribution of the Vicsek model defined by

$$P(\xi;\eta) = \begin{cases} \frac{1}{2\pi\eta} & \xi \in [-\eta\pi : \eta\pi] \\ 0 & elsewhere \end{cases}$$

However for the coarse grained equations we will set $\eta = 1$ and obtain, the more physical, classical wrapped normal distribution

$$P(\xi;\sigma) = \begin{cases} \frac{1}{\sqrt{2\pi}\sigma} \sum_{k=-\infty}^{\infty} e^{-\frac{(\xi-2\pi k)^2}{2\sigma^2}} & \xi \in [-\pi : \pi] \\ 0 & elsewhere \end{cases}$$

The reason for this choice is simple. To obtain hydrodynamic equations of collective motion we will use a Fourier series expansion on the angle. But the Vicsek like noise is a step function whose Fourier series is spoilt by the Gibbs phenomenon, i.e is not uniformly convergent. Its Fourier transform is an oscillating sinc function. We thus prefer a continuous function, whose Fourier transform is monotonic.

The particles are also subjected to collision events. In the original Vicsek model collision events correspond to the polar alignment of the particles inside some interaction radius, with an addition of a random angle from the same distribution as the angular diffusion of individual particles. However the change of angle can have not only a polar nature but also a nematic one as in ref[**?** 19]. It is also important to note that the interaction for most of the big animals with collective motion is not local by nature but topological, i.e an individual interact with the individuals that he has in sight, independently of the distance to this individuals. Thus we can also introduce a model with topological interactions as in ref[18]. A derivation of hydrodynamic equations for such a case can also be made and will be presented in the last chapter.

In the case of local interactions we can introduce the interaction radius d_0. When particles get closer than this distance, they align their angle according to the rule

$$\theta_i^{t+1} = \bar{\theta}_i + \xi_i$$

where

$$\bar{\theta}_i = \arg\left(\sum_{j \in d_0} e^{i\theta_j}\right)$$

in the case of a polar alignment rule or

$$\bar{\theta}_i = \arg\left(\sum_{j \in d_0} \mathrm{sign}\left[\cos\left(\grave{}_j - \grave{}_i\right) e^{i\grave{}_j}\right]\right)$$

in the case of a nematic alignment. In the case of topological interactions, the neighbors will be chosen as the Voronoi nearest neighbors.

While we generally choose the angle noise in the collision event ξ_i to have an equivalent distribution than the one of self-diffusion, this is not mandatory. We can however note that choosing two different angle distributions will not introduce any new state, but will only complicate the topology of the stability diagram, hence the motivation to choose them equivalent.

Finally while the original Vicsek model does not have any spatial diffusion there is no any reason to exclude such a diffusion in a general case (we can note than the diffusive dynamic is however natural in the case of nematic particles and replace the convective one). We can thus introduce two diffusions coefficients

- Diffusion along the velocity of the particles is given by $D_{\parallel} = D_0 + \delta D$
- Diffusion perpendicular to the particles velocity vector is given by $D_{\perp} = D_0 - \delta$

This coefficients can be used to introduce spatial diffusion for polar particles in hydrodynamic equations, they where however never used in microscopic simulations.

2.2 THE BOLTZMANN APPROACH

To obtain hydrodynamic equations of collective motion we will start from a Boltzmann equation for the probability $f(r, \theta, t)$ of finding an spp at position r with an angle θ at time t. However to use the Boltzmann approach some hypothesis about the underlying system should be made, namely the molecular chaos hypothesis that implies that the velocities and positions of particles are uncorrelated. We must also assume that the gas is diluted i.e the typical distance between particles is much larger than the interaction radius. All this is needed to be able to use the binary collision hypothesis. While we can argue that these conditions will not forcefully be met in a high-density collective state, especially in the band structure, we will however show that this Boltzmann equation provides coherent results compared to the microscopic models.

The classical Boltzmann equation for ideal gases is written as

$$\frac{\partial f}{\partial t} = \left(\frac{\partial f}{\partial t}\right)_{force} + \left(\frac{\partial f}{\partial t}\right)_{diff} + \left(\frac{\partial f}{\partial t}\right)_{coll}$$

and is composed of an external force term, a diffusion term and a collision term.

First as we have already noted the spp are not subjected to external forces, however they take energy from the medium for self-propulsion. Thus we will replace the force term in the original Boltzmann equation by the term corresponding to this self-propulsion. In the case of polar particles this will be a convection term with an amplitude v_0 while in the case of nematic particles this will be a spatial diffusion term.

As for the diffusion term, we must first speak about the angular diffusion term. This term will always be identical independently of the type of particles and is composed of a loss term, when a particle

with angle θ change it to another angle and a gain term when a particle with angle θ' diffuse to the angle θ. In the previous subsection we have noted that the probability of self-diffusion is given by λ, thus the angular diffusion term is given by

$$I_{diff}[f] = -\lambda f(r,\theta,t) + \lambda \int_{-\pi}^{\pi} d\theta' \int_{-\pi}^{\pi} d\xi P(\xi)\, \delta\left(\theta' + \xi - \theta\right) f\left(r,\theta',t\right)$$

We should note that in the case of nematic particles the possible values of angles for θ' are of course $\left[-\frac{\pi}{2} : \frac{\pi}{2}\right]$.

Secondly there is also a possibility to introduce a positional diffusion as defined in previous section. This diffusion terms will be given by

$$D_{\parallel}\partial_{\parallel}^2 f(r,\theta,t) + D_{\perp}\partial_{\perp}^2 f(r,\theta,t)$$

where

$$\partial_{\parallel} = e(\theta)\cdot\nabla\ \partial_{\perp} = \nabla - e(\theta)\,\partial_{\parallel}$$

Finally the collision term will also be composed of a loss and gain term. However the collision term will be different depending on the particle type and interaction type. To this end we introduce the collision kernel $K(\theta_1,\theta_2)$ which corresponds to the type of the particles and the outgoing angle term $\Psi(\theta_1,\theta_2)$ that corresponds to the type of collision. We can thus have three different cases; the simple Vicsek one, discussed in the third chapter, when particles and the collisions are polar, the mixed case, discussed in the fourth chapter, where the particle are polar but the collision are nematic and finally a fully nematic case, discussed in chapter five, when the particles and the collisions are fully nematic. A full expression of these two terms will be given in the corresponding chapters. There is also a special case for topological interactions where the collision kernel will be changed accordingly, this will be described in chapter six. The collision integral is then given by

$$\begin{aligned} I_{coll}[g,h] = &-g(r,\theta,t)\int_{-\pi}^{\pi} d\theta_2 K(\theta_1,\theta_2)\, h(r,\theta_2,t) \\ &+ \int_{-\pi}^{\pi} d\theta_1 \int_{-\pi}^{\pi} d\theta_2 \int_{-\pi}^{\pi} d\xi . P(\xi)\, K(\theta_1,\theta_2) \\ &\qquad \times g(r,\theta_1,t)\,.h(r,\theta_2,t)\,\delta\left(\Psi(\theta_1,\theta_2) + \xi - \theta\right) \end{aligned}$$

once again the integration will be performed on angles $\left[-\frac{\pi}{2} : \frac{\pi}{2}\right]$ in the case of nematic particles.

This equation of course admits a constant solution $f(r,\theta,t) = \frac{\rho_0}{2\pi}$, where ρ_0 is the global density of particles. However we must seek methods to transform this equation if we want to study more complicated analytical solutions, notably the homogeneous collective motion solutions or the band solutions. The numerical approach is more or less the only one we can use to study this equation in its full form.

2.3 DERIVATION OF HYDRODYNAMIC EQUATIONS

We want to transform the previously obtained Boltzmann equation into a set of hydrodynamic equations for density, polar and nematic order parameters. For this end we will take the Fourier transform on the angle. We will suppose that f is sufficiently smooth, as a function of θ, near the transition point, for a finite Fourier series to be applicable.

To make a Fourier transform of the Boltzmann equation we introduce the series expansion of $f(r,\theta,t)$

$$\begin{aligned} f(r,\theta,t) &= \frac{1}{2\pi}\sum_{k=-\infty}^{\infty}\hat{f}_k(r,t)\,e^{-ik\theta} \\ \hat{f}_k(r,t) &= \int_{-\pi}^{\pi} d\theta f(r,\theta,t)\,e^{ik\theta} \end{aligned}$$

Thus in order to obtain the Fourier transform of the Boltzmann equation we should multiply it by $e^{ik\theta}$ and integrate on the angle. We will then obtain an infinite set of equations. Exact expressions of these equations will be given in corresponding chapters.

The zero moment, which is just an integration on the angle, correspond to the density field

$$\rho(r,t) = f_0(r,t) = \int_{-\pi}^{\pi} f(r,\theta,t)\,d\theta$$

The first moment is given by

$$f_1(r,t) = \int_{-\pi}^{\pi} f(r,\theta,t)\,e^{i\theta}d\theta$$

its real and imaginary parts can be mapped to the polar order parameter

$$\vec{w} = \frac{1}{\rho(r,t)}\left[\Re\left(f_1(r,t)\right)\vec{x} + \Im\left(f_1(r,t)\right)\vec{y}\right]$$

Finally the second order parameter

$$f_2(r,t) = \int_{-\pi}^{\pi} f(r,\theta,t)\,e^{i2\theta}d\theta$$

can be mapped to the components of the nematic tensor Ω

$$\Omega_{11} = \Omega_{22} = \frac{1}{2\rho(r,t)}\Re\left(f_2(r,t)\right)$$

$$\Omega_{12} = \Omega_{21} = \frac{1}{2\rho(r,t)}\Im\left(f_2(r,t)\right)$$

In order to obtain a closed density conservation equation it is enough to integrate the Boltzmann equation on θ. However obtaining higher order equations is more complicated as these equations do not have a closed form, i.e we will need to introduce a closure approximation that we will discuss latter.

2.4 THE CLOSURE APPROXIMATION

One of the most important parts of the derivation of the hydrodynamic equations is the correct truncation of the infinite series. A badly controlled expansion can easily lead to an explosive set of equations with an uncontrolled growth. We want to derive a strict approach to the closure of Boltzmann equations of collective motion, that can be applied invariably to different type of simple models. For this end we introduce a Ginzburg-Landau like approach for the equation of the order parameter. Our aim is to obtain Ginzburg-Landau like terms in the polar or nematic order parameters in order to obtain the collective motion solution. Thus we shall truncate our equations at least at the order which conserve the third power order term. We can for example cite the work of Baskaran and Marchetti[6], in which the author truncated the series directly at the order of the order parameter term. Thus they were not able to obtain the third power order term, which they added manually in order for their equations to be non explosive. Such an approach is at least questionable, because not only the third order power term was neglected, but potentially other terms of the same order of magnitude.

We will derive the hydrodynamic equations near the transition point where order is low and it is safe to assume that the amplitude of the higher order moments decreases fast enough for the truncation to be valid. It is important to note that such a truncation is only meant to be valid near the transition point to collective motion, where the Ginzburg-Landau like terms of the order parameter dominate the equation. But such a restricted rage of validity is not a problem since we are interested in investigation of the phenomena near the transition point.

For our equations to be consistent, we should ensure that all the terms in our equation are of the same order of magnitude. Thus we must introduce a scaling ansatz to perform a correct truncation. We start with the most important Ginzburg-Landau terms. Let's suppose that the order parameter is given by the function ψ. Then the Ginzburg-Landau equation[26] (without external forces) has the form

$$\alpha\psi - \beta\left|\psi\right|^2\psi + \gamma\nabla^2\psi = 0 \tag{1}$$

and we want that all of these terms have the same order of magnitude. As we are near the transition point, the order parameter ψ is small, we then assign the order of magnitude to it

$$\psi \sim \epsilon$$

We immediately obtain from equation(1) the scaling of spatial derivatives

$$\nabla \sim \epsilon$$

and the scaling of the first coefficient

$$\alpha \sim \epsilon^2$$

In the classical Ginzburg-Landau theory[26] of superconductors the α term represented the distance to the transition point as a function of temperature

$$\alpha = \alpha_0 \left(T - T_c\right)$$

In our case this distance will be given as a function of density

$$\alpha = \alpha_0 \left(\rho - \rho_c\right)$$

In our case the density is not bounded to any particular value. Thus to correctly set the scaling of the density it is practical to assume that the f distribution has a small spatial variation from the global density, i.e $\rho\left(r,t\right) = \rho_0 + \Delta\rho\left(r,t\right)$ where ρ_0 is the mean density and $\Delta\rho \sim \epsilon$.

We have already assumed that the Fourier coefficient of the order parameter has the scaling ϵ, we need also to introduce a scaling for other coefficients. Near the transition point, the angular distribution of f will be near the homogenous one. Thus it is safe to assume that the other Fourier coefficients should scale as $\hat{f}_k \sim \epsilon^{|k|}$.

Finally we need to introduce a scaling for the time derivative, for this end we will assume the coherence of the continuity equation. Given that the scaling of all the other terms is already known, we will obtain the scaling of ∂_t from it.

Having introduced the scaling ansatz, we can cancel out all the terms that have a higher order than the Ginzburg-Landau terms and obtain closed hydrodynamic equations.

2.5 LIMIT OF THE VALIDITY OF THE SCALING ANSATZ.

First, we need to stress out that the scaling for the density is valid for f distributions that are more or less spatially homogeneous. In case of a large deviation, for example in the case of band structures, assuming $\Delta\rho$ small is not necessarily correct. Thus as we will show in the case of polar particles, this scaling of the density should perhaps be revised.

As for the scaling of the Fourier coefficients, we will see in next chapters, that there is no any reason to consider that this truncation will lead to well behaved equations far from the transition point i.e deep in the ordered region, because higher order unbounded harmonics will grow in this region. Moreover, there is no any reason to consider that the Fourier coefficients are at all converging to zero far from the transition point, i.e a higher order truncation is not necessary helpful in obtaining a well-behaved equation in this region.

This is actually easily understandable. When the noise is decreasing the distribution of the initial Boltzmann function as a function of

the angle converges to a Dirac function. But the Fourier transform of a Dirac function is a constant, i.e the high order Fourier coefficients are not decreasing to zero. Thus a finite truncation will always lead to explosion of neglected terms far from the transition point.

For a better insight, let's suppose that the angle distribution of the probability function is given by the wrapped normal distribution introduced in the first section of this chapter, with its variance decreasing to zero as we are going deeper in the ordered region. Its Fourier transform is given by

$$\begin{aligned}\hat{P}_k(\sigma) &= F[P(\theta,\sigma)] \\ &= \frac{1}{\sqrt{2\pi}\sigma}\sum_{q=-\infty}^{\infty}\int_{-\pi}^{\pi} d\theta e^{-\frac{(\theta-2\pi q)^2}{2\sigma^2}} e^{ik\theta} \\ &= e^{\frac{-k^2\sigma^2}{2}}\end{aligned}$$

Therefore the order of truncation must scale as $\frac{1}{\sigma}$. Or as we have said σ is going to zero, the order of truncation must go to infinity as we decrease the noise.

As a consequence, if we want to obtain a valid set of equations in this region we should seek another series decomposition than the Fourier one.

More important even near the transition point, the introduced ansatz will not necessarily give well behaved equations if we try to truncate the equations at a higher order than the one of the Ginzburg-Landau terms. The higher order terms will probably be unbalanced, leading to explosive sets of equations. An investigation in the polar case, which will be presented in the next chapter, confirms this.

2.6 LANGEVIN EQUATIONS

The original equations as introduced in BDG do not have any effective noise distribution and are completely deterministic. Or such a noise is needed to obtain the scaling parameters of the underlying model. We can of course introduce an additive noise like in ref[35]. However large density fluctuations where reported for the Vicsek like model i.e the noise that we should use must be of multiplicative nature and proportional to local density. To introduce such a noise an approach developed by Dean[16] can be used. An incomplete derivation of such noise is introduced in the paper of the active-nematic case chapter. However the complete derivation and study of Langevin like equations is very long and complicated and can easily fill an independent thesis. Thus I do not aboard this subject in my thesis.

BIBLIOGRAPHY

[1] I.S. Aranson and L.S. Tsimring. Model of coarsening and vortex formation in vibrated granular rods. *PRE*, 67(2):021305, 2003. (Cited on page 11.)

[2] I.S. Aranson and L.S. Tsimring. Pattern formation of microtubules and motors: Inelastic interaction of polar rods. *Physical Review E*, 71(5 AR 050901), 2005. (Cited on page 11.)

[3] I.S. Aranson and L.S. Tsimring. Theory of self-assembly of microtubules and motors. *PRE*, 74(3):031915, 2006. (Cited on page 11.)

[4] T. Balch and R.C. Arkin. Behavior-based formation control for multirobot teams. *Ieee Transactions on Robotics and Automation*, 14(6):926–939, 1998. (Cited on page 3.)

[5] M. Ballerini, N. Cabibbo, R. Candelier, A. Cavagna, E. Cisbani, I. Giardina, V. Lecomte, A. Orlandi, G. Parisi, A. Procaccini, M. Viale, and V. Zdravkovic. Interaction ruling animal collective behavior depends on topological rather than metric distance: Evidence from a field study. *Proceedings of the National Academy of Sciences*, 105(4):1232–1237, 2008. (Cited on page 147.)

[6] A. Baskaran and M.C. Marchetti. Hydrodynamics of self-propelled hard rods. *PRE*, 77(1):011920, 2008. (Cited on pages 10 and 24.)

[7] A. Baskaran and M.C. Marchetti. Self-regulation in self-propelled nematic fluids. *European Physical Journal E*, 35(9):95, 2012. (Cited on page 136.)

[8] E. Bertin, M. Droz, and G. Grégoire. Boltzmann and hydrodynamic description for self-propelled particles. *Physical Review E*, 74(2 AR 022101), 2006. (Cited on pages 9 and 36.)

[9] E. Bertin, M. Droz, and G. Grégoire. Hydrodynamic equations for self-propelled particles: microscopic derivation and stability analysis. *Journal of Physics A-mathematical and Theoretical*, 42(44):445001, 2009. (Cited on pages 9, 43, and 48.)

[10] D.L. Blair, T. Neicu, and A. Kudrolli. Vortices in vibrated granular rods. *PRE*, 67(3):031303, 2003. (Cited on page 130.)

[11] J.P. Boyd. *Chebyshev and Fourier spectral methods*. Dover Publications, 2001. (Cited on page 57.)

[12] J. Buhl, D. Sumpter, I.D. Couzin, J.J. Hale, E. Despland, E.R. Miller, and S.J. Simpson. From disorder to order in marching locusts. *Science*, 312(5778):1402–1406, 2006. (Cited on page 3.)

[13] A. Cavagna, A. Cimarelli, I. Giardina, G. Parisi, R. Santagati, F. Stefanini, and M. Viale. Scale-free correlations in starling flocks. *Proceedings of the National Academy of Sciences of the United States of America*, 107(26):11865–11870, 2010. (Cited on page 3.)

[14] L.-Y. Chen, N. Goldenfeld, and Y. Oono. Renormalization group and singular perturbations: Multiple scales, boundary layers, and reductive perturbation theory. *Physical Review E*, 54(1):376–394, 1996. (Cited on page 54.)

[15] L.H. Cisneros, R. Cortez, C. Dombrowski, R.E. Goldstein, and J.O. Kessler. Fluid dynamics of self-propelled microorganisms, from individuals to concentrated populations. *Experiments in Fluids*, 43(5):737–753, 2007. (Cited on page 4.)

[16] D.S. Dean. Langevin equation for the density of a system of interacting langevin processes. *Journal of Physics A-mathematical and General*, 29(24):L613–L617, 1996. (Cited on page 26.)

[17] J. Gautrais, C. Jost, M. Soria, A. Campo, S. Motsch, R. Fournier, S. Blanco, and G. Theraulaz. Analyzing fish movement as a persistent turning walker. *Journal of Mathematical Biology*, 58(3):429–445, 2009. (Cited on page 3.)

[18] F. Ginelli and H. Chaté. Relevance of metric-free interactions in flocking phenomena. *Physical Review Letters*, 105(16):168103, 2010. (Cited on pages 4, 9, 20, and 147.)

[19] F. Ginelli, F. Peruani, M. Bar, and H. Chaté. Large-scale collective properties of self-propelled rods. *Physical Review Letters*, 104(18):184502, 2010. (Cited on pages xiii, xiv, 4, 9, 20, 75, and 76.)

[20] L. Giomi, M.J. Bowick, X. Ma, and M.C. Marchetti. Defect annihilation and proliferation in active nematics. *PRL*, 110(22):228101, 2013. (Cited on page 130.)

[21] A. Gopinath, M.F. Hagan, M.C. Marchetti, and A. Baskaran. Dynamical self-regulation in self-propelled particle flows. *Physical Review E*, 85(6 AR 061903), 2012. (Cited on page 10.)

[22] Y. Hatwalne, S. Ramaswamy, M. Rao, and R.A. Simha. Rheology of active-particle suspensions. *Physical Review Letters*, 92(11):118101, 2004. (Cited on page 4.)

[23] T. Ihle. Kinetic theory of flocking: Derivation of hydrodynamic equations. *Physical Review E*, 83(3 AR 030901), 2011. (Cited on page 9.)

[24] T. Ihle. Invasion-wave induced first-order phase transition in systems of active particles. *eprint arXiv:1304.0149*, 2013. (Cited on page 10.)

[25] C. Lanczos. *Linear differential operators*. Van Nostrand, 1961. (Cited on pages 91 and 133.)

[26] L.D. Landau. *Collected papers of L.D. Landau. Edited and with an introduction by D. ter Haar*. Oxford, New York, Pergamon Press, 1965. (Cited on pages 24 and 25.)

[27] N.D. Mermin and H. Wagner. Absence of ferromagnetism or antiferromagnetism in one- or two-dimensional isotropic heisenberg models. *PRL*, 17(22):1133–1136, 1966. (Cited on page 5.)

[28] S. Mishra, A. Baskaran, and M.C. Marchetti. Fluctuations and pattern formation in self-propelled particles. *PRE*, 81(6):061916, 2010. (Cited on page 10.)

[29] M. Moussaid, D. Helbing, and G. Theraulaz. How simple rules determine pedestrian behavior and crowd disasters. *Proceedings of the National Academy of Sciences of the United States of America*, 108(17):6884–6888, 2011. (Cited on page 3.)

[30] S. Ramaswamy, R.A. Simha, and J. Toner. Active nematics on a substrate: Giant number fluctuations and long-time tails. *Europhysics Letters*, 62(2):196–202, 2003. (Cited on page 99.)

[31] P. Romanczuk and L. Schimansky-Geier. Mean-field theory of collective motion due to velocity alignment. *Ecological Complexity*, 10:83–92, 2012. (Cited on page 11.)

[32] V. Schaller, C. Weber, C. Semmrich, E. Frey, and A.R. Bausch. Polar patterns of driven filaments. *Nature*, 467(7311):73–77, 2010. (Cited on pages 3 and 35.)

[33] A. Sokolov and I.S. Aranson. Reduction of viscosity in suspension of swimming bacteria. *Physical Review Letters*, 103(14):148101, 2009. (Cited on pages 3 and 4.)

[34] A. Sokolov, R.E. Goldstein, F.I. Feldchtein, and I.S. Aranson. Enhanced mixing and spatial instability in concentrated bacterial suspensions. *Physical Review E*, 80(3):031903, 2009. (Cited on page 4.)

[35] J. Toner and Y.H. Tu. Long-range order in a 2-dimensional dynamical xy model - how birds fly together. *Physical Review Letters*, 75(23):4326–4329, 1995. (Cited on pages 5, 9, and 26.)

[36] J. Toner, Y.H. Tu, and S. Ramaswamy. Hydrodynamics and phases of flocks. *Annals of Physics*, 318(1):170–244, 2005. (Cited on pages 8, 9, and 75.)

[37] Y. Tu, J. Toner, and M. Ulm. Sound waves and the absence of galilean invariance in flocks. *PRL*, 80(21):4819–4822, 1998. (Cited on pages 7 and 35.)

[38] A.E. Turgut, H. Celikkanat, F. Gokce, and E. Sahin. Self-organized flocking in mobile robot swarms. *Swarm Intelligence*, 2(2-4):97–120, 2008. (Cited on page 3.)

[39] T. Vicsek, A. Czirok, E. Benjacob, I. Cohen, and O. Shochet. Novel type of phase-transition in a system of self-driven particles. *Physical Review Letters*, 75(6):1226–1229, 1995. (Cited on pages 3, 4, and 33.)

Part III

METRIC MODELS

3 THE POLAR MODEL

3.1 THE VICSEK POLAR MODEL

We start with the simplest case of the Vicsek model as introduced in the first paper[39] and in the introductory chapter. As already mention in the introduction a major breakthrough in the study of this model was made by G. Grégoire and H. Chaté[**?**] in 2004. The authors have found that the transition to the ordered state is discontinuous due to the appearance of a non-homogenous band state between the disordered and the ordered state. Based on ref[**?**] we can give some more insight about the microscopic model.

Repeating the introductory chapter, the classical Vicsek model is composed of N point particles, with a polar symmetry, that move in a 2D space of size $L \times L$ with periodic boundary conditions. The position of the particles are updated according to the rules

$$\begin{aligned} x_i^{t+1} &= x_i^t + v_0 \mathrm{e}\left(\theta_i^{t+1}\right)\Delta t \\ \theta_i^{t+1} &= \bar{\theta}_i + \xi_i \end{aligned}$$

where $\bar{\theta}_i$ is the mean angle of particles inside an interaction radius d_0 around particle i and $\xi_i \in [-\eta\pi : -\eta\pi]$ is delta-correlated white noise whose amplitude is controlled by a value $\eta \in [0 : 1]$. We can note that the noise as introduced here is an "angular noise" on the evaluation of the mean. In ref[**?**] authors proposed to use a vectorial noise that is dependent on local alignment, decreasing when the local alignment is increasing. Their motivation is given by the fact that in experimental systems, the error comes from the evaluation of the direction of each individual, rather than from the evaluation of the mean. This noise has the big advantage of diminishing finite size effects, while not introducing any new state or changing the nature of the order-disorder transition. As introducing such a vectorial noise inside a binary Boltzmann collision is problematic we will keep the original Vicsek angular noise for our study.

This model has the following control parameters, the speed of particles $v_0 = |\vec{v}_i|$, the interaction radius d_0, the time step Δt , the noise amplitude η and the mean density of particles $\rho = {}^{N}/_{L^2}$. The first three are not essential to the model, and can be adimensionalised as will be shown later, we can thus fix them to arbitrary values. Thus we are interested in studying the phase diagram of this model in the $\eta \times \rho$ plane.

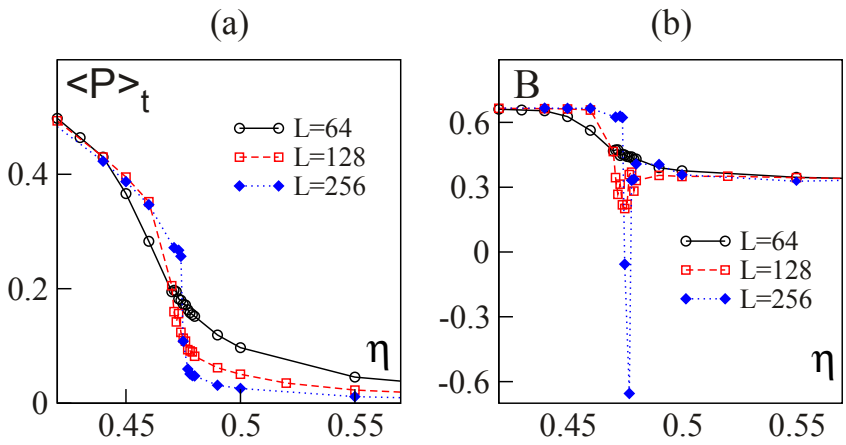

Figure 3: (a) Time averaged mean order parameter $\langle P \rangle_t$ as a function of noise amplitude η for different system sizes. (b) Time averaged Binder cummulant $\langle B \rangle_t$ as a function of noise amplitude η. Images from ref[**?**].

To study this system we can introduce the mean polar order in the system $P = \frac{1}{Nv_0}\left|\sum_{i=1}^{N} \vec{v}_i\right|$ as well as the Binder cummulant $B = 1 - \frac{\langle P^4 \rangle_t}{3\langle P^2 \rangle_t^2}$ that is useful to distinguish a first order transition.

For small system sizes the transition seems to be continuous as shown on Fig(3a), however as the size is increased the discontinuous nature of the transition appears. This can be clearly seen with the dip of the Binder cummulant on Fig(3b) for big system sizes.

It has been shown that for low values of the density, the transition noise η_t is behaving like

$$\eta_t \propto \rho^{1/d}$$

thus in a 2d space it will scale like $\sqrt{\rho}$. As the density will increase and the mean interparticle distance will become smaller that d_0, η_t will deviate from that rule, and switch to a logarithmic convergence toward a fixed value that we expect to be one. The experimental phase diagram is presented on Fig(4a).

As we have already noted the transition to the ordered state is of the first order. Thus it is naturally accompanied by a hysteresis of the polar order parameter around the transition point represented on Fig(4b).

The first order transition is due to the appearance of band structures in between the homogenous isotropic phases and the homogenous collective motion phase. This bands are composed of particles oriented perpendicularly to the band structure, i.e the movement of the band is perpendicular to the band orientation. The quantity, the height and weights of bands vary greatly depending on system size and position in the phase diagram. We can note some trends but further investigation are needed to elucidate these dependencies. First the number of bands increase with the size of the system and as we

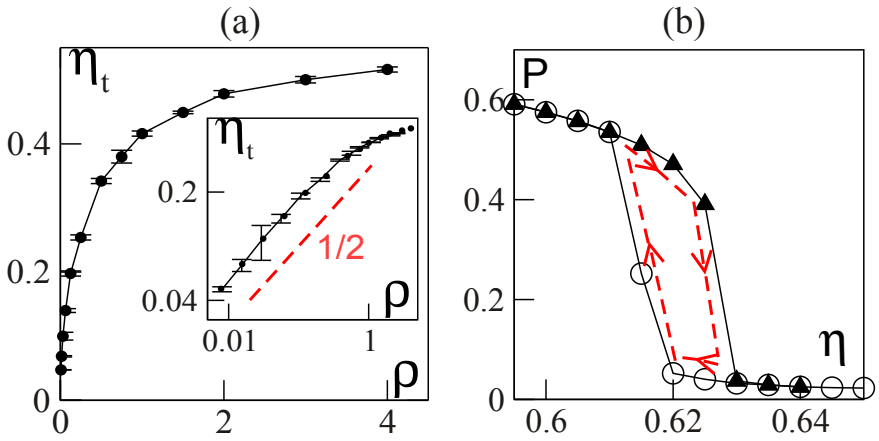

Figure 4: (a) The phase diagram of the microscopic Vicsek model. (b) The hysteresis of the order parameter as a function of angular noise. Images from ref[?].

are moving away from the transition line. After a transition time, which increase with the size of the system, all bands in the system become identical (as new results obtained in our group sugests, the separations between bands is also becoming identical). There is also a tendency to the increase of the width of the band and the decrease of the number of bands, as the angular noise is decreased. But as of today, new investigation performed in a much bigger systems in our group show that this information on the parameters of the bands can be incorrect, and new investigations are needed in order to establish correct results. The study of the bands with the hydrodynamic equations that we obtain can help elucidating the truth.

Although particles in this band are mostly oriented in the direction of the band motion, superdifusion of particles was reported along the band orientation. This is in accordance with the results of the study of Tu and Toner[37], who has found that different sound speeds exist in a homogenous polar order state, according to the orientation of the polar order.

We can note that similar structures, that can be interpreted as the Vicsek bands, have already been observed in experiments on actin microfilaments[32]. Thus this toy model, despite its extreme simplicity, presents a real interpretation of some universal process behind experimental polar systems.

In summary we can cite the following properties of the classical Vicsek model:

1. Three different states are observed while the angular noise strength is decreased; the disordered one, the polar solitonic like structures and a polarly ordered one with true long-range order.

2. The phase transition between the disordered state and the soliton state is of first order.

3. The number and size of the bands as a function of different parameters still need to be investigated.
4. They are two sound speeds, which are also different according to the orientation to the polar order.
5. The ordered state have giant density fluctuations with an exponent of 0.8

With our equations we can try to confirm the first three observations. However in an absence of an effective noise, we can not confirm the other two properties. Additional studies with are needed for that, which will not be part of this thesis.

3.2 DERIVATION OF HYDRODYNAMIC EQUATIONS

3.2.1 *Boltzmann equation*

As our particles are polar we will use a convection term in the Boltzmann equation. The equation is then given by

$$\frac{\partial f}{\partial t}(r,\theta,t) + v_0 \mathrm{e}(\theta) \cdot \nabla f(r,\theta,t) = I_{diff}[f] + I_{col}[f,f]$$

As in the Boltzmann approach the self diffusion events and the collision ones are separated, we must introduce a probability of self diffusion λ. This also implies that the noise amplitude, that is controlled by the variance σ^2 of the wrapped normal distribution, of the diffusion process is not necessarily equivalent to the one in the collision process. However, contrary to the original publication[8], we will suppose that the self-diffusion and the collision angular noises are identical, which is the case of the original Vicsek model. The difference in these terms will only lead to some transformation of the stability diagram, more or less complicated according to the dependance of the two noises, but it will not affect the possible states that we can obtain with this equation. We thus drop out this difference for the simplification of our study. As explained in the previous chapter the diffusion integral is given by

$$I_{diff}[f] = -\lambda f(r,\theta,t) + \lambda \int_{-\pi}^{\pi} d\theta_1 \int_{-\pi}^{\pi} d\xi P(\xi)\, \delta(\theta_1 + \xi - \theta)\, f(r,\theta_1,t)$$

and is composed of a loss term and a gain term.

To obtain the collision integral we need to introduce the expression of the collision kernel $K(\theta_1,\theta_2)$ and of the outcoming angle term $\Psi(\theta_1,\theta_2)$. The collision kernel represents the collision surface in which the particles should lie to collide in an interval Δt. Let's put ourselves in the reference frame of particle one. In this frame the second particle has a speed of $\vec{v}_2 = v_0(\mathrm{e}(\theta_2) - \mathrm{e}(\theta_1))$. Thus $|\vec{v}_2|\,\Delta t$

give us the length of the collision surface. Its width correspond to $2d_0$, the collision kernel is then given by

$$K(\theta_1, \theta_2) = 2d_0 v_0 \left|\mathrm{e}(\theta_2) - \mathrm{e}(\theta_1)\right|$$

Because our particles are polar, the outcoming angle term is just given by the mean orientation between the two colliding particles

$$\Psi(\theta_1, \theta_2) = \arg\left(e^{i(\theta_1+\theta_2)}\right)$$

We then obtain the expression of the collision integral

$$\begin{aligned} I_{coll}[f, f] = &-2d_0 v_0 f(r, \theta, t) \int_{-\pi}^{\pi} d\theta_2 \left|\mathrm{e}(\theta_2) - \mathrm{e}(\theta_1)\right| f(r, \theta_2, t) \\ &+ 2d_0 v_0 \int_{-\pi}^{\pi} d\theta_1 \int_{-\pi}^{\pi} d\theta_2 \int_{-\pi}^{\pi} d\xi P(\xi) \left|\mathrm{e}(\theta_2) - \mathrm{e}(\theta_1)\right| \\ &\times f(r, \theta_1, t) f(r, \theta_2, t) \delta\left(\bar{\theta} + \xi - \theta\right) \end{aligned}$$

Apart from angular distribution variance and mean density, this equation has three parameters; v_0, d_0 and λ. In the original paper of Bertin et al. the equations where studied using all these control parameters. However as we will show, most of them can be adimensionalised leaving only two essential parameters, the global density of particles and the angular noise level. We introduce a typical time scale λ^{-1}, $T = t\lambda$, and a typical length scale $\frac{v_0}{\lambda}$, $R = r\frac{\lambda}{v_0}$. We can also introduce the collision surface $S = \frac{2d_0 v_0}{\lambda}$ which will be our new control parameter. But this one can also be adimensionalised by setting $\tilde{f} = Sf$ and multiplying the Boltzmann equation by S. This give us the new equation

$$\frac{\partial \tilde{f}}{\partial T}(R, \theta, T) + \partial_{\parallel} \tilde{f}(R, \theta, T) = \tilde{I}_{diff}\left[\tilde{f}\right] + \tilde{I}_{col}\left[\tilde{f}, \tilde{f}\right]$$

where

$$\tilde{I}_{diff} = -\tilde{f}(R, \theta, T) + \int_{-\pi}^{\pi} d\theta_1 \int_{-\pi}^{\pi} d\xi p(\xi) \delta(\theta_1 + \xi - \theta) \tilde{f}(R, \theta_1, T)$$

$$\begin{aligned} \tilde{I}_{coll} = &-\tilde{f}(R, \theta, T) \int_{-\pi}^{\pi} d\theta_2 \left|\mathrm{e}(\theta_2) - \mathrm{e}(\theta)\right| \tilde{f}(R, \theta, T) \\ &+ \int_{-\pi}^{\pi} d\theta_1 \int_{-\pi}^{\pi} d\theta_2 \int_{-\pi}^{\pi} d\xi P(\xi) \left|\mathrm{e}(\theta_2) - \mathrm{e}(\theta_1)\right| \\ &\times \tilde{f}(R, \theta_1, T) \tilde{f}(R, \theta_2, T) \delta\left(\bar{\theta} + \xi - \theta\right) \end{aligned}$$

In the next sections we drop out the R, T and the $\tilde{}$ notation for simplicity.

3.2.2 *Hydrodynamic equations*

To obtain hydrodynamic equations we make a Fourier transform on the angle of the Boltzmann equation. For this end we introduce

$$\hat{f}_k(r,t) = \int_{-\pi}^{\pi} d\theta f(r,\theta,t)\, e^{ik\theta} \tag{2}$$

and its inverse transform

$$f(r,\theta,t) = \frac{1}{2\pi}\sum_{k=-\infty}^{\infty} e^{ik\theta}\hat{f}_k(r,t) \tag{3}$$

We show next how to compute the Fourier transform of each term of the Boltzmann equation; for that we need to multiply it by $e^{ik\theta}$ and integrate on $[-\pi : \pi]$.

3.2.2.1 *Convection term*

We can start by mapping $\mathrm{e}(`)$ on a plane by introducing the orthogonal plane $\mathrm{e}_x = \mathrm{e}(0)$ and $\mathrm{e}_y = \mathrm{e}(\pi/2)$. Thus $\mathrm{e}_x(\theta) = \cos(\theta)$ and $\mathrm{e}_y(\theta) = \sin(\theta)$. The convection term is then transformed into

$$\begin{aligned}
\left(\frac{\partial f}{\partial t}\right)_{conv} &= v_0 \mathrm{e}(\theta)\cdot\nabla f(r,\theta,t) \\
&= v_0\left[\mathrm{e}_x(\theta)\,\partial_x f(r,\theta,t) + \mathrm{e}_y(\theta)\,\partial_y f(r,\theta,t)\right] \\
&= v_0\left[\partial_x(\cos(\theta) f(r,\theta,t)) + \partial_y(\sin(\theta) f(r,\theta,t))\right] \\
&= v_0\left[\partial_x(C_x) + \partial_y(Cy)\right]
\end{aligned}$$

We compute the Fourier transform of each term separately

$$\begin{aligned}
F[C_x] &= \int_{-\pi}^{\pi} d\theta e^{ik\theta}\cos(\theta) f(r,\theta,t) \\
F[C_y] &= \int_{-\pi}^{\pi} d\theta e^{ik\theta}\sin(\theta) f(r,\theta,t)
\end{aligned}$$

substituting equation(3) inside we obtain

$$\begin{aligned}
F[C_x] &= \frac{1}{2\pi}\sum_{q=-\infty}^{\infty}\hat{f}_q(r,t)\int_{-\pi}^{\pi} d\theta e^{i(k-q)\theta}\cos(\theta) \\
&= \frac{1}{2}\left[\hat{f}_{k-1}(r,t) + \hat{f}_{k+1}(r,t)\right]
\end{aligned}$$

and

$$\begin{aligned}
F[C_y] &= \frac{1}{2\pi}\sum_{q=-\infty}^{\infty}\hat{f}_q(r,t)\int_{-\pi}^{\pi} d\theta e^{i(k-q)\theta}\sin(\theta) \\
&= \frac{i}{2}\left[\hat{f}_{k-1}(r,t) - \hat{f}_{k+1}(r,t)\right]
\end{aligned}$$

3.2.2.2 *Angular diffusion integral*

The Fourier transform of the loss term of the diffusion integral is evident, we need only to explicit the computation of the gain term

$$\begin{aligned} F\left[I_{diff,gain}\right] &= \int_{-\pi}^{\pi} d\theta e^{ik\theta}\left(\int_{-\pi}^{\pi} d\theta_1 \int_{-\pi}^{\pi} d\xi P\left(\xi\right)\delta\left(\theta_1+\xi-\theta\right) f\left(r,\theta_1,t\right)\right) \\ &= \int_{-\pi}^{\pi} d\theta_1 \int_{-\pi}^{\pi} d\xi P\left(\xi\right) e^{ik(\theta_1+\xi)} f\left(r,\theta_1,t\right) \\ &= \int_{-\pi}^{\pi} d\theta_1 e^{ik\theta_1} f\left(r,\theta_1,t\right) \int_{-\pi}^{\pi} d\xi P\left(\xi\right) e^{ik\xi} \\ &= \hat{f}_k\left(r,t\right)\hat{P}_k \end{aligned}$$

where

$$\hat{P}_k = F\left[P\left(\xi\right)\right] = e^{-\frac{k^2\sigma^2}{2}}$$

Thus the Fourier transform of the whole diffusion term is given by

$$F\left[I_{diff}\right] = -\hat{f}_k\left(r,t\right)\left(1-\hat{P}_k\right)$$

3.2.2.3 *Collision integral*

Once again we compute the loss and gain terms separately

$$F\left[I_{coll,loss}\right] = \int_{-\pi}^{\pi} d\theta e^{ik\theta}\left(-Sf\left(r,\theta,t\right)\int_{-\pi}^{\pi} d\theta' \left|\mathrm{e}\left(\theta'\right)-\mathrm{e}\left(\theta\right)\right| f\left(r,\theta',t\right)\right)$$

We first need to substitute $\left|e\left(\theta'\right)-e\left(\theta\right)\right|$ or

$$\begin{aligned} \left|e\left(\theta'\right)-e\left(\theta\right)\right|^2 &= \mathrm{e}\left(\theta'\right)^2 - 2\mathrm{e}\left(\theta'\right)\cdot\mathrm{e}\left(\theta\right)+\mathrm{e}\left(\theta\right)^2 \\ &= 2\left(1-\cos\left(\theta'-\theta\right)\right) \\ &= 4\sin^2\left(\frac{\theta'-\theta}{2}\right) \end{aligned}$$

thus

$$\left|e\left(\theta'\right)-e\left(\theta\right)\right| = 2\left|\sin\left(\frac{\theta'-\theta}{2}\right)\right|$$

Substituting it back to the Fourier transform we obtain

$$F\left[I_{coll,loss}\right] = -2\int_{-\pi}^{\pi} d\theta e^{ik\theta} f\left(r,\theta,t\right)\int_{-\pi}^{\pi} d\theta' \left|\sin\left(\frac{\theta'-\theta}{2}\right)\right| f\left(r,\theta',t\right)$$

We can now put inside equation(3)

$$F\left[I_{coll,loss}\right] = -\frac{1}{\pi}\sum_{q=-\infty}^{\infty}\hat{f}_q\left(r,t\right)\int_{-\pi}^{\pi} d\theta e^{ik\theta} f\left(r,\theta,t\right)\int_{-\pi}^{\pi} d\theta' \left|\sin\left(\frac{\theta'-\theta}{2}\right)\right| e^{-iq\theta'}$$

We introduce a variable substitution $\phi = \theta' - \theta$

$$\begin{aligned}
F\left[I_{coll,loss}\right] &= -\frac{1}{\pi}\sum_{q=-\infty}^{\infty}\hat{f}_q\left(r,t\right)\int_{-\pi}^{\pi}d\theta e^{ik\theta}f\left(r,\theta,t\right)\int_{-\pi}^{\pi}d\phi\left|\sin\left(\frac{\phi}{2}\right)\right|e^{-iq\phi}e^{-iq\theta} \\
&= -\frac{1}{\pi}\sum_{q=-\infty}^{\infty}\hat{f}_q\left(r,t\right)\int_{-\pi}^{\pi}d\theta e^{i(k-q)\theta}f\left(r,\theta,t\right)\int_{-\pi}^{\pi}d\phi\left|\sin\left(\frac{\phi}{2}\right)\right|e^{-iq\phi} \\
&= -\frac{1}{\pi}\sum_{q=-\infty}^{\infty}\hat{f}_{k-q}\left(r,t\right)\hat{f}_q\left(r,t\right)\int_{-\pi}^{\pi}d\theta'\left|\sin\left(\frac{\theta'-\theta}{2}\right)\right|e^{-iq\theta'} \\
&= -\frac{1}{\pi}\sum_{q=-\infty}^{\infty}\hat{f}_k\left(r,t\right)\hat{f}_q\left(r,t\right)I_q
\end{aligned}$$

where

$$I_q = \int_{-\pi}^{\pi}d\theta\left|\sin\left(\frac{\theta}{2}\right)\right|\cos\left(q\theta\right)$$

We can now compute the gain term

$$\begin{aligned}
F\left[I_{coll,gain}\right] &= \int_{-\pi}^{\pi}d\theta e^{ik\theta}\int_{-\pi}^{\pi}d\theta_1\int_{-\pi}^{\pi}d\theta_2\int_{-\pi}^{\pi}d\xi P\left(\xi\right)\left|\mathrm{e}\left(\theta_2\right)-\mathrm{e}\left(\theta_1\right)\right| \\
&\quad \times f\left(r,\theta_1,t\right)f\left(r,\theta_2,t\right)\delta\left(\bar{\theta}+\xi-\theta\right) \\
&= \int_{-\pi}^{\pi}d\theta_1\int_{-\pi}^{\pi}d\theta_2\int_{-\pi}^{\pi}d\xi P\left(\xi\right)\left|\mathrm{e}\left(\theta_2\right)-\mathrm{e}\left(\theta_1\right)\right| \\
&\quad \times e^{ik\bar{\theta}}e^{ik\xi}f\left(r,\theta_1,t\right)f\left(r,\theta_2,t\right)
\end{aligned}$$

making the same substitutions as previously we obtain

$$\begin{aligned}
F\left[I_{coll,gain}\right] = \frac{1}{2\pi^2}\sum_{q=-\infty}^{\infty}\sum_{l=-\infty}^{\infty}\hat{f}_q\hat{f}_l\hat{P}_k \\
\int_{-\pi}^{\pi}d\theta_1 e^{-iq\theta_1}\int_{-\pi}^{\pi}d\theta_2 e^{-il\theta_2}\left|\sin\left(\frac{\theta_1-\theta_2}{2}\right)\right|e^{ik\bar{\theta}}
\end{aligned}$$

we will now make a shift by θ_1 in the integration limits of θ_2 and a variable substitution. If $\theta_1 - \pi < \theta_2 < \theta_1 + \pi$ then $\bar{\theta} = \theta_1 + \frac{\theta_2-\theta_1}{2}$, we also introduce $\phi = \theta_2 - \theta_1$ to obtain

$$\begin{aligned}
F\left[I_{coll,gain}\right] &= \frac{1}{2\pi^2}\sum_{q=-\infty}^{\infty}\sum_{l=-\infty}^{\infty}\hat{f}_q\hat{f}_l\hat{P}_k \\
&\quad \int_{-\pi}^{\pi}d\theta_1 e^{-iq\theta_1}\int_{-\pi}^{\pi}d\phi e^{-il(\phi-\theta_1)}\left|\sin\left(\frac{\phi}{2}\right)\right|e^{ik\left(\theta_1+\frac{\phi}{2}\right)} \\
&= \frac{1}{2\pi^2}\sum_{q=-\infty}^{\infty}\sum_{l=-\infty}^{\infty}\hat{f}_q\hat{f}_l\hat{P}_k \\
&\quad \int_{-\pi}^{\pi}d\theta_1 e^{i(l-q+k)\theta_1}\int_{-\pi}^{\pi}d\phi e^{-i\left(l-\frac{k}{2}\right)\phi}\left|\sin\left(\frac{\phi}{2}\right)\right| \\
&= \frac{1}{\pi}\sum_{q=-\infty}^{\infty}\hat{f}_q\hat{f}_{k-q}\hat{P}_k\int_{-\pi}^{\pi}d\phi e^{-i\left(\frac{k}{2}-q\right)\phi}\left|\sin\left(\frac{\phi}{2}\right)\right| \\
&= \frac{1}{\pi}\sum_{q=-\infty}^{\infty}\hat{f}_q\hat{f}_{k-q}\hat{P}_k I_{q-\frac{k}{2}}
\end{aligned}$$

Thus the Fourier transform of the whole integral is

$$F\left[I_{coll}\right] = -\frac{1}{\pi}\sum_{q=-\infty}^{\infty}\hat{f}_k\left(r,t\right)\hat{f}_q\left(r,t\right)\left(I_q - I_{q-\frac{k}{2}}\right)$$

3.2.3 *Expansion and closure*

Combining together all the terms that we have computed we obtain the Fourier expansion of the Boltzmann equation

$$\partial_t\hat{f}_k + \nabla\hat{C} = -\hat{f}_k\left(r,t\right)\left(1-\hat{P}_k\right) - \frac{1}{\pi}\sum_{q=-\infty}^{\infty}\hat{f}_k\left(r,t\right)\hat{f}_q\left(r,t\right)\left(I_q - I_{q-\frac{k}{2}}\right)$$

To simplify notation we will drop the hat and the explicit dependence on r and t in what follows and we also introduce the following complex operators

$$\begin{aligned}\nabla &= \partial_x + i\partial_y\\ \nabla^* &= \partial_x - i\partial_y\\ \Delta &= \nabla\nabla^*\end{aligned}$$

Taking $k=0$ we immediately obtain the continuity equation

$$\partial_t\rho = -\Re\left(\nabla^* f_1\right) \tag{4}$$

For all the other equations in the series, we must introduce a closure ansatz as explained in the previous chapter. We start by introducing the scaling of the order parameter $f_1 \sim \epsilon$. The Ginzburg-Landau equation for this order parameter then imply that $\nabla \sim \epsilon$ and that the distance to the transition point scale as ϵ^2. We also suppose the spatial variations of f to be small and hence $\rho = \rho_0 + \Delta\rho$, where $\Delta\rho \sim \epsilon$ and ρ_0 is the global density. We then obtain from equation(4) that $\partial_t \sim \epsilon$. We will truncate all the equations that follow at order three in ϵ. Taking $k=1$ we obtain

$$\begin{aligned}\partial_t f_1 + \frac{1}{2}\nabla\rho + \frac{1}{2}\nabla^* f_2 = &\\ -\left[\left(1-P_1\right) + \frac{4}{\pi}\left(\frac{2}{3}-P_1\right)\rho\right]f_1 &\\ + \frac{4}{\pi}\left(\frac{2}{5}-P_1\right)f_1^* f_2 &\end{aligned} \tag{5}$$

and for k=2

$$\begin{aligned}\partial_t f_2 + \frac{1}{2}\nabla f_1 = &\\ -\left[\left(1-P_2\right) + \frac{8}{3\pi}\left(\frac{7}{5}+P_2\right)\rho\right]f_2 &\\ + \frac{4}{\pi}\left(\frac{1}{3}+P_2\right)f_1^2 &\end{aligned} \tag{6}$$

In equation(6) the time derivative of f_2 is of third order as well as the term $\Delta\rho f_2$, but all the other terms are of second order. We can thus eliminate $\partial_t f_2$ from equation(6). We will however keep the $\Delta\rho f_2$ term, explaining the reason for this later. After the elimination of $\partial_t f_2$ from equation(6) we can easily obtain the value of f_2 from it, which we substitute into equation(5) to obtain

$$\begin{aligned}\partial_t f_1 + \frac{1}{2}\nabla\rho &= \left(\mu - \xi\left|f_1\right|^2\right) f_1 + \frac{\nu}{4}\Delta f_1 \\ &\quad + \iota f_1^* \nabla f_1 - \chi f_1 \nabla^* f_1 \end{aligned} \tag{7}$$

where the coefficients are given by

$$\begin{aligned}\nu &= \left[(1-P_2) + \frac{8}{3\pi}\left(\frac{7}{5}+P_2\right)\rho\right]^{-1} \\ \mu &= -\left[(1-P_1) + \frac{4}{\pi}\left(\frac{2}{3}-P_1\right)\rho\right] \\ \xi &= \nu\frac{16}{\pi^2}\left(P_1 - \frac{2}{5}\right)\left(\frac{1}{3}+P_2\right) \\ \iota &= \nu\frac{2}{\pi}\left(P_1 - \frac{2}{5}\right) \\ \chi &= \nu\frac{4}{\pi}\left(\frac{1}{3}+P_2\right)\end{aligned}$$

First thing that we should note is the ν term which still contains the $\Delta\rho$ dependance, that we did not eliminate from equation(6). We can also remark that the term on the l.h.s. are of a lower second order compared to the other terms. As we have already said this does not mean that the equation is unbalanced. If we place ourselves in a moving convective frame, this term become of third order like the others.

We can also write these equations in a vectorial notation where we introduce $\vec{w} = \rho\vec{P}$

$$\partial_t\rho = -\nabla\vec{w}$$

$$\begin{aligned}\partial_t\vec{w} + \gamma\left(\vec{w}\cdot\nabla\right)\vec{w} = -\frac{1}{2}\nabla\rho + \frac{\kappa}{2}\nabla\vec{w}^2 + \left(\mu - \xi\left|\vec{w}\right|^2\right)\vec{w} \\ + \frac{\nu}{4}\nabla^2\vec{w} - \kappa\left(\nabla\cdot\vec{w}\right)\vec{w}\end{aligned}$$

where we have introduced two new coefficients

$$\begin{aligned}\kappa &= \chi + \iota \\ &= \nu\frac{2}{\pi}\left(2P_2 + P_1 + \frac{4}{15}\right) \\ \gamma &= \chi - \iota \\ &= \nu\frac{2}{\pi}\left(2P_2 - P_1 + \frac{16}{15}\right)\end{aligned}$$

In this notation we can easily see that we can not get rid of the advection term by placing ourselves in the Lagrangian frame, as our equation does not conserve momentum, and the coefficient in front of the advection term is a variable parameter γ and not equal to one.

While this vectorial notation was used in the original paper[9] by Bertin et al. we will stick to the complex notation which is easier to manipulate. We can also remark that the equation in ref[9] contains more terms that the one contained here. However it easy to check that these terms are of fourth order in our Ginzburg-Landau approach, i.e the truncation in the original paper was done with a less strict approach than the one we employ here.

3.3 HOMOGENEOUS SOLUTIONS AND THEIR STABILITY ANALYSIS

3.3.1 *Homogenous solution*

Discarding all temporal and spatial derivatives in equation(7) we obtain

$$\left(\mu - \xi \left|f_1\right|^2\right) f_1 = 0$$

Thus f_1 admit two homogeneous solutions. The disordered solution $f_1 = 0$ and the ordered solution $f_1 = \pm\sqrt{\frac{\mu}{\xi}}$. While the first solution always exists, the second one appears only when $\mu > 0$ and the zero solution becomes unstable to homogeneous perturbations. It is easy to check that if we do not neglect the ρ dependance of the ξ term $f_1 \propto \rho$, i.e the polar order parameter amplitude $\left|\vec{P}\right| = |f_1|/\rho$ is limited and approaches a steady value as ρ goes to infinity. However if we neglect the ρ dependance of the ν term and hence that of the ξ term, we obtain $f_1 \propto \sqrt{\rho}$, thus f_1 goes to zero as ρ goes to infinity. As can be seen on figure 5 on the next page, this difference is negligible when $\Delta\rho$ is small, but such an approximation will not necessarily be valid in the case of a band solution. In the case that we keep all the ρ dependenies when we approach the top of the band, the corresponding speed of the top should increase, effectively creating a shock wave. But if we omit the ρ dependance of the ξ term, for high enough bands, the speed at the top will decrease, thus potentially changing the dynamics of the band solution. This is a reason to keep the dependence of the ξ term on ρ, unless if numeric investigation shows no difference between the two cases.

From the equation $\mu = 0$ we can obtain the expression of the transition density

$$\rho_t = \frac{3}{4}\frac{\pi\left(1 - P_1\right)}{3P_1 - 2} \tag{8}$$

The important thing that we should note about this density is that it corresponds to the continuous second order transition of the equa-

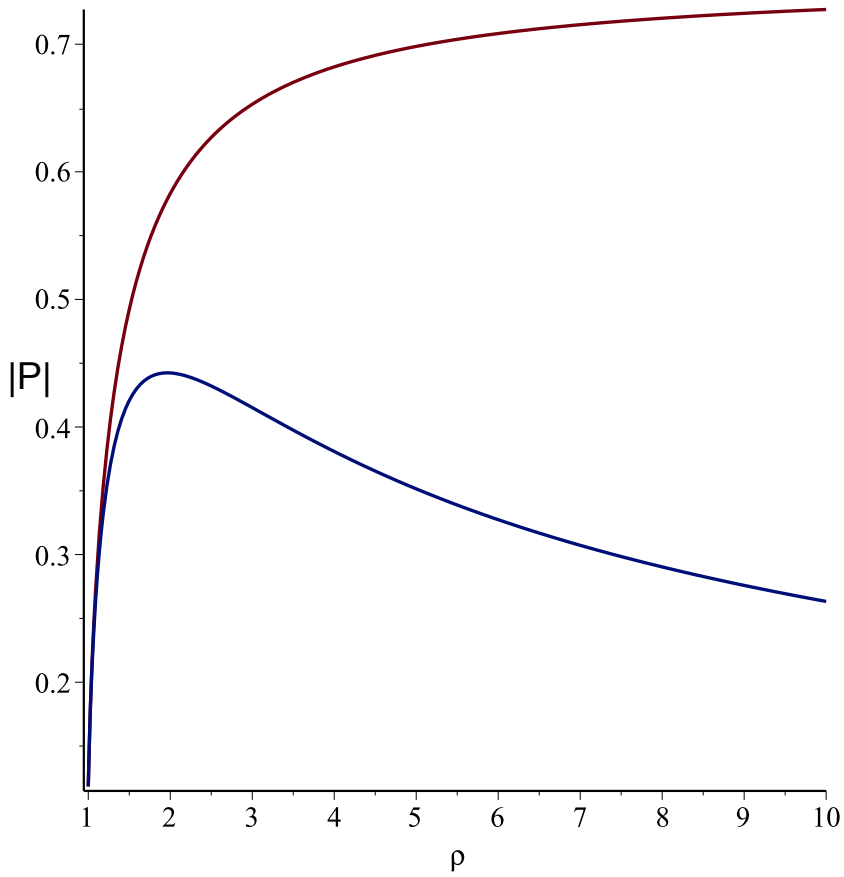

Figure 5: Amplitude of $\left|\vec{P}\right| = |f_1|/\rho$ as a function of density, for $\sigma = \sigma_t\,(\rho = 1)$. The red line correspond to the case of a density dependance of the ξ term, the blue line in the absence of such dependance.

tion(7), thus it can not be compared to the one showed on fig(4a) which correspond to the first order transition. However as we will show later, the homogeneous solution is unstable near ρ_t and our equation has a non-linear solution which introduces a subcritical bifurcation into the deterministic PDE.

We can also invert equation(8) in order to obtain the value of the transition noise given by the variance

$$\sigma_t^2 = 2\ln\left(3\frac{\pi + 4\rho}{3\pi + 8\rho}\right)$$

Taking the limit $\rho \to 0$, we obtain $\sigma_t \propto \sqrt{\rho}$, this proportionality is equivalent to the microscopic case. We can also note that the variance saturates at high density at a value $\sigma_t^\infty = \sqrt{2\ln(3/2)}$.

It is important to note that the transition values ρ_t and σ_t will not vary if we push the truncation of the Fourier series to higher orders, because they are fixed by the value of μ which will not vary. This is not the case of the value of the ordered solution $f_1 = \pm\sqrt{\frac{\mu}{\xi}}$ which will vary with the order of truncation. At zero noise we expect f_1/ρ to be equal to one as in the microscopic case, however it is easy to check that it is now equal to

$$f_1^0 = \sqrt{\frac{2}{3}}$$

Which is expected, because as we have detailed in the previous chapter the third order truncation is inappropriate far from the transition point. We can expect that this value will grow if we push the truncation further, which we will show later.

3.3.2 *Stability to inhomogeneous perturbations*

3.3.2.1 *Stability matrix*

In order to search for inhomogeneous perturbations of the homogeneous solution we will suppose that it is oriented along the $\vec{x}$ axis, i.e that f_1 is real. We introduce the following perturbations to the homogeneous solution

$$\begin{aligned} \rho(x,y,t) &= \rho_0 + \delta\rho(x,y,t) \\ f_1(x,y,t) &= f_{1,0} + \left(\delta f_1^R(x,y,t) + i\delta f_1^I(x,y,t)\right) \end{aligned}$$

we introduce this ansatz in equations(47) and limit them to the first order in perturbations and separate into real and imaginary parts to obtain

$$\begin{aligned}
\partial_t \delta\rho &= -\partial_x \delta f_1^R - \partial_y \delta f_1^I \\
\partial_t \delta f_1^R &= \left(\mu_0 - 3\xi f_{1,0}^2\right) \delta f_1^R + \left(\mu' - \xi' f_{1,0}^2\right) f_{1,0} \delta\rho - \frac{1}{2}\partial_x \delta\rho + \frac{\nu_0}{4}\Delta\delta f_1^R \\
&\quad -\gamma_0 \partial_x \delta f_1^R - \kappa_0 \partial_y \delta f_1^I \\
\partial_t \delta f_1^I &= -\frac{1}{2}\partial_y \delta\rho + \frac{\nu_0}{4}\Delta\delta f_1^I - \gamma_0 \partial_x \delta f_1^I + \kappa_0 \partial_y \delta f_1^R
\end{aligned} \tag{9}$$

where the zero pondered coefficients correspond to the one with $\rho = \rho_0$, $\mu' = \partial\mu/\partial\rho$ and $\xi' = \partial\xi/\partial\rho$. Of course the term ξ' is present only if we keep the ρ dependance of the ν term. We then introduce the new ansatz

$$\begin{aligned}
\delta\rho\,(x,y,t) &= \delta\rho_0\,(t)\, e^{\lambda t + i\left(k_x x + k_y y\right)} \\
\delta f_1^R\,(x,y,t) &= \delta f_{1,0}^R\,(t)\, e^{\lambda t + i\left(k_x x + k_y y\right)} \\
\delta f_1^I\,(x,y,t) &= \delta f_{1,0}^I\,(t)\, e^{\lambda t + i\left(k_x x + k_y y\right)}
\end{aligned}$$

In order to establish the linear stability we should look for the dispersion relation of $\lambda\,(q)$ for a given q. Our homogeneous solution will be unstable for $\lambda > 0$. We substitute this ansatz into equations(9) to obtain the matrix equation $\lambda\vec{\delta f} = M\vec{\delta f}$ where the vector $\vec{\delta f}$ is given by

$$\begin{pmatrix} \delta\rho_0\,(t) \\ \delta f_{1,0}^R\,(t) \\ \delta f_{1,0}^I\,(t) \end{pmatrix}$$

and the matrix M is given by

$$\begin{pmatrix} 0 & -ik_x & -ik_y \\ -\frac{ik_x}{2} + \left(\mu' - \xi' f_{1,0}^2\right) f_{1,0} & \left(\mu_0 - 3\xi f_{1,0}^2\right) - \frac{\nu_0}{4}\left(k_x^2 + k_y^2\right) - i\gamma_0 k_x f_{1,0} & -ik_y \kappa_0 f_{1,0} \\ -\frac{ik_y}{2} & ik_y \kappa_0 f_{1,0} & -\frac{\nu_0}{4}\left(k_x^2 + k_y^2\right) - i\gamma_0 k_x f_{1,0} \end{pmatrix} \tag{10}$$

We can now study the eigenvalues of the matrix M which are equal to λ.

3.3.2.2 *Stability of the isotropic solution*

We can first check that the isotropic solution $f_{1,0} = 0$ is stable to inhomogeneous perturbations. As the solution is isotropic, there is no any

reason to have a preferred direction for the perturbations, we then arbitrary choose $k_x = 0$, the matrix(10) is in this case transformed into

$$\begin{pmatrix} 0 & 0 & -ik_y \\ 0 & \mu_0 - \frac{\nu_0}{4}k_y^2 & 0 \\ -\frac{ik_y}{2} & 0 & -\frac{\nu_0}{4}k_y^2 \end{pmatrix}$$

The value of λ is then given by

$$\begin{aligned} \lambda\left[\left(\mu_0 - \frac{\nu_0}{4}k_y^2 - \lambda\right)\left(\frac{\nu_0}{4}k_y^2 + \lambda\right)\right] + \frac{k_y^2}{2}\left(\mu_0 - \frac{\nu_0}{4}k_y^2 - \lambda\right) &= 0 \quad (11) \\ \left[\lambda\left(\frac{\nu_0}{4}k_y^2 + \lambda\right) + \frac{k_y^2}{2}\right]\left(\mu_0 - \frac{\nu_0}{4}k_y^2 - \lambda\right) &= 0 \\ \left(\lambda^2 + \lambda\frac{\nu_0}{4}k_y^2 + \frac{k_y^2}{2}\right)\left(\mu_0 - \frac{\nu_0}{4}k_y^2 - \lambda\right) &= 0 \quad (12) \end{aligned}$$

The second parenthesis in equation(11) gives the solution

$$\lambda_1 = \mu_0 - \frac{\nu_0}{4}k_y^2$$

For the isotropic solution μ_0 is negative and ν_0 is always positive thus $\lambda_1 < 0$. The first parenthesis in equation(11) gives the two following eigenvalues

$$\lambda_{2,3} = -\frac{\nu_0}{4}k_y^2 \pm \sqrt{\frac{\nu_0{}^2}{16}k_y^4 - 2k_y^2}$$

which are again negative, i.e the isotropic solution is stable to inhomogeneous perturbations.

3.3.2.3 *Stability of the homogeneous ordered solution*

For the general case of homogeneous collective motion solution, the matrix eigenvalues are too complicated for an analytical computation. We then search for numerical eigenvalues of the matrix(10). As we remember we have kept the ρ dependence of the ν term, while this is in theory a fourth order truncation. We will give the stability analysis in both cases; one when we keep the dependance and in the other when we neglect it.

We can start by looking at figure 6 on page 49 in which the pure third order truncation is presented, i.e $\xi' = 0$. This diagram can be divided in four different regions divided by three lines. Starting at the top of the figure(6) we are in the disordered region. The first line of transition is given by σ_t which corresponds to the appearance of the collective motion solution. However as we see from the diagram this solution is unstable to parallel, or mostly parallely oriented, perturbations. We expect these parallel perturbations, because they can be seen as precursors of the band solutions that we have seen in the

microscopic case. The limit of this region is given by the stabilization value σ_s. After this value the homogeneous solution become stable. One could naively expect that the lines σ_t and σ_s of the linear stability analysis correspond to the limit where the bands solutions exists. However we will show that this is not the case, and that the nonlinear band solutions are limited by the lines σ_{max} and σ_{min} that we will explain later.

Further away from the σ_t line we see the appearance of another unstable region limited by the line σ_u, with the most unstable direction oriented mostly transversely to the polar order. As we remember there is no any other instabilities in the microscopic model. This instability was not reported in the ref[9] because the authors searched only for parallel instabilities corresponding to the microscopic model. However as we have said in the previous chapter, as the noise is decreasing, the truncation approximation $|f_k| \sim \epsilon^k$ is no more valid. Thus, this spurious instability is most probably the result of our truncation of the Fourier series of the Boltzmann equation.

Finally we can remark that the line of longitudinal instability $\sigma_{\|}$, was the only one that was investigated in ref[9], and is certainly insufficient to understand the full phase space diagram.

Looking on the case of a pseudo fourth order truncation on figure 7 on page 50 we see that all the regions have been preserved. Moreover, while our equation is now not completely balanced, the band region and the stable region between σ_s and σ_u have both become bigger. However this is not necessarily a reason to keep the ξ dependance on $\Delta\rho$, unless, as we have already said, it will be proven in numerical simulations that this is important for the dynamics of the band.

Finally we can look at the maximum growth rate in both cases on fig(8). We can see that the amplitude of the spurious instabilities is two orders of magnitude higher than that of the band instability. As a matter of fact our equations will explode in this region.

3.3.3 *Going beyond the third order truncation*

As we have noted in the previous subsection our equations present a region of spurious instability in the low noise part of the phase diagram. Having said in the previous chapter that far from the transition point the high order Fourier coefficients should become important, we can naively try to increase the order of truncation to try to push down the σ_u line.

Thus we will try in the following to obtain higher order equations and study their linear stability.

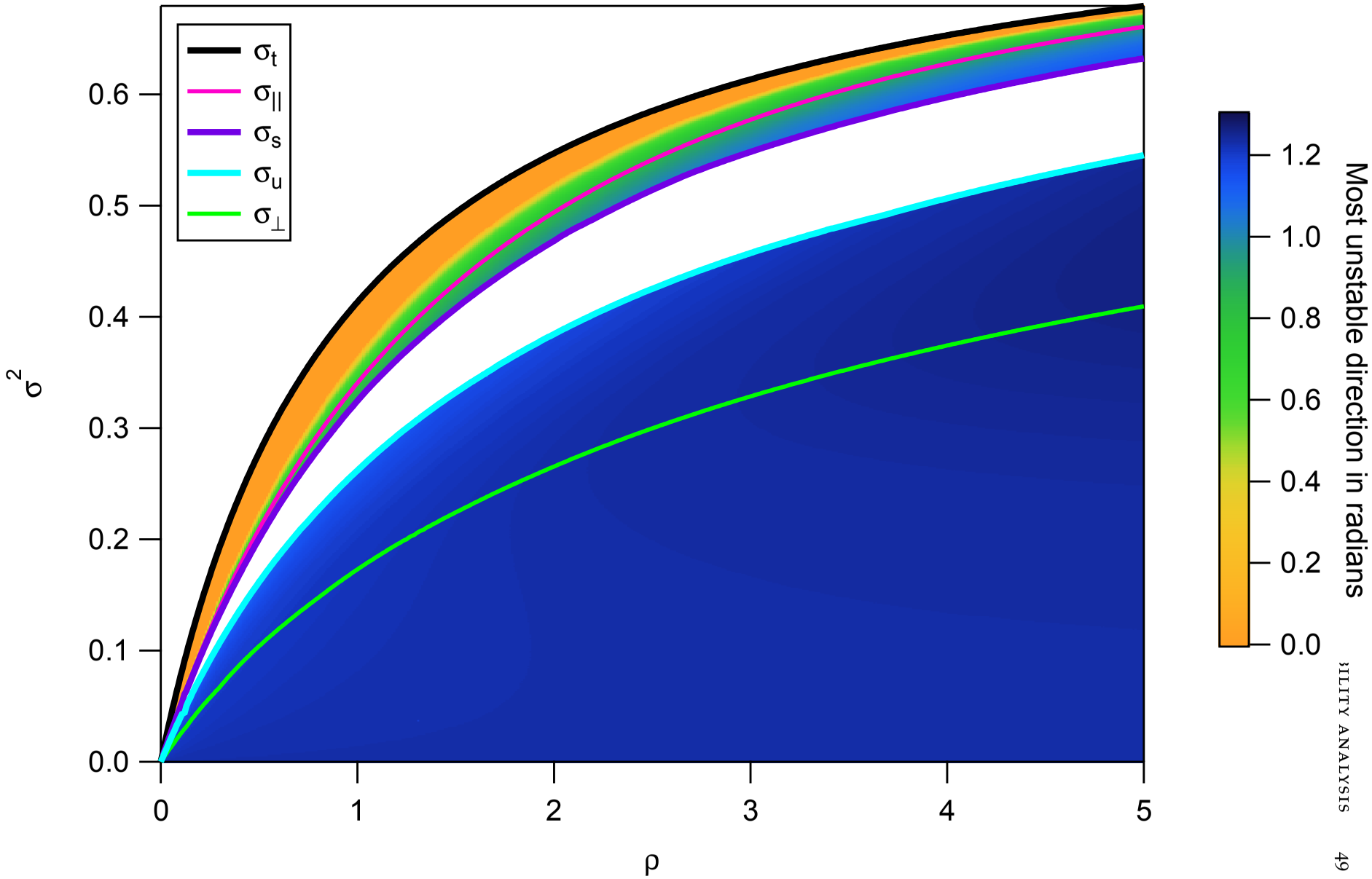

Figure 6: Stability diagram in the case of a pure third order truncation. The color code indicates the direction, in radians, in which the eigenvalue is the most unstable, as compared to the direction of the homogeneous solution. The line σ_t corresponds to the transition to collective motion solution. This solution is unstable up to the restabilisation line σ_s. Completely longitudinal instabilities exist only above line $\sigma_{\|}$. Another, probably spurious, instability appears after the line σ_u. Completely transversal instabilities exist below the line $\sigma_{\perp}$.

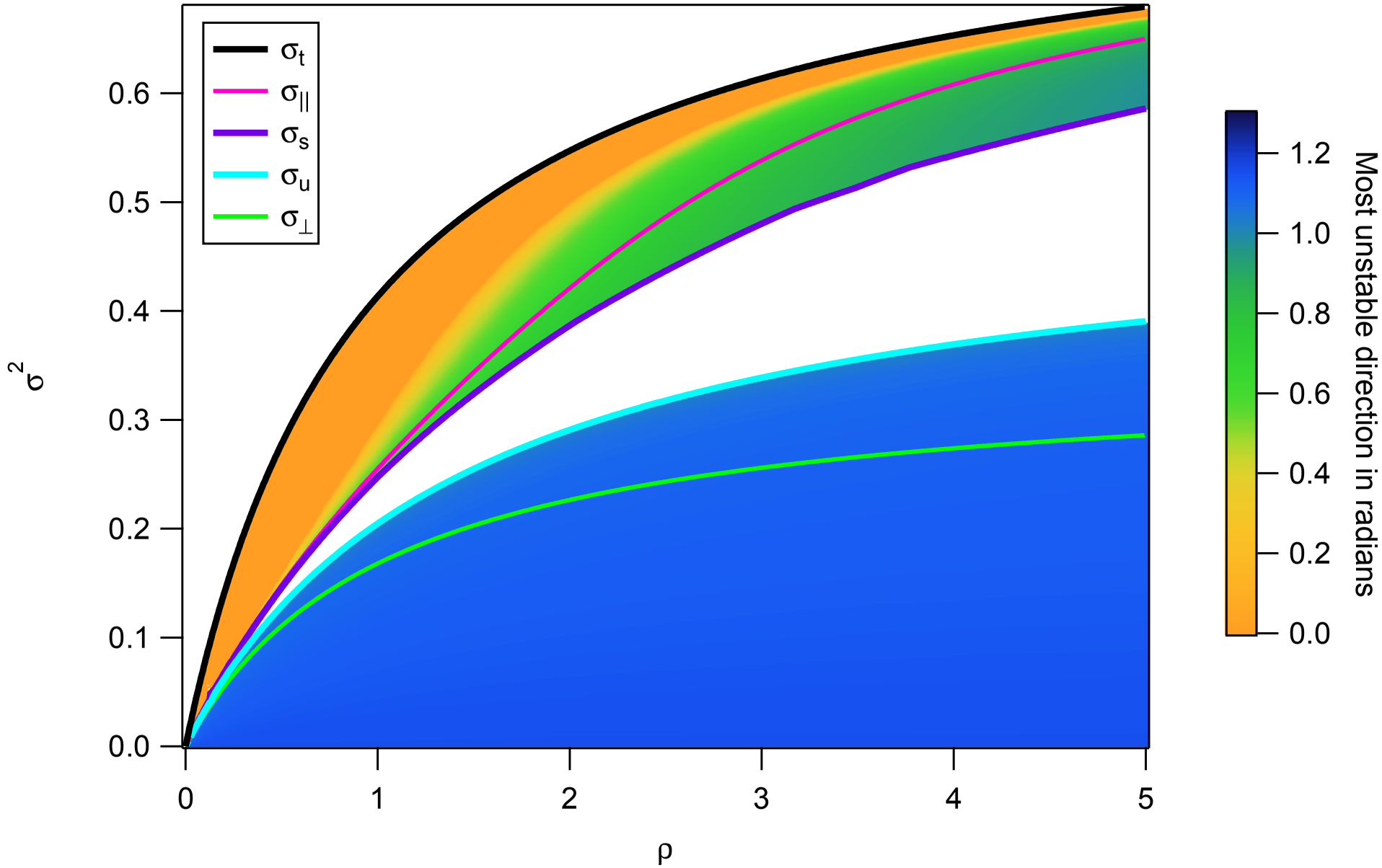

Figure 7: Stability diagram in the case of density dependance of the ξ term. The color code indicates the direction, in radians, in which the eigenvalue is the most unstable, as compared to the direction of the homogeneous solution. The line σ_t corresponds to the transition to collective motion solution. This solution is unstable up to the restabilisation line σ_s. Completely longitudinal instabilities exist only above line $\sigma_{\|}$. Another, probably spurious, instability appears after the line σ_u. Completely transversal instabilities exist below the line $\sigma_{\perp}$.

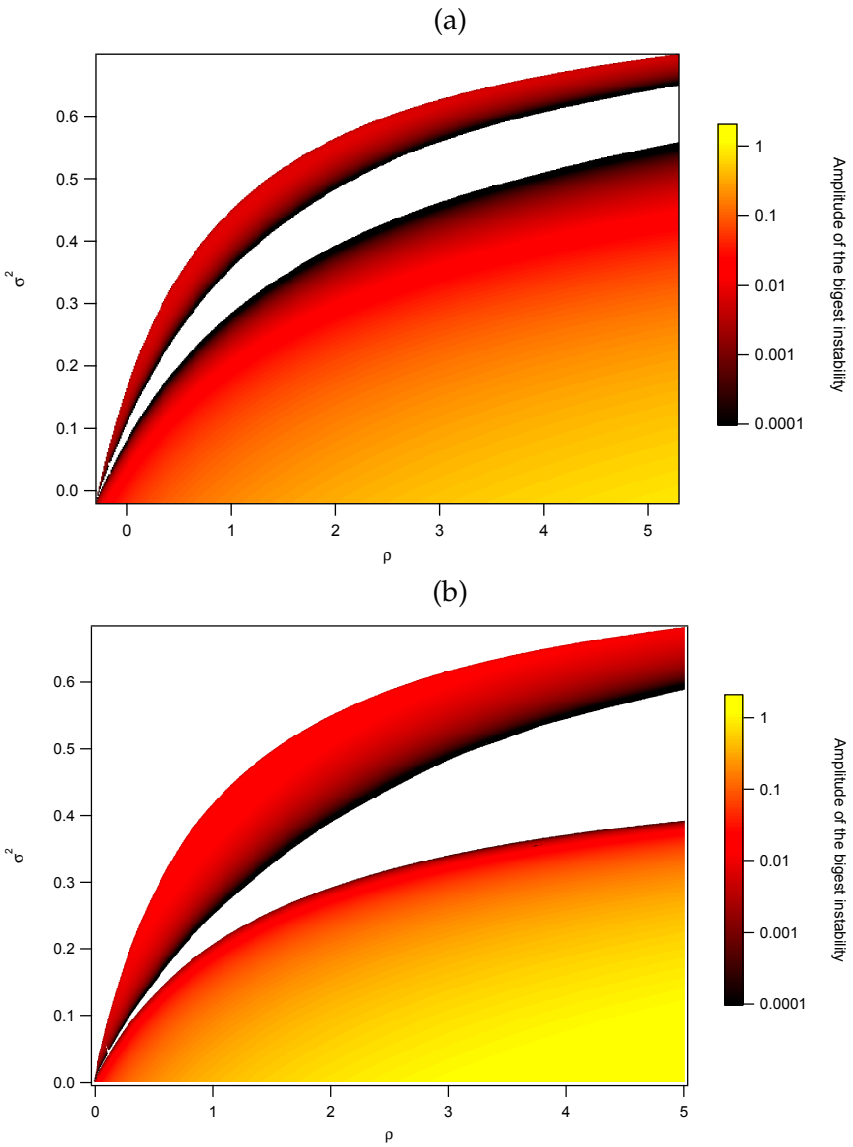

Figure 8: Modulus of largest eigenvalues in the case of a pure third order truncation (a) and if keeping the rho dependance of ξ (b).

3.3.3.1 *Fourth order expansion*

In the case of a fourth order truncation we keep the equation of f_2 and enslave the equation of f_3. We still count all the terms with the same scaling ansatz as introduced in section 2.3.

We present here only the form of the homogeneous part of the obtained equations for better explanation, without giving exact expressions of coefficients. The homogenous equations in this case have the form

$$\begin{aligned} C_{1,(1)} f_1 + C_{1,(2,1)} f_2 f_1^* &= 0 \\ C_{2,(2)} f_2 + C_{2,(1,1)} f_1^2 + C_{2,(2,1,1)} f_2 \left|f_1\right|^2 &= 0 \end{aligned}$$

First thing that we should notice is that the equation of f_2 becomes unbalanced in this case, because the new term $f_2 \left|f_1\right|^2$ is of fourth order in the Ginzburg-Landau like counting, while the two old ones are of second order. Thus we are already in the domain of uncontrolled expansion that can lead to explosive solutions. Computing numerically the stability of the obtained stability matrix, we found out that the collective motion state becomes unstable to homogeneous perturbations. This is of course due to the new unbalanced term, all the other terms were present in the old set of equations.

3.3.3.2 *Fifth and sixth order expansion*

Let's try to push the expansion forward, perhaps a new term will balance the fourth order term in the fourth order expansion. The new set of homogeneous parts of equations is given by

$$\begin{aligned} C_{1,(1)} f_1 + C_{1,(2,1)} f_2 f_1^* + C_{1,(2,3)} f_2^* f_3 &= 0 \\ C_{2,(2)} f_2 + C_{2,(1,1)} f_1^2 + C_{2,(2,1,1)} f_2 \left|f_1\right|^2 &= 0 \\ C_{3,(3)} f_3 + C_{3,(1,2)} f_1 f_2 + C_{3,(1,1,3)} \left|f_1^2\right| f_3 + C_{3,(1,2,2)} f_1^* f_2^2 &= 0 \end{aligned}$$

Now a new unbalanced term had appeared in equation of f_1 which is of fifth order while the other two are of third order. There is not any evident analytical solution to this set of equations. We thus search the homogeneous solution numerically. To do so we first obtain an approximate analytical solution, taking into account only the lowest available order terms in each equation. This is our starting solution for the search of a numerical solution. The result is presented on Fig(9). We see that for low noise a numerical solution disappears completely. This is due to the unbalanced fifth order term in the equation of f_1. If we drop out this term, a numerical solution to the set of equations is found everywhere. However even, if we drop out this term, the new set of equations is still unstable to homogeneous perturbations, because the fourth order term in equation of f_2 is still unbalanced.

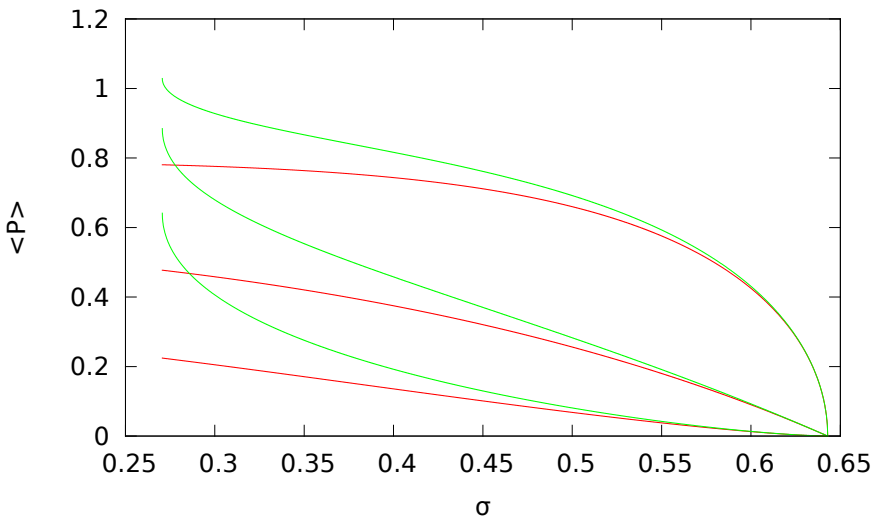

Figure 9: Homogeneous solutions to the equation truncated at fifth order. The lines represent the homogeneous solutions f_n, with n decreasing from top to bottom. In red approximate analytical solutions, in green exact numerical ones.

At the sixth order expansion no new term appears in the equation of f_1, thus this new set of equation still does not have a solution at low noise.

3.3.3.3 *Seventh order expansion*

At seventh order the homogeneous set of equations is given by

$$\begin{aligned}
C_{1,(1)}f_1 + C_{1,(2,1)}f_2 f_1^* + C_{1,(2,3)}f_2^* f_3 + C_{1,(3,4)}f_3 f_4 &= 0 \\
C_{2,(2)}f_2 + C_{2,(1,1)}f_1^2 + C_{2,(2,1,1)}f_2\,|f_1|^2 + C_{2,(2,4)}f_2 f_4 &= 0 \\
C_{3,(3)}f_3 + C_{3,(1,2)}f_1 f_2 + C_{3,(4,1)}f_1 f_4 + C_{3,(2,5)}f_2 f_5 &= 0 \\
C_{4,(4)}f_4 + C_{4,(2,2)}f_2^2 + C_{4,(1,3)}f_1 f_3 + C_{4,(1,5)}f_1 f_4 &= 0 \\
C_{5,(5)}f_7 + C_{5,(1,4)}f_1 f_4 + C_{5,(2,3)}f_2 f_3 & \\
+C_{5,(1,1,5)}f_1^2 f_5 + C_{5,(1,3,3)}f_1 f_3^2 + C_{5,(1,2,4)}f_1 f_2 f_4 &= 0
\end{aligned}$$

Now a new term has appeared in the equation of f_1, looking at Fig(10) we see that this term has balanced the previous explosive term, and now a solution exists everywhere. However studying the homogeneous stability of this solution, we once again find that it is everywhere unstable.

We stop our search at this seventh order. In sum, we understand that the Ginzburg-Landau type of scaling ansatz and expansion is appropriate exclusively to cut equations at the same order as the Ginzburg-Landau terms themselves. If we want to obtain higher order expansions of the Fourier series of the Boltzmann equation we should search for another type of expansion and closure ansatz. Perhaps a probable candidate would be the perturbed renormalization

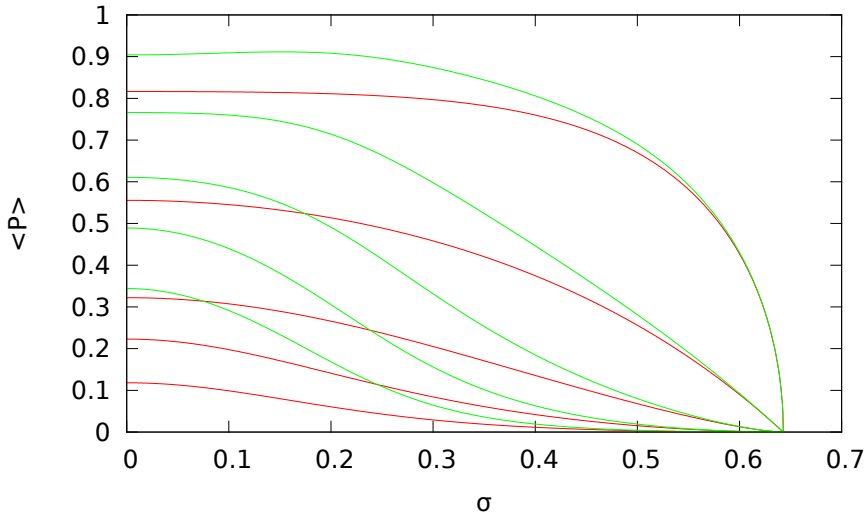

Figure 10: Homogenous solutions to the equation truncated at seventh order. The lines represent the homogeneous solutions f_n, with n decreasing from top to bottom. In red approximate analytical solutions, in green exact numerical ones.

group approach introduced by Chen et al.[14]. Although I should stress out that no investigation was done at this time to check if this approach can be at all used for the closure of the Boltzmann series.

The only positive effect of the increase in order of truncation, is the increase of the maximum value of $\left|\vec{P}\right| = f_1/\rho$, which should tend to 1 in the limit of infinite truncation.

3.4 NUMERICAL SIMULATIONS

To perform the simulation of the equation, I have developed a Fortran code based on the pseudo-spectral approach. This approach provides much more accurate solutions at a lower computational cost, than the traditional finite difference method. All the simulations where done with a simple Euler time stepping. Space and time resolutions where adjusted in order to provide well-behaved solutions, and will be detailed for each simulation.

3.4.1 *Simulation of 1D solution*

As the bands reported in microscopic simulations are invariant the in transverse direction, it is natural to start by studying one dimensional solutions of our equation.

First of all we want to confirm that in large boxes, after some lengthy transition time, all bands become equivalent as well as the spacing between them. But I have found that this rule is not always observed. In the case of a pure third order truncation of equations, we

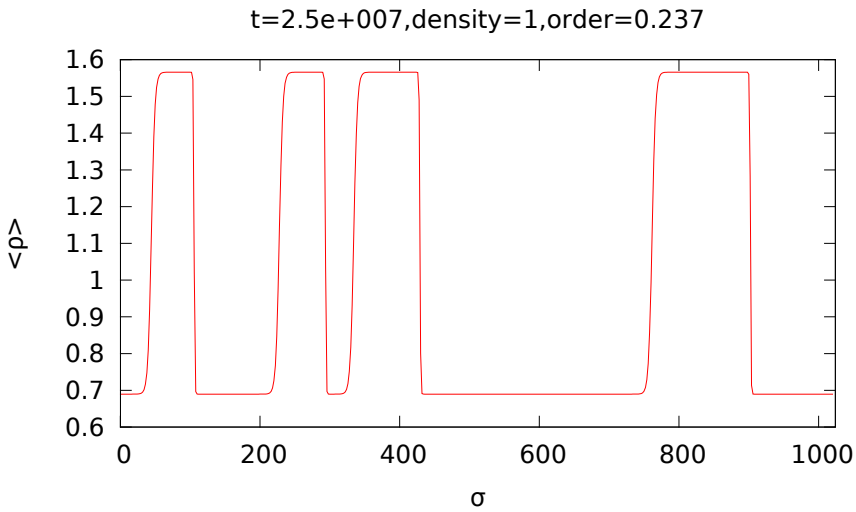

Figure 11: Final state of the density field at time $T = 2.5 \times 10^7$ in a box of size $L = 1000$ with no density dependance of the ν term starting from random initial conditions. The simulation was done with a spatial stepping of $\Delta x = 0.25$ and a time steping of $\Delta t = 0.01$. The mean density in the system is $\rho_0 = 1$ and the noise value is $\sigma = 0.64$.

found that the bands never become identical and the separation between them remains unequal. The evolution stops at some transient state as shown on Fig(11). No any further evolution of the system is observed even for huge times of about 10^7.

But if we now keep the ρ dependance of the ν term, the system evolves to a state where the bands are identical as seen on Fig(12). The separation between them is not, but this is due to an exponentially weak interaction between the bands and the absence of any effective noise. We wanted to elucidate which of the terms in our equation is responsible for such an effect. We have found that it is sufficient to keep only the ρ dependance of the ξ term, to make the bands equivalent as shown in Fig(13).

Note also the difference between the top of the bands. In the case of no density dependance the bands are very wide. In the case of a full density dependance the bands are much slimmer. Finally in the intermediate case of only ξ dependance on ρ the top of the bands is abrupt like in shock waves.

Thus we have found that in order to obtain an equation that behaves like the microscopical model it is insufficient to truncate the equation at the pure third order as we initially thought. A pseudo-fourth order truncation is needed in order to have correct behavior of the bands. An open question remains how must we change the rules of truncation introduced in the previous part, in order to account for such an effect? We can however say in advance, that the truncation

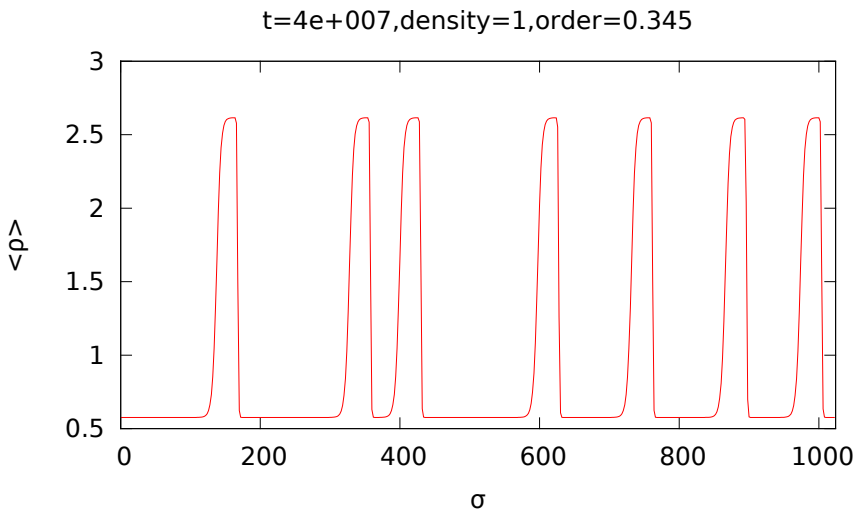

Figure 12: Final state of the density field at time $T = 4 \times 10^7$ in a box of size $L = 1000$ with density dependance of the ν term starting from random initial conditions. The simulation was done with a spatial stepping of $\Delta x = 0.25$ and a time steping of $\Delta t = 0.01$. The mean density in the system is $\rho_0 = 1$ and the noise value is $\sigma = 0.64$.

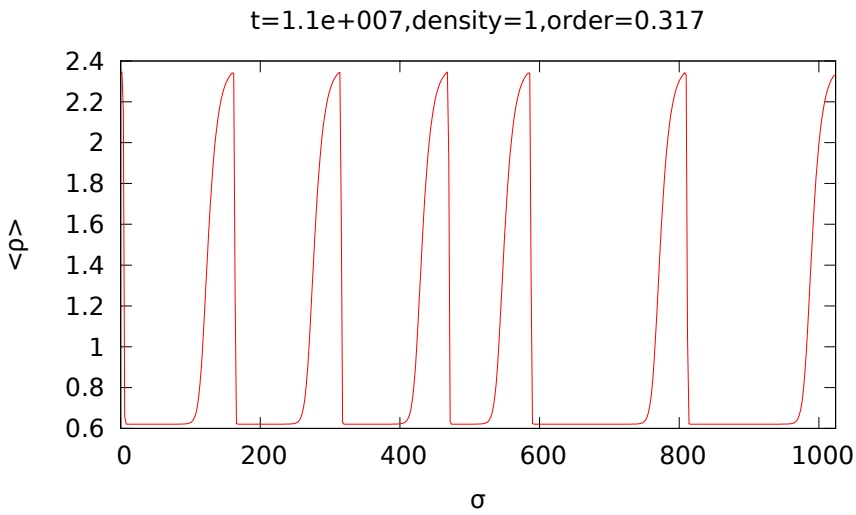

Figure 13: Final state of the density field at time $T = 1.1 \times 10^7$ in a box of size $L = 1000$ with density dependance of the ξ term only starting from random initial conditions. The simulation was done with a spatial stepping of $\Delta x = 0.25$ and a time steping of $\Delta t = 0.01$. The mean density in the system is $\rho_0 = 1$ and the noise value is $\sigma = 0.64$.

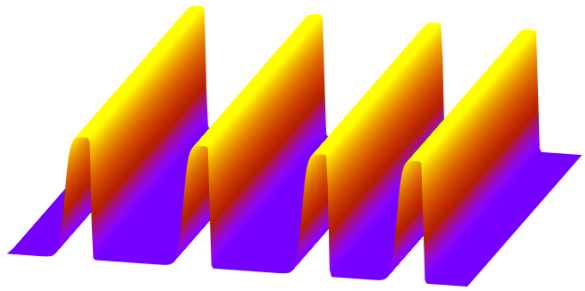

Figure 14: Band solution in a 2d simulation box. The orientation of the bands in the system correspond to the initial orientation of a periodic perturbation on density and polar order.

rules introduced in Part I, were found correct for other Vicsek like models.

Due to the very long evolution times, it is however extremely time-consuming to study the behavior of band solutions by simulation. We will thus try to study them, by obtaining numerically exact solutions and studying their stability as will be explained latter.

3.4.2 *2D simulations*

In two dimensions we want to confirm that the soliton like and the fully ordered solutions are the only ones that can be obtained. We start by simulating in 2d the evolution of a perturbation oriented in only one dimension. As shown on Fig(14), independently of the initial orientation of the perturbation, the system will evolve to a soliton structure in the direction of the initial perturbation.

If now I simulate the 2d equation starting from an initial condition disordered in both dimensions, I obtain, after some lengthy transition time, once again a soliton like solution in a small simulation box (for sizes up to about 100x100). However if I try to perform this simulation in bigger boxes, the equations explode at some point of time when two soliton like structures cross each other. This numerical difficulty of simulating these equations for large box sizes is certainly due to the advection terms in equation 7 on page 42, which is known to be extremely hard to simulate[11]. As of now I was not able to overcome this numerical instability. However, in recent microscopical simulations in our group, more complicated 2d solutions where found for very large system sizes. We can expect that such kind of structures could also be found in our equations.

3.5 SOLUTIONS OF THE ODE EQUATION

As soliton-like solutions have been reported in microscopic simulations, and since I have observed them in simulations of the equation, we can try to obtain analytical expressions of these structures. To this end we put ourselves in the frame of the moving soliton, which we suppose to move along the $\vec{x}$ axis with speed c. As these solitons are 1D solutions, we will neglect all variations of our fields along the $\vec{y}$ axis. We introduce the variable $\zeta = x - ct$, the new frame density $R(\zeta) = \rho(x - ct)$ and polar order parameter $P(\zeta) = f_1(x - ct)$ functions. In the new reference frame our derivatives become

$$\begin{aligned} \frac{\partial}{\partial t} &= -c\frac{\partial}{\partial \zeta} \\ \frac{\partial}{\partial x} &= \frac{\partial}{\partial \zeta} \end{aligned}$$

The density equation(4) then become

$$-cR' = -P'$$

Thus $R = \frac{P}{c} + \rho_{gas}$ where ρ_{gas} is the value of density in the disordered sea between the solitons. Making the same transformation to the polar order equation(7) we obtain, after substituting inside the R solution

$$P'' = (a_0 + a_1 P)\, P' - b_1 P - b_2 P^2 - b_3 P^3 \tag{13}$$

where in the case of a ρ dependance of the ν term we have

$$\begin{aligned} a_0 &= \left(\frac{2}{c} - 4c\right)\frac{1}{\nu^*} \\ a_1 &= \left(\frac{2}{c^2} - 4\right)\tilde{\nu} + 4\gamma_2 \\ b_1 &= 4\frac{\mu^*}{\nu^*} \\ b_2 &= \frac{4}{c}\left(\frac{\mu'}{\nu^*} + \mu^*\tilde{\nu}\right) \\ b_3 &= \frac{4}{c^2}\left(\mu'\tilde{\nu} - c^2\xi_2\right) \\ \mu^* &= \mu\left(\rho = \rho_{gas}\right) \\ \nu^* &= \nu\left(\rho = \rho_{gas}\right) \\ \mu' &= \frac{\partial \mu}{\partial \rho} \\ \tilde{\nu} &= \frac{\partial}{\partial \rho}\left(\frac{1}{\nu}\right) \\ \gamma_2 &= \frac{\gamma}{\nu} \\ \xi_2 &= \frac{\xi}{\nu} \end{aligned}$$

and in the case of a no ρ dependance the terms will be

$$\begin{aligned}
b_1 &= 4\frac{\mu^*}{\nu_0} \\
b_2 &= \frac{4}{c}\frac{\mu'}{\nu_0} \\
b_3 &= -4\xi_2 \\
a_0 &= \left(\frac{2}{c} - 4c\right)\frac{1}{\nu_0} \\
a_1 &= 4\gamma_2 \\
\nu_0 &= \nu\left(\rho = \rho_0\right)
\end{aligned}$$

In the second case our coefficients depend on a supplementary parameter ρ_0, the mean density in the system. However this parameter is already known and in both cases the solution of the equation will depend on ρ_0 through the relation $\int_L R = L\rho_0$, where L is the linear size of the system.

Note that we don't treat one of the possible cases that we studied in simulations, when ξ depend on ρ and ν is independent of this. In this case our ODE will go to the fourth order in P further complicating calculations.

This type of equations is known to mathematicians and have been extensively studied[**?**]. They are nonlinear parabolic equations generally referenced as Fisher-KPP (Kolmogorov-Petrovskij-Peskunov) equations. Many traveling front solutions have been identified[**? ? ? ? ?**] for this type of equations. However as of now I was not able to identify a soliton like solution to our equation. We are thus obliged to search for numerical solutions using the shooting method. We will also try to derive traveling front solutions that will perhaps give us an analytical relation between the speed c and the asymptotic density ρ_{gas}.

3.5.1 *Shooting of the ODE*

As of writing of this thesis, the study of the ODE equations was not yet completed. Thus only an introduction to the methods to perform such a study is presented. I will give only the results corresponding to the case with a density dependence of ν.

3.5.1.1 *One-soliton solution*

We can start to search for a one-soliton solution by the shooting method. To use the shooting method we should fix the conditions at the border. Since at both ends our solution should decay to zero, we take the linearized version of the equation(13) to obtain the decay exponent $k = \frac{a_0 \pm \sqrt{a_0^2 - 4b_1}}{2}$. We will then impose the border conditions on both ends to be equal to $A_1 e^{\pm kx}$, where A_1 is a parameter to be

determined by shooting. We have only two equations (the first and second derivatives of P), and three unknowns; c, ρ_{gas} and A_1. We have thus two options, first fix the value of c and search for A_1 and ρ_{gas}, or fix ρ_{gas} and search for values of c and A_1. During our analysis we have found that for a given ρ_{gas} the value of the speed is not necessarily unique, thus we will fix the value of the speed c.

Note that to have k with two different signs $b_1$must be negative. In the case of ρ dependence of ν $b_1 = 4\nu^*\mu^*$ and $b_1 = 4\nu_0\mu^*$ in the case of absence of such a dependence. In all cases ν is a positive quantity, thus we must have $\mu^* \leq 0$. As we know from equation(8) this condition is equivalent to $\rho_{gas} \leq \rho_t$. In the case $\rho_{gas} \to \rho_t$ we have

$$k_\pm \quad \to \quad 2a_0$$

i.e. the soliton in this limit is symmetric. Note as we will see later that in this limit the width of the soliton is diverging due to the fact that $a_0 \to 0$. So we already known that the maximum of ρ_{gas} is fixed by ρ_t, and that the soliton will become of infinite width as it approaches that limit.

We start by fixing a value of sigma and examine the obtained solutions. We will do this at a value $\sigma = 0.1$. As can be seen on Fig(15) , the $\rho_{gas} - c$ diagram is not monotonic. Starting from a maximum value predicted by theory of ρ_t, ρ_{gas} goes down to a minimal value ρ_{gas}^{min} and then increases again to some final value. We can also trace other parameters of the obtained soliton; the height of the soliton, the width at half-height and the mass of the soliton. The latter is defined as the area under the soliton. The results are presented on Fig(16). First we see that the height of the soliton is going from zero at $\rho_{gas} = \rho_t$ to some finite value. Note that the height of the soliton is not diverging at maximum speed. The width at half-height and the mass of the soliton, are in contrary diverging at both ends. The divergence of the mass of the soliton for $c \to c_{min}$ indicates that the width of the soliton increases faster than the decrease of the height to zero. Note that the minimu of ρ_{gas}, of the width at half-height and of the mass of the soliton do not coincide. They are respectively $c \approx 0.85$, $c \approx 0.81$ and $c \approx 0.73$. But if we trace the $^{height}/_{width}$ parameter (Fig(17)), we find that the maximum of this value will coincide with the minimum of ρ_{gas}, i.e. for $\rho_{gas} \in \left[\rho_t : \rho_{gas}^{min}\right]$ the soliton will mostly grow in height, and after that the height of the soliton will hardly evolve, but its width will grow rapidly.

We can also study the asymmetry of the soliton which we can do via the exponents $k_\pm$ represented on Fig(18). To an easier study of the asymmetry it is practical to introduce the symmetry coefficient $\varsigma(\sigma, c) = \left|\frac{k_-}{k_+}\right|$ which varies from one for a perfectly symmetric soliton to zero for a completely asymmetric one. As we have said previously in the limit $c \to 1/\sqrt{2}$ both exponents are equal and the soliton is perfectly symmetric. As we increase the speed the symmetry of the

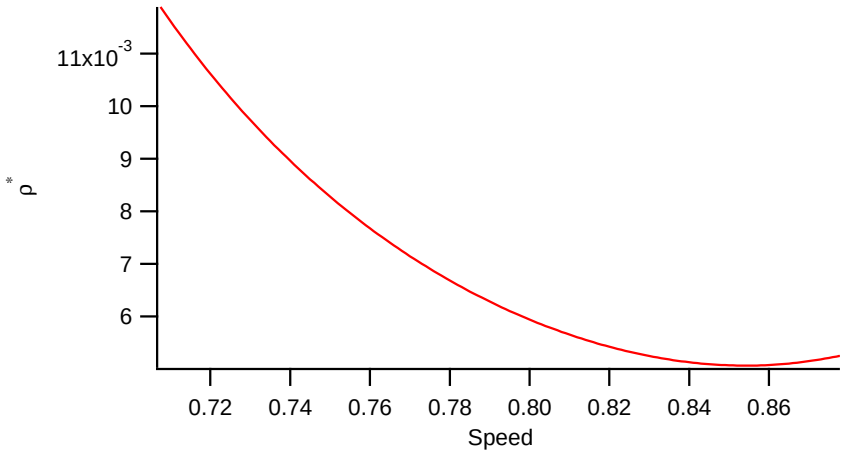

Figure 15: The asymptotic density ρ_{gas} versus the speed c. Values obtained at $\sigma = 0.1$.

soliton is decreasing without going to zero, though. The profiles of the solitons at three locations; near the minimum speed c_{min}, near the minimum asymptotit density ρ_{gas}^{min} and near the maximum speed c_{max} are represented on Fig(19).

We next examine the speed c, the asymptotic density ρ_{gas} and other parameters of the soliton as a function of noise σ. All the parameters are plotted for c_{min}, ρ_{gas}^{min} and c_{max}.

We first look at the Fig(20) representing the three different speed values as a function of σ. We first see that the line c_{min} is a constant with an approximate value of 0.707. This value is actually $c = 1/\sqrt{2}$ which is the speed that we obtain from the condition $a_0 = 0$ (the energy conservation relation implies $a_0 > 0$). This value of a_0 explains the divergence of the soliton width in this limit. The values of the speed corresponding to the cases ρ_{gas}^{min} and c_{max} decrease from high values at low σ to c_{sound} at $\sigma \to \sigma_t^{\infty} \approx 0.9$. At $\sigma \approx 0.76$ the lines corresponding to the casesρ_{gas}^{min} and c_{max} become indistinguishable. Also note that for $\sigma \to 0$, the maximum speed converges to a fixed value $c_{max} \approx 0.88$ which is lower than one. As of now I do not know why this value is not one.

Next we plot the different values of ρ_{gas} as a function of σ on Fig(21). As we have already said the value of ρ_{gas} corresponding to c_{min} is actually ρ_t. Of course ρ_{gas} is smaller than ρ_t for the soliton solution to exist. The value of ρ_{gas} corresponding to ρ_{gas}^{min} is hardly distinguishable from ρ_t. I caution the reader not to confuse the values of ρ_{gas} for c_{max} and c_{min} with the values ρ_{max} and ρ_{min} that will be introduced for the mixed and for the nematic models.

Next, we plot the height of the solitons on Fig(22). The height of the soliton for c_{min} is of course always zero. For ρ_{gas}^{min} and c_{max} they are increasing up to a maximum at $\sigma \approx 0.785$ and then decrease slightly. I am not sure if the decrease of the height after this critical noise value

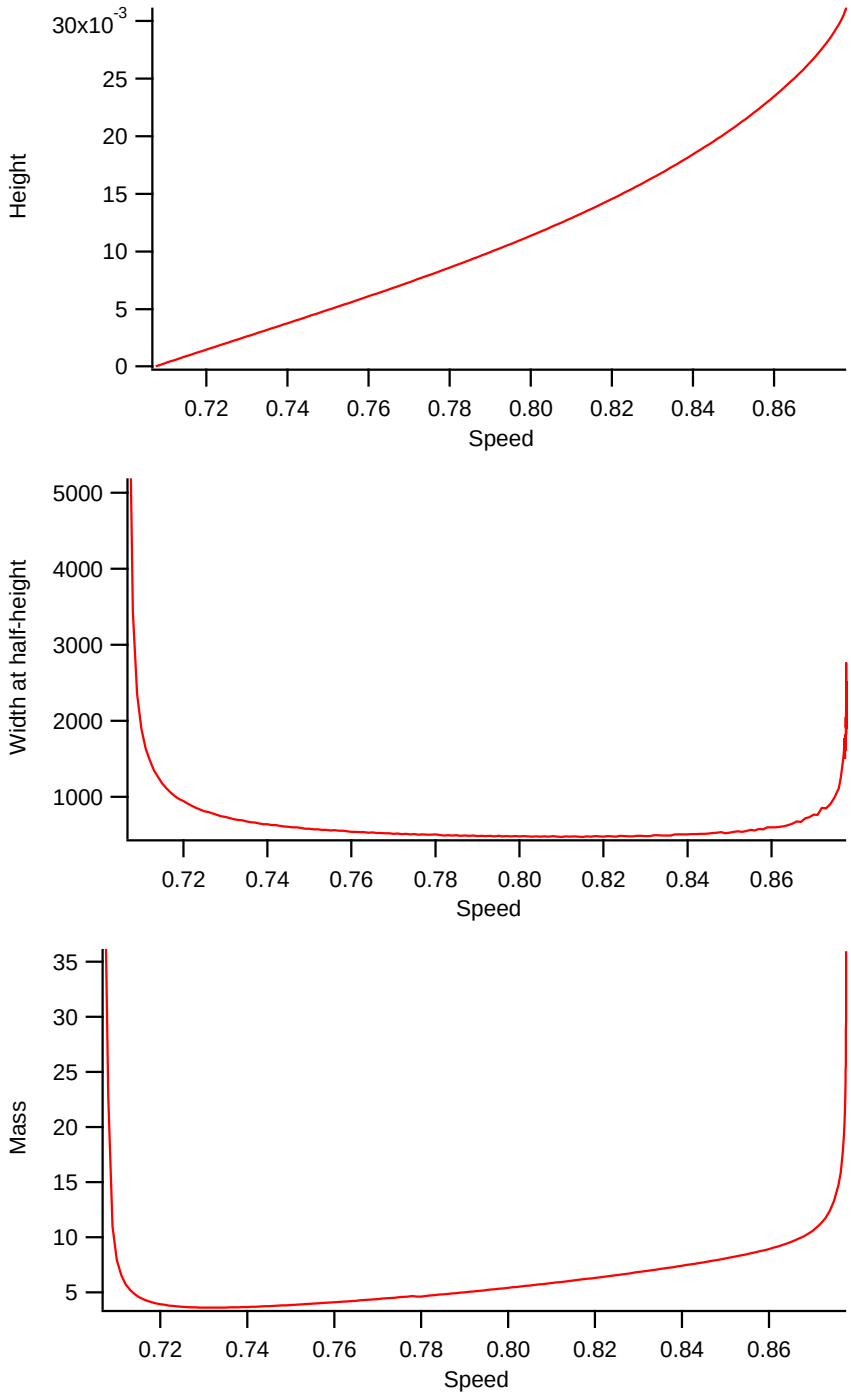

Figure 16: The height, the width at half-height and the mass of the soliton versus speed c. Results obtained at $\sigma = 0.1$.

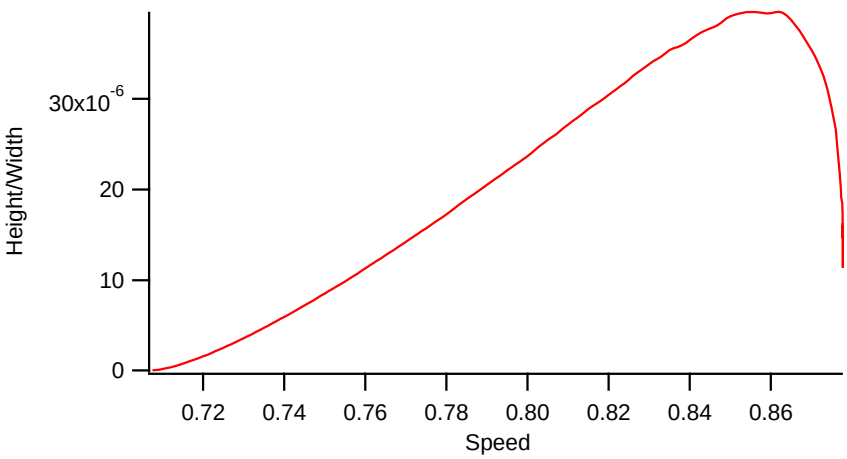

Figure 17: The $^{height}/_{width}$ parameter as a function of speed c. Values obtained at a noise $\sigma = 0.1$.

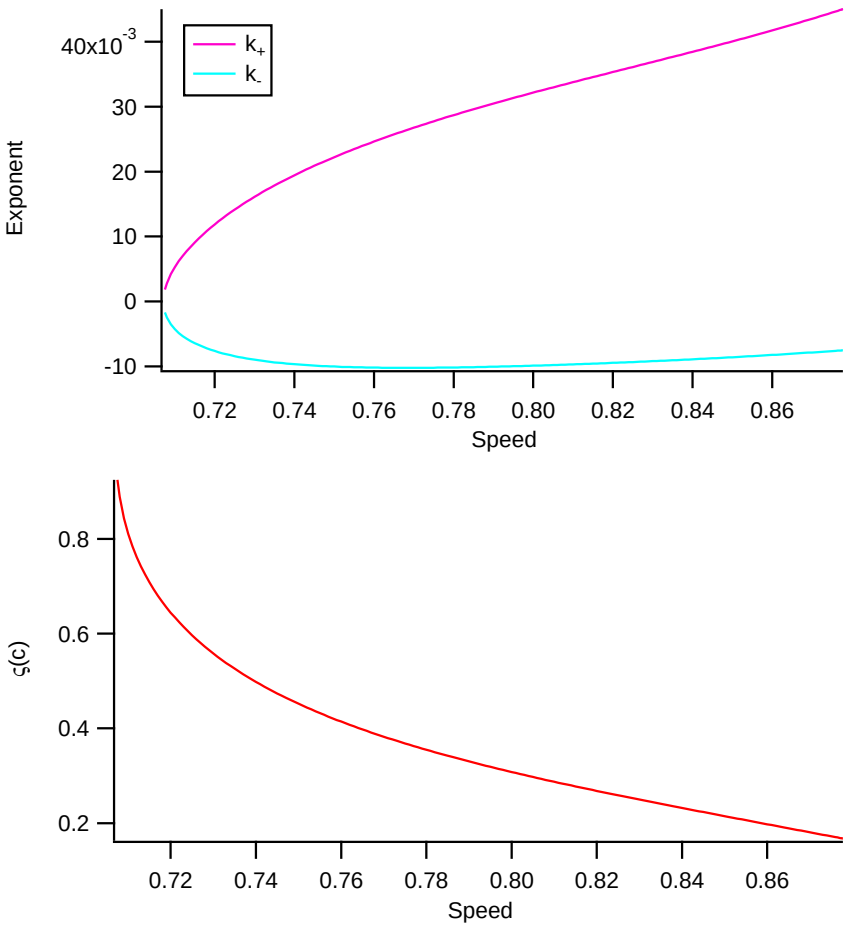

Figure 18: Exponents $k_{\pm}$ and the symmetry coefficient $\varsigma(c)$ as a function of speed. Measured for $\sigma = 0.1$.

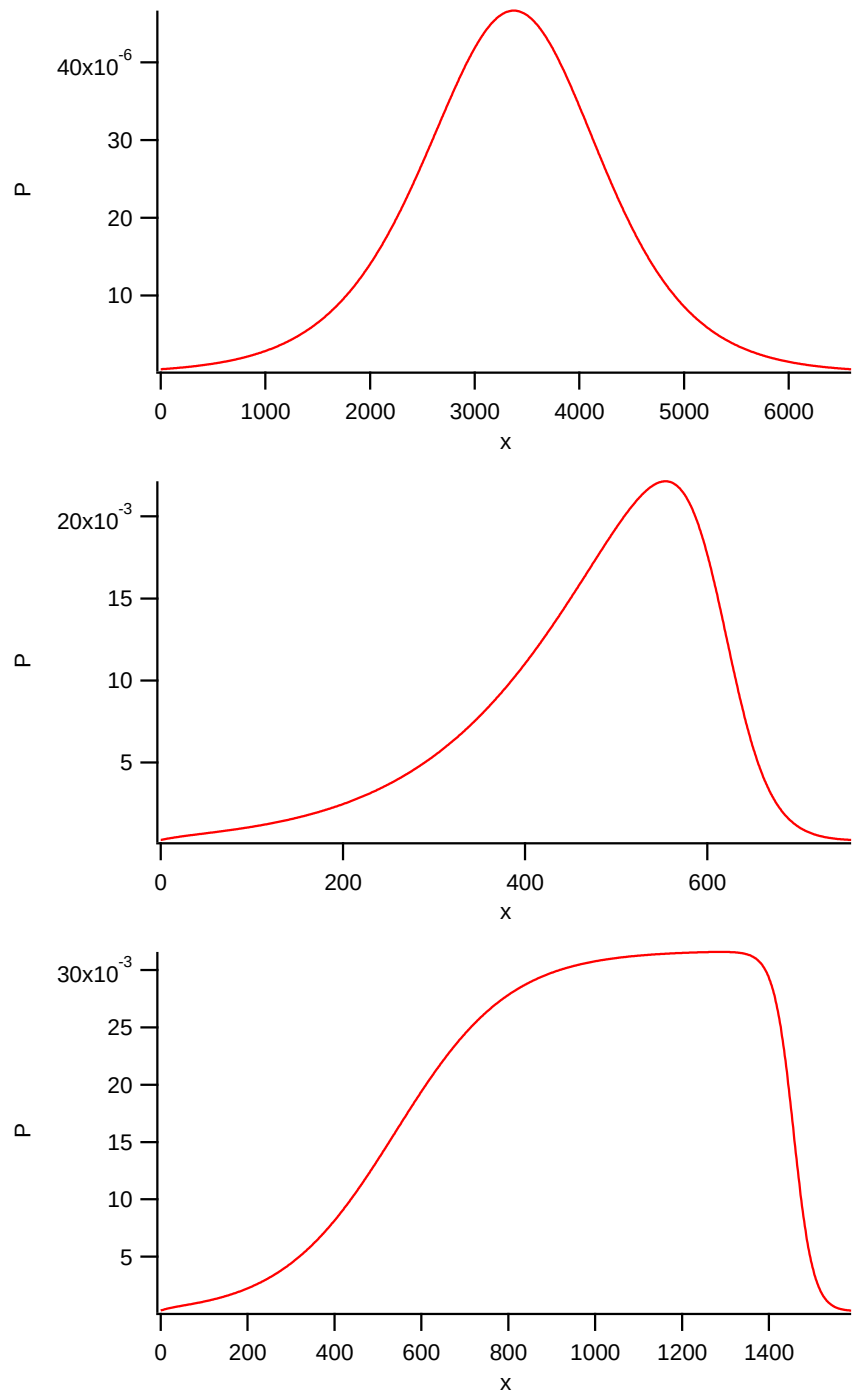

Figure 19: Profiles of the solitons for speed values near c_{min}, ρ_{gas}^{min} and c_{max}. The exact values of speed are $c = 0.708$, $c = 0.854$ and $c = 0.877$. The noise value is $\sigma = 0.1$.

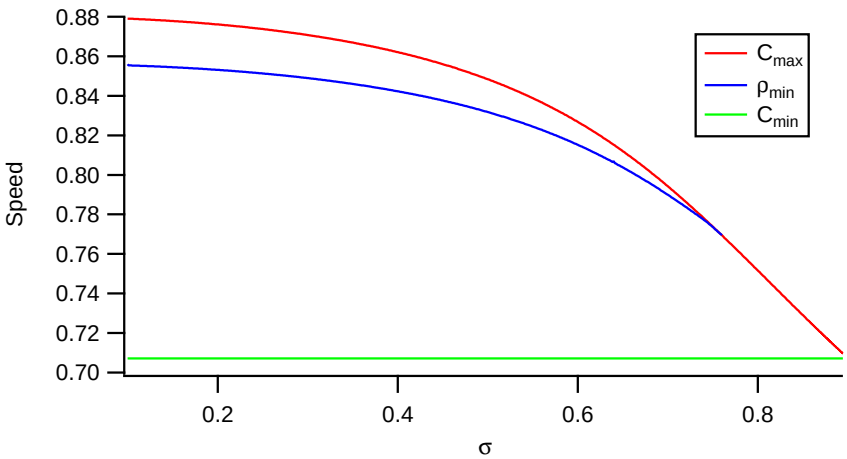

Figure 20: The speed of solitons as a function of noise σ.

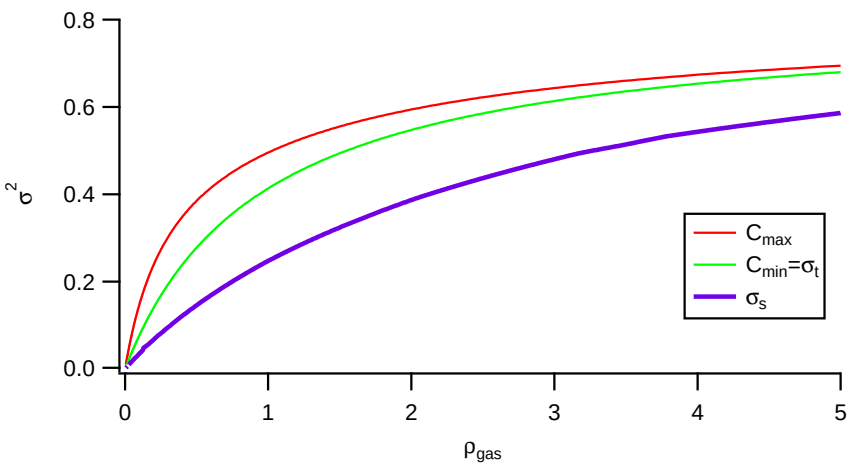

Figure 21: Values of ρ_{gas} as a function of noise σ. Note that the values for c_{max} and ρ_{gas}^{min} are indistinguishable on this graph, those the latter is not ploted. The restabilisation noies σ_s is given for reference.

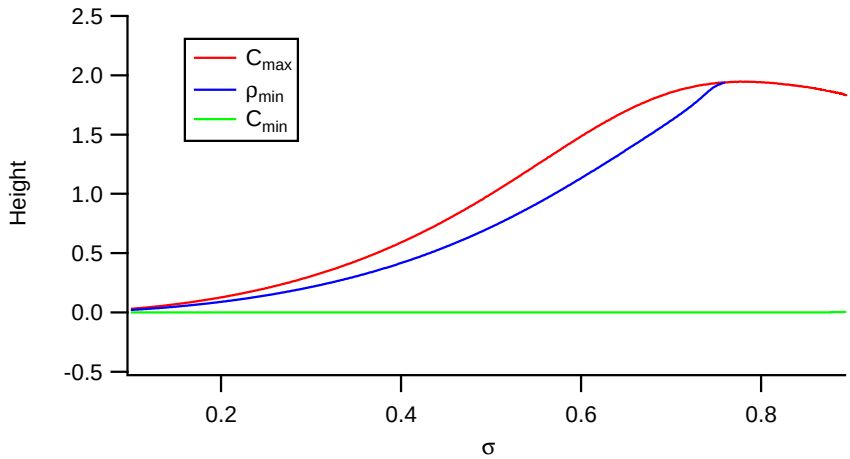

Figure 22: Height of the solitons as a function of noise σ.

is real or is just due to a numerical difficulty of obtaining solitons in this zone.

Finally we plot the width at half-height and the mass. This parameters are of course plotted only for ρ_{gas}^{min} as we have seen that they diverge for c_{min} and c_{max}. As can be seen on Fig(23) both the width and the mass diverge in both limits $\sigma \to 0$ and $\sigma \to \sigma_t$. The divergence of the width of the solitons in the limit $\sigma \to 0$ can perhaps explain why no soliton can be observed at small noise for finite size boxes.

3.5.1.2 *Many-soliton solutions*

As we have seen in microscopic simulations and in simulations of our equations, there are generally many solitons in the simulation box. Thus we can try to search by shooting for a periodic solution. To do so, we must suppose that the order parameter P will not decay to zero between the solitons, but to a small value p_{gas}. Thus we will now need to impose the speed c and the asymptotic order parameter p_{gas}. As we have one additional parameter, the phase diagram will become complicated, we will then study the solutions only for some fixed values of the noise σ.

As of now I can only say that the width of the periodic soliton decreases when p_{gas} is increased. The limit $p_{gas} \to 0$ corresponds of course to the infinite width soliton, the case that we studied previously.

3.5.1.3 *Stability analysis*

As the family of obtained soliton solutions is very big, a unique solution should be selected by the stability considerations and the dynamics. There are two ways of finding numerically the stability of the soliton. The first is just to introduce the obtained shooting solution

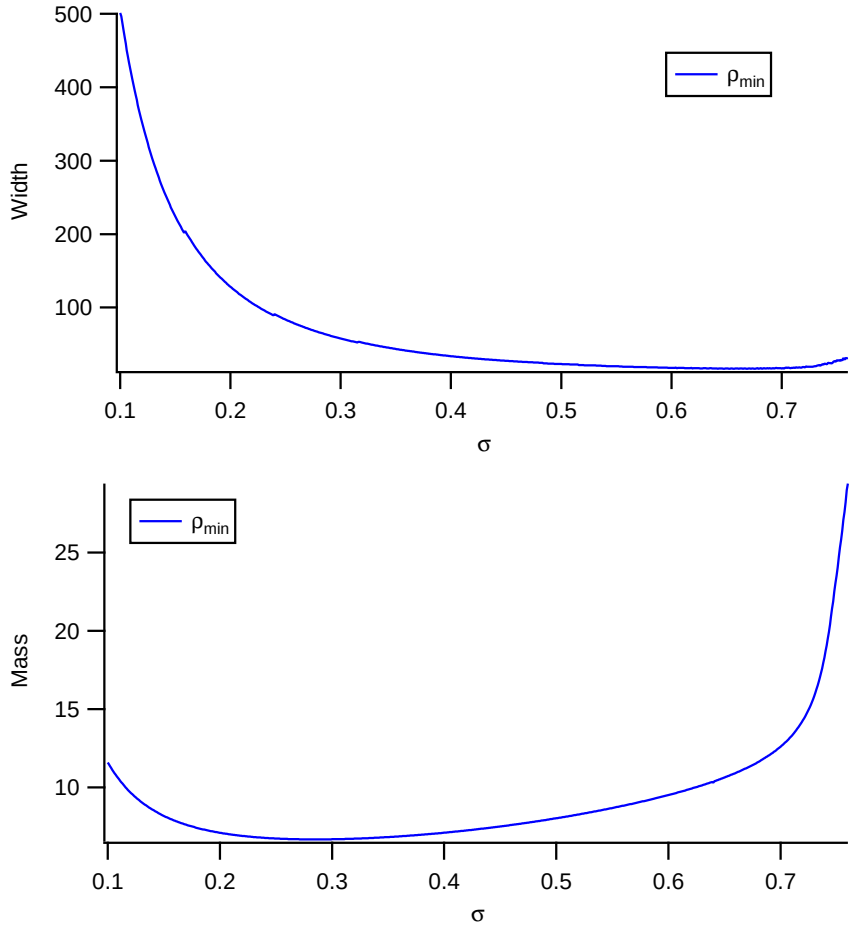

Figure 23: The width at half-height and the mass of the soliton for the case ρ_{gas}^{min} as a function of noise σ.

inside the simulation program and look if the solution will survive past an adaptation period. When trying to do such an investigation, I have quickly found that this method is not robust and is extremely time consuming. We have already seen in the simulation section, that the time to the full adaptation of the soliton is extremely long.

Another way would be to study the linear stability of these solutions, by linearizing the equations for a perturbation of the soliton solution and to study the obtained stability matrix numerically. However our solution is dependent on position x, thus we will need to obtain eigenvalues of an extremely large matrix, whose size will depend on the number of points along the x directions that we will take. As this procedure is time consuming, it was not yet done at the time of writing of this thesis. This work will be addressed in the future and included in a new article on the study of the polar BGL equation.

3.5.2 *Analytic front solution*

We try to find a front solution to the ODE equation found previously. We will search for a solution in the form

$$P(\zeta) = \sum_{j=0}^{p} A_j G^j(\zeta)$$

where $G(y) = \frac{e^{ky+\varphi}}{1+e^{ky+\varphi}}$, p is the order of the pole of the solution and A_j coefficients are to be determined. It is easy to check that the order of the pole of this equation is 1, thus we will be searching for a solution given by $P(\zeta) = A_0 + A_1 G(\zeta)$. Inserting it inside equation (13) and using relations $G' = kG - kG^2$ and $G'' = k^2G - 3k^2G^2 + 2k^2G^3$ we obtain the following set of equations to fulfill

$$\begin{aligned} 2k^2 &= -a_1A_1k - b_3A_1^2 \\ -3k^2 &= -a_0k - a_1k(A_0 - A_1) - b_2A_1 - 3b_3A_0A_1 \\ k^2 &= -2b_2A_0 + k(a_0 + a_1A_0) - b_1 - 3b_3A_0^2 \end{aligned}$$

We have three equations with four unknowns ρ_{gas}, c, k and A_1.

We want to have a zero P field outside the front region, so we put $A_0 = 0$. We are thus left with the equations

$$\begin{aligned} 2k^2 &= -a_1A_1k - b_3A_1^2 \\ -3k^2 &= -a_0k + a_1kA_1 - b_2A_1 \\ k^2 &= ka_0 - b_1 \end{aligned}$$

From the last equation we obtain $k = \frac{a_0 \pm \sqrt{a_0^2 - 4b_1}}{2}$. As we can see, apart from the opposite sign solutions that come from the change of the sign of k with c, there are two different solutions that correspond to different exponential decays for the front of the soliton and the rear.

The first two equations can be reformulated as

$$\begin{aligned} 2k^2 &= -a_1 A_1 k - b_3 A_1^2 \\ 2k^2 &= b_1 - a_1 k A_1 + b_2 A_1 \end{aligned}$$

Taking the difference of this two equations gives

$$0 = -b_1 - b_2 A_1 - b_3 A_1^2$$

which is a logical result implying that the value of A_1 at infinity should be independent of all gradients. This give us the solution

$$A_1 = \frac{-b_2 \pm \sqrt{b_2^2 - 4b_1 b_3}}{2b_3}$$

I find that b_2 is a positive quantity in the region of band existence, so to have a positive value of A_1 (for positive c) we must choose the solution with a plus sign (and respectively with a minus sign in the case of negative c).

We are left with an equation that gives a relation between ρ_{gas} and c.

$$2ka_0 = 3b_1 - a_1 k A_1 + b_2 A_1$$

The analytic $\rho_{gas} - c$ phase diagram is extremely similar in its shape to the one found by the shooting method, however the values of ρ_{gas} and c are not the same as the ones found in shooting. As of now I don't have any explanation to this difference, further investigations are needed to understand this.

3.6 CONCLUSION

I have obtained hydrodynamic equations that are able to reproduce the different phases observed in the microscopic model. I was also able to confirm the first-order nature of the order-disorder transition. Thus the transition line of the hydrodynamic equations is not given by the line of existence and the stability of the homogenous solution. The determination of the exact line of transition requires to add an effective noise term to our equations.

I was also able to study the solitonic structures obtained in our equations. I have found that the truncation rules introduced in the previous part are not sufficient to obtain the behavior of bands equivalent to the microscopic model. A higher order truncation is needed to obtain equivalent and equally spaced solitons.

While we can obtain a semi-analytical solution of our bands using the shooting method, the study of the stability of the obtained solutions has not yet been done due to its complexity. This is the subject of an ongoing work.

In sum, I have obtained equations that faithfully reproduce the qualitative properties of the microscopic model. A deeper study of

these equations, including a derivation of an effective noise term, will lead to a better understanding of the microscopical model.

BIBLIOGRAPHY

[1] I.S. Aranson and L.S. Tsimring. Model of coarsening and vortex formation in vibrated granular rods. *PRE*, 67(2):021305, 2003. (Cited on page 11.)

[2] I.S. Aranson and L.S. Tsimring. Pattern formation of microtubules and motors: Inelastic interaction of polar rods. *Physical Review E*, 71(5 AR 050901), 2005. (Cited on page 11.)

[3] I.S. Aranson and L.S. Tsimring. Theory of self-assembly of microtubules and motors. *PRE*, 74(3):031915, 2006. (Cited on page 11.)

[4] T. Balch and R.C. Arkin. Behavior-based formation control for multirobot teams. *Ieee Transactions on Robotics and Automation*, 14(6):926–939, 1998. (Cited on page 3.)

[5] M. Ballerini, N. Cabibbo, R. Candelier, A. Cavagna, E. Cisbani, I. Giardina, V. Lecomte, A. Orlandi, G. Parisi, A. Procaccini, M. Viale, and V. Zdravkovic. Interaction ruling animal collective behavior depends on topological rather than metric distance: Evidence from a field study. *Proceedings of the National Academy of Sciences*, 105(4):1232–1237, 2008. (Cited on page 147.)

[6] A. Baskaran and M.C. Marchetti. Hydrodynamics of self-propelled hard rods. *PRE*, 77(1):011920, 2008. (Cited on pages 10 and 24.)

[7] A. Baskaran and M.C. Marchetti. Self-regulation in self-propelled nematic fluids. *European Physical Journal E*, 35(9):95, 2012. (Cited on page 136.)

[8] E. Bertin, M. Droz, and G. Grégoire. Boltzmann and hydrodynamic description for self-propelled particles. *Physical Review E*, 74(2 AR 022101), 2006. (Cited on pages 9 and 36.)

[9] E. Bertin, M. Droz, and G. Grégoire. Hydrodynamic equations for self-propelled particles: microscopic derivation and stability analysis. *Journal of Physics A-mathematical and Theoretical*, 42(44):445001, 2009. (Cited on pages 9, 43, and 48.)

[10] D.L. Blair, T. Neicu, and A. Kudrolli. Vortices in vibrated granular rods. *PRE*, 67(3):031303, 2003. (Cited on page 130.)

[11] J.P. Boyd. *Chebyshev and Fourier spectral methods*. Dover Publications, 2001. (Cited on page 57.)

[12] J. Buhl, D. Sumpter, I.D. Couzin, J.J. Hale, E. Despland, E.R. Miller, and S.J. Simpson. From disorder to order in marching locusts. *Science*, 312(5778):1402–1406, 2006. (Cited on page 3.)

[13] A. Cavagna, A. Cimarelli, I. Giardina, G. Parisi, R. Santagati, F. Stefanini, and M. Viale. Scale-free correlations in starling flocks. *Proceedings of the National Academy of Sciences of the United States of America*, 107(26):11865–11870, 2010. (Cited on page 3.)

[14] L.-Y. Chen, N. Goldenfeld, and Y. Oono. Renormalization group and singular perturbations: Multiple scales, boundary layers, and reductive perturbation theory. *Physical Review E*, 54(1):376–394, 1996. (Cited on page 54.)

[15] L.H. Cisneros, R. Cortez, C. Dombrowski, R.E. Goldstein, and J.O. Kessler. Fluid dynamics of self-propelled microorganisms, from individuals to concentrated populations. *Experiments in Fluids*, 43(5):737–753, 2007. (Cited on page 4.)

[16] D.S. Dean. Langevin equation for the density of a system of interacting langevin processes. *Journal of Physics A-mathematical and General*, 29(24):L613–L617, 1996. (Cited on page 26.)

[17] J. Gautrais, C. Jost, M. Soria, A. Campo, S. Motsch, R. Fournier, S. Blanco, and G. Theraulaz. Analyzing fish movement as a persistent turning walker. *Journal of Mathematical Biology*, 58(3):429–445, 2009. (Cited on page 3.)

[18] F. Ginelli and H. Chaté. Relevance of metric-free interactions in flocking phenomena. *Physical Review Letters*, 105(16):168103, 2010. (Cited on pages 4, 9, 20, and 147.)

[19] F. Ginelli, F. Peruani, M. Bar, and H. Chaté. Large-scale collective properties of self-propelled rods. *Physical Review Letters*, 104(18):184502, 2010. (Cited on pages xiii, xiv, 4, 9, 20, 75, and 76.)

[20] L. Giomi, M.J. Bowick, X. Ma, and M.C. Marchetti. Defect annihilation and proliferation in active nematics. *PRL*, 110(22):228101, 2013. (Cited on page 130.)

[21] A. Gopinath, M.F. Hagan, M.C. Marchetti, and A. Baskaran. Dynamical self-regulation in self-propelled particle flows. *Physical Review E*, 85(6 AR 061903), 2012. (Cited on page 10.)

[22] Y. Hatwalne, S. Ramaswamy, M. Rao, and R.A. Simha. Rheology of active-particle suspensions. *Physical Review Letters*, 92(11):118101, 2004. (Cited on page 4.)

[23] T. Ihle. Kinetic theory of flocking: Derivation of hydrodynamic equations. *Physical Review E*, 83(3 AR 030901), 2011. (Cited on page 9.)

[24] T. Ihle. Invasion-wave induced first-order phase transition in systems of active particles. *eprint arXiv:1304.0149*, 2013. (Cited on page 10.)

[25] C. Lanczos. *Linear differential operators*. Van Nostrand, 1961. (Cited on pages 91 and 133.)

[26] L.D. Landau. *Collected papers of L.D. Landau. Edited and with an introduction by D. ter Haar*. Oxford, New York, Pergamon Press, 1965. (Cited on pages 24 and 25.)

[27] N.D. Mermin and H. Wagner. Absence of ferromagnetism or antiferromagnetism in one- or two-dimensional isotropic heisenberg models. *PRL*, 17(22):1133–1136, 1966. (Cited on page 5.)

[28] S. Mishra, A. Baskaran, and M.C. Marchetti. Fluctuations and pattern formation in self-propelled particles. *PRE*, 81(6):061916, 2010. (Cited on page 10.)

[29] M. Moussaid, D. Helbing, and G. Theraulaz. How simple rules determine pedestrian behavior and crowd disasters. *Proceedings of the National Academy of Sciences of the United States of America*, 108(17):6884–6888, 2011. (Cited on page 3.)

[30] S. Ramaswamy, R.A. Simha, and J. Toner. Active nematics on a substrate: Giant number fluctuations and long-time tails. *Europhysics Letters*, 62(2):196–202, 2003. (Cited on page 99.)

[31] P. Romanczuk and L. Schimansky-Geier. Mean-field theory of collective motion due to velocity alignment. *Ecological Complexity*, 10:83–92, 2012. (Cited on page 11.)

[32] V. Schaller, C. Weber, C. Semmrich, E. Frey, and A.R. Bausch. Polar patterns of driven filaments. *Nature*, 467(7311):73–77, 2010. (Cited on pages 3 and 35.)

[33] A. Sokolov and I.S. Aranson. Reduction of viscosity in suspension of swimming bacteria. *Physical Review Letters*, 103(14):148101, 2009. (Cited on pages 3 and 4.)

[34] A. Sokolov, R.E. Goldstein, F.I. Feldchtein, and I.S. Aranson. Enhanced mixing and spatial instability in concentrated bacterial suspensions. *Physical Review E*, 80(3):031903, 2009. (Cited on page 4.)

[35] J. Toner and Y.H. Tu. Long-range order in a 2-dimensional dynamical xy model - how birds fly together. *Physical Review Letters*, 75(23):4326–4329, 1995. (Cited on pages 5, 9, and 26.)

[36] J. Toner, Y.H. Tu, and S. Ramaswamy. Hydrodynamics and phases of flocks. *Annals of Physics*, 318(1):170–244, 2005. (Cited on pages 8, 9, and 75.)

[37] Y. Tu, J. Toner, and M. Ulm. Sound waves and the absence of galilean invariance in flocks. *PRL*, 80(21):4819–4822, 1998. (Cited on pages 7 and 35.)

[38] A.E. Turgut, H. Celikkanat, F. Gokce, and E. Sahin. Self-organized flocking in mobile robot swarms. *Swarm Intelligence*, 2(2-4):97–120, 2008. (Cited on page 3.)

[39] T. Vicsek, A. Czirok, E. Benjacob, I. Cohen, and O. Shochet. Novel type of phase-transition in a system of self-driven particles. *Physical Review Letters*, 75(6):1226–1229, 1995. (Cited on pages 3, 4, and 33.)

4 MIXED POLAR-NEMATIC MODEL

4.1 THE MICROSCOPIC MODEL

In this microscopic model introduced by Ginelli et al.[19], the considered point-like particles are still polar like the one used in the polar Vicsek model. However their interaction is nematic as explained in fig(24). If the angle of collision between particles is less than $\frac{\pi}{2}$, i.e. a head to tail collision, then the particles align polarly. If the angle of collision is greater that $\frac{\pi}{2}$, i.e. a head to head collision, then the particles align nematicaly.

In this case the classical Vicsek equations are modified to

$$\begin{aligned} x_i^{t+1} &= x_i^t + v_0 \mathrm{e}\left(\theta_i^{t+1}\right)\Delta t \\ \theta_i^{t+1} &= \arg\left[\sum_{j\in R} \mathrm{sign}\left[\cos\left(\theta_j^t - \theta_i^t\right)\right] e^{i\theta_j^t}\right] + \xi_i \end{aligned}$$

Where the summation is done on particles inside a radius R of the particle i, and $\xi_i \in \left[-\eta\frac{\pi}{2} : \eta\frac{\pi}{2}\right]$ is a delta-correlated white noise whose amplitude is controlled by the parameter $\eta \in [0:1]$.

The authors have found four different phases in this model, as presented on Fig(25). At low noise values (or at high values of density), the system has long range nematic order, Fig(25a). This order is characterized by two polar phases moving in opposite directions, with statistically the same number of particles in each phases. Both of these polar phases have long range order (at least at the system sizes studied by the authors), thus the whole nematic phase also has this non-equilibrium property. As predicted earlier by Toner et al.[36], the homogenous phase should exhibit giant number fluctuations with the fluctuations $\Delta n^2 = \left\langle (n - \langle n \rangle)^2 \right\rangle$ following a power law behavior $\Delta n \sim \langle n \rangle^1$. However the exponent observed in this simulations was

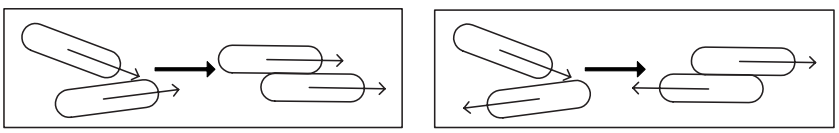

Figure 24: Rules of nematic collision for polar particles. In the case of a head-tail collision, the particles align polarly. In the case of a head-head collision, they align nematicaly. Note that the finite size of the particles is only for representation purpose, the particles in the model are point-like. Image from ref[19].

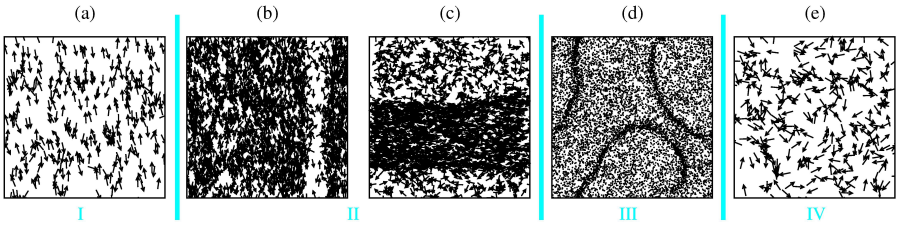

Figure 25: The four different phases observed in microscopic mixed polar-nematic model. (a) At low noise, a long-range nematic order exist. (b,c) At a higher noise, a disordered band appear which grow with increase of noise. (d) At a critical noise parameter this band destabilise, leading to a chaotic phase. The transition between phase II and III mark the order-disorder transition. (e) At even higher noise, the system become completely disordere. Figure from ref[19].

0.8. This exponent is identical to the one predicted by Toner. and Tu. for polar particles and observed in simulations[**?**] of the polar Vicsek model and is higher than the one for equilibrium systems equal to $1/2$.

At larger values of noise, a narrow band of isotropic particles appear as seen on Fig(25b). The band is oriented along the nematic order direction and is not traveling. As the noise is further increased this band becomes larger and larger as seen on Fig(25c). Contrary to the completely polar case, where many polar solitonic objects can be observed for large system sizes, in this model only one band is always observed independently of the system size. At some critical noise parameter this band destabilizes and breaks down leading to a chaotic state as seen on Fig(25d). This state is really chaotic, i.e. the total order parameter in the system goes to zero as the system size is increased. Thus a first order phase transition is present between this chaotic phase and the stable band phase. Finally at even higher noise, a completely disordered phase appears as seen on Fig(25e). No pure polar order was observed in this system.

In summary we can try to verify the following properties of the model using our approach with hydrodynamic equations:

1. There are four different phases present in the system; a long range nematicaly ordered phase, a stable nematic band phase, a chaotic band phase and an isotropic phase.

2. The transition between the second and the third phases, is discontinuous.

3. They are giant density fluctuations in the ordered nematic phase and inside the bands.

The last point can not be verified with our current equations, due to the lack of an effective noise term. The derivation of such a noise term is beyond the scope of this thesis.

4.2 DERIVATION OF HYDRODYNAMIC EQUATIONS

Next follows an article that includes; the derivation of hydrodynamic equations, the study of the stability of a homogenous solution and an analytical derivation of a non homogenous solution.

Nonlinear Field Equations for Aligning Self-Propelled Rods

Anton Peshkov,[1,2,3] Igor S. Aranson,[4,3] Eric Bertin,[5,3] Hugues Chaté,[1,2,3] and Francesco Ginelli[6]

[1]*Service de Physique de l'Etat Condensé, CEA-Saclay, URA 2464 CNRS, 91191 Gif-sur-Yvette, France*
[2]*LPTMC, CNRS-UMR 7600, Université Pierre et Marie Curie, 75252 Paris, France*
[3]*Max Planck Institute for the Physics of Complex Systems, Nöthnitzer Strasse 38, 01187 Dresden, Germany*
[4]*Materials Science Division, Argonne National Laboratory, 9700 South Cass Avenue, Argonne, Illinois 60439, USA*
[5]*Université de Lyon, Laboratoire de Physique, ENS Lyon, CNRS, 46 Allée d'Italie, 69007 Lyon, France*
[6]*Institute for Complex Systems and Mathematical Biology, King's College, University of Aberdeen, Aberdeen AB24 3UE, United Kingdom*

(Received 24 July 2012; published 27 December 2012)

We derive a set of minimal and well-behaved nonlinear field equations describing the collective properties of self-propelled rods from a simple microscopic starting point, the Vicsek model with nematic alignment. Analysis of their linear and nonlinear dynamics shows good agreement with the original microscopic model. In particular, we derive an explicit expression for density-segregated, banded solutions, allowing us to develop a more complete analytic picture of the problem at the nonlinear level.

DOI: 10.1103/PhysRevLett.109.268701 PACS numbers: 87.18.Gh, 05.65.+b, 45.70.Vn

Collective motion is a central theme in the rapidly growing field of active matter studies which loosely groups together all situations where energy is spent locally to produce coherent motion [1]. In spite of the emergence of better-controlled, larger-scale experiments [2–6], our understanding of collective motion mostly comes from the study of mathematical models, and particularly of models of "dry" active matter systems, where the fluid which surrounds the moving objects can be neglected.

Microscopic models, then, usually consist of interacting self-propelled particles, as in the Vicsek model [7], where constant-speed point particles locally align their velocities. Their study, together with some more theoretical approaches, revealed a wealth of phenomena such as true long-range orientational order in two dimensions, spontaneous segregation of dense and ordered regions, anomalously strong number fluctuations, etc. [8–10].

These results have given rise to an emerging picture of universality classes, typically depending on the symmetries involved, which one would ideally characterize by some coarse-grained field equations. Different routes can be followed to obtain such equations: one can write *a priori* all terms allowed by symmetries up to some arbitrary order in gradients once hydrodynamic fields have been identified. One can also derive them from some microscopic starting point under more or less controlled and constraining assumptions, yielding more or less complete, well-behaved equations. There is, nevertheless, shared belief, based mostly on renormalization-group approaches, that in each case there exists a set of minimal equations accounting for all large-scale physics.

For polar particles aligning ferromagnetically (as in the Vicsek model), there is now near consensus about this minimal set of equations: the phenomenological theory initially proposed by Toner and Tu [11] is essentially correct if one takes into account the dependencies of its coefficients on density and parameters initially overlooked but later derived from microscopic dynamics in Refs. [12,13]. It has been shown to reproduce many of the phenomena observed in microscopic models [14], although a complete study of its nonlinear solutions and dynamics is still lacking.

For the other important universality class of polar particles aligning *nematically*—e.g., self-propelled rods—the situation is less satisfactory: Baskaran and Marchetti [15] first derived rather lengthy yet mostly linear hydrodynamic equations for hard rods interacting via excluded volume, showing in particular the presence of global nematic, not polar, order, in agreement with microscopic observations [16]. Very recently [17], they added some nonlinear terms and performed a linear stability analysis of the homogeneous ordered state within an arbitrary choice of parameters. These even longer equations do not benefit from the same consensus as the Toner-Tu theory.

In this Letter, we derive a set of minimal nonlinear field equations describing the collective properties of self-propelled rods from a simple microscopic starting point, the Vicsek model with nematic alignment studied in Ref. [16]. We use a "Boltzmann-Ginzburg-Landau" approach, a controlled expansion scheme [18], which is a refined version of that used in Ref. [12]. Analysis of the solutions of these equations shows good agreement with the original microscopic model. In particular, we derive explicit expressions for density-segregated, banded solutions, allowing us to develop a more complete analytic picture of the problem at the nonlinear level.

In the Vicsek model with nematic alignment [16], point particles move off lattice at constant speed v_0. Orientations and positions are updated following (here in two dimensions):

 © 2012 American Physical Society

$$\theta_j^{t+1} = \arg\left[\sum_{k\sim j} \mathrm{sign}[\cos(\theta_k^t - \theta_j^t)]e^{i\theta_k^t}\right] + \eta_j^t, \quad (1)$$

$$\mathbf{r}_j^{t+1} = \mathbf{r}_j^t + v_0\mathbf{e}(\theta_j^{t+1}), \quad (2)$$

where $\mathbf{e}(\theta)$ is the unit vector along θ, the sum is taken over particles k within distance d_0 of particle j (including j itself), and η is a white noise with zero average and variance σ^2. Like all Vicsek-style models, it shows orientational order at large-enough global density ρ_0 and/or small-enough noise strength σ. It was shown in Ref. [16] that the order is nematic and that both the ordered and disordered phases are subdivided in two: The homogeneous nematic phase observed at low noise is replaced at larger σ values by a segregated phase where a dense, ordered band occupying a fraction of space coexists with a disordered, dilute, gas. The transition to disorder is given by the onset of a long-wavelength instability of this band leading to a chaotic regime where bands constantly form, elongate, meander, and disappear over very long time scales. At still larger σ values, a "microscopically disordered" phase is observed.

Following Ref. [12], we write, in a dilute limit where only binary interactions are considered and assuming that orientations are decorrelated between them ("molecular chaos hypothesis"), a Boltzmann equation governing the evolution of the one-particle distribution $f(\mathbf{r}, \theta, t)$:

$$\partial_t f(\mathbf{r}, \theta, t) + v_0\mathbf{e}(\theta)\cdot\nabla f(\mathbf{r}, \theta, t) = I_{\mathrm{dif}}[f] + I_{\mathrm{col}}[f], \quad (3)$$

with the angular diffusion and collision integrals

$$\begin{aligned} I_{\mathrm{dif}}[f] &= -\lambda f(\theta) + \lambda\int_{-\pi}^{\pi} d\theta' f(\theta') \\ &\quad\times\int_{-\infty}^{\infty} d\eta P_\sigma(\eta)\delta_{2\pi}(\theta' - \theta + \eta), \\ I_{\mathrm{col}}[f] &= -f(\theta)\int_{-\pi}^{\pi} d\theta' K(\theta', \theta) f(\theta') \\ &\quad+ \int_{-\pi}^{\pi} d\theta_1 f(\theta_1)\int_{-\pi}^{\pi} d\theta_2 K(\theta_1, \theta_2) f(\theta_2) \\ &\quad\times\int_{-\infty}^{\infty} d\eta P_\sigma(\eta)\delta_{2\pi}(\Psi(\theta_1, \theta_2) - \theta + \eta), \end{aligned} \quad (4)$$

where $P_\sigma(\eta)$ is the microscopic noise distribution, $\delta_{2\pi}$ is a generalized Dirac delta imposing that the argument is equal to zero modulo 2π, $K(\theta_1, \theta_2) = 2d_0 v_0|\mathbf{e}(\theta_1) - \mathbf{e}(\theta_2)|$ is the collision kernel for dilute gases [12], and $\Psi(\theta_1, \theta_2) = \frac{1}{2}(\theta_1 + \theta_2) + \frac{\pi}{2}[H[\cos(\theta_1 - \theta_2)] - 1]$ for $-\frac{\pi}{2} < \theta_2 - \theta_1 < \frac{3\pi}{2}$ [with $H(x)$ the Heaviside step function] codes for the nematic alignment. Rescaling of time, space, and density allows us to set the "collision surface" $S \equiv 2d_0 v_0/\lambda = 1$ and $v_0 = 1$ below, without loss of generality.

Next, the distribution function is expanded in the Fourier series of the angle: $f(\mathbf{r}, \theta, t) = \frac{1}{2\pi}\sum_{k=-\infty}^{\infty} f_k(\mathbf{r}, t)e^{-ik\theta}$, with $f_k = f_{-k}^*$ and $|f_k| \le f_0$. The zero mode is nothing but the local density, while f_1 and f_2 give access to the polar and nematic order parameter fields $\mathbf{P}$ and $\mathbf{Q}$:

$$\rho = f_0, \qquad \rho\mathbf{P} = \begin{pmatrix} \mathrm{Re} f_1 \\ \mathrm{Im} f_1 \end{pmatrix},$$
$$\rho\mathbf{Q} = \frac{1}{2}\begin{pmatrix} \mathrm{Re} f_2 & \mathrm{Im} f_2 \\ \mathrm{Im} f_2 & -\mathrm{Re} f_2 \end{pmatrix}. \quad (5)$$

As a matter of fact, it is convenient to use f_1 and f_2, together with the "complex" operators $\nabla \equiv \partial_x + i\partial_y$ and $\nabla^* \equiv \partial_x - i\partial_y$. The continuity equation governing ρ is given by integrating the Boltzmann equation over angles:

$$\partial_t\rho + \mathrm{Re}(\nabla^* f_1) = 0. \quad (6)$$

In Fourier space, the Boltzmann equation (3) yields an infinite hierarchy of equations:

$$\begin{aligned} &\partial_t f_k + \frac{1}{2}(\nabla f_{k-1} + \nabla^* f_{k+1}) \\ &\quad= (\hat{P}_k - 1)f_k + \frac{2}{\pi}\sum_{q=-\infty}^{\infty}\left[\hat{P}_k J_{kq} - \frac{4}{1-4q^2}\right] f_q f_{k-q}, \end{aligned} \quad (7)$$

where $\hat{P}_k = \int_{-\infty}^{\infty} d\eta P_\sigma(\eta)e^{ik\eta}$ and

$$\begin{aligned} J_{kq} &= \int_{-\pi/2}^{\pi/2} d\phi \left|\sin\frac{\phi}{2}\right| e^{i((k/2)-q)\phi} + \cos\frac{k\pi}{2} \\ &\quad\times\int_{\pi/2}^{3\pi/2} d\phi \left|\sin\frac{\phi}{2}\right| e^{i((k/2)-q)\phi}. \end{aligned} \quad (8)$$

To truncate and close this hierarchy, we adopt the following scaling structure, valid near onset of *nematic* order, assuming, in a Ginzburg-Landau-like approach [18], small and slow variations of the density and of the polar and nematic fields:

$$\rho - \rho_0 \sim \epsilon, \quad \{f_{2k-1}, f_{2k}\}_{k\ge1} \sim \epsilon^k, \quad \nabla \sim \epsilon, \quad \partial_t \sim \epsilon. \quad (9)$$

Note that the scaling of space and time is in line with the propagative structure of our system, as seen in the continuity equation (6), which contains no diffusion term.

The first nontrivial order yielding well-behaved equations is ϵ^3: keeping only terms up to this order, equations for $f_{k>4}$ identically vanish, while those for f_3 and f_4 provide expressions of these quantities in terms of ρ, f_1, and f_2, which allows us to write the closed equations:

$$\begin{aligned} \partial_t f_1 &= -\frac{1}{2}(\nabla\rho + \nabla^* f_2) + \frac{\gamma}{2} f_2^* \nabla f_2 \\ &\quad- (\alpha - \beta|f_2|^2)f_1 + \zeta f_1^* f_2, \end{aligned} \quad (10)$$

$$\begin{aligned} \partial_t f_2 &= -\frac{1}{2}\nabla f_1 + \frac{\nu}{4}\nabla^2 f_2 - \frac{\kappa}{2} f_1^* \nabla f_2 - \frac{\chi}{2}\nabla^*(f_1 f_2) \\ &\quad+ (\mu - \xi|f_2|^2)f_2 + \omega f_1^2 + \tau|f_1|^2 f_2, \end{aligned} \quad (11)$$

where all coefficients depend only on the noise strength σ (via the $\hat{P}_k$ coefficients) and the local density ρ:

$$\nu = \left[\frac{136}{35\pi}\rho + 1 - \hat{P}_3\right]^{-1} \qquad \omega = \frac{8}{\pi}\left[\frac{1}{6} - \frac{\sqrt{2}-1}{2}\hat{P}_2\right]$$
$$\mu = \frac{8}{\pi}\left[\frac{2\sqrt{2}-1}{3}\hat{P}_2 - \frac{7}{5}\right]\rho - 1 + \hat{P}_2 \qquad \zeta = \frac{8}{5\pi}$$
$$\alpha = \frac{8}{\pi}\left[\frac{1}{3} - \frac{1}{4}\hat{P}_1\right]\rho + 1 - \hat{P}_1 \qquad \chi = \nu\frac{2}{\pi}\left[\frac{4}{5} + \hat{P}_3\right]$$
$$\kappa = \nu\frac{8}{15}\left[\frac{19}{7} - \frac{\sqrt{2}+1}{\pi}\hat{P}_2\right] \qquad \gamma = \nu\frac{4}{3\pi}\left[\hat{P}_1 - \frac{2}{7}\right]$$
$$\tau = \chi\frac{8}{15}\left[\frac{19}{7} - \frac{\sqrt{2}+1}{\pi}\hat{P}_2\right] \qquad \beta = \gamma\frac{2}{\pi}\left[\frac{4}{5} + \hat{P}_3\right]$$
$$\xi = \frac{32}{35\pi}\left[\frac{1}{15} + \hat{P}_4\right]\left[\frac{13}{9} - \frac{6\sqrt{2}+1}{\pi}\hat{P}_2\right] \times \left[\frac{8}{3\pi}\left(\frac{31}{21} + \frac{\hat{P}_4}{5}\right)\rho + 1 - \hat{P}_4\right]^{-1}. \tag{12}$$

Below, for convenience, we choose the Gaussian noise distribution $P_\sigma(\eta) = \frac{1}{\sigma\sqrt{2\pi}}\exp[-\frac{\eta^2}{2\sigma^2}]$ for which $\hat{P}_k = \exp[-\frac{1}{2}k^2\sigma^2]$ [19]. A few remarks are, then, in order. First, μ can change sign and become positive for large enough ρ, while α is always positive. The homogeneous disordered state ($f_1 = f_2 = 0$) undergoes an instability to nematic order when $\mu = 0$, defining the basic transition line $\sigma_t(\rho_0)$ in the (ρ_0, σ) plane [Fig. 1(a)]. Next, ξ being positive in the $\mu > 0$ region where the disordered solution is unstable, Eqs. (10) and (11) possess a homogeneous nematically ordered solution $(f_1, f_2) = (0, \sqrt{\mu/\xi})$ (assuming order along $\mathbf{x}$, so that f_2 is real positive) [20]. The nonlinear terms express the complicated relation between the polar and nematic fields, which are both slow modes. In particular, nonlinearities in Eq. (10) do depend on f_2 and prevent the trivial exponential decay of f_1, as predicted by linear theories [17], which would result in active nematic field equations [9]. On the other hand, the familiar nonlinearities of the Toner-Tu theory for polar systems may only be recovered if f_2 would get enslaved to f_1 [12], which is not possible in a system with nematic interactions where $\mu > 0$.

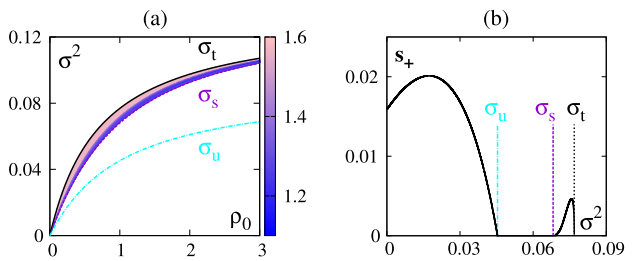

FIG. 1 (color online). (a) Linear stability of homogeneous solutions in the (ρ_0, σ) plane (plotted as a function of σ^2 to enhance clarity). The line $\rho = \frac{15\pi(\hat{P}_2-1)}{40\hat{P}_2(2\sqrt{2}-1)-64}$, given by $\mu = 0$, is the basic instability line defining $\rho_t(\sigma)$ or $\sigma_t(\rho_0)$: above it, the disordered homogeneous solution is linearly stable; below, it becomes unstable and the ordered solution $f_2 = \sqrt{\mu/\xi}$ exists. This solution is unstable between the σ_t and the σ_s lines. It is linearly stable between σ_s, and σ_u, which marks the border of a region where $q = 0$ is the most unstable mode. The color scale codes for the angle between the most unstable wave vector and the direction of nematic order. (b) Largest eigenvalue s_+ (when positive) as a function of σ^2 for $\rho_0 = 1$.

In the following, we further expand coefficients up to ϵ^3 in $\rho - \rho_0$, which amounts to keeping the crucial ρ dependence in μ and α and replacing ρ by ρ_0 in all other coefficients. This does not change any of our main results, but allows us to find exact band solutions (see below).

We have studied the linear stability of the homogeneous nematic solution with respect to perturbations of an arbitrary wave vector in the full (ρ_0, σ) parameter plane (Fig. 1). Similar to the polar case with ferromagnetic alignment [12–14,21], this solution is unstable to long wavelengths in a region bordering the basic transition line. The most unstable modes in this region are roughly—but not exactly—transversal to the order of the solution [22]. The homogeneous nematic solution becomes linearly stable deeper in the ordered phase [line σ_s in Fig. 1(a)], but its stability domain is limited by another instability region where $q = 0$ is the most unstable mode (line σ_u, which can be shown to be given by $\alpha + \zeta\sqrt{\mu/\xi} - \beta\mu/\xi = 0$). This strong instability, which occurs at large densities and/or weak noise, may be an artifact introduced by our truncation [24].

To go beyond the linear stability analysis of spatially homogeneous solutions, we performed numerical integrations of Eqs. (6), (10), and (11) in rectangular domains with periodic boundary conditions of typical linear sizes 50–200 [25]. For parameter values in the instability region of the nematic homogeneous solution, we observe stationary asymptotic solutions in which nematic order is confined to and oriented along a dense band with local density ρ_{band} amidst a homogeneous disordered "gas" with ρ_{gas} such that $\rho_{\text{band}} > \rho_s > \rho_t > \rho_{\text{gas}}$ [Fig. 2(a)], where $\rho_s(\sigma)$ is given by inverting $\sigma_s(\rho_0)$. Varying system size and using various domain aspect ratios, we find most often a single band oriented along the shortest dimension of the domain, which occupies a size-independent fraction Ω of space. All these observations are in agreement with the behavior of the original microscopic model [16].

Band solutions are also present *beyond* the region of instability of the homogeneous ordered state. Starting from, e.g., sufficiently inhomogeneous initial conditions, we find band solutions both for ρ_0 values larger than ρ_s, where they coexist with the homogeneous ordered phase, and below ρ_t, where the disordered homogeneous solution is linearly stable. Working at fixed ρ_0 varying σ for clarity, we thus find bands in a $[\sigma_{\min}, \sigma_{\max}]$ interval larger than the linear-instability interval $[\sigma_s, \sigma_t]$ (Fig. 3). Along it, the fraction occupied by the ordered band decreases from $\Omega \lesssim 1$ near $\sigma_{\min}$ to $\Omega \gtrsim 0$ near $\sigma_{\max}$. Furthermore, within a small layer $\sigma_{\max} < \sigma \leq \sigma_c$, the bands are unstable, giving rise to a chaotic regime where they twist, elongate, break, and form again, in a manner strikingly similar to

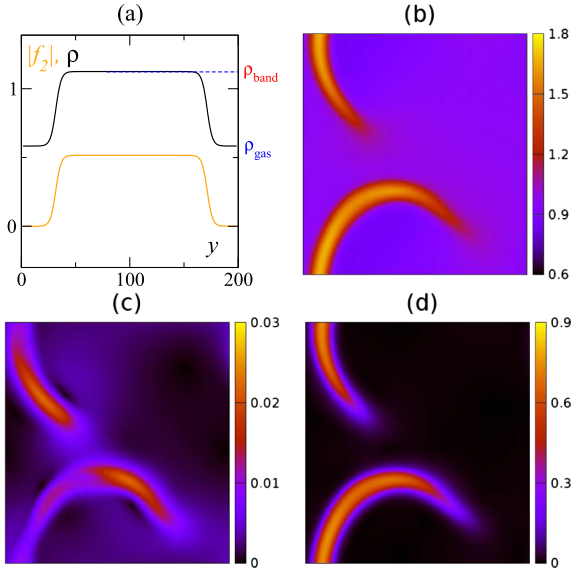

FIG. 2 (color online). Numerically obtained density-segregated solutions. (a) density and f_2 profiles of a stationary banded solution ($f_1 = 0$ throughout). The fronts linking the disordered and ordered domains can be perfectly fitted to hyperbolic tangents (not shown). ($\sigma = 0.26$, $\rho_0 = 1$, $L = 100$) (b, c, d) chaotic band regime: snapshots of (respectively) ρ, $|f_1|$, and $|f_2|$. ($\sigma = 0.2826$, $\rho_0 = 1$, $L = 200$).

observations made in the original microscopic model (Figs. 2(b)–2(d), [26]).

Thus the region of linear instability of the homogeneous ordered solution does *not* correspond to the existence (and stability) domain of band solutions, which is wider. In the original microscopic model, with its built-in fluctuations, coexistence of band solutions and homogeneous order has not been reported, but the homogeneous solution was found metastable near the threshold of emergence of bands where these appear "suddenly" [16]. At the other end of the band existence region, no coexistence was reported between band solutions and the homogeneous disordered state, suggesting that the latter is always driven to the former by intrinsic fluctuations. All this suggests that transitions found in the microscopic model do *not* correspond to the linear stability limits of homogeneous solutions of our *deterministic* continuous equations, pointing to a subcritical bifurcation scenario.

We now derive band solutions analytically. Suppose that, as observed, $f_1 = 0$ for band solutions and that f_2 is real and positive (i.e., nematic order is along x), and depends only on y. For a stationary solution, Eq. (10) then yields, after integration over y,

$$\rho - f_2 - \frac{1}{2}\gamma f_2^2 = \tilde{\rho}, \tag{13}$$

where $\tilde{\rho}$ is a constant. This allows us to write Eq. (11), again looking for stationary solutions, in terms of f_2 only:

$$\frac{\nu}{4}\partial_{yy} f_2 = -\mu' f_2(\tilde{\rho} - \rho_t + f_2) + \left[\xi - \frac{\gamma}{2}\mu'\right] f_2^3, \tag{14}$$

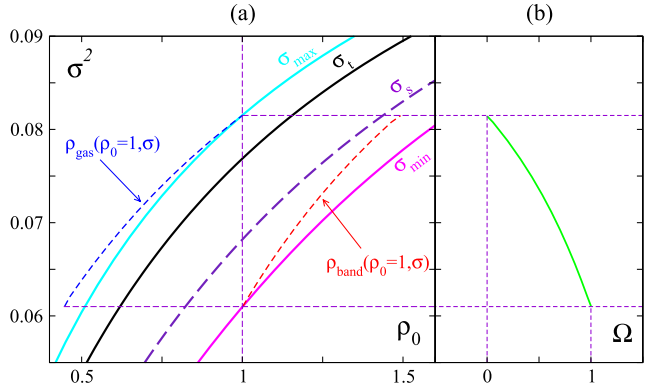

FIG. 3 (color online). Analytic band solutions for the slightly simplified system (see text). (a) (ρ_0, σ) parameter plane with basic instability line σ_t, stability limit of homogeneous ordered phase σ_s, and limits of existence of band solutions $\sigma_{\min}$ and $\sigma_{\max}$. The short-dashed blue and red lines show the ρ_{gas} and ρ_{band} density values of the band solutions for $\rho_0 = 1$ as a function of σ over their existence range [$\sigma_{\min}$, $\sigma_{\max}$], indicated by the thin horizontal dashed violet lines. (b) variation with σ of Ω, the fraction of space occupied by the ordered part of the band solution, for $\rho_0 = 1$.

where we have rewritten $\mu = \mu'(\rho - \rho_t)$, with μ' independent of ρ. Direct integration of Eq. (14) yields, under the condition $\lim_{y\to\pm\infty} f_2(y) = 0$, the following solution

$$f_2(y) = \frac{3(\rho_t - \tilde{\rho})}{1 + a\cosh(2y\sqrt{\mu'(\rho_t - \tilde{\rho})/\nu})}, \tag{15}$$

where $a = \sqrt{1 + 9b(\tilde{\rho} - \rho_t)/2\mu'}$ and $b = \xi - \mu'\gamma/2$. The value of $\tilde{\rho}$ can be obtained from the condition $\int_L \rho(y)dy = L\rho_0$, where L is the size of the box. We can neglect the exponentially decreasing tails in the integral and solve the equation $\int_{-\infty}^{\infty}[\rho(y) - \tilde{\rho}]dy = L(\rho_0 - \tilde{\rho})$. Under the assumption $L \to \infty$ we obtain

$$\tilde{\rho} \approx \rho_t - \frac{2\mu'}{9b}(1 - K_1 e^{-K_2 L}), \tag{16}$$

where K_1 and K_2 are positive quantities depending on σ and ρ_0 whose expression we omit for compactness. Substituting this value in the expression of a gives us $a = K_1 e^{-K_2 L/2}$, yielding a width of the band proportional to L, in agreement with observations on the microscopic model. As $L \to \infty$, the value of $\tilde{\rho}$ converges to the asymptotic value $\tilde{\rho}_{\text{gas}}$.

To determine the surface fraction Ω occupied by the ordered band, we use the relation $\Omega(\rho_{\text{band}} - \rho_{\text{gas}}) + \rho_{\text{gas}} = \rho_0$. Substituting the value of ρ_{band} obtained from Eqs. (13) and (15) at $y = 0$, we find for $L \to \infty$

$$\Omega = \frac{9b^2(\rho_0 - \rho_t) + 2b\mu'}{2\mu'(\gamma\mu' + 3b)}. \tag{17}$$

The condition $0 < \Omega < 1$ yields the lower limit $\sigma_{\min}$ and the upper limit $\sigma_{\max}$ of existence of the band solution.

Its stability will be analyzed in a forthcoming paper [27]. All these results are presented in Fig. 3.

To summarize, using a "Boltzmann-Ginzburg-Landau" controlled expansion scheme, we derived a set of minimal yet complete nonlinear field equations from the Vicsek model with nematic alignment studied in Ref. [16]. This simple setting allowed for a comprehensive analysis of the linear and nonlinear dynamics of the field equations obtained because our approach automatically yields a "meaningful manifold" parametrized by global density and noise strength in the high-dimensional space spanned by all coefficients of the continuous equations. Excellent agreement was found (at a qualitative level) with the simulations of the original microscopic model. The banded solutions were studied analytically. Their existence domain was found different from the region of linear instability of the homogeneous ordered phase, stressing the importance of a nonlinear analysis. More work, beyond the scope of this Letter, is needed to obtain a better understanding of the chaotic regimes observed. To this aim, we plan to study the linear stability of the band solutions in two dimensions.

Our equations (10) and (11) are simpler than those written by Baskaran and Marchetti in Refs. [15,17], not only because our microscopic starting point does not include positional diffusion of particles. The method used there seems intrinsically different, yielding more terms, many with a different structure from ours, while some of our nonlinear ones do not appear. It is not known yet whether the equations of Ref. [17] can also account for the nonlinear phenomena described above. Future work should explore this point in some detail.

Finally, experiments showed that microtubules displaced by a "carpet" of dynein motors move collectively and form large vortical structures [6]. It was shown that a Vicsek model with nematic alignment, but one in which the microscopic noise is colored, accounts quantitatively for the observed phenomena. Extending the approach followed here to this case is the subject of ongoing work.

We thank the Max Planck Institute for the Physics of Complex Systems, Dresden, for providing the framework of the Advanced Study Group "Statistical Physics of Collective Motion" within which much of this work was conducted. The work of I. S. A. was supported by the U.S. Department of Energy, Office of Basic Energy Sciences, Division of Materials Science and Engineering, under Contract No. DEAC02-06CH11357.

[1] S. Ramaswamy, Annu. Rev. Condens. Matter Phys. **1**, 323 (2010).

[2] J. Deseigne, O. Dauchot, and H. Chaté, Phys. Rev. Lett. **105**, 098001 (2010); J. Deseigne, S. Léonard, O. Dauchot, and H. Chaté, Soft Matter **8**, 5629 (2012).

[3] V. Schaller, C. Weber, C. Semmrich, E. Frey, and A. R. Bausch, Nature (London) **467**, 73 (2010); V. Schaller, C. Weber, E. Frey, and A. R. Bausch, Soft Matter **7**, 3213 (2011); V. Schaller, C. A. Weber, B. Hammerich, E. Frey, and A. R. Bausch, Proc. Natl. Acad. Sci. U.S.A. **108**, 19 183 (2011).

[4] H. P. Zhang, A. Béer, E. L. Florin, and H. L. Swinney, Proc. Natl. Acad. Sci. U.S.A. **107**, 13 626 (2010); X. Chen, X. Dong, A. Beer, H. L. Swinney, and H. P. Zhang, Phys. Rev. Lett. **108**, 148101 (2012).

[5] A. Sokolov, I. S. Aranson, J. O. Kessler, and R. E. Goldstein, Phys. Rev. Lett. **98**, 158102 (2007).

[6] Y. Sumino, K. H. Nagai, Y. Shitaka, D. Tanaka, K. Yoshikaw, H. Chaté, and K. Oiwa, Nature (London) **483**, 448 (2012).

[7] T. Vicsek, A. Czirok, E. Ben-Jacob, I. Cohen, and O. Shochet, Phys. Rev. Lett. **75**, 1226 (1995).

[8] J. Toner, Y. Tu, and S. Ramaswamy, Ann. Phys. (Amsterdam) **318**, 170 (2005).

[9] S. Ramaswamy, R. A. Simha, and J. Toner, Europhys. Lett. **62**, 196 (2003); S. Mishra and S. Ramaswamy, Phys. Rev. Lett. **97**, 090602 (2006); H. Chaté, F. Ginelli, and R. Montagne, Phys. Rev. Lett. **96**, 180602 (2006).

[10] H. Chaté, F. Ginelli, G. Grégoire, and F. Raynaud, Phys. Rev. E **77**, 046113 (2008); G. Grégoire and H. Chaté, Phys. Rev. Lett. **92**, 025702 (2004).

[11] J. Toner, and Y. Tu, Phys. Rev. Lett. **75**, 4326 (1995); Phys. Rev. E **58**, 4828 (1998); J. Toner, Phys. Rev. E **86**, 031918 (2012).

[12] E. Bertin, M. Droz, and G. Grégoire, Phys. Rev. E **74**, 022101 (2006); J. Phys. A **42**, 445001 (2009).

[13] T. Ihle, Phys. Rev. E **83**, 030901 (2011).

[14] S. Mishra, A. Baskaran, and M. C. Marchetti, Phys. Rev. E **81**, 061916 (2010).

[15] A. Baskaran and M. C. Marchetti, Phys. Rev. E **77**, 011920 (2008); Phys. Rev. Lett. **101**, 268101 (2008).

[16] F. Ginelli, F. Peruani, M. Bär, and H. Chaté, Phys. Rev. Lett. **104**, 184502 (2010).

[17] A. Baskaran and M. C. Marchetti, Eur. Phys. J. E **35**, 95 (2012).

[18] I. S. Aranson and L. S. Tsimring, Phys. Rev. E **71**, 050901 (2005); **74**, 031915 (2006).

[19] For Gaussian noise, and other unimodal, centered noise distributions, most of the coefficients above do not change sign and are positive in the parameter region of interest.

[20] Other homogeneous solutions with both f_1 and f_2 nonzero exist, but they are not observed in simulations, being either unphysical (having a modulus larger than f_0) and/or unstable.

[21] A. Gopinath, M. F. Hagan, M. C. Marchetti, and A. Baskaran, Phys. Rev. E **85**, 061903 (2011).

[22] This near-threshold instability is generically present in all dry active matter systems with metric interactions. See, e.g., Refs. [21,23].

[23] A. Peshkov, S. Ngo, E. Bertin, H. Chaté, and F. Ginelli, Phys. Rev. Lett. **109**, 098101 (2012).

[24] Simulations of Eqs. (6), (10), and (11) in this region lead to unbounded growth, whereas the original Vicsek model with nematic alignment shows no sign of instability.

[25] We used a pseudospectral code with Euler time stepping ($\Delta t = 0.01$), with at least 400×400 Fourier modes on square domains of linear size $L = 200$.

[26] Compare with Fig. 2(d) of Ref. [16]. See Supplemental Material at http://link.aps.org/supplemental/10.1103/PhysRevLett.109.268701 for a movie, and compare with Supplemental Material movie of Ref. [16].

[27] A. Peshkov *et al.* (to be published).

4.3 NUMERICAL SIMULATIONS

As the nematic order in this system is perpendicular to the variation of the nematic order parameter, there is no point in studying this system in one dimension. Only two dimensional studies are those performed.

I simulate the equation using the pseudo-spectral code used for all the other simulations. I typically used a time step of $\Delta t = 0.05$ and a spatial step of $\Delta x = 0.25$.

At small sizes of the system all the four states reported in the microscopic simulations where observed as shown on Fig(26). However we would expect that as the system size is increased the region, in the noise parameter σ, of the chaotic solution will become smaller and smaller. This correspond to the case when the critical width of the band that would be stabilised is fixed. Or for a fixed σ, the width of the band increase with the system size, thus the chaotic region will become smaller. However this is not what I have found. While increasing the noise the chaotic region becomes bigger. Moreover, at lower values of noise, even if the band is never completely destroyed, the border of the band are always chaotic at large enough size system sizes as shown on Fig(27).

To better study this effect, we measure the mean difference between density fields at a time interval τ

$$\langle \Delta\rho \rangle_\tau (t) = \int\int \text{abs}\left(\rho(x, y, t+\tau) - \rho\left(x, y, t\right)\right) dxdy$$

The time evolution of $\langle \Delta\rho \rangle_\tau$ is studied for various noise parameters at different system sizes. The simulation is started with the analytical band solution as obtained in equations(13,15) in the article. This solution is perturbed with a random conserving noise on the density of amplitude $1E-3$.

In all cases the mean density is $\rho_0 = 1$. At this density the critical parameters are the minimum noise for the band $\sigma_{min} \approx 0.247$, the transition noise $\sigma_t \approx 0.277$ and the maximum noise for the band $\sigma_{max} \approx 0.286$. As can be seen on Figures(29,29), the parameter $\langle \Delta\rho \rangle_\tau$ can have three different behaviors as a function of time. First the band can decay to a homogeneous solution, which will be isotropic if the noise is bigger than σ_t or ordered if the noise is lower than σ_t. The second case, observed at high values of noise, is that $\langle \Delta\rho \rangle_\tau$ increases to some high values, after which it chaotically oscillate around this value indicating a completely chaotic solution. Finally the last case, is when $\langle \Delta\rho \rangle_\tau$ increase to lower values indicating a not completely destructed band solution with oscillating borders. We can see that in this case at initial times $\langle \Delta\rho \rangle_\tau$ is periodically oscillating, however at very long times the periodic oscillations always transform into a chaotic oscillation of the borders. Sometimes the chaotically oscillat-

Figure 26: The four different phases observed in simulation of hydrodynamic equations. Compare this image with Fig 25 on page 76. Obtained for $L = 200 \times 200$, $\rho_0 = 1$ and different noise values.

ing band can transform into a completely chaotic solution at big sizes of the system as seen on Fig(29).

It is also interesting to investigate if the critical value σ_t plays any particular role in the type of the instability, i.e. if for $\sigma > \sigma_t$ the solution is always completely chaotic and for $\sigma < \sigma_t$ the band always persist. To this end I simulate a very big system size $L = 2000 \times 2000$ at a noise value above $\sigma = 0.278$ and below $\sigma = 0.275$ the critical value $\sigma_t \approx 0.277$. As we see on Fig(30) both solutions transform into a completely chaotic one. Thus the nature of the instability is independent of the the "critical" noise value.

As the system size increases we have seen than there is no stable non homogeneous solutions anymore. Going back to microscopic simulations, it was found in our group, that for larger system sizes the bands that at small sizes was supposed to be stable, also exhibited oscillations at the borders. Thus our hydrodynamics equations are able to predict a behavior not previously found in microscopic simulations.

4.4 STABILITY OF THE BAND SOLUTION

4.4.1 *Analytical investigation*

As we have seen in numerical simulations, the band solution is unstable in large enough systems. Depending on the noise value and system size, the band is completely destroyed for noise near σ_{max} or is kept alive but have fluctuating borders for σ near σ_{min}. This is due to the finite size of the instability, which is insufficient to destroy the band in low noise regimes, where the band is very large.

As we have the analytical form of the band solution we can try to investigate its linear stability.

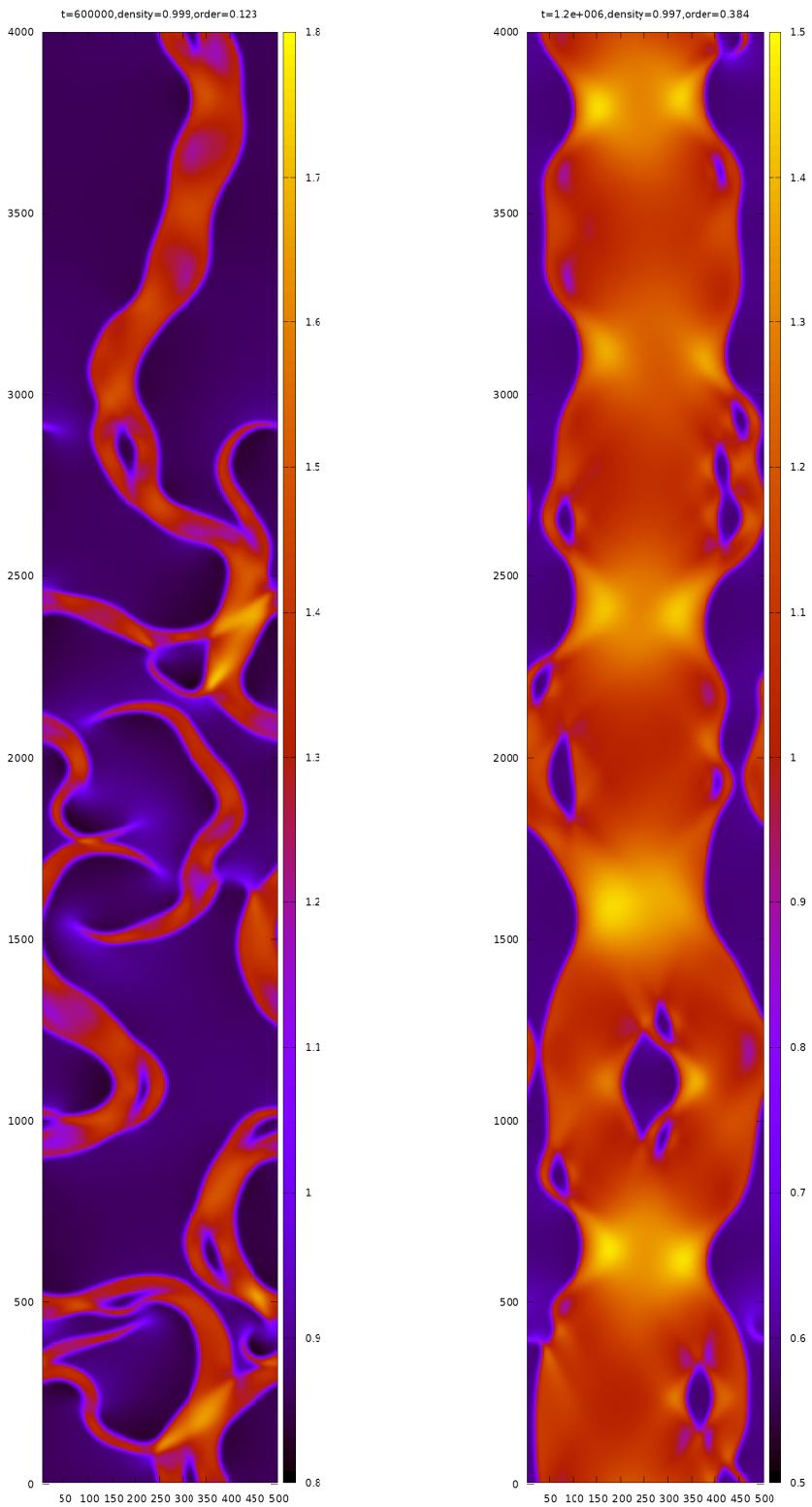

Figure 27: Density field comparison of two chaotic solutions in the mixed case. Both are obtained for $L = 4000 \times 500$ and $\rho_0 = 1$ from a perturbed band solution. On the left a completely chaotic solution obtained for $\sigma^2 = 0.278$ at time $T = 6E5$. On the right, while the border are chaotic, the band solution survives, for $\sigma^2 = 0.26$ at time $T = 1.2E6$.

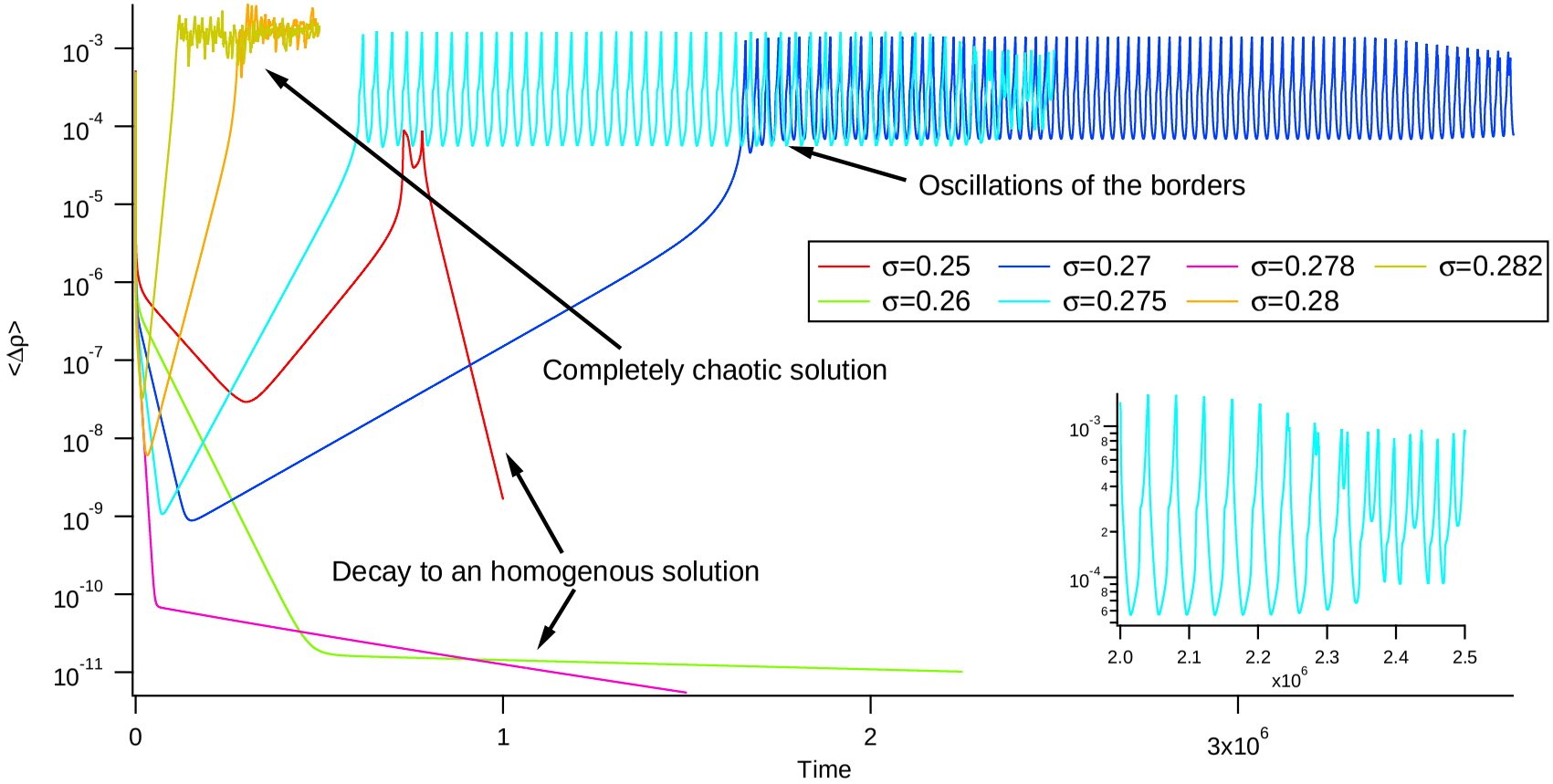

Figure 28: Study of the time series of $\langle \Delta\rho \rangle_\tau$ at $L = 400 \times 400$. The difference is recorded at time intervals $\tau = 40$. At high values of noise ($\sigma = (0.282, 0.28)$) the solution converges to a completely chaotic one. At a lower noise values ($\sigma = (0.282, 0.275)$) a band persists, but its borders are unstable. Initially, the instability of the borders is oscillating, but at later times it becomes chaotic. The inset shows the transformation from a periodic to a chaotic instability of the border at $\sigma = 0.275$. Finally at low noise values ($\sigma = (0.26, 0.25)$) the solution decays to a homogeneous ordered solution. Note that at the value of noise $\sigma = 0.278$ the solution decayed to an isotropic disordered one, because this value of noise is bigger than $\sigma_t \approx 0.277$.

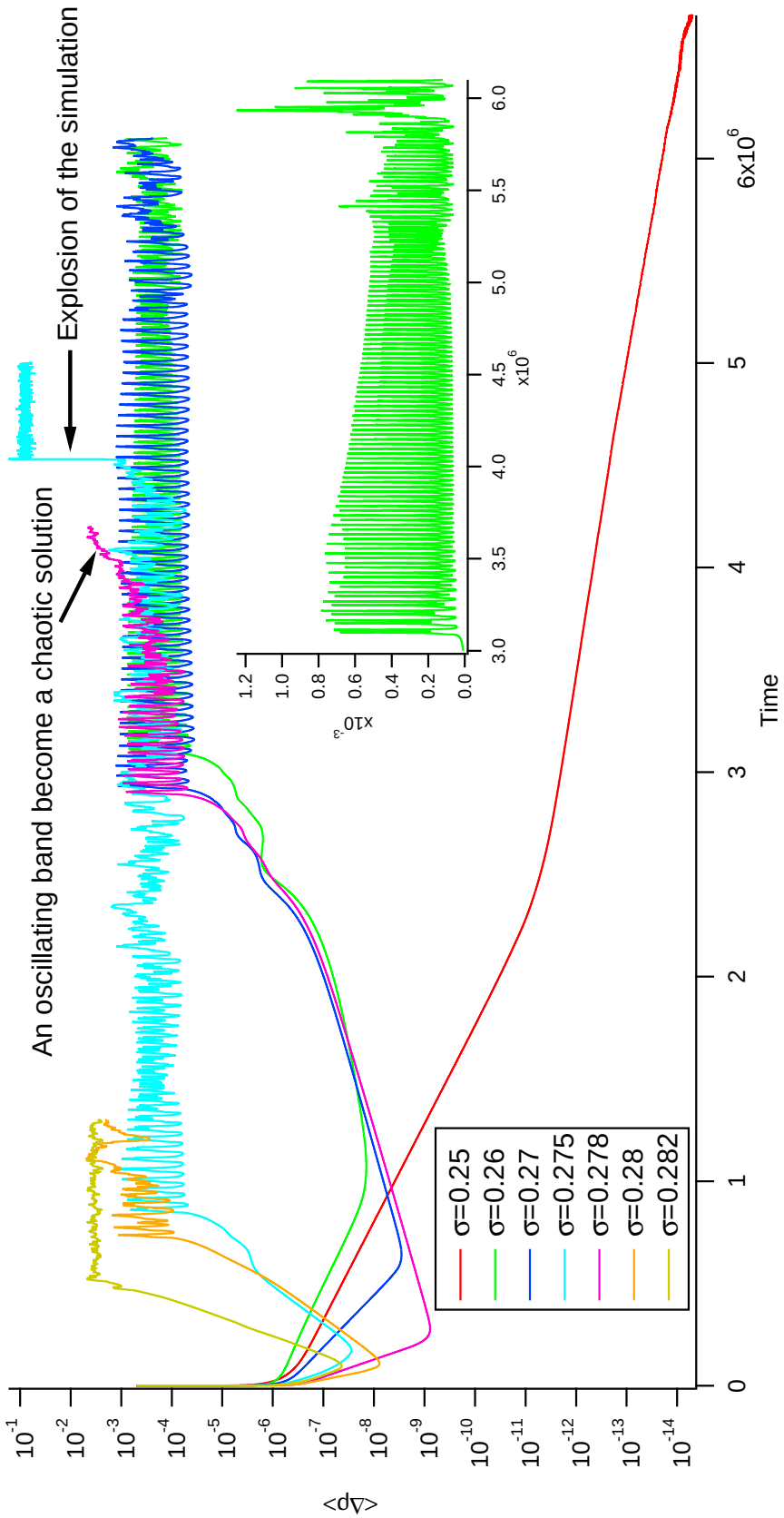

Figure 29: Study of the time series of $\langle \Delta\rho \rangle_\tau$ at $L = 1000 \times 1000$. The difference is recorded at time intervals $\tau = 100$. At high values of noise ($\sigma = (0.282, 0.28)$) the solution converges to a completely chaotic one. At a lower noise values ($\sigma = (0.278, 0.275)$) a band with oscillating borders exists initially, but transforms into a completely chaotic one after some time. Note that at $\sigma = 0.275$ the simulation explodes during this transformation, due to the numerical stiffness of our equations. At a lower noise values ($\sigma = (0.27, 0.26)$) a band persists, but its borders are unstable. The inset shows the transformation from a periodic to a chaotic instability of the border at $\sigma = 0.27$. Finally at low noise value $\sigma = 0.25$ the solution decays to a homogeneous ordered solution.

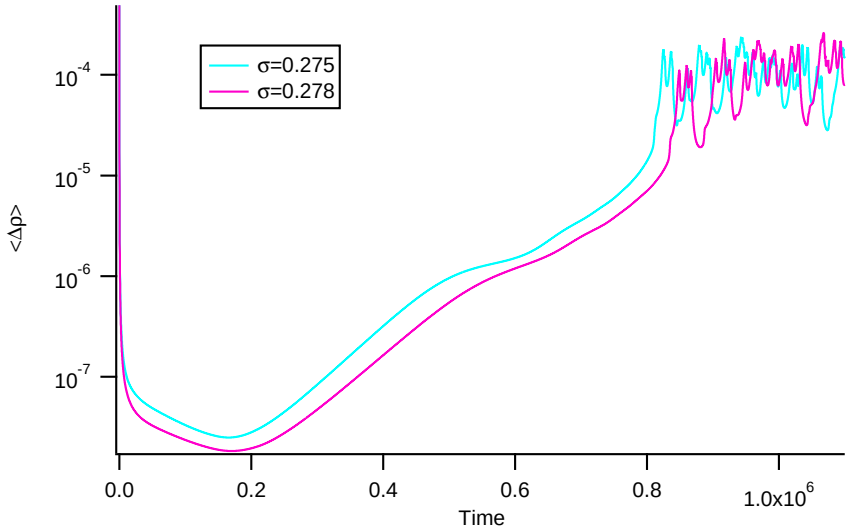

Figure 30: Study of the time series of $\langle \Delta\rho \rangle_\tau$ at $L = 2000 \times 2000$. The difference between the means is recorded at time interval $\tau = 100$. We see that both at a noise above and below the transition noise $\sigma_t \approx 0.277$ the final obtained solution is the completely chaotic one.

We start with the generic equations (6,10,11 in the article)

$$
\begin{aligned}
\partial_t \rho &= -\Re(\nabla^* f_1) \\
\partial_t f_1 &= -\frac{1}{2}\nabla\rho - \frac{1}{2}\nabla^* f_2 - \left(\alpha - \beta|f_2|^2\right) f_1 + \frac{\gamma}{2} f_2^* \nabla f_2 t + \zeta f_1^* f_2 \\
\partial_t f_2 &= -\frac{1}{2}\nabla f_1 + \frac{\nu}{4}\Delta f_2 + (\mu - \xi|f_2|^2) f_2 \\
&\quad -\frac{\kappa}{2} f_1^* \nabla f_2 - \frac{\chi}{2}\nabla^*(f_1 f_2) + \omega f_1^2 + \tau |f_1|^2 f_2
\end{aligned}
$$

As in the derivation of the band solution, we will suppose that the nematic order is oriented along the $\vec{x}$ axis, thus the band solution will vary along the y direction. We will search for an instability along the x direction which, if found, is sufficient to prove that the band is unstable. We thus use the following ansatz

$$
\begin{aligned}
\rho\,(x,y,t) &= \rho\,(y) + \delta\rho\,(y)\, e^{ikx+\lambda t} \\
f_1^{(R)}\,(x,y,t) &= \delta p^{(R)}\,(y)\, e^{ikx+\lambda t} \\
f_1^{(I)}\,(x,y,t) &= \delta p^{(I)}\,(y)\, e^{ikx+\lambda t} \\
f_2^{(R)}\,(x,y,t) &= f\,(y) + \delta n^{(R)}\,(y)\, e^{ikx+\lambda t} \\
f_2^{(I)}\,(x,y,t) &= \delta n^{(I)}\,(y)\, e^{ikx+\lambda t}
\end{aligned}
$$

Where $\rho\,(y)$ and $f\,(y)$ are the band solutions corresponding to equations(13,15) in the article. We also expand the coefficient $\mu =$

$\mu'(\rho - \rho_t)$. Substituting this ansatz into our equations and limiting them into first order in perturbations we obtain

$$\begin{aligned}
\lambda\delta\rho &= -(ik\delta p^{(R)} + \partial_y \delta p^{(I)}) \qquad (14)\\
\lambda\delta p^{(R)} &= -\left(\alpha - \beta f^2\right)\delta p^{(R)} - \frac{1}{2}ik\delta\rho - \frac{1}{2}(ik\delta n^{(R)} + \partial_y \delta n^{(I)})\\
&\quad +\zeta f \delta p^{(R)} + \frac{1}{2}\gamma\left[f\left(ik\delta n^{(R)} - \partial_y \delta n^{(I)}\right) + \delta n^{(I)}\partial_y f\right]\\
\lambda\delta p^{(I)} &= -\left(\alpha - \beta f^2\right)\delta p^{(I)} - \frac{1}{2}\partial_y\delta\rho - \frac{1}{2}(ik\delta n^{(I)} - \partial_y \delta n^{(R)})\\
&\quad -\zeta f \delta p^{(I)} + \frac{1}{2}\gamma\left[f\left(ik\delta n^{(I)} + \partial_y \delta n^{(R)}\right) + \delta n^{(R)}\partial_y f\right]\\
\lambda\delta n^{(R)} &= (\mu'\rho_t - 3\xi f^2)\delta n^{(R)} + \mu'\rho\delta n^{(R)} + \mu'\delta\rho f\\
&\quad -\frac{1}{2}(ik\delta p^{(R)} - \partial_y \delta p^{(I)}) + \frac{\nu}{4}(\partial_y^2 \delta n^{(R)} - k^2\delta n^{(R)}) - \frac{\chi}{2}f(ik\delta p^{(R)} + \partial_y \delta p^{(I)})\\
\lambda\delta n^{(I)} &= (\mu'\rho_t - \xi f^2)\delta n^{(I)} + \mu'\rho\delta n^{(I)}\\
&\quad -\frac{1}{2}(ik\delta p^{(I)} + \partial_y \delta p^{(R)}) + \frac{\nu}{4}(\partial_y^2 \delta n^{(I)} - k^2\delta n^{(I)}) - \frac{\chi}{2}f(ik\delta p^{(I)} - \partial_y \delta p^{(R)})
\end{aligned}$$

This set of equations does not have any evident eigenfunctions and eigenvalues. Thus we will suppose $k \to 0$ and will search for perturbated solutions. For this end we introduce the following ansatz

$$\begin{aligned}
\lambda &= \lambda_0 + \lambda_1 k + \lambda_2 k^2 + \dots\\
\delta\rho &= \delta\rho_0 + \delta\rho_1 k + \delta\rho_2 k^2 + \dots\\
\delta p^{(R)} &= \delta p_0^{(R)} + \delta p_1^{(R)} k + \delta p_2^{(R)} k^2 + \dots\\
\delta p^{(I)} &= \delta p_0^{(I)} + \delta p_1^{(I)} k + \delta p_2^{(I)} k^2 + \dots\\
\delta n^{(R)} &= \delta n_0^{(R)} + \delta n_1^{(R)} k + \delta n_2^{(R)} k^2 + \dots\\
\delta n^{(I)} &= v_0 + \delta n_1^{(I)} k + \delta n_2^{(I)} k^2 + \dots
\end{aligned}$$

Substituting it into our set of equations we obtain at order $k = 0$

$$\begin{aligned}
\lambda_0\delta\rho_0 &= -\partial_y \delta p_0^{(I)} \qquad (15)\\
\lambda_0\delta p_0^{(R)} &= -\left(\alpha - \beta f^2\right)\delta p_0^{(R)} + \frac{1}{2}\partial_y \delta n_0^{(I)} \qquad (16)\\
&\quad +\zeta f \delta p_0^{(R)} + \frac{1}{2}\gamma\left[-f\partial_y \delta n_0^{(I)} + \delta n_0^{(I)}\partial_y f\right] \qquad (17)\\
\lambda_0\delta p_0^{(I)} &= -\left(\alpha - \beta f^2\right)\delta p_0^{(I)} - \frac{1}{2}\partial_y\delta\rho_0 + \frac{1}{2}\partial_y \delta n_0^{(R)} \qquad (18)\\
&\quad -\zeta f \delta p_0^{(I)} + \frac{1}{2}\gamma\left[f\partial_y \delta n_0^{(R)} + \delta n_0^{(R)}\partial_y f\right] \qquad (19)\\
\lambda_0\delta n_0^{(R)} &= (\mu'\rho_t - 3\xi f^2)\delta n_0^{(R)} + \mu'\rho\delta n_0^{(R)} + \mu'\delta\rho_0 f \qquad (20)\\
&\quad +\frac{1}{2}\partial_y \delta p_0^{(I)} + \frac{\nu}{4}\partial_y^2 \delta n_0^{(R)} - \frac{\chi}{2}f\partial_y \delta p_0^{(I)} \qquad (21)\\
\lambda_0\delta n_0^{(I)} &= (\mu'\rho_t - \xi f^2)\delta n_0^{(I)} + \mu'\rho\delta n_0^{(I)} \qquad (22)\\
&\quad -\frac{1}{2}\partial_y \delta p_0^{(R)} + \frac{\nu}{4}\partial_y^2 \delta n_0^{(I)} + \frac{\chi}{2}f\partial_y \delta p_0^{(R)} \qquad (23)
\end{aligned}$$

Setting $\lambda_0 = 0$, we obtain from the first equation $\delta p_0^{(I)} = cnst$ that we set to zero. The second and the last equations are decoupled from the other two, we then also set $\delta p_0^{(R)} = \delta n_0^{(I)} = \delta p_0^{(I)} = 0$. The two equations left now read

$$\begin{aligned} 0 &= -\frac{1}{2}\partial_y \delta\rho_0 + \frac{1}{2}\partial_y \delta n_0^{(R)} + \frac{1}{2}\gamma\left[f\partial_y \delta n_0^{(R)} + \delta n_0^{(R)}\partial_y f\right] && (24)\\ 0 &= (\mu'\rho_t - 3\xi f^2)\delta n_0^{(R)} + \mu'\rho\delta n_0^{(R)} + \mu'\delta\rho_0 f + \frac{\nu}{4}\partial_y^2 \delta n_0^{(R)} && (25) \end{aligned}$$

Comparing the to equations(13,14) in the article we immediately see that

$$\begin{aligned} \delta\rho_0 &= \partial_y \rho \\ \delta n_0^{(R)} &= \partial_y f \end{aligned}$$

At order k=1 we obtain

$$\begin{aligned} \lambda_1 \partial_y \rho &= -\partial_y \delta p_1^{(I)} && (26)\\ 0 &= -\left(\alpha - \beta f^2\right)\delta p_1^{(R)} - \frac{1}{2} i\partial_y \rho - \frac{1}{2}(i\partial_y f + \partial_y \delta n_1^{(I)}) && (27)\\ &\quad +\zeta f \delta p_1^{(R)} + \frac{1}{2}\gamma\left[f\left(i\partial_y f - \partial_y \delta n_1^{(I)}\right) + \delta n_1^{(I)}\partial_y f\right] && (28)\\ 0 &= -\left(\alpha - \beta f^2\right)\delta p_1^{(I)} - \frac{1}{2}\partial_y \delta\rho_1 - \frac{1}{2}(ik\delta n_1^{(I)} - \partial_y \delta n_1^{(R)}) \\ &\quad -\zeta f \delta p_1^{(I)} + \frac{1}{2}\gamma\left[f\left(i\delta n_1^{(I)} + \partial_y \delta n_1^{(R)}\right) + \delta n_1^{(R)}\partial_y f\right] && (29)\\ \lambda_1 \partial_y f &= (\mu'\rho_t - 3\xi f^2)\delta n_1^{(R)} + \mu'\rho\delta n_1^{(R)} + \mu'\delta\rho_1 f && (30)\\ &\quad +\frac{1}{2}\partial_y \delta p_1^{(I)} + \frac{\nu}{4}\partial_y^2 \delta n_1^{(R)} - \frac{\chi}{2} f\partial_y \delta p_1^{(I)} && (31)\\ 0 &= (\mu'\rho_t - \xi f^2)\delta n_1^{(I)} + \mu'\rho\delta n_1^{(I)} && (32)\\ &\quad -\frac{1}{2}\partial_y \delta p_1^{(R)} + \frac{\nu}{4}\partial_y^2 \delta n_1^{(I)} + \frac{\chi}{2} f\partial_y \delta p_1^{(R)} && (33) \end{aligned}$$

Setting $\delta p_1^{(R)} = 0$, we obtain from the second and the last equation which are decoupled from the others

$$\begin{aligned} 0 &= -\frac{1}{2} i\partial_y \rho - \frac{1}{2}(i\partial_y f + \partial_y \delta n_1^{(I)}) \\ &\quad +\frac{1}{2}\gamma\left[f\left(i\partial_y f - \partial_y \delta n_1^{(I)}\right) + \delta n_1^{(I)}\partial_y f\right] \\ 0 &= -(\mu'\rho_t + \xi f^2)\delta n_1^{(I)} + \mu'\rho\delta n_1^{(I)} + \frac{\nu}{4}\partial_y^2 \delta n_1^{(I)} \end{aligned}$$

These two equations admit a solution $\delta n_1^{(I)} = -2if$. As for the other three equations, they are the same as the one at order $k = 0$, we thus set $\lambda_1 = \delta p_1^{(I)} = \delta n_1^{(R)} = \delta\rho_1 = 0$ without loss of generality.

Finally at order $k = 2$ we obtain

$$\begin{aligned}
\lambda_2 \partial_y \rho &= -\partial_y \delta p_2^{(I)} \\
0 &= -\left(\alpha - \beta f^2\right) \delta p_2^{(R)} - \frac{1}{2}\partial_y \delta n_2^{(I)} \\
&\quad + \zeta f \delta p_2^{(R)} - \frac{1}{2}\gamma \left[f \partial_y \delta n_2^{(I)} - \delta n_2^{(I)} \partial_y f \right] \\
0 &= -\left(\alpha - \beta f^2\right) \delta p_2^{(I)} - \frac{1}{2}\partial_y \delta \rho_2 + \frac{1}{2}\partial_y \delta n_2^{(R)} - f \\
&\quad - \zeta f \delta p_2^{(I)} + \frac{1}{2}\gamma \left[2f^2 + \partial_y \left(\delta n_2^{(R)} f \right) \right] \\
\lambda_2 \partial_y f &= (\mu' \rho_t - 3\xi f^2) \delta n_2^{(R)} + \mu' \rho \delta n_2^{(R)} + \mu' \delta \rho_2 f \\
&\quad + \frac{1}{2}\partial_y \delta p_2^{(I)} + \frac{\nu}{4}(\partial_y^2 \delta n_2^{(R)} - \partial_y f) - \frac{\chi}{2} f \partial_y \delta p_2^{(I)} \\
0 &= 0
\end{aligned}$$

As the second equation is decoupled from the others, we set $\delta p_2^{(R)} = \delta n_2^{(I)} = 0$. From the first equation we obtain $\delta p_2^{(I)} = -\lambda_2 \left(\rho + cnst\right)$. Inserting it into the third equation we obtain

$$\begin{aligned}
0 &= \left(\alpha - \beta f^2\right) \lambda_2 \left(\rho + cnst\right) - \frac{1}{2}\partial_y \delta \rho_2 + \frac{1}{2}\partial_y \delta n_2^{(R)} - f \\
&\quad + \lambda_2 \zeta f \left(\rho + cnst\right) + \frac{1}{2}\gamma \left[2f^2 + \partial_y \left(\delta n_2^{(R)} f \right) \right] \\
\delta \rho_2 &= \left(1 + \gamma f\right) \delta n_2^{(R)} + 2 \int_{-\infty}^{\infty} dy \left[\lambda_2 \left(\alpha + \zeta f - \beta f^2\right) \left(\rho + cnst\right) - f + \gamma f^2 \right]
\end{aligned}$$

As we want the integral on the r.h.s to be finite, we adjust the integration constant of $\delta p_2^{(I)}$ accordingly $\delta p_2^{(I)} = -\lambda_2 \left(\rho - \rho_{gas}\right)$. Finally inserting this relation to the last equation we obtain

$$\begin{aligned}
&\lambda_2 \left(\partial_y f + \frac{1}{2}\left(1 - \chi f\right) \partial_y \rho \right) + \frac{\nu}{4}\partial_y f \\
&\quad - \mu' f 2 \int_{-\infty}^{\infty} dy \left[\lambda_2 \left(\alpha + \zeta f - \beta f^2\right) \left(\rho - \rho_{gas}\right) - f + \gamma f^2 \right] \\
&= (\mu' \rho_t - 3\xi f^2) \delta n_2^{(R)} + \mu' \rho \delta n_2^{(R)} + \mu' \left(f + \gamma f^2\right) \delta n_2^{(R)} + \frac{\nu}{4}\partial_y^2 \delta n_2^{(R)}
\end{aligned} \tag{34}$$

The homogeneous equation on the r.h.s admits the solution $\delta n_2^{(R)} = \partial_y f$. Or it can be wrote in the form $L \delta n_2^{(R)}$ where

$$L = (\mu' \rho_t - 3\xi f^2) + \mu' \rho + \mu' \left(f + \gamma f^2\right) + \frac{\nu}{4}\partial_y^2$$

We know from math analysis that the operator L is self-adjoint (see for example ref[25]). In the same way we known that for a linear inhomogeneous differential equation $Lu\left(x\right) = v\left(x\right)$, the equation $Lu\left(x\right) - \lambda_i u\left(x\right) = v\left(x\right)$ has a solution if and only if $< \beta_i | v >= 0$. Where L is a self-adjoint operator, and β_i and λ_i are respectively the

eigenfunctions and eigenvalues of this operator. Or we have said that our homogeneous equation has an eigenfunction $\beta = \partial_y f$ with the corresponding eigenvalue $\lambda = 0$ thus the solvability condition for equation(34) is given by

$$\int_{-\infty}^{\infty} dy \partial_y f \left[\lambda_2 \left(\partial_y f + \frac{1}{2}\left(1 - \chi f\right)\partial_y \rho\right) + \frac{\nu}{4}\partial_y f\right] = \int_{-\infty}^{\infty} dy \partial_y f \left[\mu' f 2 \int_{-\infty}^{\infty} dy \left[\lambda_2 \left(\alpha + \zeta f - \beta f^2\right)\left(\rho - \rho_{gas}\right) - f + \gamma f^2\right]\right] \tag{35}$$

We now use the relation $\rho - \rho_{gas} = \frac{\gamma}{2} f^2 + f$ to obtain

$$\int_{-\infty}^{\infty} dy \left(\partial_y f\right)^2 \left[\lambda_2 \left(\frac{3}{2} + \frac{1}{2}\left(\chi + \gamma\right) f - \chi\gamma f^2\right) + \frac{\nu}{4}\right] = + \lambda_2 2\mu' \int_{-\infty}^{\infty} dy \partial_y f \left(\alpha + \left(\zeta + \gamma\frac{\alpha}{2}\right) f + \left(\zeta\frac{\gamma}{2} - \beta\right) f^2 - \frac{\gamma}{2}\beta f^3\right) 2\mu' \int dy \partial_y f \left[f \int dy f \left[\gamma f - 1\right]\right] \tag{36}$$

$$\lambda_2 \int_{-\infty}^{\infty} dy \left(\partial_y f\right)^2 \left[\frac{3}{2} + \frac{1}{2}\left(\chi + \gamma\right) f - \chi\gamma f^2\right] - 2\lambda_2\mu' \int_{-\infty}^{\infty} dy \left(\partial_y f\right) f \int_{-\infty}^{\infty} dy f \left(\alpha + \left(\zeta + \gamma\frac{\alpha}{2}\right) f + \left(\zeta\frac{\gamma}{2} - \beta\right) f^2 - \frac{\gamma}{2}\beta f^3\right) = -\int_{-\infty}^{\infty} dy \left(\partial_y f\right)^2 \frac{\nu}{4} + 2\mu' \int dy \partial_y f \left[f \int dy f \left(\gamma f - 1\right)\right] \tag{37}$$

After performing an integration by part this equation simplifies to

$$\lambda_2 \int_{-\infty}^{\infty} dy \left(\partial_y f\right)^2 \left[\frac{3}{2} + \frac{1}{2}\left(\chi + \gamma\right) f - \chi\gamma f^2\right] + \lambda_2\mu' \int_{-\infty}^{\infty} dy f^3 \left(\alpha + \left(\zeta + \gamma\frac{\alpha}{2}\right) f + \left(\zeta\frac{\gamma}{2} - \beta\right) f^2 - \frac{\gamma}{2}\beta f^3\right) = -\int_{-\infty}^{\infty} dy \left(\partial_y f\right)^2 \frac{\nu}{4} - \mu' \int dy f^3 \left(\gamma f - 1\right) \tag{38}$$

This equation has the form $\lambda_2 A = B$, thus the set of equations(14) is unstable if $B/A > 0$. The band solution has the form

$$f\left(y\right) = \frac{c}{1 + a\cosh\left(by\right)}$$

n	p_0	p_1	p_2	q_0	q_1	q_2
3	3	0	0	4	2	0
4	11	4	0	12	18	0
5	50	55	0	48	144	18
6	274	607	64	240	1200	450

n	r_0	r_1	r_2	s_0	s_1	s_2
0	1	2	0	0	6	0
1	2	13	0	0	24	6
2	6	83	16	0	120	90

Table 1: Coefficients of the integrals(39,40)

where

$$\begin{aligned} c &= \frac{2\mu'}{3\left(\xi - \mu'\gamma/2\right)} \\ b &= \frac{4\mu'}{3\sqrt{\nu\left(2\xi - \mu'\gamma\right)}} \\ a &= \sqrt{K_1}e^{-\frac{K_2 L}{2}} \\ K_1 &= 4\exp\left(-\frac{2c\gamma}{c\gamma+2}\right) \\ K_2 &= \frac{4}{9}\sqrt{\frac{c\mu'}{3\nu}}\frac{\left(c+\left(\rho_0-\rho_t\right)\right)}{\left(c\gamma+2\right)} \end{aligned}$$

Direct integration give the following relations

$$\int_{-\infty}^{\infty} dy f^n = \frac{2c^n\left(-1\right)^n}{b\left(n-1\right)!\left(a^2-1\right)^{n-1}\sqrt{1-a^2}} \sum_{i=0}^{\lfloor\frac{n-1}{2}\rfloor}\left(p_i^n\sqrt{1-a^2}+q_i^n\operatorname{arctanh}\left(\frac{a-1}{\sqrt{1-a^2}}\right)\right)a^{2i} \quad (39)$$

$$\int_{-\infty}^{\infty} dy \left(\partial_y f\right)^2 f^n = \frac{2c^{n+2}b\left(-1\right)^n}{\left(n+3\right)!\left(a^2-1\right)^{n+2}\sqrt{1-a^2}} \sum_{i=0}^{\lceil\frac{n+2}{2}\rceil}\left(r_i^n\sqrt{1-a^2}+s_i^n\operatorname{arctanh}\left(\frac{a-1}{\sqrt{1-a^2}}\right)\right)a^{2i} \quad (40)$$

where the coefficients p_i^n, q_i^n, r_i^n, and s_i^n are given in table(1). Note that the above integral can be expressed in a "compact" form through the Appell hypergeometric series, which I omit for a easier understanding by a non-specialist.

Note that c, b and ν are always positive and that $a \in]0:1[$. We can numerically prove that λ_2 is always positive, i.e that the band

solution is always unstable. Depending on the characteristic length of the perturbation and that of the band, either the band is completely destroyed by the perturbation for noise value near the transition one, or only the borders of the band are perturbed.

4.5 CONCLUSION

I derived equations that are able to faithfully reproduce the qualitative behavior of the microscopic system. As in the microscopic model, four different phases are observed; a completely ordered one, a band phase, a chaotic phase and a completely disordered phase.

I was able to obtain an analytical solution of the band phase. We was also able to prove that this band solution is always unstable, which translates into a completely chaotic state near the transition point and in oscillating border of the band solution at lower noise. We can note that the oscillations of the borders of the band solution was not previously found in microscopic simulations. However they where confirmed latter, for larger system sizes, after the discovery of the instability of the band solution in the coarse-grained case. The fact that the band is not completely destroyed by the noise, at lower noise, confirm the first order type of the phase transition.

Thus our hydrodynamic equations give a faithful representation of the underlying microscopical model. Derivation of an effective noise should confirm, or predict, other properties of the polar rods.

BIBLIOGRAPHY

[1] I.S. Aranson and L.S. Tsimring. Model of coarsening and vortex formation in vibrated granular rods. *PRE*, 67(2):021305, 2003. (Cited on page 11.)

[2] I.S. Aranson and L.S. Tsimring. Pattern formation of microtubules and motors: Inelastic interaction of polar rods. *Physical Review E*, 71(5 AR 050901), 2005. (Cited on page 11.)

[3] I.S. Aranson and L.S. Tsimring. Theory of self-assembly of microtubules and motors. *PRE*, 74(3):031915, 2006. (Cited on page 11.)

[4] T. Balch and R.C. Arkin. Behavior-based formation control for multirobot teams. *Ieee Transactions on Robotics and Automation*, 14(6):926–939, 1998. (Cited on page 3.)

[5] M. Ballerini, N. Cabibbo, R. Candelier, A. Cavagna, E. Cisbani, I. Giardina, V. Lecomte, A. Orlandi, G. Parisi, A. Procaccini, M. Viale, and V. Zdravkovic. Interaction ruling animal collective behavior depends on topological rather than metric distance: Evidence from a field study. *Proceedings of the National Academy of Sciences*, 105(4):1232–1237, 2008. (Cited on page 147.)

[6] A. Baskaran and M.C. Marchetti. Hydrodynamics of self-propelled hard rods. *PRE*, 77(1):011920, 2008. (Cited on pages 10 and 24.)

[7] A. Baskaran and M.C. Marchetti. Self-regulation in self-propelled nematic fluids. *European Physical Journal E*, 35(9):95, 2012. (Cited on page 136.)

[8] E. Bertin, M. Droz, and G. Grégoire. Boltzmann and hydrodynamic description for self-propelled particles. *Physical Review E*, 74(2 AR 022101), 2006. (Cited on pages 9 and 36.)

[9] E. Bertin, M. Droz, and G. Grégoire. Hydrodynamic equations for self-propelled particles: microscopic derivation and stability analysis. *Journal of Physics A-mathematical and Theoretical*, 42(44):445001, 2009. (Cited on pages 9, 43, and 48.)

[10] D.L. Blair, T. Neicu, and A. Kudrolli. Vortices in vibrated granular rods. *PRE*, 67(3):031303, 2003. (Cited on page 130.)

[11] J.P. Boyd. *Chebyshev and Fourier spectral methods*. Dover Publications, 2001. (Cited on page 57.)

[12] J. Buhl, D. Sumpter, I.D. Couzin, J.J. Hale, E. Despland, E.R. Miller, and S.J. Simpson. From disorder to order in marching locusts. *Science*, 312(5778):1402–1406, 2006. (Cited on page 3.)

[13] A. Cavagna, A. Cimarelli, I. Giardina, G. Parisi, R. Santagati, F. Stefanini, and M. Viale. Scale-free correlations in starling flocks. *Proceedings of the National Academy of Sciences of the United States of America*, 107(26):11865–11870, 2010. (Cited on page 3.)

[14] L.-Y. Chen, N. Goldenfeld, and Y. Oono. Renormalization group and singular perturbations: Multiple scales, boundary layers, and reductive perturbation theory. *Physical Review E*, 54(1):376–394, 1996. (Cited on page 54.)

[15] L.H. Cisneros, R. Cortez, C. Dombrowski, R.E. Goldstein, and J.O. Kessler. Fluid dynamics of self-propelled microorganisms, from individuals to concentrated populations. *Experiments in Fluids*, 43(5):737–753, 2007. (Cited on page 4.)

[16] D.S. Dean. Langevin equation for the density of a system of interacting langevin processes. *Journal of Physics A-mathematical and General*, 29(24):L613–L617, 1996. (Cited on page 26.)

[17] J. Gautrais, C. Jost, M. Soria, A. Campo, S. Motsch, R. Fournier, S. Blanco, and G. Theraulaz. Analyzing fish movement as a persistent turning walker. *Journal of Mathematical Biology*, 58(3):429–445, 2009. (Cited on page 3.)

[18] F. Ginelli and H. Chaté. Relevance of metric-free interactions in flocking phenomena. *Physical Review Letters*, 105(16):168103, 2010. (Cited on pages 4, 9, 20, and 147.)

[19] F. Ginelli, F. Peruani, M. Bar, and H. Chaté. Large-scale collective properties of self-propelled rods. *Physical Review Letters*, 104(18):184502, 2010. (Cited on pages xiii, xiv, 4, 9, 20, 75, and 76.)

[20] L. Giomi, M.J. Bowick, X. Ma, and M.C. Marchetti. Defect annihilation and proliferation in active nematics. *PRL*, 110(22):228101, 2013. (Cited on page 130.)

[21] A. Gopinath, M.F. Hagan, M.C. Marchetti, and A. Baskaran. Dynamical self-regulation in self-propelled particle flows. *Physical Review E*, 85(6 AR 061903), 2012. (Cited on page 10.)

[22] Y. Hatwalne, S. Ramaswamy, M. Rao, and R.A. Simha. Rheology of active-particle suspensions. *Physical Review Letters*, 92(11):118101, 2004. (Cited on page 4.)

[23] T. Ihle. Kinetic theory of flocking: Derivation of hydrodynamic equations. *Physical Review E*, 83(3 AR 030901), 2011. (Cited on page 9.)

[24] T. Ihle. Invasion-wave induced first-order phase transition in systems of active particles. *eprint arXiv:1304.0149*, 2013. (Cited on page 10.)

[25] C. Lanczos. *Linear differential operators*. Van Nostrand, 1961. (Cited on pages 91 and 133.)

[26] L.D. Landau. *Collected papers of L.D. Landau. Edited and with an introduction by D. ter Haar*. Oxford, New York, Pergamon Press, 1965. (Cited on pages 24 and 25.)

[27] N.D. Mermin and H. Wagner. Absence of ferromagnetism or antiferromagnetism in one- or two-dimensional isotropic heisenberg models. *PRL*, 17(22):1133–1136, 1966. (Cited on page 5.)

[28] S. Mishra, A. Baskaran, and M.C. Marchetti. Fluctuations and pattern formation in self-propelled particles. *PRE*, 81(6):061916, 2010. (Cited on page 10.)

[29] M. Moussaid, D. Helbing, and G. Theraulaz. How simple rules determine pedestrian behavior and crowd disasters. *Proceedings of the National Academy of Sciences of the United States of America*, 108(17):6884–6888, 2011. (Cited on page 3.)

[30] S. Ramaswamy, R.A. Simha, and J. Toner. Active nematics on a substrate: Giant number fluctuations and long-time tails. *Europhysics Letters*, 62(2):196–202, 2003. (Cited on page 99.)

[31] P. Romanczuk and L. Schimansky-Geier. Mean-field theory of collective motion due to velocity alignment. *Ecological Complexity*, 10:83–92, 2012. (Cited on page 11.)

[32] V. Schaller, C. Weber, C. Semmrich, E. Frey, and A.R. Bausch. Polar patterns of driven filaments. *Nature*, 467(7311):73–77, 2010. (Cited on pages 3 and 35.)

[33] A. Sokolov and I.S. Aranson. Reduction of viscosity in suspension of swimming bacteria. *Physical Review Letters*, 103(14):148101, 2009. (Cited on pages 3 and 4.)

[34] A. Sokolov, R.E. Goldstein, F.I. Feldchtein, and I.S. Aranson. Enhanced mixing and spatial instability in concentrated bacterial suspensions. *Physical Review E*, 80(3):031903, 2009. (Cited on page 4.)

[35] J. Toner and Y.H. Tu. Long-range order in a 2-dimensional dynamical xy model - how birds fly together. *Physical Review Letters*, 75(23):4326–4329, 1995. (Cited on pages 5, 9, and 26.)

[36] J. Toner, Y.H. Tu, and S. Ramaswamy. Hydrodynamics and phases of flocks. *Annals of Physics*, 318(1):170–244, 2005. (Cited on pages 8, 9, and 75.)

[37] Y. Tu, J. Toner, and M. Ulm. Sound waves and the absence of galilean invariance in flocks. *PRL*, 80(21):4819–4822, 1998. (Cited on pages 7 and 35.)

[38] A.E. Turgut, H. Celikkanat, F. Gokce, and E. Sahin. Self-organized flocking in mobile robot swarms. *Swarm Intelligence*, 2(2-4):97–120, 2008. (Cited on page 3.)

[39] T. Vicsek, A. Czirok, E. Benjacob, I. Cohen, and O. Shochet. Novel type of phase-transition in a system of self-driven particles. *Physical Review Letters*, 75(6):1226–1229, 1995. (Cited on pages 3, 4, and 33.)

5 ACTIVE-NEMATIC MODEL

5.1 INTRODUCTION TO THE MICROSCOPIC MODEL

The last metric model that we consider is a fully nematic case that was introduced by Chaté et al.[?]. In this Vicsek like model not only the interaction is nematic, but also the particle themselves. Once again N point particles move off-lattice in a 2D space. Each particle have an orientation θ_i. As particles are nematic, at each time step they randomly choose to move in the direction θ_i or $\theta_i + \pi$. The equations of Vicsek dynamics then become

$$\begin{aligned} x_i^{t+1} &= x_i^t + v_0 \mathrm{e}\left(\theta_i^{t+1}\right)\Delta t \\ \theta_i^{t+1} &= \Theta\left(Q_i^t\right) + \xi_i \end{aligned}$$

Where $\xi_i \in \left[-\eta\frac{\pi}{2} : \eta\frac{\pi}{2}\right]$ is a delta-correlated white noise whose amplitude is controlled by the parameter $\eta \in [0:1]$ and $\Theta\left(Q_i\right)$ is the direction of the first eigenvector of the local nematic order parameter

$$Q_i = \sum_{j\in R}\begin{pmatrix} \left\langle\cos^2\left(\theta_j\right)\right\rangle - \frac{1}{2} & \left\langle\cos\left(\theta_j\right)\sin\left(\theta_j\right)\right\rangle \\ \left\langle\cos\left(\theta_j\right)\sin\left(\theta_j\right)\right\rangle & \left\langle\sin^2\left(\theta_j\right)\right\rangle - \frac{1}{2} \end{pmatrix}$$

where the summation is taken on particles within the interaction radius R of the particle i.

The authors measured the global nematic order parameter $\langle S\rangle$ for different values of noise η. Varying η from 0 to 1 it was discovered that the order parameter undergoes a continuous Kosterlitz-Thouless like transition from a disordered to an ordered system. The order is only quasi-long-range like in equilibrium systems. However the quasi-long-range order phase exhibits the non-equilibrium properties of giant density fluctuations like predicted by Ramaswamy and coworkers[30]. The observed power law behavior is $\Delta n \sim \langle n\rangle^1$, which is higher than the equilibrium exponent of $1/2$ and the one for polar particles of 0.8. These giant fluctuations imply that the density and the nematic fields are coupled together, in contrast to the equilibrium systems where such coupling is absent.

The quasi-ordered phase is characterized by an ordered band along which nematic order exist. These bands are not evolve bending, merging and dissolving. The characteristic evolution time of a band increase with the system size. However typically only one band is observed in the system independent of it's size like in the mixed polar-nematic case and contrary to the many polar solitons observed in the classical Vicsek model. Newer insights in our group suggests that the

observed instabilities of the band have a chaotic nature. And while the evolution time of the instabilities of the band increase with the system size, the statistical importance of such events also increase, suggesting that the band state could be completely chaotic.

In summary, in the hydrodynamic equation we can study and confirm

1. Three different states, a completely disordered one, a state with a single nematic band which is probably unstable and/or chaotic and a quasi-long-range order state.
2. A continuous transition between the disordered and the ordered state.
3. Giant number fluctuations with an exponent of one.

Once again, as we don't deal with the Langevin equations in this thesis, the last question will not be treated.

5.2 DERIVATION OF HYDRODYNAMIC EQUATIONS

Next follows an article that includes; the derivation of the hydrodynamic equations, some study of the obtained equations and an insight on derivation of Langevin equations.

IOPscience iopscience.iop.org

Home Search Collections Journals About Contact us My IOPscience

Mesoscopic theory for fluctuating active nematics

This article has been downloaded from IOPscience. Please scroll down to see the full text article.

2013 New J. Phys. 15 085032

(http://iopscience.iop.org/1367-2630/15/8/085032)

View the table of contents for this issue, or go to the journal homepage for more

Download details:
IP Address: 132.166.16.225
The article was downloaded on 11/09/2013 at 10:18

Please note that terms and conditions apply.

New Journal of Physics
The open access journal for physics

Mesoscopic theory for fluctuating active nematics

Eric Bertin[1,2], **Hugues Chaté**[2,3,4,9], **Francesco Ginelli**[5], **Shradha Mishra**[6], **Anton Peshkov**[2,3,4] **and Sriram Ramaswamy**[2,7,8]

[1] Université de Lyon, Laboratoire de Physique, ENS Lyon, CNRS, 46 Allée d'Italie, F-69007 Lyon, France
[2] Max Planck Institute for the Physics of Complex Systems, Nöthnitzer Straße 38, D-01187 Dresden, Germany
[3] Service de Physique de l'Etat Condensé, CEA-Saclay, URA 2464 CNRS, F-91191 Gif-sur-Yvette, France
[4] LPTMC, CNRS-UMR 7600, Université Pierre et Marie Curie, F-75252 Paris, France
[5] SUPA, Department of Physics and Institute for Complex Systems and Mathematical Biology, King's College, University of Aberdeen, Aberdeen AB24 3UE, UK
[6] Department of Physics and Meteorology, Indian Institute of Technology Kharagpur, Kharagpur 721 302, India
[7] TIFR Centre for Interdisciplinary Sciences, Tata Institute of Fundamental Research, 21 Brundavan Colony, Narsingi, Hyderabad 500 075, India
E-mail: hugues.chate@cea.fr

New Journal of Physics **15** (2013) 085032 (27pp)
Received 3 May 2013
Published 28 August 2013
Online at http://www.njp.org/
doi:10.1088/1367-2630/15/8/085032

Abstract. The term active nematics designates systems in which apolar elongated particles spend energy to move randomly along their axis and interact by inelastic collisions in the presence of noise. Starting from a simple Vicsek-style model for active nematics, we derive a mesoscopic theory, complete with effective multiplicative noise terms, using a combination of kinetic theory and Itô calculus approaches. The stochastic partial differential equations thus obtained

[8] On leave from Department of Physics, Indian Institute of Science, Bangalore 560 012 India.
[9] Author to whom any correspondence should be addressed.

Content from this work may be used under the terms of the Creative Commons Attribution 3.0 licence. Any further distribution of this work must maintain attribution to the author(s) and the title of the work, journal citation and DOI.

© IOP Publishing Ltd and Deutsche Physikalische Gesellschaft

are shown to recover the key terms argued in Ramaswamy *et al* (2003 *Europhys. Lett.* **62** 196) to be at the origin of anomalous number fluctuations and long-range correlations. Their deterministic part is studied analytically, and is shown to give rise to the long-wavelength instability at onset of nematic order (see Shi X and Ma Y 2010 arXiv:1011.5408). The corresponding nonlinear density-segregated band solution is given in a closed form.

Contents

1. Introduction **2**
2. Kinetic approach **3**
2.1. Microscopic dynamics . . . 3
2.2. Timescales and lengthscales . . . 4
2.3. Master equation . . . 5
2.4. Hydrodynamic description . . . 6
2.5. Homogeneous solutions . . . 9
3. Linear stability analysis **11**
3.1. Stability of the disordered isotropic solution . . . 11
3.2. Stability of the ordered solution . . . 12
4. Inhomogeneous solution **13**
5. Langevin formulation **15**
5.1. Density field fluctuations . . . 16
5.2. Nematic field fluctuations . . . 17
6. Conclusions **20**
Acknowledgments **20**
Appendix A. Fourier expansion of the master equation **21**
Appendix B. Curvature-induced current and equilibrium limit **23**
Appendix C. Correlation of the nematic field fluctuations **23**
References **26**

1. Introduction

The study of collective properties of systems of interacting active particles [1–3] is currently attracting a great deal of interest. In active matter, particles extract energy from their surrounding and dissipate it to propel themselves in some coherent way in a viscous fluid and/or over a dissipative substrate. In this last case, or whenever hydrodynamic effects can be neglected, physicists speak of 'dry active matter' [3]. Systems as diverse as animal flocks [4–6], human crowds [7, 8], subcellular proteins [9], bacterial colonies [10] and driven granular matter [11–13] have been described in this framework.

In the context of dry active matter, there is now some consensus in the physics community that minimal models such as the celebrated Vicsek model [14, 15] play a crucial role, since they stand as simple representatives of universality classes which have started to emerge from a combination of numerical and theoretical results: for instance, many different microscopic (particle) models have been shown to exhibit the same collective properties as the Vicsek model, and the continuous equation proposed by Toner and Tu [16] is widely believed to account for its

collective properties. Such hydrodynamic theories formulated at the mesoscopic level through stochastic partial differential equations (PDEs) are the natural framework to characterize and define universality classes.

In early approaches these mesoscopic theories have been built on the principle of including all that is not explicitly forbidden, retaining all leading terms (in a gradient expansion sense) allowed by symmetries and conservation laws [16, 17]. This grants access to the general structure of these equations and has been successful in describing relevant features of active matter systems such as their anomalously large number density fluctuations [12, 13, 16, 18]. Despite the attractions of a gradient expansion, it typically contains many transport coefficients of unknown dependence on microscopic control parameters and hydrodynamic fields such as local density. Moreover, the dependence of the noise terms on the dynamical fields in such equations remains arbitrary, and frequently neglected, whereas it could have profound consequences for important phenomena such as spontaneous segregation, clustering and interface dynamics.

Ideally, thus, one would be able to derive well-behaved mesoscopic theories using a systematic procedure starting from a given microscopic model. Kinetic-theory-like approaches [19–23] go one step toward this goal, by allowing one to compute hydrodynamic transport coefficients and nonlinear terms. One of the most successful versions is arguably the 'Boltzmann–Ginzburg–Landau' (BGL) framework recently put forward by some of us [24, 25], where, in the spirit of weakly nonlinear analysis, one performs well-controlled expansions in the vicinity of ordering transitions. Kinetic approaches alone thus yield good deterministic 'mean-field' equations but one still needs to 'reintroduce' fluctuations in order to get *bona fide* mesoscopic descriptions.

In this work, we show how this complete program can be achieved for the case of active nematics, i.e. systems where particles are energized individually but not really self-*propelled*, moving along the axis of the nematic degree of freedom they carry, with equal probability forward or back (think of shaken apolar rods aligning by inelastic collisions [12]). Starting from the Vicsek-style model for active nematics introduced in [26], we formulate a version of the BGL scheme mentioned above adapted to problems dominated by diffusion, derive the corresponding hydrodynamic equations and study their homogeneous and inhomogeneous solutions. In a last section, we show how these equations can be complemented by appropriate noise terms using a direct coarse-graining approach.

2. Kinetic approach

2.1. Microscopic dynamics

We consider the microscopic model for active nematics of [26] in two space dimensions. This Vicsek-style model can be thought of as a minimal model for a single layer of vibrated granular rods [12] although it does not deal explicitly with any volume exclusion forces. Here, rather, pointwise particles $j = 1, \ldots, N$ are characterized by their position $\mathbf{x}_j^t$ and an axial direction $\theta_j^t \in [-\pi/2, \pi/2]$. They interact synchronously with all neighboring particles situated within distance r_0 in a characteristic driven-overdamped dynamics implemented at discrete timesteps Δt:

$$\theta_j^{t+\Delta t} = \frac{1}{2}\mathrm{Arg}\left[\sum_{k\in V_j} \mathrm{e}^{\mathrm{i}2\theta_k^t}\right] + \psi_j^t, \tag{1}$$

$$\mathbf{x}_j^{t+\Delta t} = \mathbf{x}_j^t + d_0\, \kappa_j^t\, \hat{\mathbf{n}}_j^t, \tag{2}$$

where V_j is the neighborhood of particle j, $d_0 < r_0$ is the elementary displacement, $\hat{\mathbf{n}}_j^t \equiv (\cos\theta_j^t, \sin\theta_j^t)^{\mathrm{T}}$ is the nematic director and ψ and κ are two white noises: the random angle ψ_j^t, familiar of Vicsek-style models, is drawn from a symmetric distribution $\tilde{P}_\eta(\psi)$ of variance η^2, and the zero average bimodal noise $\kappa_j^t = \pm 1$ determines the actual orientation of motion. Both noises are delta correlated, namely $\langle \kappa_j^t \kappa_k^{t'} \rangle \sim \langle \psi_j^t \psi_k^{t'} \rangle \sim \delta_{t\,t'} \delta_{j\,k}$. Note that the factor 2 in the exponential terms of equation (1) implements an alignment interaction which fulfills the nematic symmetry $\theta \to \theta + \pi$. In other words, particles align their axial direction but do not carry any polar orientation.

In the following, we adopt the convention $[\hat{\mathbf{n}}\hat{\mathbf{n}}]_{\alpha\beta} \equiv \hat{n}_\alpha \hat{n}_\beta$ and label coordinates by greek indices, $\alpha, \beta, \ldots = 1, 2$, summing over repeated indices.

2.2. Timescales and lengthscales

We consider low density systems in which particles, at a given time, are either non-interacting or involved in a binary interaction. In this dilute limit we can neglect interactions between more than two particles. We also treat interactions as collision-like events, with the mean intercollision time

$$\tau_{\mathrm{free}} \approx \frac{\tau_{\mathrm{d}}}{d_0^2\, \rho_0}, \tag{3}$$

where ρ_0 is the global particle density and τ_{d} is the shortest microscopic timescale of the dynamics, associated to the inversion of the rods direction of motion $\tau_{\mathrm{d}} \sim \Delta t$. This intercollision time is much larger than the collision timescale

$$\tau_{\mathrm{coll}} \approx \tau_{\mathrm{d}} \left(\frac{r_0}{d_0}\right)^2. \tag{4}$$

For driven granular rods, τ_{d} may be thought of as the inverse of the shaking frequency, and for typical parameters it is much smaller than both the collision (τ_{coll}) and the mean intercollision (τ_{free}) timescales; at low enough densities $\tau_{\mathrm{d}} \ll \tau_{\mathrm{coll}} \ll \tau_{\mathrm{free}}$. Note that the timescales (4)–(3) are different from the ones characteristic of ballistic dynamics [20].

To develop a kinetic approach we consider a mesoscopic timescale τ_{B} such that $\tau_{\mathrm{coll}} \ll \tau_{\mathrm{B}} \ll \tau_{\mathrm{free}}$. As a consequence, we will treat the inversion of the direction of motion as a noisy term through Itô stochastic calculus [27]. We also consider a mesoscopic coarse-graining lengthscale ℓ_{B} which, while being much smaller than the system size L, is larger than the microscopic scales, such as the step-size d_0, the mean interparticle distance $\rho_0^{-1/2}$ and the interaction range r_0. To summarize, in a dilute system one has

$$\tau_{\mathrm{d}} \ll \tau_{\mathrm{d}} \left(\frac{r_0}{d_0}\right)^2 \ll \tau_{\mathrm{B}} \ll \frac{\tau_{\mathrm{d}}}{d_0^2 \rho_0} \tag{5}$$

and

$$d_0 < r_0 \ll \frac{1}{\sqrt{\rho_0}} \ll \ell_{\mathrm{B}} \ll L, \tag{6}$$

where we have made explicit the condition that the typical coarse-graining lengthscale ℓ_{B} is such that many particles are contained in a box of linear size ℓ_{B}, that is $\rho_0 \ell_{\mathrm{B}}^2 \gg 1$.

2.3. Master equation

We now write down a Boltzmann-like master equation in terms of the single particle probability distribution $f(\mathbf{x}, \theta, t)$, with $-\frac{\pi}{2} < \theta \leqslant \frac{\pi}{2}$, evolving over the timescale $\Delta t \approx \tau_{\mathrm{B}}$. The minimal spatial resolution is such that many particles are contained in a spatial volume d^2x centered around the position $\mathbf{x}$. Moreover, we consider a dilute system, so that interactions (collisions) between particles are sufficiently rare to justify (i) *binary interactions* (as explained above, particles then either self-diffuse or experience noisy binary, collision-like interactions), (ii) decorrelation of the orientation between successive binary collisions of the same pair of particles, that is $f_2(\mathbf{x}, \theta_1, \theta_2, t) \approx f(\mathbf{x}, \theta_1, t) f(\mathbf{x}, \theta_2, t)$.

We first omit collisions and angular diffusion, only considering equation (2) to get

$$f(\mathbf{x}, \theta, t + \Delta t) = \tfrac{1}{2}[f(\mathbf{x} + \hat{\mathbf{n}}(\theta) d_0, \theta, t) + f(\mathbf{x} - \hat{\mathbf{n}}(\theta) d_0, \theta, t)], \tag{7}$$

where we have considered that a particle moves along one of the two orientations of $\hat{\mathbf{n}}$ with equal probability. On the mesoscopic timescale $\tau_{\mathrm{B}} \gg \tau_{\mathrm{d}} \sim \Delta t$, Itô calculus [27] to second order gives

$$\partial_t f(\mathbf{x}, \theta, t) = D_0 \partial_\alpha \partial_\beta [\hat{n}_\alpha(\theta) \hat{n}_\beta(\theta) f(\mathbf{x}, \theta, t)], \tag{8}$$

where

$$D_0 = \frac{d_0^2}{2\tau_{\mathrm{d}}} \tag{9}$$

is the microscopic diffusion parameter.

To account for angular diffusion and binary collisions, the appropriate integrals need to be added to the right-hand side of equation (8):

$$\partial_t f(\mathbf{x}, \theta, t) = D_0\, \partial_\alpha \partial_\beta [\hat{n}_\alpha(\theta) \hat{n}_\beta(\theta) f(\mathbf{x}, \theta, t)] + I_{\mathrm{diff}}[f] + I_{\mathrm{coll}}[f, f]. \tag{10}$$

The diffusion integral describes self-diffusion which takes place at a rate $\lambda \approx 1/\tau_{\mathrm{d}}$

$$I_{\mathrm{diff}}[f] = -\lambda f(\theta) + \lambda \int_{-\pi/2}^{\pi/2} \mathrm{d}\theta' f(\theta') \int_{-\infty}^{\infty} \mathrm{d}\zeta\, P(\zeta)\, \delta_\pi(\theta' - \theta + \zeta), \tag{11}$$

where we used the simplified notation $f(\theta) \equiv f(\mathbf{x}, \theta, t)$, δ_π is a generalized Dirac delta imposing that the argument is equal to zero modulo π and $P(\zeta)$ is a symmetric noise distribution of variance σ^2, corresponding to the effective noise arising at the timescale τ_{B} from the sum of the microscopic stochastic contributions to angular dynamics.

Binary collisions are described by

$$\begin{aligned} I_{\mathrm{coll}}[f, f] = &- f(\theta) \int_{-\pi/2}^{\pi/2} \mathrm{d}\theta' f(\theta') K(\theta, \theta') \\ &+ \int_{-\pi/2}^{\pi/2} \mathrm{d}\theta_1 \int_{-\pi/2}^{\pi/2} \mathrm{d}\theta_2 f(\theta_1) K(\theta_1, \theta_2) f(\theta_2) \int_{-\infty}^{\infty} \mathrm{d}\zeta\, P(\zeta)\, \delta_\pi(\Psi(\theta_1, \theta_2) - \theta + \zeta), \end{aligned} \tag{12}$$

where, for the sake of simplicity, we have used the same noise distribution $P(\zeta)$ as in the self-diffusion integral, and the out-coming angle Ψ from deterministic binary collisions is, for $-\frac{\pi}{2} < \theta_1, \theta_2 \leqslant \frac{\pi}{2}$,

$$\Psi(\theta_1, \theta_2) = \tfrac{1}{2}(\theta_1 + \theta_2) + h(\theta_1 - \theta_2) \quad \text{with } h(\theta) = \begin{cases} 0 & \text{if } |\theta| \leqslant \dfrac{\pi}{2}, \\ \dfrac{\pi}{2} & \text{if } \dfrac{\pi}{2} < |\theta| \leqslant \pi. \end{cases} \tag{13}$$

Note that the role of the function $h(\theta)$ is to ensure that $\Psi(\theta_1, \theta_2)$ is π-periodic with respect to θ_1 and θ_2 independently, as dictated by the nematic symmetry of the system. The collision kernel $K(\theta_1, \theta_2)$, i.e. the number of collisions per unit time and volume, is calculated as follows, modifying the standard collision kernel of kinetic theory to take into account the fact that active nematic particles can move either along $\hat{\mathbf{n}}$ or $-\hat{\mathbf{n}}$ [19, 20, 28]. Consider two particles with nematic axis $\hat{\mathbf{n}}(\theta)$ and $\hat{\mathbf{n}}(\theta')$ located in the volume d^2x centered around position $\mathbf{x}$. In the reference frame of the first particle the second one diffuses either along the $|\hat{\mathbf{n}}(\theta) - \hat{\mathbf{n}}(\theta')|$ or the $|\hat{\mathbf{n}}(\theta) + \hat{\mathbf{n}}(\theta')|$ nematic axis. In unit time, taking into account the characteristic timescales τ_d and step-size d_0 of its motion, it sweeps a surface (its cross section, which is conserved going back to the lab reference frame) equal to

$$\begin{aligned} K(\theta, \theta') &= \frac{r_0 d_0}{\tau_\mathrm{d}}[|\hat{\mathbf{n}}(\theta) - \hat{\mathbf{n}}(\theta')| + |\hat{\mathbf{n}}(\theta) + \hat{\mathbf{n}}(\theta')|] \\ &= 2\alpha_0 \left[\left|\sin\frac{\theta - \theta'}{2}\right| + \left|\cos\frac{\theta - \theta'}{2}\right|\right], \end{aligned} \tag{14}$$

where we have introduced the microscopic collision parameter

$$\alpha_0 = \frac{r_0 d_0}{\tau_\mathrm{d}}. \tag{15}$$

Note that $K(\theta, \theta') \equiv \tilde{K}(\theta - \theta')$ is an even function of the difference $(\theta - \theta')$, and fulfills the nematic symmetry, being invariant under rotation of either angle by π.

Before proceeding to derive hydrodynamic equations, we simplify all notations by rescaling time $\tilde{t} = \lambda t = t/\tau_\mathrm{d}$ and space $\tilde{x} = \frac{\sqrt{2}}{d_0}x$. As in [24, 25] we also set the collision surface $S = 2r_0 d_0$ to 1 by a global rescaling of the one-particle probability density f, without loss of generality. This amounts to set $\lambda = 1$, $D_0 = 1$ and $2\alpha_0 = 1$, so that, dropping the tildes, our Boltzmann-like master equation now depends only on the global density ρ_0 and the noise intensity σ.

2.4. Hydrodynamic description

In two spatial dimensions, hydrodynamic fields can be obtained by expanding the single particle probability density f in Fourier series of its angular variable $\theta \in [-\pi/2, \pi/2]$:[10]

$$f(\mathbf{x}, \theta, t) = \frac{1}{\pi}\sum_{k=-\infty}^{k=\infty} \hat{f}_k(\mathbf{x}, t)\,\mathrm{e}^{-\mathrm{i}2k\theta} \tag{16}$$

and

$$\hat{f}_k(\mathbf{x}, t) = \int_{-\pi/2}^{\pi/2} \mathrm{d}\theta f(\mathbf{x}, \theta, t)\,\mathrm{e}^{\mathrm{i}2k\theta}. \tag{17}$$

The number density and the density-weighted nematic tensor field $\mathbf{w} \equiv \rho\mathbf{Q}$ are then given by

$$\rho(\mathbf{x}, t) = \int_{-\pi/2}^{\pi/2} \mathrm{d}\theta f(\mathbf{x}, \theta, t) = \hat{f}_0(\mathbf{x}, t) \tag{18}$$

[10] These k-modes are equivalent to even harmonics if one would define particles orientation in $[-\pi, \pi]$ in spite of the symmetry under rotations by π (with odd ones being zero by symmetry).

and

$$w_{11}(\mathbf{x},t) = -w_{22}(\mathbf{x},t) = \frac{1}{2}\int_{-\pi/2}^{\pi/2} \mathrm{d}\theta f(\mathbf{x},\theta,t)\cos(2\theta) = \frac{1}{2}\mathrm{Re}\,\hat{f}_1(\mathbf{x},t), \tag{19}$$

$$w_{12}(\mathbf{x},t) = w_{21}(\mathbf{x},t) = \frac{1}{2}\int_{-\pi/2}^{\pi/2} \mathrm{d}\theta f(\mathbf{x},\theta,t)\sin(2\theta) = \frac{1}{2}\mathrm{Im}\,\hat{f}_1(\mathbf{x},t). \tag{20}$$

Note that when $\mathrm{Im}\,\hat{f}_1 = 0$ the nematic field is aligned either along the x ($\mathrm{Re}\,\hat{f}_1 > 0$) or the y ($\mathrm{Re}\,\hat{f}_1 < 0$) axis.

Injecting the Fourier expansion (16) in the master equation (10), one gets, after some lengthy calculations detailed in appendix A, the infinite hierarchy:

$$\partial_t \hat{f}_k(\mathbf{x},t) = \frac{1}{2}\Delta \hat{f}_k(\mathbf{x},t) + \frac{1}{4}(\nabla^{*2}\hat{f}_{k+1} + \nabla^2 \hat{f}_{k-1}) + [\hat{P}_k - 1]\hat{f}_k(\mathbf{x},t)$$
$$+\frac{1}{\pi}\sum_q \hat{f}_q(\mathbf{x},t)\hat{f}_{k-q}(\mathbf{x},t)\left[\hat{P}_k\hat{J}_{k,q} - \frac{4}{1-16q^2}\right], \tag{21}$$

where $\hat{P}_k$ is the Fourier transform of the noise distribution $P(\zeta)$ (namely, $\hat{P}_k = \int_{-\infty}^{\infty} \mathrm{d}\zeta\, P(\zeta)\,\mathrm{e}^{\mathrm{i}2k\zeta}$) and

$$\hat{J}_{k,q} = 4\,\frac{1 + 2\sqrt{2}(2q-k)(-1)^q \sin\left(\frac{k\pi}{2}\right)}{1 - 4(2q-k)^2} \tag{22}$$

and we have introduced the following 'complex' operators

$$\begin{aligned}
\nabla &\equiv \partial_x + \mathrm{i}\partial_y,\\
\nabla^* &\equiv \partial_x - \mathrm{i}\partial_y,\\
\Delta &\equiv \nabla\nabla^*,\\
\nabla^2 &\equiv \nabla\nabla,\\
\nabla^{*2} &\equiv \nabla^*\nabla^*.
\end{aligned}$$

The equation at order $k = 0$ is thus expressed in the simple form

$$\partial_t \rho = \tfrac{1}{2}\Delta\rho + \tfrac{1}{2}\mathrm{Re}(\nabla^{*2}\hat{f}_1) \tag{23}$$

and is nothing but the continuity equation for diffusive active matter with local anisotropy characterized by $\hat{f}_1$.

Equation (21) possesses a trivial, isotropic and homogeneous solution: $\rho(\mathbf{x},t) \equiv \hat{f}_0(\mathbf{x},t) = \rho_0$ and $\hat{f}_k(\mathbf{x},t) = 0$ for $|k| > 0$. We are interested in a nematically ordered homogeneous solution which could eventually arise following some instability of the isotropic solution above. In analogy to the scaling ansatz used for polar particles [20, 25], the interaction term in equation (21) suggests a simple scaling ansatz to close the infinite hierarchy of equations on $\hat{f}_k(\mathbf{x},t)$. Near an instability threshold with continuous onset, Fourier coefficients should scale as $\hat{f}_k(\mathbf{x},t) \sim \epsilon^{|k|}$ where ϵ is a small parameter characterizing the distance to threshold. Moreover, the curvature induced current (last term of (23)) also induces an order ϵ variation in the density field, $\rho(\mathbf{x},t) - \rho_0 \sim \epsilon$. Then, assuming spatial derivatives to be of order ϵ, the request that all terms in equation (23) are of the same order also fixes the diffusive structure of the scaling of time and spatial gradients: $\partial_t \sim \nabla^2 \sim \Delta \sim \epsilon^2$.

Using the above scaling ansatz, we proceed by discarding all terms appearing in (21) of order higher than ϵ^3. For $k = 1, 2$ we get

$$\partial_t \hat{f}_1 = \tfrac{1}{2}\Delta \hat{f}_1 + \tfrac{1}{4}\nabla^2\rho + a_1(\rho)\hat{f}_1 + b_1 \hat{f}_1^* \hat{f}_2 \tag{24}$$

and

$$0 = \tfrac{1}{4}\nabla^2 \hat{f}_1 - a_2(\rho)\hat{f}_2 + b_2 \hat{f}_1^2, \tag{25}$$

where the coefficients are

$$a_1(\rho) = \frac{8}{3\pi}\left[(2\sqrt{2}-1)\hat{P}_1 - \frac{7}{5}\right]\rho - (1-\hat{P}_1), \tag{26}$$

$$b_1 = \frac{8}{315\pi}[13 - 9\hat{P}_1(1+6\sqrt{2})], \tag{27}$$

$$a_2(\rho) = (1-\hat{P}_2) + \frac{8}{3\pi}\left(\frac{\hat{P}_2}{5} + \frac{31}{21}\right)\rho \tag{28}$$

and

$$b_2 = \frac{4}{\pi}\left(\frac{1}{15} + \hat{P}_2\right). \tag{29}$$

Equation (25) shows that at this order $\hat{f}_2$ is enslaved to $\hat{f}_1$ (given that $a_2 > 0$) and, further,

$$a_2(\rho_0)\hat{f}_2 \approx \tfrac{1}{4}\nabla^2 \hat{f}_1 + b_2 \hat{f}_1^2, \tag{30}$$

where the coefficient a_2 is evaluated at the mean density ρ_0, since the $\delta\rho = \rho - \rho_0$ corrections are of higher order. By substituting equations (25) into (24) one finally gets, neglecting the term $\hat{f}_1^*\nabla^2\hat{f}_1 \sim \epsilon^4$,

$$\partial_t \hat{f}_1 = (\mu - \xi|\hat{f}_1|^2)\hat{f}_1 + \tfrac{1}{4}\nabla^2\rho + \tfrac{1}{2}\Delta\hat{f}_1, \tag{31}$$

where we have introduced the transport coefficients

$$\mu = \frac{8}{3\pi}\left[(2\sqrt{2}-1)\hat{P}_1 - \frac{7}{5}\right]\rho - (1-\hat{P}_1), \tag{32}$$

$$\xi = \frac{32\nu}{35\pi^2}\left[\frac{1}{15} + \hat{P}_2\right]\left[(1+6\sqrt{2})\hat{P}_1 - \frac{13}{9}\right] \tag{33}$$

$$\text{with } \nu = \left[\frac{8}{3\pi}\left(\frac{31}{21} + \frac{\hat{P}_2}{5}\right)\rho_0 + (1-\hat{P}_2)\right]^{-1}. \tag{34}$$

Note that the coefficient ξ is only a function of the average density ρ_0, as space and time dependent corrections are of order ϵ^4. Note also that the coefficients μ and ξ are exactly the same as those found for the nematic field equation of nematically aligning polar particles [25][11].

[11] Note that in [25], the equations obtained are not entirely correct: (i) there is a sign error and a misplaced factor π in the expression of ξ; (ii) the term $\frac{\nu}{4}\nabla^2 f_2$ should read $\frac{\nu}{4}\Delta f_2$, where Δ is the Laplacian. In addition, let us emphasize that the Fourier coefficients $\hat{P}_k$ have a different definition in [25], due to the absence of global nematic symmetry: $\hat{P}_k$ here corresponds to $\hat{P}_{2k}$ in [25], leading to (only apparent) differences.

Equations (23) and (31) can be expressed in tensorial notation. To this aim, we introduce the linear differential operator $\mathbf{\Gamma}$, such that $\Gamma_{11} = -\Gamma_{22} \equiv \partial_1\partial_1 - \partial_2\partial_2$ and $\Gamma_{12} = \Gamma_{21} \equiv 2\partial_1\partial_2$, and the Frobenius inner product $\mathbf{A}{:}\mathbf{B} = A_{\alpha\beta}B_{\alpha\beta}$ (note that $\mathbf{w}{:}\mathbf{w} = ||\mathbf{w}||^2$ and $\mathbf{\Gamma}{:}\mathbf{w} = 2\partial_\alpha\partial_\beta w_{\alpha\beta}$). After some manipulation of the terms and the use of equations (19) and (20), we obtain the hydrodynamic equations for the density and nematic field

$$\partial_t\rho = \tfrac{1}{2}\Delta\rho + \tfrac{1}{2}(\mathbf{\Gamma}{:}\mathbf{w}), \tag{35}$$

$$\partial_t\mathbf{w} = \mu\,\mathbf{w} - 2\xi\,\mathbf{w}\,(\mathbf{w}{:}\mathbf{w}) + \tfrac{1}{2}\Delta\mathbf{w} + \tfrac{1}{8}\mathbf{\Gamma}\rho. \tag{36}$$

Although the tensorial notation might be more familiar to some readers, it is in fact easier here to continue manipulating the complex field $\hat{f}_1$ and the complex operators defined above. Moreover, in the following we drop the '^' superscript to ease notations. Note also that equations (35) and (36) were also derived from an apolar Vicsek-style model in [29].

The parameter-free character of the Laplacian term in (36) means, consistently with our expansion in ϵ, that the nematic phase of our system will be characterized by a single Frank constant [30]. The nonlinearities studied in [31] are therefore also absent to this order. The last term in equation (23) (or equation (35)), i.e. $\frac{1}{2}\mathrm{Re}\left(\nabla^2 f_1\right)$ (or $\frac{1}{2}(\mathbf{\Gamma} : \mathbf{w})$), is a curvature induced current which couples the density and the nematic field. While its existence was first deduced from general principles [17], here we have computed it directly from microscopic dynamics. Our calculations also give an exact expression for the corresponding transport coefficient, which is equal to the diffusive one (in equation (23) or (35)), here set to 1/2 by our rescaling. In appendix B, we show explicitly that this curvature-induced current originates from the coupling of orientation with motility.

We note finally that equations (35) and (36) are similar to those found by Baskaran and Marchetti [22] but simpler, largely due to our simpler starting point.

2.5. Homogeneous solutions

From now on, we use for $P(\zeta)$ a centered Gaussian distribution of variance σ^2, in which case $\hat{P}_k = \mathrm{e}^{-2k^2\sigma^2}$. The linear stability with respect to homogeneous perturbations of the disordered solution $\rho(\mathbf{x}, t) = \rho_0$, $\hat{f}_1(\mathbf{x}, t) = 0$ is given by the sign of $\mu(\rho_0)$ which yields the basic transition line

$$\sigma_\mathrm{t} = \sqrt{\frac{1}{2}\ln\left[5\,\frac{8(2\sqrt{2}-1)\rho_0 + 3\pi}{56\rho_0 + 15\pi}\right]}. \tag{37}$$

Note that in the dilute limit $\rho_0 \ll 1$, where the equations have been derived, one has $\sigma_\mathrm{t} \sim \sqrt{\rho_0}$.

For $\sigma < \sigma_\mathrm{t}$, $\mu > 0$, and the homogeneous nematically ordered solution

$$|f_1| = \sqrt{\frac{\mu}{\xi}} \tag{38}$$

exists and is stable w.r.t. homogeneous perturbations. The critical line is shown in figure 1(a) (black solid line). Note that for $\sigma < \sigma_\mathrm{t}$, all transport coefficients (32)–(34) are positive. This will be useful in the rest of the paper.

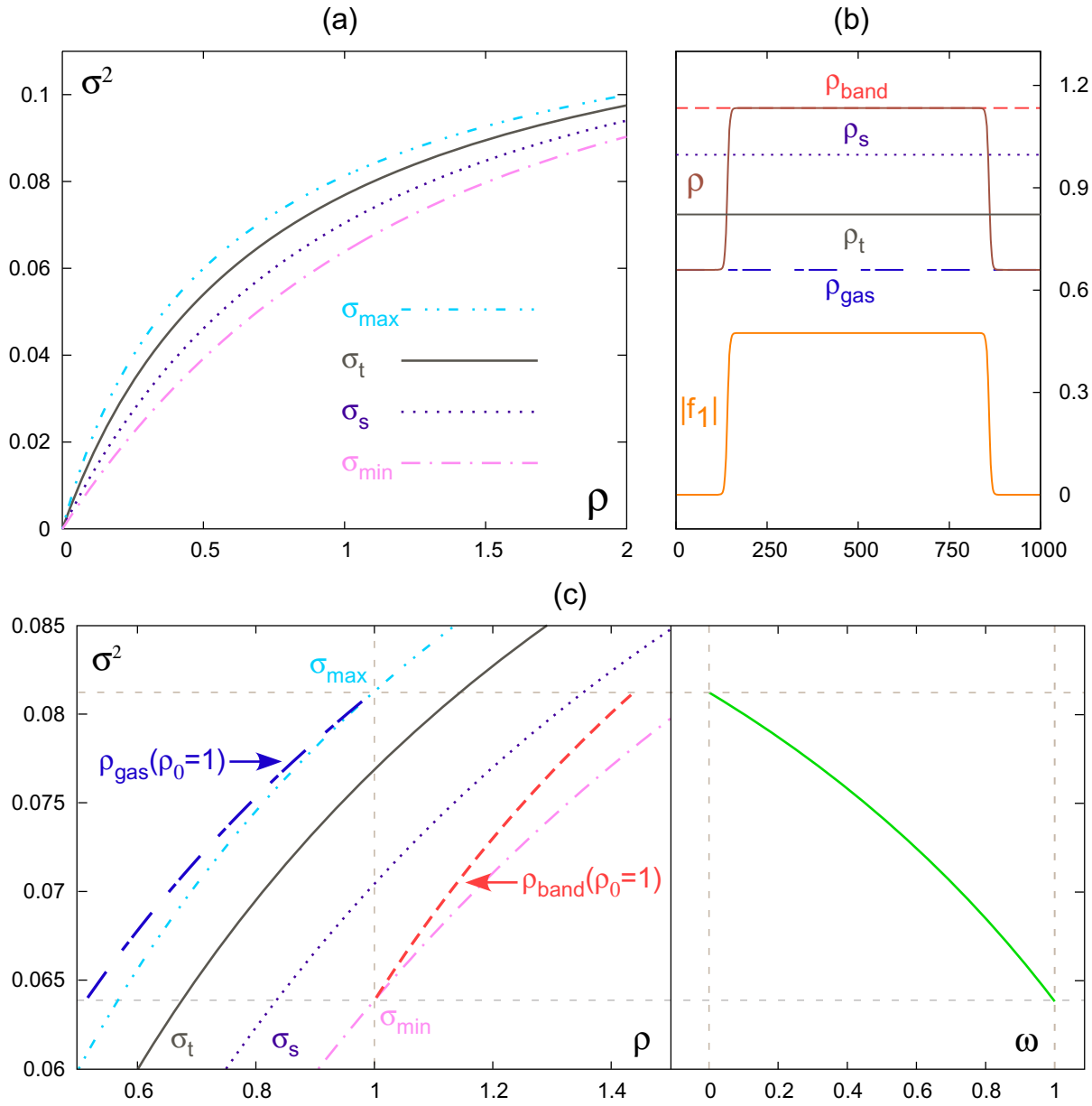

Figure 1. (a) Basic stability diagram. The line σ_t (solid, black) marks the linear instability of the disordered homogeneous solution. The ordered homogeneous solution is linearly unstable to large wavelengths between the σ_t and σ_s (dotted, purple) lines, and linearly stable below the σ_s line. The σ_{min} and σ_{max} lines mark the domain of existence of the band solution (62). (b) Density and order profile of the band solution for $\rho_0 = 1$, $\sigma = 0.265$, $L = 1000$; note that the lower and upper levels (ρ_{gas} and ρ_{band}) are respectively lower than ρ_t and higher than ρ_s, i.e. such that the corresponding homogeneous solution are lineally stable. (c) Properties of the band solutions for $\rho_0 = 1$: left: values of ρ_{gas} (long dash, dark blue line) and ρ_{band} (dashed, red line) as σ varies between σ_{min} and σ_{max}; right: corresponding variation of the surface fraction ω.

3. Linear stability analysis

We now study the linear stability of the above homogeneous solutions w.r.t. to arbitrary perturbations. Linearizing equations (23) and (31) around a homogeneous solution, $f_1 = f_{1,0} + \delta f_1$ and $\rho = \rho_0 + \delta\rho$, one has

$$\partial_t \delta\rho = \tfrac{1}{2}\Delta\delta\rho + \tfrac{1}{2}\mathrm{Re}(\nabla^{*2}\delta f_1), \tag{39}$$

$$\partial_t \delta f_1 = (\mu_0 - \xi|f_{1,0}|^2)\delta f_1 + \mu' f_{1,0}\,\delta\rho - 2\xi f_{1,0}\,\mathrm{Re}(f_{1,0}^*\,\delta f_1) + \tfrac{1}{4}\nabla^2\delta\rho + \tfrac{1}{2}\Delta\delta f_1, \tag{40}$$

where $\mu_0 \equiv \mu(\rho_0)$ and μ' is the derivative of μ w.r.t. ρ. We then introduce the real and imaginary parts of the order parameter perturbation, $\delta f_1 = \delta f_1^{(\mathrm{R})} + \mathrm{i}\delta f_1^{(\mathrm{I})}$, and express the spatial dependence of all perturbation fields in Fourier space, with a wavevector $\mathbf{q} = (q_x, q_y)$, by introducing the ansatz

$$\delta\rho(\mathbf{x}, t) = \delta\rho_{\mathbf{q}}\,\mathrm{e}^{st+\mathrm{i}\mathbf{qr}}, \tag{41}$$

$$\delta f_1^{(\mathrm{R})}(\mathbf{x}, t) = \delta f_{1,\mathbf{q}}^{(\mathrm{R})}\,\mathrm{e}^{st+\mathrm{i}\mathbf{qr}}, \quad \delta f_1^{(\mathrm{I})}(\mathbf{x}, t) = \delta f_{1,\mathbf{q}}^{(\mathrm{I})}\,\mathrm{e}^{st+\mathrm{i}\mathbf{qr}}. \tag{42}$$

The stability of the stationary solution $f_{1,0}$ is then ruled by the real part of the growth rate s.

3.1. Stability of the disordered isotropic solution

We first study the stability of the disordered solution $f_{1,0} = 0$, in the case $\mu_0 < 0$. Substituting equations (41), (42) in equations (39), (40), one has

$$\begin{aligned} s\,\delta\rho_{\mathbf{q}} &= -\frac{q^2}{2}\,\delta\rho_{\mathbf{q}} - \frac{1}{2}(q_x^2 - q_y^2)\delta f_{1,\mathbf{q}}^{(\mathrm{R})} - q_x q_y \delta f_{1,\mathbf{q}}^{(\mathrm{I})}, \\ s\,\delta f_{1,\mathbf{q}}^{(\mathrm{R})} &= -\frac{1}{4}(q_x^2 - q_y^2)\delta\rho_{\mathbf{q}} + \left(\mu_0 - \frac{q^2}{2}\right)\delta f_{1,\mathbf{q}}^{(\mathrm{R})}, \\ s\,\delta f_{1,\mathbf{q}}^{(\mathrm{I})} &= -\frac{1}{2}q_x q_y\,\delta\rho_{\mathbf{q}} + \left(\mu_0 - \frac{q^2}{2}\right)\delta f_{1,\mathbf{q}}^{(\mathrm{I})}, \end{aligned} \tag{43}$$

where $q^2 = q_x^2 + q_y^2$. All directions of the wavevector $\mathbf{q}$ being equivalent, we choose for simplicity $q_x = q$ and $q_y = 0$. From equation (43), one then sees that the component $\delta f_{1,\mathbf{q}}^{(\mathrm{I})}$ becomes independent from $\delta\rho_{\mathbf{q}}$ and $\delta f_{1,\mathbf{q}}^{(\mathrm{R})}$, yielding the negative eigenvalue $s = \mu_0 - \frac{q^2}{2}$. The eigenvalues of the remaining 2×2 block of the stability matrix are solutions of the second order polynomial

$$s^2 + s[q^2 - \mu_0] + \frac{q^2}{2}\left[\frac{q^2}{4} - \mu_0\right] \equiv s^2 + \beta_1\,s + \beta_0 = 0. \tag{44}$$

In the disordered state $\mu_0 < 0$, so that β_1 and β_2 are positive and one always has $\mathrm{Re}\,(s) < 0$. Therefore, the homogeneous disordered solution is stable w.r.t. to all perturbations if $\mu_0 < 0$, i.e. $\sigma > \sigma_{\mathrm{t}}$.

3.2. Stability of the ordered solution

To study the stability of the anisotropic ordered solution, it is convenient to choose a reference frame in which order is along one of the axes:

$$\mathrm{Re}(f_{1,0}) = \pm\sqrt{\frac{\mu_0}{\xi}}, \quad \mathrm{Im}(f_{1,0}) = 0. \tag{45}$$

This solution is aligned along x, if $f_{1,0}$ is positive, or along y if negative. For simplicity we will concentrate further on the case $f_{1,0} \geqslant 0$, i.e. on the nematic solution aligned along the x-axis. The real part $\delta f_1^{(\mathrm{R})}$ of the nematic field perturbation describes changes in the modulus $|f_{1,0}|$, and the imaginary part $\delta f_1^{(\mathrm{I})}$ describes perturbations perpendicular to the nematic orientation. The ansatz (41), (42) then yields the three coupled linear equations

$$\begin{aligned} s\,\delta\rho_{\mathbf{q}} &= -\frac{q^2}{2}\,\delta\rho_{\mathbf{q}} - \frac{1}{2}(q_x^2 - q_y^2)\delta f_{1,\mathbf{q}}^{(\mathrm{R})} - q_x q_y\,\delta f_{1,\mathbf{q}}^{(\mathrm{I})}, \\ s\,\delta f_{1,\mathbf{q}}^{(\mathrm{R})} &= \left[\mu' f_{1,0} - \frac{1}{4}(q_x^2 - q_y^2)\right]\delta\rho_{\mathbf{q}} - \left[2\mu_0 + \frac{q^2}{2}\right]\delta f_{1,\mathbf{q}}^{(\mathrm{R})}, \\ s\,\delta f_{1,\mathbf{q}}^{(\mathrm{I})} &= -\frac{1}{2}q_x q_y\,\delta\rho_{\mathbf{q}} - \frac{q^2}{2}\delta f_{1,\mathbf{q}}^{(\mathrm{I})}. \end{aligned} \tag{46}$$

We performed a full numerical stability analysis of these equations. The results are presented in figure 1. The transition to the homogeneous solution is given by the line σ_{t}. This solution is unstable to finite wavelength transversal perturbations of angle $|\theta| > \frac{\pi}{4}$ between the lines σ_{t} and σ_{s} (dotted purple line in figure 1), but is stable deeper in the ordered phase.

Two remarks are in order. Firstly, the angle of the most unstable mode is here always perfectly $\frac{\pi}{2}$. It is thus possible to obtain the 'restabilization' line σ_{s} analytically as shown below. Secondly, there is no spurious instability at low noise and/or high density (although we have found that such an instability appears if the truncation of the equations is made to the fourth order).

To obtain the analytic expression of the line σ_{s}, we write the wavevector in terms of its modulus q and its angle $\theta_{\mathbf{q}}$, so that $q_x^2 - q_y^2 = q^2\cos 2\theta_{\mathbf{q}}$ and $2q_x q_y = q^2\sin 2\theta_{\mathbf{q}}$. We can then analyze equations (46) in the longitudinal and perpendicular wavedirections $\theta_{\mathbf{q}} = 0, \pm\frac{\pi}{2}$, where the imaginary perturbation $\delta f_{1,\mathbf{q}}^{(\mathrm{I})}$ decouples from the other two. The latter is stable toward long-wavelength perturbations, since the corresponding eigenvalue $s = -q^2/2$ is negative. The stability toward density and real perturbations depends on a 2×2 matrix which yields the quadratic eigenvalue equation

$$s^2 + [2\mu_0 + q^2]s + \left[\left(\frac{\pm\mu' f_{1,0}}{2} + \mu_0\right)q^2 + \frac{q^4}{8}\right] = 0 \tag{47}$$

whose solutions are

$$s = \frac{1}{2}\left[-2\mu_0 - q^2 \pm \sqrt{4\mu_0^2 \mp 2\mu' f_{1,0}q^2 + \frac{q^4}{2}}\right]. \tag{48}$$

The sign $\pm$ in front of the $\mu' f_{1,0}$ term in equation (47) corresponds to the case $\theta_{\mathbf{q}} = 0$ (positive sign) and $\theta_{\mathbf{q}} = \frac{\pi}{2}$ (negative sign) respectively. Note that μ' is strictly positive, as typical for all active matter system with metric interactions, where the interaction rate grows with local density. Also μ_0 is positive and of order ϵ^2 (see equation (45)). It it thus easy to see that in

the case of large q, $\Re[s] \leqslant 0$. For small values of q, we perform an expansion to order q^2 of the largest growth rate s_+, obtained by taking the positive sign in front of the square root in equation (48), leading to

$$s_+ = \frac{q^2}{2}\left[\mp\frac{\mu'}{2\mu_0}f_{1,0} - 1\right]. \tag{49}$$

We can then conclude that for longitudinal perturbations ($\theta_{\mathbf{q}} = 0$, negative sign in front of μ'), the homogenous solution is stable confirming the results of numerical analysis. In the case of transversal perturbations ($\theta_{\mathbf{q}} = \pm\pi/2$), the stability condition is given by

$$\mu_0 > \frac{\mu'^2}{4\xi} \tag{50}$$

meaning that close to the instability threshold of the disordered solution, when μ_0 is positive but small, the state of homogeneous order is unstable with respect to long-wavelength perturbations. This instability was first identified in a kinetic-equation analysis by Shi and Ma [23]. Note that condition (50) is valid up to the third order in ϵ (or, equivalently, in the order parameter $||\mathbf{w}||$). It yields the stability line

$$\rho_s = \frac{4\mu_2 - \mu'^2\xi_2}{\mu'^2\xi_1 - 4\mu'}, \tag{51}$$

where $\mu_2 = \mu(\rho = 0)$, $\xi_1 = (1/\xi)'$ and $\xi_2 = (1/\xi(\rho_0 = 0))$. We do not provide here the explicit analytical expression for σ_s because this requires solving a sixth order polynomial.

We remark that the near-threshold instability discussed above is rather generic and appears in 'dry' active matter systems with metric interactions, as opposed to systems with metric-free ones, where the interaction rate is density-independent, and $\mu' = 0$ [24, 32, 33]. In this case (topological active nematics), stability would be enforced by the positive higher order corrections $\mu_0 q^2$ which dominates arbitrarily close to threshold.

4. Inhomogeneous solution

We now show how a spatially inhomogeneous stationary 'band' solution to our hydrodynamic equations can be found. First we remark that our equation for the nematic field, equation (31), is formally the same as that derived in [25] for polar particles with nematic alignment when the polar field is set to zero, as it is imposed here by the complete nematic symmetry of our system. We thus expect an ordered band solution made of two fronts connecting a linearly stable homogeneous disordered state ($\rho = \rho_{\text{gas}} < \rho_t$) and a linearly stable homogeneous ordered state ($\rho = \rho_{\text{band}} > \rho_s$) (see figure 1). Following [25], we rewrite

$$\mu(\rho) = \mu'(\rho - \rho_t) \tag{52}$$

with $\rho_t = (1 - \hat{P}_1)/\mu'$, suppose that the nematic field is aligned along one of the axes and varies only along y. In other words

$$\text{Re}\,(f_1) = f_1(y), \quad \text{Im}\,(f_1) = 0, \quad \rho = \rho(y). \tag{53}$$

Equation (35) then becomes

$$\partial_y^2\rho = \partial_y^2 f_1 \tag{54}$$

which can be integrated to give

$$\rho = f_1 + Ay + \rho_{\text{gas}}, \tag{55}$$

where A and ρ_{gas} are integration constants. Furthermore, to keep the fields finite for $|y| \to \infty$, one has $A = 0$. By substituting equations (54) and (55) into equation (31) one gets

$$\partial_{yy} f_1 = -4\mu'(\rho_{\text{gas}} - \rho_{\text{t}}) f_1 - 4\mu' f_1^2 + 4\xi f_1^3. \tag{56}$$

We multiply equation (56) by $\partial_y f_1$ and integrate it once to obtain

$$\frac{1}{2}(\partial_y f_1)^2 = -2\mu'(\rho_{\text{gas}} - \rho_{\text{t}}) f_1^2 - \frac{4}{3}\mu' f_1^3 + \xi f_1^4. \tag{57}$$

Separating the variables we obtain

$$\int \mathrm{d}y = \pm \int \frac{\mathrm{d} f_1}{\sqrt{-4\mu'(\rho_{\text{gas}} - \rho_{\text{t}}) f_1^2 - \frac{8}{3}\mu' f_1^3 + 2\xi f_1^4}}. \tag{58}$$

Integration of this equation under the condition $\lim_{y\to\pm\infty} f_1(y) = 0$ gives after simplifications

$$f_1(y) = \frac{3(\rho_{\text{t}} - \rho_{\text{gas}})}{1 + a\cosh\left(2y\sqrt{\mu'(\rho_{\text{t}} - \rho_{\text{gas}})}\right)}, \tag{59}$$

where $a = \sqrt{1 - \frac{9\xi}{2\mu'}(\rho_{\text{t}} - \rho_{\text{gas}})}$. We still need to obtain the value of ρ_{gas} which is fixed by the condition $\int_L \rho(y)\,\mathrm{d}y = \rho_0 L$, where L is the length of the box. In the integral on the lhs we can neglect the exponentially decaying tails and integrate instead on the infinite domain. Furthermore, in the limit $L \to \infty$ we can neglect the exponentially weak dependence of ρ_{gas} on L everywhere except the a term. We then obtain

$$\rho_{\text{gas}} \approx \rho_{\text{t}} - \frac{2\mu'}{9\xi}\left(1 - 4\,\mathrm{e}^{-KL}\right), \tag{60}$$

$$K = \frac{2\sqrt{2}\mu'}{9\sqrt{\xi}}\left(1 + \frac{9\xi}{2\mu'}(\rho_0 - \rho_{\text{t}})\right). \tag{61}$$

Substituting it back into equation (59) we get, under the assumption $L \to \infty$:

$$f_1(y) = \frac{f_1^{\text{band}}}{\left(1 + 2\,\mathrm{e}^{-\frac{KL}{2}}\cosh\left(y\frac{2\sqrt{2}\mu'}{3\sqrt{\xi}}\right)\right)} \quad \text{where} \quad f_1^{\text{band}} = \frac{2\mu'}{3\xi} \tag{62}$$

and we finally obtain the ordered solution density

$$\rho_{\text{band}} = f_1^{\text{band}} + \rho_{\text{gas}} = \rho_{\text{t}} + \frac{4\mu'}{9\xi}\left(1 + 2\,\mathrm{e}^{-KL}\right) \tag{63}$$

with, as expected, $\rho_{\text{band}} > \rho_{\text{t}} > \rho_{\text{gas}}$, which guarantees the stability of both the ordered and disordered parts of the solution. Note that since $f_1^{\text{band}} > 0$ the nematic order is parallel to the x direction (i.e. along the band orientation). This is the opposite of what happens in the Vicsek model, where bands extend transversally with respect to their polarization [15].

We can introduce the band fraction Ω which indicates the fraction of the box occupied by the band. If we suppose that the front width is negligible (once again justified in the limit $L \to \infty$), this band fraction is determined by the equation

$$\Omega(\rho_{\text{band}} - \rho_{\text{gas}}) + \rho_{\text{gas}} = \rho_0. \tag{64}$$

Substituting inside the values of ρ_{gas} and ρ_{band}, we obtain

$$\Omega = \frac{9\xi\,(\rho_0 - \rho_{\text{t}}) + 2\mu'}{6\mu'}. \tag{65}$$

The condition $0 < \Omega < 1$ gives us the lower $\sigma_{\min}$ and upper $\sigma_{\max}$ limits of the existence of bands. As found for polar particles aligning nematically, these limits of existence of the band solution extend *beyond* the region of linear instability of the homogeneous ordered solution (given by $\sigma \in [\sigma_{\text{s}}, \sigma_{\text{t}}]$, see figure 1). In figure 1, we provide a graphical illustration of the shape and properties of the band solution.

An important problem left for future work is the linear stability analysis of the band solution in two space dimensions. This is all the more important as the unpublished work of Shi and Ma [23] suggests the existence of some instability mechanism.

5. Langevin formulation

Being based on a master equation, the derivation we have discussed in the previous sections leads to a set of deterministic PDEs. This is a standard approach in equilibrium statistical physics, where the microscopic fluctuations are integrated out in the coarse-graining process implicit in the definition of a mesoscopic cell size ℓ_{B}. Fluctuations, when needed, can be eventually introduced as an additive, delta correlated stochastic term as in [16]. However, the presence of large density fluctuations [17] suggests that fluctuations may not be faithfully accounted for by some additive noise term. The precise nature of noise correlations at the mesoscopic level cannot be safely overlooked in non-equilibrium systems, as it is known that stochastic terms multiplicative in the relevant fields can radically alter the universality class of mesoscopic theories [34].

In this section, we perform in the same spirit as in [35] a direct coarse-graining of the microscopic dynamics in order to compute the (multiplicative) stochastic terms which emerge at the mesoscopic level. In the following, we restrict the computation to the stochastic terms emerging from the collisionless dynamics. In the dilute, low density regime, where collisions are sparse, this is not a major limitation, since one can reformulate the microscopic dynamics as composed of deterministic collisions separated by several self-diffusion events—see section 5.2 for more details.

For real-space coarse-graining, we make use of a smooth, isotropic, normalized (to one) filter $g_s(r)$ decaying exponentially or faster for $r > s$, e.g. a Gaussian of width s. The fluctuating coarse-grained density and nematic order field are then defined as

$$\rho(\mathbf{x}, t) \equiv \sum_{i=1}^{N} g_s(\mathbf{x}_i^t - \mathbf{x}) \tag{66}$$

and

$$\mathbf{w}(\mathbf{x}, t) \equiv \sum_{i=1}^{N} g_s(\mathbf{x}_i^t - \mathbf{x})\tilde{\mathbf{Q}}_i^t, \tag{67}$$

where we have introduced the microscopic traceless tensor

$$\tilde{\mathbf{Q}}_i^t = \hat{\mathbf{n}}_i^t\hat{\mathbf{n}}_i^t - \frac{\mathbb{I}}{2} = \frac{1}{2}\begin{pmatrix} \cos 2\theta_i^t & \sin 2\theta_i^t \\ \sin 2\theta_i^t & -\cos 2\theta_i^t \end{pmatrix} \equiv \mathbf{Q}(\theta_i^t). \tag{68}$$

5.1. Density field fluctuations

The correlations of density field fluctuations can be derived by generalizing an approach first outlined by Dean [36] for Brownian particles. As mentioned above, we use the collisionless dynamics. We are interested in the time evolution of the density field (66), which is given by

$$\rho(\mathbf{x}, t+\Delta t) = \sum_{i=1}^{N} g_s(\mathbf{x}_i^{t+\Delta t} - \mathbf{x}) = \sum_{i=1}^{N} g_s(\mathbf{x}_i^t + \Delta\mathbf{x}_i^t - \mathbf{x}), \tag{69}$$

where $\Delta\mathbf{x}_i^t = \mathbf{x}_i^{t+\Delta t} - \mathbf{x}_i^t = d_0\,\kappa_j^t\,\hat{\mathbf{n}}_j^t$ (see equation (2)).

Expanding up to second order in powers of $\Delta\mathbf{x}_i^t$ according to Itô calculus [27] one has

$$\partial_t \rho(\mathbf{x}, t) = T_0(\mathbf{x}, t) + T_1(\mathbf{x}, t), \tag{70}$$

where

$$T_0(\mathbf{x}, t) = \frac{d_0^2}{2\tau_\mathrm{d}} \sum_{i=1}^{N} [\hat{\mathbf{n}}_i^t]_\alpha [\hat{\mathbf{n}}_i^t]_\beta \partial_\alpha \partial_\beta g_s(\mathbf{x}_i^t - \mathbf{x}) \tag{71}$$

and

$$T_1(\mathbf{x}, t) = \frac{d_0}{\tau_\mathrm{d}} \sum_{i=1}^{N} \kappa_i^t \left(\hat{\mathbf{n}}_i^t \cdot \nabla\right) g_s(\mathbf{x}_i^t - \mathbf{x}). \tag{72}$$

The second order term T_0 yields the deterministic part of the density dynamics. By equations (66), (67) and the definition of the microscopic nematic tensor $\tilde{\mathbf{Q}}$ (equation (68)) one easily gets

$$T_0 = \frac{D_0}{2}(\mathbf{\Gamma} : \mathbf{w}) + \frac{D_0}{2}\Delta\rho, \tag{73}$$

that is, the right-hand side of the diffusion equation (35) in non-rescaled time and space units. The first-order term T_1 gives rise to the (zero average) stochastic term we are interested in. At this stage, T_1 is not a simple function of the mesoscopic fields; however, following [36] it is possible to show that its two point correlation can be recast as a function of ρ and $\mathbf{w}$. Averaging over the random numbers κ_i^t, we have, in the limit $s \to 0$,

$$\begin{aligned}\langle T_1(\mathbf{x}, t) T_1(\mathbf{y}, t')\rangle &= d_0^2 \frac{\delta(t-t')}{\tau_\mathrm{d}} \sum_{i=1}^{N} (\hat{\mathbf{n}}_i^t \cdot \nabla_x)(\hat{\mathbf{n}}_i^t \cdot \nabla_y) g_s(\mathbf{x}_i^t - \mathbf{x}) g_s(\mathbf{x}_i^t - \mathbf{y}) \\ &\simeq d_0^2 \frac{\delta(t-t')}{\tau_\mathrm{d}} \sum_{i=1}^{N} (\hat{\mathbf{n}}_i^t \cdot \nabla_x)(\hat{\mathbf{n}}_i^t \cdot \nabla_y)(g_s(\mathbf{x}-\mathbf{y}) g_s(\mathbf{x}_i^t - \mathbf{x})).\end{aligned} \tag{74}$$

Using equation (68), one then finds, approximating the filter g_s by a Dirac delta in the limit $s \to 0$,

$$\langle T_1(\mathbf{x}, t) T_1(\mathbf{y}, t')\rangle = d_0^2 \frac{\delta(t-t')}{\tau_\mathrm{d}} \partial_\alpha \partial_\beta \left[\delta(\mathbf{x}-\mathbf{y}) \left(w_{\alpha\beta}(\mathbf{x}, t) + \frac{1}{2}\rho(\mathbf{x}, t)\delta_{\alpha\beta}\right)\right]. \tag{75}$$

We can rewrite the noise term T_1 in the stochastically equivalent (i.e. with the same correlations on the mesoscopic scale) form

$$T_1(\mathbf{x}, t) = \nabla \cdot \mathbf{h}(\mathbf{x}, t), \tag{76}$$

where $\mathbf{h}$ is a Gaussian, zero-average vectorial noise, delta-correlated in time with correlations

$$\langle h_\alpha(\mathbf{x},t)h_\beta(\mathbf{y},t')\rangle \simeq \frac{d_0^2}{\tau_\mathrm{d}}\,\delta(t-t')\,\delta(\mathbf{x}-\mathbf{y})\left(w_{\alpha\beta}(\mathbf{x},t)+\frac{\delta_{\alpha\beta}}{2}\rho(\mathbf{x},t)\right). \tag{77}$$

Such a noise term can finally be expressed in the more convenient form

$$h_\alpha(\mathbf{x},t) = K_{\alpha\beta}(\mathbf{x},t)\tilde{h}_\beta(\mathbf{x},t), \tag{78}$$

where the Gaussian noise $\tilde{\mathbf{h}}$ has correlations independent from the hydrodynamic fields

$$\langle \tilde{h}_\alpha(\mathbf{x},t)\tilde{h}_\beta(\mathbf{x}',t')\rangle = 2D_0\,\delta_{\alpha\beta}\,\delta(t-t')\,\delta(\mathbf{x}-\mathbf{x}') \tag{79}$$

and the tensor $\mathbf{K}$ is implicitly defined from the relation $\mathbf{K}\cdot\mathbf{K} = (\rho/2)\mathbf{I}+\mathbf{w}$ (with $\mathbf{I}$ being the identity matrix). In the limit of small $\mathbf{w}$ considered here, we can expand $\mathbf{K}$ to first order in $\mathbf{w}$, yielding

$$\mathbf{K} = \frac{1}{\sqrt{2}}\rho^{1/2}\left(\mathbf{I}+\frac{\mathbf{w}}{\rho}\right). \tag{80}$$

The divergence term $\nabla\cdot$ appearing in T_1 reflects global density conservation, while the proportionality of noise variance to number density can be interpreted as a consequence of the central limit theorem. Adding up the two contributions, one finally gets

$$\partial_t\rho = \frac{D_0}{2}(\mathbf{\Gamma}:\mathbf{w}) + \frac{D_0}{2}\Delta\rho + \nabla\cdot\,(\mathbf{K}\cdot\tilde{\mathbf{h}}). \tag{81}$$

The coupling of density fluctuations to the density weighted nematic field $\mathbf{w} = \rho\mathbf{Q}$ can be better understood if we express the deterministic part appearing in the rhs of equation (81) as the sum of an active, non-equilibrium term

$$T_\mathrm{a} = \frac{D_0}{2}\partial_\alpha\left(\rho\partial_\beta\,[\mathbf{Q}]_{\alpha\beta}\right) \tag{82}$$

and a locally anisotropic diffusion term

$$T_\mathrm{m} = \frac{D_0}{2}\partial_\alpha\left([\mathbf{Q}]_{\alpha\beta}\,\partial_\beta\rho\right) + \frac{D_0}{2}\Delta\rho \tag{83}$$

whose mobility, proportional to $(2\mathbf{Q}+\mathbf{I})\rho$, stands in a fluctuation–dissipation relation [37][12] to the multiplicative noise term $\nabla\cdot\,(\mathbf{K}\cdot\tilde{\mathbf{h}})$, since the noise amplitude in equation (77) is proportional to $(2\mathbf{Q}+\mathbf{I})\rho$.

5.2. Nematic field fluctuations

We next discuss fluctuations of the nematic tensor. As seen from equation (67), $\mathbf{w}$ is a function of the $2N$ microscopic stochastic variables $\mathbf{x}_i^t$ and—through the microscopic nematic tensor (68)—θ_i^t, whose dynamics is given by equations (1) and (2). According to Itô calculus, one has

$$\partial_t\mathbf{w} = \mathbf{\Omega}_0 + \mathbf{\Omega}_1 + \mathbf{\Omega}_2, \tag{84}$$

where $\mathbf{\Omega}_0$ is the deterministic part of the coarse-grained collisionless dynamics (which we do not write here explicitly), arising from quadratic contributions in the Itô expansion, while $\mathbf{\Omega}_1$

[12] Kumaran discusses fluctuation–dissipation relations when the kinetic coefficient is field dependent.

and $\mathbf{\Omega}_2$ are two stochastic contributions, obtained by first order expansion in, respectively, the angular and spatial stochastic variables,

$$\mathbf{\Omega}_1 = \frac{2}{\tau_\mathrm{d}} \sum_{i=1}^{N} g_s(\mathbf{x}_i^t - \mathbf{x})\, \mathbf{A} \cdot \tilde{\mathbf{Q}}_i^t\, \psi_i^t, \tag{85}$$

$$\mathbf{\Omega}_2 = \frac{d_0}{\tau_\mathrm{d}} \sum_{i=1}^{N} \kappa_i^t \hat{\mathbf{n}}_i^t \cdot \nabla g_s(\mathbf{x}_i^t - \mathbf{x})\, \tilde{\mathbf{Q}}_i^t, \tag{86}$$

where ψ_i^t and κ_i^t are the microscopic noises and $\partial_\theta\, \tilde{\boldsymbol{Q}}_i^t = 2\,\mathbf{A} \cdot \tilde{\mathbf{Q}}_i^t$, with

$$\mathbf{A} = \begin{pmatrix} 0 & -1 \\ 1 & 0 \end{pmatrix}. \tag{87}$$

Note that in $\mathbf{\Omega}_1$ we have retained only the linear contribution in the microscopic noise ψ_i^t. We first focus on the stochastic terms $\mathbf{\Omega}_1$. On coarse-graining scales, averaging over the microscopic noise ψ_i^t, correlations of $\mathbf{\Omega}_1$ are given by

$$\begin{aligned}\langle [\mathbf{\Omega}_1(\mathbf{x}, t)]_{\alpha\beta} \left[\mathbf{\Omega}_1(\mathbf{y}, t')\right]_{\gamma\delta} \rangle &= 4\eta^2 \frac{\delta(t-t')}{\tau_\mathrm{d}} \sum_{i=1}^{N} g_s(\mathbf{x}_i^t - \mathbf{x}) g_s(\mathbf{x}_i^t - \mathbf{y}) \left[\mathbf{A} \cdot \tilde{\mathbf{Q}}_i^t\right]_{\alpha\beta} \left[\mathbf{A} \cdot \tilde{\mathbf{Q}}_i^t\right]_{\gamma\delta} \\ &\approx 4\eta^2 \frac{\delta(t-t')}{\tau_\mathrm{d}} g_s(\mathbf{y}-\mathbf{x}) \sum_{i=1}^{N} g_s(\mathbf{x}_i^t - \mathbf{x}) \left[\mathbf{A} \cdot \tilde{\mathbf{Q}}_i^t\right]_{\alpha\beta} \left[\mathbf{A} \cdot \tilde{\mathbf{Q}}_i^t\right]_{\gamma\delta}.\end{aligned} \tag{88}$$

To evaluate this correlator, we determine the average value $\langle \sum_i g_s\, (\mathbf{A} \cdot \tilde{\mathbf{Q}}_i^t)(\mathbf{A} \cdot \tilde{\mathbf{Q}}_i^t) \rangle$, in the framework of the deterministic dynamics studied in section 2, namely

$$\left\langle \sum_{i=1}^{N} g_s(\mathbf{x}_i^t - \mathbf{x}) \left[\mathbf{A} \cdot \tilde{\mathbf{Q}}_i^t\right]_{\alpha\beta} \left[\mathbf{A} \cdot \tilde{\mathbf{Q}}_i^t\right]_{\gamma\delta} \right\rangle = \int_{-\frac{\pi}{2}}^{\frac{\pi}{2}} \mathrm{d}\theta\, f(\mathbf{x}, \theta, t)\, [\mathbf{A} \cdot \mathbf{Q}(\theta)]_{\alpha\beta}\, [\mathbf{A} \cdot \mathbf{Q}(\theta)]_{\gamma\delta}\,. \tag{89}$$

After some rather lengthy calculations (see appendix C), one finds

$$\begin{aligned}\int_{-\frac{\pi}{2}}^{\frac{\pi}{2}} \mathrm{d}\theta\, f(\mathbf{x}, \theta, t)\, [\mathbf{A} \cdot \mathbf{Q}(\theta)]_{\alpha\beta}\, [\mathbf{A} \cdot \mathbf{Q}(\theta)]_{\gamma\delta} &= \rho\, J_{\alpha\beta\gamma\delta} + \frac{2b_2}{a_2} \left[(w_{\mu\nu} w_{\mu\nu}) J_{\alpha\beta\gamma\delta} - 2 w_{\alpha\beta} w_{\gamma\delta}\right] \\ &\quad + \frac{1}{4a_2} \left[\Gamma_{\mu\nu} w_{\mu\nu} J_{\alpha\beta\gamma\delta} - \Gamma_{\alpha\beta} w_{\gamma\delta} - \Gamma_{\gamma\delta} w_{\alpha\beta}\right],\end{aligned} \tag{90}$$

where we have introduced the tensor

$$J_{\alpha\beta\gamma\delta} = \tfrac{1}{2} \left(\delta_{\alpha\gamma}\delta_{\beta\delta} + \delta_{\alpha\delta}\delta_{\beta\gamma} - \delta_{\alpha\beta}\delta_{\gamma\delta}\right) \tag{91}$$

which plays the role of a unit tensor for the double contraction of symmetric traceless tensors, e.g. $w_{\alpha\beta} = J_{\alpha\beta\mu\nu}\, w_{\mu\nu}$. In order to characterize the noise $\mathbf{\Omega}_1$, we introduce the following change of variables:

$$[\mathbf{\Omega}_1(\mathbf{x}, t)]_{\alpha\beta} = H_{\alpha\beta\mu\nu}(\mathbf{x}, t)\, \tilde{\Omega}_{\mu\nu}(\mathbf{x}, t), \tag{92}$$

where $\tilde{\mathbf{\Omega}}$ is a tensorial symmetric traceless white noise, such that

$$\langle \tilde{\Omega}_{\alpha\beta}(\mathbf{x}, t)\tilde{\Omega}_{\gamma\delta}(\mathbf{y}, t')\rangle = 2D\delta(\mathbf{x}-\mathbf{y})\,\delta(t-t')\,J_{\alpha\beta\gamma\delta} \tag{93}$$

with $D = 2\eta^2/\tau_{\mathrm{d}}$. The correlation of $\mathbf{\Omega}_1$ then reads

$$\langle [\mathbf{\Omega}_1(\mathbf{x}, t)]_{\alpha\beta}\left[\mathbf{\Omega}_1(\mathbf{y}, t')\right]_{\gamma\delta}\rangle = 2D\delta(\mathbf{x}-\mathbf{y})\,\delta(t-t')\,H_{\alpha\beta\mu\nu}(\mathbf{x}, t)H_{\gamma\delta\mu\nu}(\mathbf{x}, t). \tag{94}$$

By identification with equation (88), and using equation (90), one eventually finds for $\mathbf{H}$

$$\begin{aligned} H_{\alpha\beta\gamma\delta} = \rho^{1/2}\,J_{\alpha\beta\gamma\delta} &+ \frac{b_2}{a_2\,\rho^{1/2}}\left[w_{\mu\nu}w_{\mu\nu}J_{\alpha\beta\gamma\delta} - 2w_{\alpha\beta}w_{\gamma\delta}\right] \\ &+ \frac{1}{8a_2\,\rho^{1/2}}\left[\Gamma_{\mu\nu}w_{\mu\nu}J_{\alpha\beta\gamma\delta} - \Gamma_{\alpha\beta}w_{\gamma\delta} - \Gamma_{\gamma\delta}w_{\alpha\beta}\right]. \end{aligned} \tag{95}$$

Note that, in agreement with the central limit theorem, $\mathbf{\Omega}_1$ is (at least to first order in $\mathbf{w}$) proportional to the square root of local density.

The second stochastic term $\mathbf{\Omega}_2$, finally, can be treated similarly, but it would give rise to a conserved noise (due to the presence of ∇ terms) akin to the one discussed for the density equations, thus related to density fluctuations affecting the $\mathbf{w} = \rho\mathbf{Q}$ field. We discard such conserved term as irrelevant (in the renormalization group sense) with respect to the non-conserved multiplicative noise $\mathbf{\Omega}_1$.

In order to write down the complete Langevin equation, one also needs to evaluate the contribution of the deterministic part $\mathbf{\Omega}_0$. However, expressing this contribution in terms of the fluctuating fields ρ and $\mathbf{w}$ turns out to be a very complicated task. One should also take into account collisions between particles, and not only the collisionless dynamics described by $\mathbf{\Omega}_0$. However, as mentioned earlier in this section, in the low density limit where our kinetic approach is justified, the microscopic dynamics (1)–(2) can be reformulated as deterministic binary collisions separated by several self-diffusion events, at the cost of a rescaling of the angular noise amplitude (note that this reformulation is not exact, in the sense that self-diffusion events no-longer have a Poissonian statistics). As a first approximation, this rescaling of the angular noise amplitude results in a global rescaling of the noise term $\tilde{\Omega}$ by a phenomenological factor χ. Therefore, we believe our method to provide essentially the correct relevant stochastic correlations for the nematic Langevin dynamics, up to an order one unknown multiplicative constant.

In addition, microscopic collisions could provide a further fluctuation source due to disorder below the coarse-graining scale, like the randomness of collision times. While we conjecture them to be irrelevant, we leave a final settlement of this difficult problem for future work, and use for the deterministic part of the dynamics the hydrodynamic equation (36), derived from the Boltzmann approach.

We thus finally obtain the stochastic equation for the nematic field (in rescaled units)

$$\partial_t\mathbf{w} = \mu\,\mathbf{w} - 2\xi\,\mathbf{w}\,(\mathbf{w}:\mathbf{w}) + \tfrac{1}{2}\Delta\mathbf{w} + \tfrac{1}{8}\mathbf{\Gamma}\rho + \chi\mathbf{H}:\tilde{\mathbf{\Omega}}. \tag{96}$$

A few remarks are in order: firstly, our expressions of the noise amplitudes $\mathbf{K}$ and $\mathbf{H}$ (equations (80) and (95)) suggest that the stochastic terms might be better expressed in terms of the field $\mathbf{Q}$, rather than $\mathbf{w} = \rho\mathbf{Q}$; secondly, equations similar to equations (81) and (96) were also derived from an apolar Vicsek-style model in [29].

In spite of the limitations listed above, the present approach already provides us with useful information on the statistics of the noise terms, which is seen to differ significantly from the white noise postulated on a phenomenological basis in previous works. On top of the overal $\rho^{1/2}$ dependency, our calculation reveals a non-trivial dependence of the correlation of the noise on the nematic order parameter (see equations (80), (81), (94) and (95)).

6. Conclusions

To summarize, using as a starting point the simple active nematics model of [26], we have demonstrated how one can derive in a systematic manner a continuous mesoscopic description. We formulated a version of the BGL approach put forward in [24, 25] for this case where (anisotropic) diffusion dominates, deriving a simple hydrodynamic equation for the nematic ordering field –equation (36). We have then used a direct coarse-graining approach to endow the hydrodynamic equations with proper noise terms.

The next stage, left for future work, consists in studying the stochastic PDEs obtained. At the linear level, it is clear that in the long-wavelength limit, standard results on giant density fluctuations [17] are recovered. However, the large amplitude of density fluctuations calls for a nonlinear analysis (which turns out to be very difficult), where the density dependence of the noise derived in section 5 may play an important role. Ideally, one should try to tackle this issue by applying methods from field theory and renormalization group analysis. In addition, we note that the multiplicative nature of the noise may also affect finite-wavelength properties, like coarsening behavior. The analysis of the stochastic PDEs can be done numerically, but some care must be taken when dealing with the multiplicative, conserved noise terms in (81).

Pending such attempts, some remarks and comments are already in order: like all previous cases studied before, the hydrodynamic equations found exhibit a domain of linear instability of the homogeneous ordered solution bordering the basic transition line σ_t. This solution does become linearly stable deeper in the ordered phase (for σ below σ_s). Moreover, we have found that the long-wavelength instability of the homogeneous ordered solution leads to a nonlinear, inhomogeneous band solution—see equation (62)—and that this band solution exists beyond the $[\sigma_s, \sigma_t]$ interval. These coexistence regions suggest, at the fluctuating level, *discontinuous* transitions.

This seems to be at odds with the reported behavior of the original microscopic model: (i) the order/disorder transition has been reported to be of the Kosterlitz–Thouless type [26]; (ii) there is no trace, at the microscopic level, of the existence of a non-segregated, homogeneous phase; (iii) coming back to giant number fluctuations, we note that the standard calculation is made in the homogeneous ordered phase whereas the numerical evidence for them reported in [26] appears now to have been obtained in the inhomogeneous phase. All this calls for revisiting the simple particle-based model and, eventually, understanding its behavior in the context of the stochastic continuum theory constructed here.

Acknowledgments

Part of this work was performed at the Max Planck Institute for the Physics of Complex Systems in Dresden, Germany, within the Advanced Study Group 2011/2012 'Statistical Physics of Collective Motion'. FG acknowledges support by EPSRC First Grant EP/K018450/1.

Appendix A. Fourier expansion of the master equation

We provide in this appendix details of the Fourier expansion of the master equation (10), leading to equation (21). Multiplying equation (10) by $e^{i2\theta}$ and integrating over θ, one gets

$$\partial_t \hat{f}_k = \partial_\alpha \partial_\beta \int_{-\pi/2}^{\pi/2} d\theta\, e^{i2k\theta} \hat{n}_\alpha(\theta)\hat{n}_\beta(\theta) f(\mathbf{x}, \theta, t) + \int_{-\pi/2}^{\pi/2} d\theta\, e^{i2k\theta} I_{\text{diff}}[f] + \int_{-\pi/2}^{\pi/2} d\theta\, e^{i2k\theta} I_{\text{coll}}[f, f]. \tag{A.1}$$

In the following, we successively compute each term of the rhs of equation (A.1).

A.1. Diffusion-like term

Let us define $Q_{\alpha\beta}(\theta)$ as

$$Q_{\alpha\beta}(\theta) = \hat{n}_\alpha(\theta)\hat{n}_\beta(\theta) - \frac{\delta_{\alpha\beta}}{2}. \tag{A.2}$$

We then have

$$\begin{aligned} Q_{11}(\theta, t) = -Q_{22}(\theta, t) &= \frac{1}{2}\cos 2\theta = \frac{e^{i2\theta} + e^{-i2\theta}}{4}, \\ Q_{12}(\theta, t) = Q_{21}(\theta, t) &= \frac{1}{2}\sin 2\theta = \frac{e^{i2\theta} - e^{-i2\theta}}{4i}. \end{aligned} \tag{A.3}$$

As a result,

$$\begin{aligned} \partial_\alpha \partial_\beta \int_{-\pi/2}^{\pi/2} d\theta\, e^{i2k\theta} \hat{n}_\alpha(\theta)\hat{n}_\beta(\theta) f(\theta) &= \partial_\alpha \partial_\beta \int_{-\pi/2}^{\pi/2} d\theta\, e^{i2k\theta} \left(Q_{\alpha\beta}(\theta) + \frac{\delta_{\alpha\beta}}{2} \right) f(\theta) \\ &= \frac{1}{2}\Delta \hat{f}_k + \frac{1}{4}\left(\nabla^{*2} \hat{f}_{k+1} + \nabla^2 \hat{f}_{k-1} \right). \end{aligned} \tag{A.4}$$

A.2. Self-diffusion term

We have rather straightforwardly

$$\begin{aligned} \int_{-\pi/2}^{\pi/2} d\theta\, e^{i2k\theta} I_{\text{diff}}[f] &= -\hat{f}_k + \int_{-\pi/2}^{\pi/2} d\theta'\, e^{i2k\theta'} f(\theta') \int_{-\infty}^{\infty} d\zeta\, e^{i2k\zeta} P(\zeta) \\ &= \left[\hat{P}_k - 1 \right] \hat{f}_k, \end{aligned} \tag{A.5}$$

where

$$\hat{P}_k = \int_{-\infty}^{\infty} d\zeta\, e^{i2k\zeta} P(\zeta) \tag{A.6}$$

is the Fourier transform of $P(\zeta)$.

A.3. Binary collisions term

Let us split the Fourier transformed collision integral into an outgoing (negative) collision term $I_k^{(-)}$ and an ingoing (positive) collision term $I_k^{(+)}$. A direct integration of the outgoing collision term yields, using $K(\theta,\theta') = \tilde{K}(\theta-\theta')$,

$$I_k^{(-)} \equiv -\int_{-\pi/2}^{\pi/2} \mathrm{d}\theta\, \mathrm{e}^{\mathrm{i}2k\theta} f(\theta) \int_{-\pi/2}^{\pi/2} \mathrm{d}\theta' f(\theta')\tilde{K}(\theta-\theta') = -\frac{1}{\pi}\sum_q \hat{K}_q \hat{f}_q \hat{f}_{k-q}, \tag{A.7}$$

where $\hat{K}_q$ is the Fourier coefficient of $\tilde{K}(\theta-\theta')$ given by, using equation (14),

$$\hat{K}_q = \int_{-\pi/2}^{\pi/2} \mathrm{d}\theta\, \mathrm{e}^{\mathrm{i}2q\theta}\left[\left|\sin\frac{\theta-\theta'}{2}\right| + \left|\cos\frac{\theta-\theta'}{2}\right|\right] = \frac{4}{1-16q^2}. \tag{A.8}$$

Then, the calculation of the ingoing collision term requires a few steps. After integration of the (generalized) Dirac delta δ_π, we have

$$I_k^{(+)} = \hat{P}_k \int_{-\pi/2}^{\pi/2} \mathrm{d}\theta_1 \int_{-\pi/2}^{\pi/2} \mathrm{d}\theta_2\, \mathrm{e}^{\mathrm{i}2k\Psi(\theta_1,\theta_2)} f(\theta_1)\tilde{K}(\theta_1-\theta_2) f(\theta_2). \tag{A.9}$$

By the change of variables $\phi = \theta_1 - \theta_2$, one gets

$$I_k^{(+)} = \hat{P}_k \int_{-\pi/2}^{\pi/2} \mathrm{d}\theta_2 \int_{-\pi/2-\theta_2}^{\pi/2-\theta_2} \mathrm{d}\phi\, \mathrm{e}^{\mathrm{i}2k\Psi(\theta_2+\phi,\theta_2)} f(\theta_2+\phi)\tilde{K}(\phi) f(\theta_2). \tag{A.10}$$

Using the π-periodicity of the integrand with respect to ϕ, we can change the integration interval on ϕ, yielding

$$I_k^{(+)} = \hat{P}_k \int_{-\pi/2}^{\pi/2} \mathrm{d}\theta_2 \int_{-\pi/2}^{\pi/2} \mathrm{d}\phi\, \mathrm{e}^{\mathrm{i}2k\Psi(\theta_2+\phi,\theta_2)} f(\theta_2+\phi)\tilde{K}(\phi) f(\theta_2). \tag{A.11}$$

On this interval of ϕ, one has from equation (13)

$$\Psi(\theta_2+\phi,\theta_2) = \theta_2 + \frac{\phi}{2}. \tag{A.12}$$

Expanding f in Fourier series (see equations (16) and (17)), we get

$$I_k^{(+)} = \frac{\hat{P}_k}{\pi^2}\sum_{q,q'} \hat{f}_q \hat{f}_{q'} \int_{-\pi/2}^{\pi/2} \mathrm{d}\theta_2\, \mathrm{e}^{\mathrm{i}2(k-q-q')\theta_2} \int_{-\pi/2}^{\pi/2} \mathrm{d}\phi\, \mathrm{e}^{\mathrm{i}(k-2q)\phi}\tilde{K}(\phi). \tag{A.13}$$

The integral over θ_2 is equal to $\pi\delta_{k,q+q'}$. Defining

$$\hat{J}_{k,q} = \int_{-\pi/2}^{\pi/2} \mathrm{d}\phi\, \mathrm{e}^{\mathrm{i}(k-2q)\phi}\tilde{K}(\phi), \tag{A.14}$$

we finally obtain

$$I_k^{(+)} = \frac{\hat{P}_k}{\pi}\sum_q \hat{J}_{k,q}\hat{f}_q\hat{f}_{k-q}. \tag{A.15}$$

The coefficient $\hat{J}_{k,q}$ can be computed explicitly, leading to

$$\hat{J}_{k,q} = 4\,\frac{1+2\sqrt{2}(2q-k)(-1)^q \sin\left(\frac{k\pi}{2}\right)}{1-4(2q-k)^2}. \tag{A.16}$$

Note finally that $\hat{J}_{0,q} = \hat{K}_q$.

Appendix B. Curvature-induced current and equilibrium limit

In this appendix, we show explicitly that the curvature-induced current, that is the term $\frac{1}{2}\mathrm{Re}(\nabla^{*2}\hat{f}_1)$ appearing in the continuity equation (23), originates from the coupling of orientation with motility. To this aim, we consider a slightly generalized microscopic process w.r.t. equations (1) and (2), where particles are also allowed to move perpendicular w.r.t. to the nematic tensor. Replace equation (2) by

$$\mathbf{x}_i^{t+\Delta t} = \mathbf{x}_i^t + d_0\,\mathbf{R}\left(\theta_i^t\right), \tag{B.1}$$

where $\mathbf{R}(\theta)$ is a stochastic operator defining the coupling between orientation and particle motion

$$\mathbf{R}(\theta) = \begin{cases} \hat{\mathbf{n}}(\theta) & \text{w.p. } p/2, \\ -\hat{\mathbf{n}}(\theta) & \text{w.p. } p/2, \\ \hat{\mathbf{n}}^{\perp}(\theta) & \text{w.p. } (1-p)/2, \\ -\hat{\mathbf{n}}^{\perp}(\theta) & \text{w.p. } (1-p)/2, \end{cases} \tag{B.2}$$

where $0 \leqslant p \leqslant 1$, w.p. stands for 'with probability' and $\hat{\mathbf{n}}^{\perp}(\theta) = \hat{\mathbf{n}}(\theta + \pi/2)$ is the perpendicular director. The standard active nematic case is recovered for $p = 1$, while $p = 1/2$ corresponds to an isotropic random walk, a case for which motion is decorrelated from order. The corresponding collisionless master equation reads

$$\begin{aligned} f(\mathbf{x}, \theta, t+\Delta t) = {} & \frac{p}{2}\left[f(\mathbf{x} - \hat{\mathbf{n}}(\theta)d_0, \theta, t) + f(\mathbf{x} + \hat{\mathbf{n}}(\theta)d_0, \theta, t)\right] \\ & + \frac{(1-p)}{2}\left[f(\mathbf{x} - \hat{\mathbf{n}}^{\perp}(\theta)d_0, \theta, t) + f(\mathbf{x} + \hat{\mathbf{n}}^{\perp}(\theta)d_0, \theta, t)\right]. \end{aligned} \tag{B.3}$$

By making use of Itô calculus, one gets at the mesoscopic timescale τ_{B}

$$\partial_t f(\mathbf{x}, \theta, t) = (2p-1)\partial_\alpha\partial_\beta\left[\hat{n}_\alpha(\theta)\hat{n}_\beta(\theta) - \frac{\delta_{\alpha\beta}}{2}\right] f(\mathbf{x}, \theta, t) + \frac{1}{2}\Delta f(\mathbf{x}, \theta, t), \tag{B.4}$$

where we have used the identity $\hat{n}_\alpha^{\perp}(\theta)\hat{n}_\beta^{\perp}(\theta) = \delta_{\alpha\beta} - \hat{n}_\alpha(\theta)\hat{n}_\beta(\theta)$. By considering the zeroth-order Fourier term of f (for which collision and angular diffusion terms vanish), one obtains the continuity equation (see also [29] for a similar result)

$$\partial_t \rho = \frac{1}{2}\Delta\rho + \frac{2p-1}{2}\mathrm{Re}\left(\nabla^{*2} f_1\right) \tag{B.5}$$

which shows that the non-equilibrium current vanishes for $p = \frac{1}{2}$.

Appendix C. Correlation of the nematic field fluctuations

In this appendix, we wish to compute the rhs of equation (89), that is, the non-trivial part of the noise correlation in the nematic order parameter equation. In other words, we need to compute the fourth-rank tensor

$$R_{\alpha\beta\gamma\delta} = \int_{-\frac{\pi}{2}}^{\frac{\pi}{2}} \mathrm{d}\theta\; f(\mathbf{x}, \theta, t)\,[\mathbf{A}\cdot\mathbf{Q}(\theta)]_{\alpha\beta}\,[\mathbf{A}\cdot\mathbf{Q}(\theta)]_{\gamma\delta}\,. \tag{C.1}$$

This is *a priori* a complicated task, and it will be useful to use a mapping between tensors and 'multicomplex' numbers (see, e.g. http://en.wikipedia.org/wiki/Multicomplex_number).

Although such a mapping is perhaps not a standard method, it will prove a very convenient technique in the following. We present this mapping in appendix C.1, and we sketch the main steps of the calculation in appendix C.2.

C.1. Mapping between tensors and 'multicomplex' numbers

Let us first emphasize that the mapping presented here is restricted to two-dimensional spaces. Before turning to tensors, we recall the rather natural correspondence between two-dimensional vectors and complex numbers: a vector $\mathbf{V} = (V_1, V_2)$ can be mapped onto a complex number $\mathcal{V} = V_1 + \mathrm{i}V_2$, where $\mathrm{i}^2 = -1$. Denoting the mapping by a double arrow $\leftrightarrow$, we can write

$$\mathbf{V} = (V_1, V_2) \longleftrightarrow \mathcal{V} = V_1 + \mathrm{i}V_2 = V_\alpha \mathrm{i}^{\alpha-1}. \tag{C.2}$$

Here, and in what follows, a sum over repeated indices is understood. The scalar product between two vectors $\mathbf{V}$ and $\mathbf{V}'$ can be expressed in complex notations as

$$\mathbf{V}\cdot\mathbf{V}' = \frac{1}{2}\left(\mathcal{V}\mathcal{V}'^* + \mathcal{V}^*\mathcal{V}'\right). \tag{C.3}$$

Such a mapping can be generalized to describe tensors by introducing several imaginary numbers i, j, ..., which commute one with the other. For instance, a second rank tensor $\mathbf{Q}$ of components $Q_{\alpha\beta}$ can be mapped onto a 'bicomplex' number

$$Q_{\alpha\beta} \longleftrightarrow \mathcal{Q} = Q_{11} + \mathrm{i}Q_{21} + \mathrm{j}Q_{12} + \mathrm{ij}Q_{22} = Q_{\alpha\beta}\,\mathrm{i}^{\alpha-1}\mathrm{j}^{\beta-1} \tag{C.4}$$

where $\mathrm{i}^2 = \mathrm{j}^2 = -1$ and i,j commute. The contraction operation between two tensors can also be expressed in complex notations, through a generalization of equation (C.3). A symmetric traceless tensor $\mathbf{Q}$ reads in complex notations

$$\mathcal{Q} = Q_{11} + (\mathrm{i}+\mathrm{j})Q_{12} - \mathrm{ij}Q_{11} = (1-\mathrm{ij})(Q_{11} + \mathrm{i}Q_{12}) \tag{C.5}$$

and is thus fully characterized by the complex number $Q_{11} + \mathrm{i}Q_{12}$. For instance, the local nematic tensor $\mathbf{Q}(\theta)$ defined in equation (68) maps onto $\frac{1}{2}(1-\mathrm{ij})\,\mathrm{e}^{2\mathrm{i}\theta}$, and the nematic field $\mathbf{w}$ maps onto $\frac{1}{2}(1-\mathrm{ij})\,f_1$. These simple relations will be useful in the following.

In addition, one of the interests of the complex notation is that tensorial products simply map onto products of complex numbers. Starting from two vectors $\mathbf{V}$ and $\mathbf{V}'$, their tensorial product maps as follows:

$$P_{\alpha\beta} = V_\alpha V'_\beta \longleftrightarrow \mathcal{P} = (V_1 + \mathrm{i}V_2)(V'_1 + \mathrm{j}V'_2). \tag{C.6}$$

The introduction of fourth rank tensors follows the same line. Introducing four independent imaginary numbers i, j, k, l ($\mathrm{i}^2 = \mathrm{j}^2 = \mathrm{k}^2 = \mathrm{l}^2 = -1$), a tensor of components $R_{\alpha\beta\gamma\delta}$ can be mapped onto a 'quadricomplex' number:

$$R_{\alpha\beta\gamma\delta} \longleftrightarrow \mathcal{R} = R_{\alpha\beta\gamma\delta}\,\mathrm{i}^{\alpha-1}\mathrm{j}^{\beta-1}\mathrm{k}^{\gamma-1}\mathrm{l}^{\delta-1}. \tag{C.7}$$

If $\mathbf{R}$ is the tensorial product of two second rank tensors $\mathbf{Q}$ and $\mathbf{Q}'$, namely $R_{\alpha\beta\gamma\delta} = Q_{\alpha\beta}Q'_{\gamma\delta}$, the associated 'quadricomplex' number is the product of two bicomplex numbers

$$\mathcal{R} = \left(Q_{\alpha\beta}\,\mathrm{i}^{\alpha-1}\mathrm{j}^{\beta-1}\right)\left(Q'_{\gamma\delta}\,\mathrm{k}^{\gamma-1}\mathrm{l}^{\delta-1}\right). \tag{C.8}$$

In particular, if $\mathbf{Q}$ and $\mathbf{Q}'$ are symmetric traceless tensors, the above expression simplifies to

$$\mathcal{R} = (1-\mathrm{ij})(1-\mathrm{kl})(Q_{11} + \mathrm{i}Q_{12})(Q'_{11} + \mathrm{k}Q'_{12}). \tag{C.9}$$

Such relations will turn useful in the following calculations.

C.2. Calculation of the correlation

We now turn to the calculation of the fourth rank tensor defined in equation (C.1), using the mapping to 'multicomplex' numbers introduced above. We first need to evaluate $\mathbf{A}\cdot\mathbf{Q}(\theta)$ in these notations. It is rather straightforward to show that

$$(\mathbf{A}\cdot\mathbf{Q}(\theta))_{\alpha\beta} \longleftrightarrow \mathrm{i}\mathcal{Q}(\theta) = \tfrac{1}{2}(\mathrm{i}+\mathrm{j})\,\mathrm{e}^{2\mathrm{i}\theta}. \tag{C.10}$$

This can be shown from the mapping $\mathbf{A}\leftrightarrow \mathrm{i}-\mathrm{j}$, using a generalization of equation (C.3). The resulting expression is however simple to interpret, since the multiplication by i corresponds to a rotation by an angle of $\frac{\pi}{2}$ in the complex plane. Computing the tensorial product $(\mathbf{A}\cdot\mathbf{Q})(\mathbf{A}\cdot\mathbf{Q})$, one finds

$$(\mathbf{A}\cdot\mathbf{Q}(\theta))_{\alpha\beta}(\mathbf{A}\cdot\mathbf{Q}(\theta))_{\gamma\delta} \longleftrightarrow \tfrac{1}{4}(\mathrm{i}+\mathrm{j})(\mathrm{k}+\mathrm{l})\,\mathrm{e}^{2\mathrm{i}\theta}\,\mathrm{e}^{2k\theta}. \tag{C.11}$$

Expanding the two exponentials and using standard trigonometric relations leads to

$$\mathrm{e}^{2\mathrm{i}\theta}\,\mathrm{e}^{2k\theta} = \tfrac{1}{2}(1+\mathrm{ik}) + \tfrac{1}{2}(1-\mathrm{ik})\,\mathrm{e}^{4\mathrm{i}\theta}. \tag{C.12}$$

As a result,

$$(\mathbf{A}\cdot\mathbf{Q}(\theta))_{\alpha\beta}(\mathbf{A}\cdot\mathbf{Q}(\theta))_{\gamma\delta} \longleftrightarrow \tfrac{1}{8}(1+\mathrm{ik})(\mathrm{i}+\mathrm{j})(\mathrm{k}+\mathrm{l}) + \tfrac{1}{8}(1-\mathrm{ik})(\mathrm{i}+\mathrm{j})(\mathrm{k}+\mathrm{l})\,\mathrm{e}^{4\mathrm{i}\theta}. \tag{C.13}$$

Computing the average over the phase-space distribution $f(\mathbf{x},\theta,t)$ leads to

$$\int_{-\frac{\pi}{2}}^{\frac{\pi}{2}} \mathrm{d}\theta\, f(\mathbf{x},\theta,t)\,[\mathbf{A}\cdot\mathbf{Q}(\theta)]_{\alpha\beta}\,[\mathbf{A}\cdot\mathbf{Q}(\theta)]_{\gamma\delta} \longleftrightarrow \frac{1}{8}(1+\mathrm{ik})(\mathrm{i}+\mathrm{j})(\mathrm{k}+\mathrm{l})\rho(\mathbf{x},t) + \frac{1}{8}(1-\mathrm{ik})(\mathrm{i}+\mathrm{j})(\mathrm{k}+\mathrm{l})\,f_1(\mathbf{x},t). \tag{C.14}$$

It is then necessary to use the closure relation (30), yielding

$$\int_{-\frac{\pi}{2}}^{\frac{\pi}{2}} \mathrm{d}\theta\, f(\mathbf{x},\theta,t)\,[\mathbf{A}\cdot\mathbf{Q}(\theta)]_{\alpha\beta}\,[\mathbf{A}\cdot\mathbf{Q}(\theta)]_{\gamma\delta} \longleftrightarrow \frac{1}{8}(1+\mathrm{ik})(\mathrm{i}+\mathrm{j})(\mathrm{k}+\mathrm{l})\rho + \frac{b_2}{8a_2}(1-\mathrm{ik})(\mathrm{i}+\mathrm{j})(\mathrm{k}+\mathrm{l})\,f_1^2 + \frac{1}{32a_2}(1-\mathrm{ik})(\mathrm{i}+\mathrm{j})(\mathrm{k}+\mathrm{l})\nabla^2 f_1. \tag{C.15}$$

We now need to perform the inverse mapping onto tensors. Let us start with the first term in the rhs of equation (C.15). Looking for a tensor of the form $a\delta_{\alpha\gamma}\delta_{\beta\delta} + b\delta_{\alpha\delta}\delta_{\beta\gamma} + c\delta_{\alpha\beta}\delta_{\gamma\delta}$, one finds by identification of the associated complex expressions that

$$(1+\mathrm{ik})(\mathrm{i}+\mathrm{j})(\mathrm{k}+\mathrm{l}) \longleftrightarrow \delta_{\alpha\gamma}\delta_{\beta\delta} + \delta_{\alpha\delta}\delta_{\beta\gamma} - \delta_{\alpha\beta}\delta_{\gamma\delta} \equiv 2J_{\alpha\beta\gamma\delta}. \tag{C.16}$$

The second and third terms in the rhs of equation (C.15) can be computed along the same line. Both terms have a similar structure, which can be formally written as $(1-\mathrm{ik})(\mathrm{i}+\mathrm{j})(\mathrm{k}+\mathrm{l})(C_{11}+\mathrm{i}C_{12})(D_{11}+\mathrm{i}D_{12})$, where $C_{\alpha\beta}$ and $D_{\alpha\beta}$ are symmetric traceless tensors that do not necessarily commute ($C_{\alpha\beta}$ may include derivation operators). One then finds, again by identification of the complex forms

$$(1-\mathrm{ik})(\mathrm{i}+\mathrm{j})(\mathrm{k}+\mathrm{l})(C_{11}+\mathrm{i}C_{12})(D_{11}+\mathrm{i}D_{12}) \longleftrightarrow C_{\mu\nu}D_{\mu\nu}J_{\alpha\beta\gamma\delta} - C_{\alpha\beta}D_{\gamma\delta} - C_{\gamma\delta}D_{\alpha\beta}. \tag{C.17}$$

As a result, we find

$$(1-\mathrm{ik})(\mathrm{i}+\mathrm{j})(\mathrm{k}+\mathrm{l})\,f_1^2 \longleftrightarrow 4\left[(w_{\mu\nu}w_{\mu\nu})J_{\alpha\beta\gamma\delta}-2w_{\alpha\beta}w_{\gamma\delta}\right], \tag{C.18}$$

$$(1-\mathrm{ik})(\mathrm{i}+\mathrm{j})(\mathrm{k}+\mathrm{l})\nabla^2 f_1 \longleftrightarrow 2\left[\Gamma_{\mu\nu}w_{\mu\nu}J_{\alpha\beta\gamma\delta}-\Gamma_{\alpha\beta}w_{\gamma\delta}-\Gamma_{\gamma\delta}w_{\alpha\beta}\right]. \tag{C.19}$$

Gathering all terms, one then recovers equation (90) from equation (C.15).

References

[1] Ramaswamy S 2010 *Annu. Rev. Condens. Matter Phys.* **1** 323
[2] Romanczuk P, Bär M, Ebeling W, Lindner B and Schimansky-Geier L 2012 *Eur. Phys. J. Spec. Top.* **202** 1162
[3] Marchetti M C *et al* 2013 *Rev. Mod. Phys.* **85** 1143
[4] Parrish J K and Hamner W M (ed) 1997 *Animal Groups in Three Dimensions* (Cambridge: Cambridge University Press)
[5] Couzin I D, Krause J, Franks N and Levin S 2005 *Nature* **433** 513
Buhl J *et al* 2006 *Science* **312** 1402
[6] Ballerini M *et al* 2008 *Proc. Natl Acad. Sci. USA* **105** 1232
[7] Helbing D, Farkas I and Vicsek T 2000 *Nature* **407** 487
Helbing D, Farkas I J and Vicsek T 2000 *Phys. Rev. Lett.* **84** 1240
[8] Moussaïd M, Helbing D and Théraulaz G 2011 *Proc. Natl Acad. Sci. USA* **108** 6884
[9] Schaller V, Weber C A, Semmerich C, Frey E and Bausch A 2010 *Nature* **467** 73
Schaller V, Weber C, Frey E and Bausch A R 2011 *Soft Matter* **7** 3213
Schaller V, Weber C A, Hammerich B, Frey E and Bausch A R 2011 *Proc. Natl Acad. Sci. USA* **108** 19183
Sumino Y, Nagai K H, Shitaka Y, Tanaka D, Yoshikawa K, Chaté H and Oiwa K 2012 *Nature* **483** 448
[10] Peruani F, Starruß J, Jakovljevic V, Sogaard-Andersen L, Deutsch A and Bär M 2012 *Phys. Rev. Lett.* **108** 098102
[11] Kudrolli A, Lumay G, Volfson D and Tsimring L S 2008 *Phys. Rev. Lett.* **100** 058001
[12] Narayan V, Ramaswamy S and Menon N 2007 *Science* **317** 105
[13] Deseigne J, Dauchot O and Chaté H 2010 *Phys. Rev. Lett.* **105** 098001
Deseigne J, Léonard S, Dauchot O and Chaté H 2012 *Soft. Matter* **8** 5629
[14] Vicsek T *et al* 1995 *Phys. Rev. Lett.* **75** 1226
[15] Grégoire G and Chaté H 2004 *Phys. Rev. Lett.* **92** 025702
Chaté H *et al* 2008 *Phys. Rev.* E **77** 046113
[16] Toner J and Tu Y 1995 *Phys. Rev. Lett.* **75** 4326
Toner J and Tu Y 1998 *Phys. Rev.* E **58** 4828
Toner J 2012 *Phys. Rev.* E **86** 031918
[17] Ramaswamy S, Simha R A and Toner J 2003 *Europhys. Lett.* **62** 196
Toner J, Tu Y and Ramaswamy S 2005 *Ann. Phys. (NY)* **318** 170
[18] Zhang H P, Beer A, Florin E-L and Swinney H L 2010 *Proc. Natl Acad. Sci. USA* **107** 13626
[19] Bertin E, Droz M and Grégoire G 2006 *Phys. Rev.* E **74** 022101
[20] Bertin E, Droz M and Grégoire G 2009 *J. Phys. A: Math. Theor.* **42** 445001
[21] Ihle T 2011 *Phys. Rev.* E **83** 030901
[22] Baskaran A and Marchetti M C 2008 *Phys. Rev. Lett.* **101** 268101
Baskaran A and Marchetti M C 2008 *Phys. Rev.* E **77** 011920
Baskaran A and Marchetti M C 2012 *Eur. Phys. J.* E **35** 95
[23] Shi X and Ma Y 2010 arXiv:1011.5408
[24] Peshkov A, Ngo S, Bertin E, Chaté H and Ginelli F 2012 *Phys. Rev. Lett.* **109** 098101
[25] Peshkov A, Aranson I S, Bertin E, Chaté H and Ginelli F 2012 *Phys. Rev. Lett.* **109** 268701

[26] Chaté H, Ginelli F and Montagne R 2006 *Phys. Rev. Lett.* **96** 180602
[27] Oksendal B 1992 *Stochastic Differential Equations* (Berlin: Springer)
[28] Huang K 1987 *Statistical Mechanics* 2nd edn (New York: Wiley)
[29] Mishra S 2009 *PhD Thesis* Indian Institute of Science (www.openthesis.org/document/view/6011220)
[30] Oseen C W 1933 *Trans. Faraday Soc.* **29** 883
Frank F C 1958 *Discuss. Faraday Soc.* **25** 19
[31] Mishra S, Simha R A and Ramaswamy S 2010 *J. Stat. Mech.* P02003
[32] Gopinath A, Hagan M F, Marchetti M C and Baskaran A 2012 *Phys. Rev.* E **85** 061903
[33] Chou Y-L, Wolfe R and Ihle T 2012 *Phys. Rev.* E **86** 021120
[34] Muñoz M A 1998 *Phys. Rev.* E **57** 1377
[35] Tailleur J and Cates M E 2008 *Phys. Rev. Lett.* **100** 218103
[36] Dean D S 1996 *J. Phys. A: Math. Gen.* **29** L613
[37] Kumaran V 1996 *J. Chem. Phys.* **104** 3120

5.3 NUMERICAL SIMULATIONS

I performed numerical simulations of the obtained hydrodynamic equations using my own pseudo-spectral code. As the nematic order is always perpendicular to the variation of the order parameter, there is no sense in performing a 1D simulation of the equations. Only a two dimensional simulation is useful.

Performing the simulation we have found at small system sizes, the presence of three different states. At high noise the system is completely disordered. When we lower the noise we found that a narrow band of nematic order appears. The width of this band increases with the decrease of the noise up to the point where the nematic order occupies the whole domain.

5.3.1 *Band solution*

At large system sizes (approximately bigger than 200x200) I have found that the band solution is unstable as in the mixed-polar nematic model. The obtained chaotic solutions completely destroy the band for higher values of the noise, which can however shortly almost reform as in the case of the microscopic model. The time of reformation of the band increases with system size. However at lower noise values a band with chaotic borders persists. As of now I do not know if the band will be completely destroyed at larger system sizes. A simulation at very big system sizes is needed to confirm it. This study should also answer if there is a real difference between the nematic and the mixed polar-nematic model. A deeper study of the stability of the chaotic solution is presented in the next section where we study the stability of the band solution.

At noise values lower than that of the band existence a homogenous ordered solution exists. This state can be considered as equivalent to the quasi-long-range order observed in microscopic simulations. An effective noise term is needed to exactly determine if this two states are equivalent.

5.3.2 *Nematic defects*

At very low noise values, if we start from random initial conditions our equations will explode after some more or less long simulation time. This can seem strange as no spurious instability, at low noise values, was found for this model contrary to the polar and mixed polar-nematic models. Closer analysis shows that nematic defects appear in the simulation. The explosion of the equations happens when such defects collide as can be seen on Fig(31). We can first note that nematic defects where already observed in experimental systems

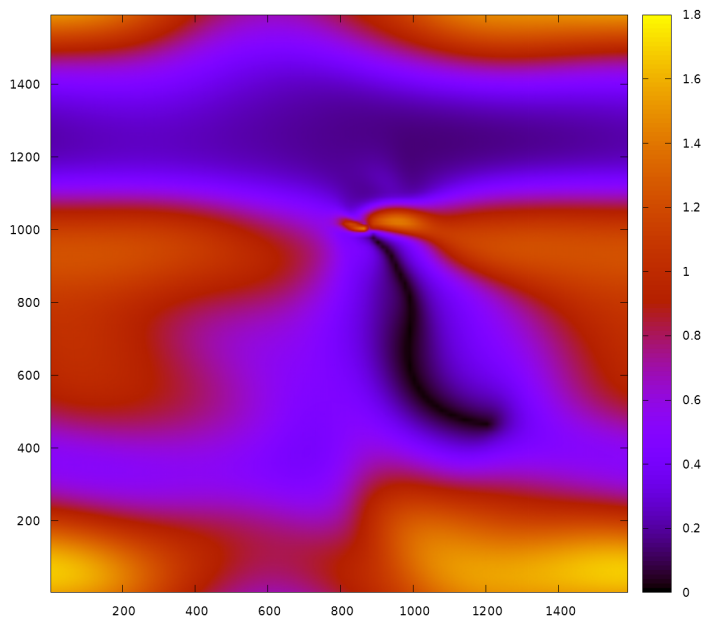

Figure 31: Density field of a simulation at $\sigma = 0.04$ and $L = 1600 \times 1600$. A collision of nematic defects can be seen in the center of the figure, which lead to the explosion of the simulation code.

of shaken rods[10]. Thus nematic defects should be natural for dry active matter.

A much better study of the defects must be performed in our equations. For this end we must find a way to stabilize the equations, for them not to explode at defect collision. We have tried to do this by setting the density field to a constant. However in this case all the defects annihilate, thus another way should be found. It is however important to note, that no fluid is necessary to the formation of defects, contrary to what have been pretended by Giomi et al.[20].

5.4 STABILITY OF THE BAND SOLUTION

5.4.1 *Analytical investigation*

As we have seen in numerical simulations, the band solution is always unstable, in sufficiently large systems. The band breaks and reforms, resembling a spatio-temporal chaotic solution. We first want to investigate analytically the stability of the band solution that we have found to linear non-homogeneous perturbations.

Our starting point are the hydrodynamic equations

$$\partial_t \rho = \frac{1}{2}\Delta\rho + \frac{1}{2}\Re\left(\nabla^{*2} f_1\right) \tag{41}$$

$$\partial_t f_1 = \left(\mu - \xi\left|f_1\right|^2\right) f_1 + \frac{1}{4}\nabla^2\rho + \frac{1}{2}\Delta f_1 \tag{42}$$

As previously we will suppose that the nematic order in the band is oriented in the $\vec{x}$ direction, i.e the band solution varies across y. We will search for an instability along the x direction which, if found, is sufficient to prove that the band is unstable. Our perturbed solutions then read

$$\begin{aligned} \rho(x,y,t) &= \rho(y) + \delta\rho(y)\, e^{ikx+\lambda t} \\ f^{(R)}(x,y,t) &= f(y) + \delta f^{(R)}(y)\, e^{ikx+\lambda t} \\ f^{(I)}(x,y,t) &= \delta f^{(I)}(y)\, e^{ikx+\lambda t} \end{aligned} \tag{43}$$

As previously we expand the μ coefficient that depends on density using

$$\mu(\rho) = \mu'(\rho - \rho_t)$$

where $\mu' = {}^{\partial\mu}/_{\partial\rho}$. Substituting equations(43) into equations(41,42) linearizing them in perturbations and separating the real and imaginary parts we obtain

$$\begin{aligned} \lambda\delta\rho &= \frac{1}{2}\left(\partial_y^2\delta\rho - k^2\delta\rho\right) + \frac{1}{2}\left(-\left(k^2+\partial_y^2\right)\delta f^{(R)} + 2ik\partial_y\delta f^{(I)}\right) \\ \lambda\delta f^{(R)} &= -\left(\mu'\rho_t + 3\xi f^2\right)\delta f^{(R)} + \mu'\rho\delta f^{(R)} + \mu' f\delta\rho \\ &\quad -\frac{1}{4}\left(k^2+\partial_y^2\right)\delta\rho + \frac{1}{2}\left(\partial_y^2 - k^2\right)\delta f^{(R)} \\ \lambda\delta f^{(I)} &= -\left(\mu'\rho_t + \xi f^2\right)\delta f^{(I)} + \mu'\rho\delta f^{(I)} - \frac{1}{2}ik\partial_y\delta\rho + \frac{1}{2}\left(\partial_y^2 - k^2\right)\delta f^{(I)} \end{aligned}$$

This set of equations does not have any evident solution. We are thus obliged to search for a perturbed solution, supposing $k \to 0$. For this end we introduce the following ansatz

$$\begin{aligned} \lambda &= \lambda_0 + \lambda_1 k + \lambda_2 k^2 + \dots \\ \delta\rho &= \delta\rho_0 + r_1 k + \delta\rho_2 k^2 + \dots \\ \delta f^{(R)} &= \delta f_0^{(R)} + \delta f_1^{(R)} k + \delta f_2^{(R)} k^2 + \dots \\ \delta f^{(I)} &= \delta f_0^{(I)} + \delta f_1^{(I)} k + \delta f_2^{(I)} k^2 + \dots \end{aligned}$$

Substituting this ansatz back into our equations and taking $k = 0$ we obtain

$$\begin{aligned} \lambda_0\delta\rho_0 &= \frac{1}{2}\partial_y^2\delta\rho_0 - \frac{1}{2}\partial_y^2\delta f_0^{(R)} \\ \lambda_0\delta f_0^{(R)} &= -\left(\mu'\rho_t + 3\xi f^2\right)\delta f_0^{(R)} + \mu'\rho\delta f_0^{(R)} + \mu' f\delta\rho_0 \\ &\quad -\frac{1}{4}\partial_y^2\delta\rho_0 + \frac{1}{2}\partial_y^2\delta f_0^{(R)} \\ \lambda_0\delta f_0^{(I)} &= -\left(\mu'\rho_t + \xi f^2\right)\delta f_0^{(I)} + \mu'\rho\delta f_0^{(I)} + \frac{1}{2}\partial_y^2\delta f_0^{(I)} \end{aligned}$$

Setting $\lambda_0 = 0$ we immediately see that the two first equations completely decouple from the third one. We thus set $\delta f_0^{(I)} = 0$. The first two equations left are just the derivatives along y of the band equations (54,56) in the article, thus we immediately know the solution $\delta\rho_0 = \delta f_0^{(R)} = \partial_y f$.

At order $k = 1$ we obtain

$$\begin{aligned}
\lambda_1 \partial_y f &= \frac{1}{2}\partial_y^2 \delta\rho_1 - \frac{1}{2}\partial_y^2 \delta f_1^{(R)} \\
\lambda_1 \partial_y f &= -\left(\mu'\rho_t + 3\xi f^2\right)\delta f_1^{(R)} + \mu'\rho\delta f_1^{(R)} + \mu' f \delta\rho_1 \\
&\quad -\frac{1}{4}\partial_y^2\delta\rho_1 + \frac{1}{2}\partial_y^2 \delta f_1^{(R)} \\
-\frac{1}{2} i\partial_y^2 f &= -\left(\mu'\rho_t + \xi f^2\right)\delta f_1^{(I)} + \mu'\rho\delta f_1^{(I)} + \frac{1}{2}\partial_y^2\delta f_1^{(I)}
\end{aligned}$$

Once again we have two decoupled sets of equations. As the first two equations are just the repetition of the set of equations at order $k = 0$, we just set $\lambda_1 = \delta\rho_1 = \delta f_1^{(R)} = 0$ without loss of generality. Comparing the third equation to equation (56) in the article we immediately obtain the solution $\delta f_1^{(I)} = -2if$.

At order $k = 2$ we obtain

$$\begin{aligned}
(\lambda_2 - 1)\,\partial_y f &= \frac{1}{2}\partial_y^2\delta\rho_2 - \frac{1}{2}\partial_y^2 \delta f_2^{(R)} \\
\left(\lambda_2 + \frac{3}{4}\right)\partial_y f &= -(\mu'\rho_t + 3\xi f^2)\delta f_2^{(R)} + \mu'\rho\delta f_2^{(R)} + \mu' f\delta\rho_2 \\
&\quad -\frac{1}{4}\partial_y^2\delta\rho_2 + \frac{1}{2}\partial_y^2\delta f_2^{(R)} \\
0 &= -\left(\mu'\rho_t + \xi f^2\right)\delta f_2^{(I)} + \mu'\rho\delta f_2^{(I)} + \frac{1}{2}\partial_y^2\delta f_2^{(I)}
\end{aligned}$$

The last equation is the same as the one at order $k = 0$, and is as always decoupled from the other two, we thus set $\delta f_2^{(I)} = 0$. As for the first two equations we introduce a change of variables $w = \delta\rho_2 - \delta f_2^{(R)}$ to obtain

$$\begin{aligned}
(\lambda_2 - 1)\partial_y f &= \frac{1}{2}\partial_y^2 w \\
(\frac{3}{2}\lambda_2 + \frac{1}{4})\partial_y f &= -(\mu'\rho_t + 3\xi f^2)\delta f_2^{(R)} + \mu'\rho\delta f_2^{(R)} \\
&\quad +\mu'(w + \delta f_2^{(R)})f + \frac{1}{4}\partial_y^2\delta f_2^{(R)}
\end{aligned}$$

From the first equation we obtain the exact solution $w = 2(\lambda_2 - 1)\int dy f(y)$. Substituting it to the second equation we obtain

$$\begin{aligned}
&(\frac{3}{2}\lambda_2 + \frac{1}{4})\partial_y f - 2\mu' f(\lambda_2 - 1)\int dy f = \\
&\quad -(\mu'\rho_t + 3\xi f^2)\delta f_2^{(R)} + \mu'\rho\delta f_2^{(R)} + \mu' f\delta f_2^{(R)} + \frac{1}{4}\partial_y^2\delta f_2^{(R)} \qquad (44)
\end{aligned}$$

The r.h.s of this equation can be written as $L\delta f_2^{(R)}$, where the differential operator L is given by

$$L = \frac{1}{4}\partial_y^2 + \left[-(\mu'\rho_t + 3\xi f^2) + \mu'\rho + \mu' f\right]$$

This operator is self-adjoint (see for example ref[25]). We know from the zero order set of equations that its eigenfunction $\delta f_2^{(R)} = \partial_y f$ corresponds to the zero eigenvalue.

We know from math analysis (see once again ref[25]) that for a linear inhomogeneous differential equation $Lu(x) = v(x)$, the equation $Lu(x) - \lambda_i u(x) = v(x)$ has a solution if and only if $< \beta_i | v >= 0$. Here$L$ is a self-adjoint operator, and β_i and λ_i are respectively the eigenfunction and eigenvalues of this operator.

In our case the eigenvalue is zero, thus the condition of solvability of equation(44) is given by

$$\begin{aligned}
\int dy \partial_y f \left((\frac{3}{2}\lambda_2 + \frac{1}{4})\partial_y f - 2\mu' f(\lambda_2 - 1) \int dy f \right) &= 0 \\
(\frac{3}{2}\lambda_2 + \frac{1}{4}) \int dy \left(\partial_y f\right)^2 - 2\mu'(\lambda_2 - 1) \int dy \left(\left(\partial_y f\right) f \int dy f \right) &= 0
\end{aligned}$$

We can proceed to an integration by part of the second integral of this equation

$$\begin{aligned}
\int dy \left(\left(\partial_y f\right) f \int dy f \right) &= \left[f^2 \int dy f \right]_{-\infty}^{\infty} - \int dy \left(f \left(\partial_y f\right) \int dy f + f^3 \right) \\
2 \int dy \left(\left(\partial_y f\right) f \int dy f \right) &= -\int dy f^3
\end{aligned}$$

because of the symmetry $f(-x) = f(x)$ of the band solution.

The solvability condition is thus given by

$$\begin{aligned}
(\frac{3}{2}\lambda_2 + \frac{1}{4}) \int dy \left(\partial_y f\right)^2 + \mu'(\lambda_2 - 1) \int dy f^3 &= 0 \\
\lambda_2 \left(\frac{3}{2} \int dy \left(\partial_y f\right)^2 + \mu' \int dy f^3 \right) &= -\frac{1}{4} \int dy \left(\partial_y f\right)^2 + \mu' \int dy f^3
\end{aligned}$$

The band solution f is strictly positive and μ' also thus

$$\left(\frac{3}{2} \int dy \left(\partial_y f\right)^2 + \mu' \int dy f^3 \right) > 0$$

The band solution is then unstable if

$$d = -\frac{1}{4} \int dy \left(\partial_y f\right)^2 + \mu' \int dy f^3 > 0$$

Our band solution has the form

$$f(y) = \frac{c}{1 + a\cosh(by)}$$

where $a = 2e^{\frac{-KL}{2}}$, $b = \frac{2\sqrt{2}\mu'}{3\sqrt{3}}$, $c = \frac{2\mu'}{3\xi}$, K is a positive quantity defined in section 2 of the article and L is the system size. Using the values of the integrals already computed in the previous chapter we obtain

$$d = \frac{c^2 b}{6} g(a)$$

where

$$\begin{aligned} g(a) &= \frac{\left(14 + a^2\right) \mathrm{sq}(a) - 3\left(3 + 2a^2\right) \mathrm{lg}(a)}{\mathrm{sq}(a)\left(a^2 - 1\right)^2} \\ \mathrm{lg}(a) &= \log\left(\frac{1 + \mathrm{sq}(a)}{a}\right) \\ \mathrm{sq}(a) &= \sqrt{1 - a^2} \end{aligned}$$

Since $c^2 b$ is a positive quantity, to prove that the band solution is unstable we only need to prove that $g(a)$ is positive. The quantity a is positive and varies from zero for $L \to \infty$ to one for $L \to 0$. It is easy to check that

$$\begin{aligned} \lim_{a \to 0^+} g(a) &= 9 \ln\left(\frac{2}{a}\right) - 14 + O\left(a^2\right) > 0 \\ \lim_{a \to 1^-} g(a) &= 1 + O\left((1 - a)^{7/2}\right) > 0 \end{aligned}$$

A plot on the whole domain $]0 : 1[$ show that $g(a)$ is always positive as can be seen on figure 32 on the next page. The instability of the solution increases with the system size. Thus for sufficiently large systems, the band solution is always unstable, confirming the result of numerical analysis.

5.4.2 *Numerical analysis*

To study the nature of the chaotic regime, I performed simulations to study the mean order parameter in the system and the spatial correlations. This study is performed for various system sizes, at global density $\rho_0 = 1$ and at three different values of the noise parameter $\sigma = 0.275$, $\sigma = 0.2775$ and $\sigma = 0.28$. Note that for $\rho_0 = 1$ the limit of existence of the band solution is given by $\sigma_{min} \approx 0.253$ and $\sigma_{max} \approx 0.285$ and the critical transition noise is $\sigma_t \approx 0.277$.

First we want to study the behavior of the mean global order parameter as the system size is increased. For a spatio-temporal chaotic solution with finite correlation length and times we expect that the mean order parameter will decrease with a power law of $\langle Q \rangle \sim L^{-1}$. However as we can see on Fig(33) not only this exponent is not exactly observed, but its value changes for different values of noise. For lower values of noise ($\sigma = (0.275, 0.2775)$) this can be explained by the insufficient size of the systems that we study, we see that at sufficiently big size there is a crossover to the correct behavior. However

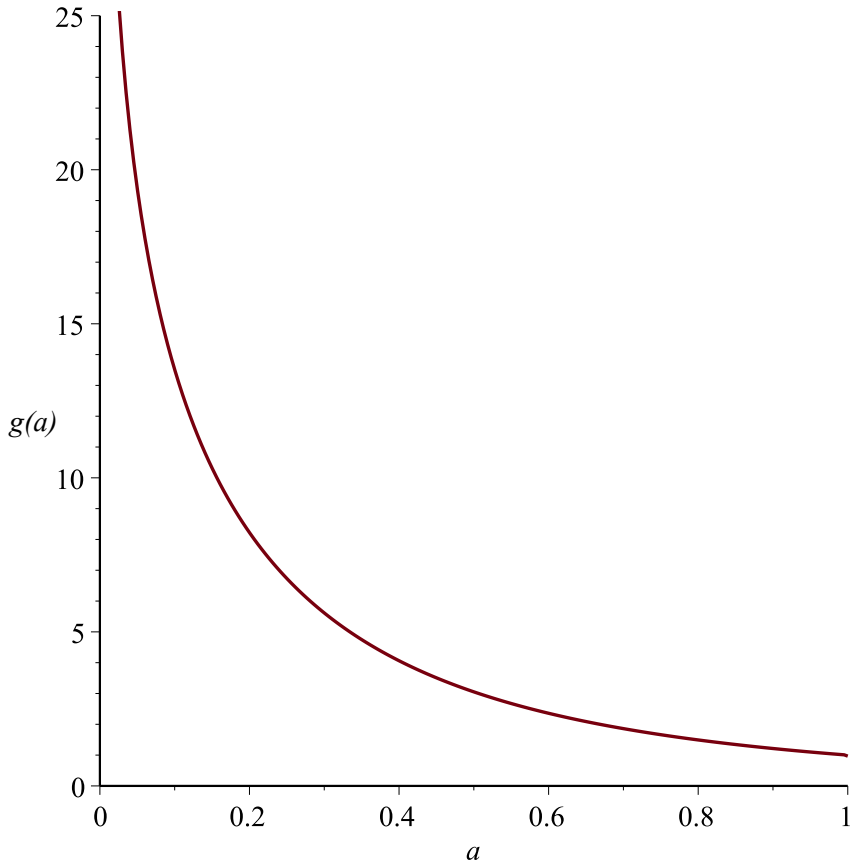

Figure 32: Values of the function $g(a)$ on the domain $]0:1[$. We see that the function is strictly positive, thus the band solution is unstable.

for the highest value of the noise $\sigma^2 = 0.28$ the observed exponent is approximately 1.14, thus it is bigger than one. This can hardly be an effect of an insufficient system size. However this can be due to an insufficient number of measure points.

As shown on the Fig(34), for $\sigma = 0.28$ the approximate auto-correlation time of the nematic order parameter is $1E5$ while we have time series of about $5E6$. Thus the time series that we have represent about 50 correlation times at best, i.e. there is perhaps no strange behavior of the decrease of the order parameter, but just insufficient statistics. It is however numerically difficult to obtain better results than that.

We can also study the spatial density auto-correlation function to prove that the typical correlation length in the system does not increase with system size. To better analyze the spatial auto-correlation function we will suppose that the 2D spatial auto-correlation function is isotropic. As shown on Fig(35), this is a valid approximation for large sizes of the system. We can thus study simply the 1D auto-correlation function. Plotting the azimuthally-averaged spatial auto-correlation function on Fig(36) we see that as the system size increases it converges to a fixed function, confirming a typical size of the structures and thus a decrease to zero of the order parameter in the thermodynamic limit. We can also see that the auto-correlation length decreases as the noise is increased (we do not have enough points to deduct a power law from it).

5.5 CONCLUSIONS

We have obtained equations that faithfully reproduce the behavior of the microscopic system. We were able to confirm that the band structures present in the system are always unstable. This instability leads to spatio-temporal chaos. However we still do not exactly know if this instability will lead to a complete destruction of the bands in the thermodynamic limit. If yes, that will confirm that the order-disorder transition in the system is continuous. This will also confirm that this system is different from the mixed polar-nematic case, and that in the latter case polar order can not be completely neglected as was done by Baskaran and Marchetti[7].

More studies are needed for a better knowledge of the chaotic phase. We need as well to perform the study of the defects presented in our equations. As always, effective noise should be deducted in order to study the giant density fluctuations that should be present in the system. However recent studies of the microscopic model in our group tend to predict that the giant number fluctuations in the quasi-long-range ordered phase are simply due to the phase separation in the chaotic regime. Thus an effective noise would not be needed to confirm giant density fluctuations with the hydrodynamic equations, further studies are needed for that.

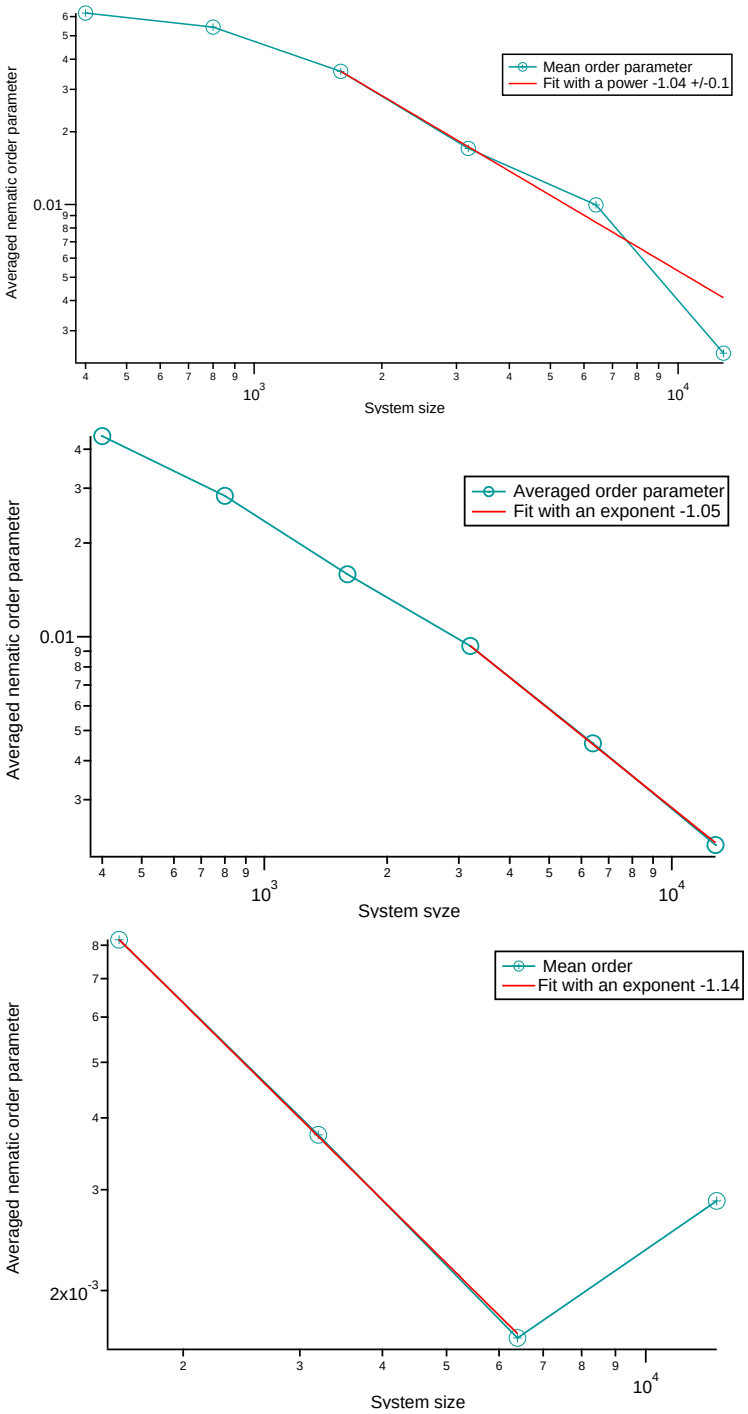

Figure 33: Fit of the order parameter as a function of system size, for different noise values. From top to bottom the noise values are $\sigma = 0.275$, $\sigma = 0.2775$ and $\sigma = 0.28$.

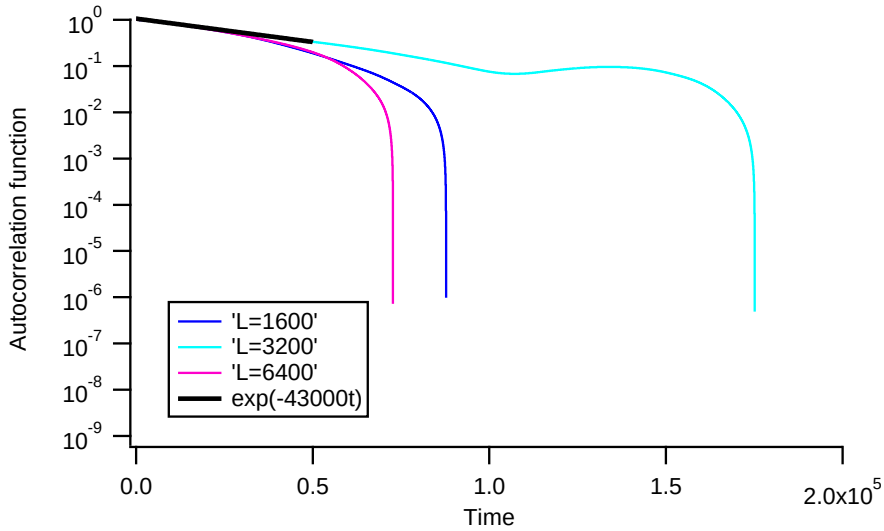

Figure 34: Temporal auto-correlation function of the mean nematic order parameter for different system sizes at $\sigma = 0.28$.

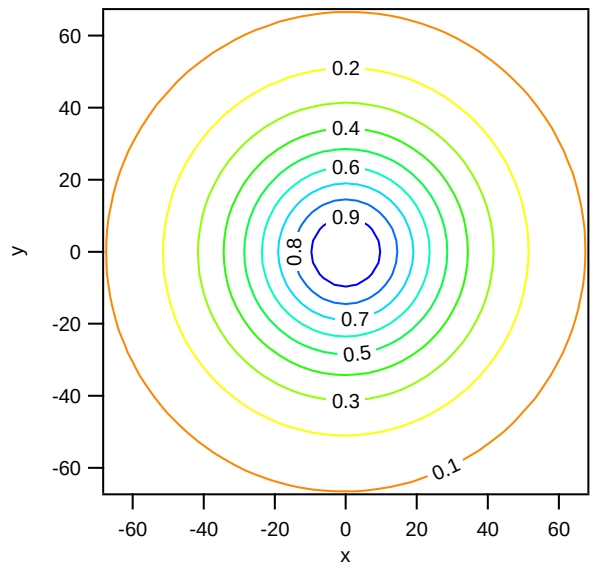

Figure 35: 2D Spatial auto-correlation function of the density for $L = 6400$ and $\sigma = 0.28$.

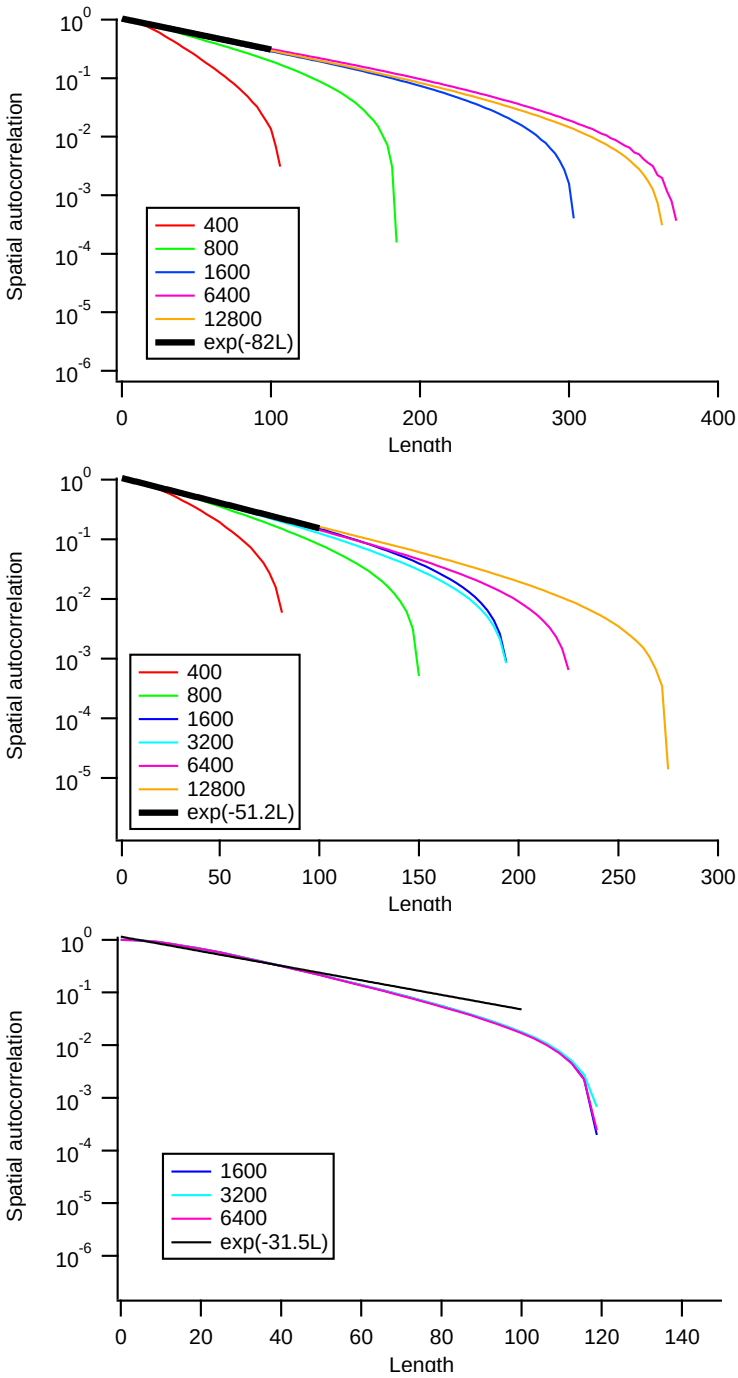

Figure 36: 1D Density spatial auto-correlation function. From top to bottom the noise values are $\sigma = 0.275$, $\sigma = 0.2775$ and $\sigma = 0.28$.

BIBLIOGRAPHY

[1] I.S. Aranson and L.S. Tsimring. Model of coarsening and vortex formation in vibrated granular rods. *PRE*, 67(2):021305, 2003. (Cited on page 11.)

[2] I.S. Aranson and L.S. Tsimring. Pattern formation of microtubules and motors: Inelastic interaction of polar rods. *Physical Review E*, 71(5 AR 050901), 2005. (Cited on page 11.)

[3] I.S. Aranson and L.S. Tsimring. Theory of self-assembly of microtubules and motors. *PRE*, 74(3):031915, 2006. (Cited on page 11.)

[4] T. Balch and R.C. Arkin. Behavior-based formation control for multirobot teams. *Ieee Transactions on Robotics and Automation*, 14(6):926–939, 1998. (Cited on page 3.)

[5] M. Ballerini, N. Cabibbo, R. Candelier, A. Cavagna, E. Cisbani, I. Giardina, V. Lecomte, A. Orlandi, G. Parisi, A. Procaccini, M. Viale, and V. Zdravkovic. Interaction ruling animal collective behavior depends on topological rather than metric distance: Evidence from a field study. *Proceedings of the National Academy of Sciences*, 105(4):1232–1237, 2008. (Cited on page 147.)

[6] A. Baskaran and M.C. Marchetti. Hydrodynamics of self-propelled hard rods. *PRE*, 77(1):011920, 2008. (Cited on pages 10 and 24.)

[7] A. Baskaran and M.C. Marchetti. Self-regulation in self-propelled nematic fluids. *European Physical Journal E*, 35(9):95, 2012. (Cited on page 136.)

[8] E. Bertin, M. Droz, and G. Grégoire. Boltzmann and hydrodynamic description for self-propelled particles. *Physical Review E*, 74(2 AR 022101), 2006. (Cited on pages 9 and 36.)

[9] E. Bertin, M. Droz, and G. Grégoire. Hydrodynamic equations for self-propelled particles: microscopic derivation and stability analysis. *Journal of Physics A-mathematical and Theoretical*, 42(44):445001, 2009. (Cited on pages 9, 43, and 48.)

[10] D.L. Blair, T. Neicu, and A. Kudrolli. Vortices in vibrated granular rods. *PRE*, 67(3):031303, 2003. (Cited on page 130.)

[11] J.P. Boyd. *Chebyshev and Fourier spectral methods*. Dover Publications, 2001. (Cited on page 57.)

[12] J. Buhl, D. Sumpter, I.D. Couzin, J.J. Hale, E. Despland, E.R. Miller, and S.J. Simpson. From disorder to order in marching locusts. *Science*, 312(5778):1402–1406, 2006. (Cited on page 3.)

[13] A. Cavagna, A. Cimarelli, I. Giardina, G. Parisi, R. Santagati, F. Stefanini, and M. Viale. Scale-free correlations in starling flocks. *Proceedings of the National Academy of Sciences of the United States of America*, 107(26):11865–11870, 2010. (Cited on page 3.)

[14] L.-Y. Chen, N. Goldenfeld, and Y. Oono. Renormalization group and singular perturbations: Multiple scales, boundary layers, and reductive perturbation theory. *Physical Review E*, 54(1):376–394, 1996. (Cited on page 54.)

[15] L.H. Cisneros, R. Cortez, C. Dombrowski, R.E. Goldstein, and J.O. Kessler. Fluid dynamics of self-propelled microorganisms, from individuals to concentrated populations. *Experiments in Fluids*, 43(5):737–753, 2007. (Cited on page 4.)

[16] D.S. Dean. Langevin equation for the density of a system of interacting langevin processes. *Journal of Physics A-mathematical and General*, 29(24):L613–L617, 1996. (Cited on page 26.)

[17] J. Gautrais, C. Jost, M. Soria, A. Campo, S. Motsch, R. Fournier, S. Blanco, and G. Theraulaz. Analyzing fish movement as a persistent turning walker. *Journal of Mathematical Biology*, 58(3):429–445, 2009. (Cited on page 3.)

[18] F. Ginelli and H. Chaté. Relevance of metric-free interactions in flocking phenomena. *Physical Review Letters*, 105(16):168103, 2010. (Cited on pages 4, 9, 20, and 147.)

[19] F. Ginelli, F. Peruani, M. Bar, and H. Chaté. Large-scale collective properties of self-propelled rods. *Physical Review Letters*, 104(18):184502, 2010. (Cited on pages xiii, xiv, 4, 9, 20, 75, and 76.)

[20] L. Giomi, M.J. Bowick, X. Ma, and M.C. Marchetti. Defect annihilation and proliferation in active nematics. *PRL*, 110(22):228101, 2013. (Cited on page 130.)

[21] A. Gopinath, M.F. Hagan, M.C. Marchetti, and A. Baskaran. Dynamical self-regulation in self-propelled particle flows. *Physical Review E*, 85(6 AR 061903), 2012. (Cited on page 10.)

[22] Y. Hatwalne, S. Ramaswamy, M. Rao, and R.A. Simha. Rheology of active-particle suspensions. *Physical Review Letters*, 92(11):118101, 2004. (Cited on page 4.)

[23] T. Ihle. Kinetic theory of flocking: Derivation of hydrodynamic equations. *Physical Review E*, 83(3 AR 030901), 2011. (Cited on page 9.)

[24] T. Ihle. Invasion-wave induced first-order phase transition in systems of active particles. *eprint arXiv:1304.0149*, 2013. (Cited on page 10.)

[25] C. Lanczos. *Linear differential operators*. Van Nostrand, 1961. (Cited on pages 91 and 133.)

[26] L.D. Landau. *Collected papers of L.D. Landau. Edited and with an introduction by D. ter Haar*. Oxford, New York, Pergamon Press, 1965. (Cited on pages 24 and 25.)

[27] N.D. Mermin and H. Wagner. Absence of ferromagnetism or antiferromagnetism in one- or two-dimensional isotropic heisenberg models. *PRL*, 17(22):1133–1136, 1966. (Cited on page 5.)

[28] S. Mishra, A. Baskaran, and M.C. Marchetti. Fluctuations and pattern formation in self-propelled particles. *PRE*, 81(6):061916, 2010. (Cited on page 10.)

[29] M. Moussaid, D. Helbing, and G. Theraulaz. How simple rules determine pedestrian behavior and crowd disasters. *Proceedings of the National Academy of Sciences of the United States of America*, 108(17):6884–6888, 2011. (Cited on page 3.)

[30] S. Ramaswamy, R.A. Simha, and J. Toner. Active nematics on a substrate: Giant number fluctuations and long-time tails. *Europhysics Letters*, 62(2):196–202, 2003. (Cited on page 99.)

[31] P. Romanczuk and L. Schimansky-Geier. Mean-field theory of collective motion due to velocity alignment. *Ecological Complexity*, 10:83–92, 2012. (Cited on page 11.)

[32] V. Schaller, C. Weber, C. Semmrich, E. Frey, and A.R. Bausch. Polar patterns of driven filaments. *Nature*, 467(7311):73–77, 2010. (Cited on pages 3 and 35.)

[33] A. Sokolov and I.S. Aranson. Reduction of viscosity in suspension of swimming bacteria. *Physical Review Letters*, 103(14):148101, 2009. (Cited on pages 3 and 4.)

[34] A. Sokolov, R.E. Goldstein, F.I. Feldchtein, and I.S. Aranson. Enhanced mixing and spatial instability in concentrated bacterial suspensions. *Physical Review E*, 80(3):031903, 2009. (Cited on page 4.)

[35] J. Toner and Y.H. Tu. Long-range order in a 2-dimensional dynamical xy model - how birds fly together. *Physical Review Letters*, 75(23):4326–4329, 1995. (Cited on pages 5, 9, and 26.)

[36] J. Toner, Y.H. Tu, and S. Ramaswamy. Hydrodynamics and phases of flocks. *Annals of Physics*, 318(1):170–244, 2005. (Cited on pages 8, 9, and 75.)

[37] Y. Tu, J. Toner, and M. Ulm. Sound waves and the absence of galilean invariance in flocks. *PRL*, 80(21):4819–4822, 1998. (Cited on pages 7 and 35.)

[38] A.E. Turgut, H. Celikkanat, F. Gokce, and E. Sahin. Self-organized flocking in mobile robot swarms. *Swarm Intelligence*, 2(2-4):97–120, 2008. (Cited on page 3.)

[39] T. Vicsek, A. Czirok, E. Benjacob, I. Cohen, and O. Shochet. Novel type of phase-transition in a system of self-driven particles. *Physical Review Letters*, 75(6):1226–1229, 1995. (Cited on pages 3, 4, and 33.)

Part IV

METRIC-FREE MODEL

6 THE POLAR METRIC-FREE MODEL

6.1 INTRODUCTION TO THE MICROSCOPIC MODEL

While the metric interactions used for the previous models are an adequate representation of what arise between microscopic particles, for example bacteria or microtubules, in the case of big organisms like fish or birds such interactions are not pertinent. For example during the StarFlag project investigation, it was established[5] that starlings align themselves on neighbors located as certain angles, but irrespective of any particular distance. This is especially important as the large animals are not able to locate other animals that are screened by others using only their sight. Thus a metric-free interaction should be introduced for such a case.

In ref[18] Ginelli and Chaté introduce a metric-free variant of the polar Vicsek model. Once again we have N polar particles with constant speed amplitude v_0 that evolve off-lattice in a 2D space in a streaming and collision succession of events. To determine the neighbors irrespective of the distance, a Voronoi tessellation of the spp's positions is used. Particle i in this case interacts only with particles that are located in its first Voronoi shell. The streaming and collision rules are then given by

$$\begin{aligned} x_i^{t+1} &= x_i^t + v_0 \mathrm{e}\left(\theta_i^{t+1}\right)\Delta t \\ \theta_i^{t+1} &= \arg\left[\sum_{j\in V_i} e^{i\theta_j^t} + \eta\vec{\xi}_i \mathbf{N_i}\right] \end{aligned}$$

Where the summation is taken on the first neighbors V_i of particle i. Note that in this case the authors used a vectorial and not an angular noise, as explained in chapter 3. Thus $\vec{\xi}_i$ is a random unit vector, $\mathbf{N_i}$is the number of neighbors of the particle i and $\eta \in [0:1]$ is the noise amplitude.

As the noise amplitude η is decreased, the polar order parameter $\left\langle \vec{P} \right\rangle = \frac{1}{Nv_0}\sum_{i=1}^{N}\vec{v}_i$ undergoes a continuous transition from disorder, $\left\langle \vec{P} \right\rangle = 0$, to order $\left\langle \vec{P} \right\rangle = 1$. At low noise, true long range order exists in this model as in the metric case of polar particles. However as the interactions are now metric-free, the local order parameter is decorrelated from the local density. This in turn does not provide any mechanism for density segregation and formation of high density solitonic structures, which are never observed in this system, further corroborating the hypothesis that the phase transition is of second order. This conclusion, about the nature of the phase transition, is

also confirmed by the study of the Binder cummulant $B = 1 - \frac{\langle P^4 \rangle_t}{3\langle P^2 \rangle_t^2}$, that does not reach to negative values, as it would for a first order transition.

Nevertheless as in the metric case, giant density fluctuations are observed in this model, with the power law behavior $\Delta n \sim \langle n \rangle^{0.875}$. This exponent is not only higher than the equilibrium exponent of $1/2$ but also bigger than the exponent predicted and observed in the case of the polar metric model which is $4/5$.

In summary:

1. The metric free polar model present a transition to true long-range order as in the case of metric interactions;

2. Contrary to the metric case, the phase transition is of second order, due to the absence of any density segregated structures.

3. Giant density fluctuations are present, but with a slightly higher exponent than in the case of metric interactions.

6.2 DERIVATION OF HYDRODYNAMIC EQUATIONS

Next follows an article on the derivation of the hydrodynamic equations and some studies of obtained equations.

Continuous Theory of Active Matter Systems with Metric-Free Interactions

Anton Peshkov,[1,2,6] Sandrine Ngo,[1,6] Eric Bertin,[3,6] Hugues Chaté,[1,2,6] and Francesco Ginelli[4,5]

[1]*Service de Physique de l'Etat Condensé, CEA-Saclay, 91191 Gif-sur-Yvette, France*
[2]*LPTMC, CNRS-UMR 7600, Université Pierre et Marie Curie, 75252 Paris, France*
[3]*Laboratoire de Physique, Université de Lyon, ENS Lyon, CNRS, 46 Allée d'Italie, 69007 Lyon, France*
[4]*Istituto dei Sistemi Complessi, CNR, via dei Taurini 19, I-00185 Roma, Italy*
[5]*SUPA, Institute for Complex Systems and Mathematical Biology, King's College, University of Aberdeen, Aberdeen AB24 3UE, United Kingdom*
[6]*Max Planck Institute for the Physics of Complex Systems, Nothnitzer Str. 38, 01187 Dresden, Germany*

(Received 30 March 2012; published 28 August 2012)

We derive a hydrodynamic description of metric-free active matter: starting from self-propelled particles aligning with neighbors defined by "topological" rules, not metric zones—a situation advocated recently to be relevant for bird flocks, fish schools, and crowds—we use a kinetic approach to obtain well-controlled nonlinear field equations. We show that the density-independent collision rate per particle characteristic of topological interactions suppresses the linear instability of the homogeneous ordered phase and the nonlinear density segregation generically present near threshold in metric models, in agreement with microscopic simulations.

DOI: 10.1103/PhysRevLett.109.098101 PACS numbers: 87.10.Ca, 05.20.Dd, 05.65.+b, 87.18.−h

Collective motion is a central theme in the emerging field of active matter studies [1]. For physicists, the interest largely lies in the nontrivial cases where the emergence of collective motion can be seen as an instance of spontaneous symmetry breaking out of equilibrium: without leaders, guiding external fields, or confinement by boundaries, large groups inside of which an "individual" can only perceive local neighbors are able to move coherently. After this was realized in the seminal papers of Vicsek *et al.* [2] and Toner and Tu [3], much progress has been recorded in the physics community [1,4], alongside continuing modeling work in ethology and biology [5,6].

Most models consist of self-propelled particles interacting with neighbors defined to be those particles within some finite distance [7]. Among those "metric models," that introduced by Vicsek *et al.* [2] is arguably the simplest: in the presence of noise, point particles move at constant speed, aligning ferromagnetically with others currently within unit distance. The study of the Vicsek model has revealed rather unexpected behavior. Of particular importance in the following is the emergence of phase segregation, under the form of high-density high-order traveling bands [8], in a large part of the orientationally ordered phase bordering the onset of collective motion, relegating further the spatially homogeneous fluctuating phase treated by Toner and Tu. Similar observations of density segregation were made for important variants of the Vicsek model, such as polar particles with nematic alignment [9] (self-propelled rods) or the active nematics model of Refs. [10,11]. The genericity of these observations has been confirmed, in the Vicsek case, by the derivation and analysis of continuous field equations [12,13] (see also Refs. [14,15]). It was shown in particular that the homogeneous ordered solution is linearly unstable near onset, and that solitary wave structures akin to the traveling bands, arise at the nonlinear level.

Even though metric interaction zones are certainly of value in cases such as shaken granular media [16,17] and motility assays [18,19] where alignment arises mostly from inelastic collisions, it has been argued recently [20–22] that they are not realistic in the context of higher organisms such as birds, fish, or pedestrians, whose navigation decisions are likely to rely on interactions with neighbors defined using metric-free, "topological" criteria. Statistical analysis of flocks of hundreds to a few thousand of individuals revealed that a typical starling interacts mostly with its 7 or 8 closest neighbors, regardless of the flock density [20]. The realistic, data-based, model of pedestrian motion developed by Moussaid *et al.* relies on the "angular perception landscape" formed by neighbors screening out others [21].

At a more theoretical level, the study of the Vicsek model with Voronoi neighbors [23] (those whose associated Voronoi cells form the first shell around the central cell) has shown that metric-free interactions are relevant at the collective scale: in particular, the traveling bands mentioned above disappear, leaving only a Toner-Tu-like phase. Below, we show that the introduction of Voronoi neighbors suppresses the density-segregated phase in other variants of the Vicsek model. In spite of the recognized importance of metric-free interactions, no continuous field equations describing the above models are available which would help put the above findings on firmer theoretical ground.

In this Letter, starting from Vicsek-style microscopic models with Voronoi neighbors, we derive nonlinear field equations for active matter with metric-free interactions using a kinetic approach well controlled near the onset of

 © 2012 American Physical Society

orientational order. We show that the density-independent collision rate per particle characteristic of these systems suppresses the linear instability of the homogeneous ordered phase and the nonlinear density segregation in agreement with microscopic simulations. We finally discuss the consequences of our findings for the relevance of metric-free interactions.

Let us first stress that with metric-free interactions, say with Voronoi neighbors, the tenet of the Boltzmann equation approach [24]—the assumption that the system is dilute enough so that it is dominated by binary collisions—is never justified since, after all, a particle is constantly interacting with almost the same number of neighbors. Here, instead, we introduce an effective interaction rate per unit time, which renders binary interactions dominant in the small rate limit. Apart from the mathematical convenience, it is not unrealistic to think that the stimulus or response function of superior animals—due to the physical constraints induced by the information processing in various cognitive layers [25]—does not treat visual cues continuously.

Our starting point is thus a Vicsek-style model in which information is processed according to some stochastic rates: N point particles move at a constant speed v_0 on a $L \times L$ torus; their heading θ is submitted to two different dynamical mechanisms, "self-diffusion" and aligning binary "collisions." In self-diffusion, θ is changed into $\theta' = \theta + \eta$ with a probability λ per unit time, where η is a random variable drawn from a symmetric distribution $P_\sigma(\eta)$ of variance σ^2. Aligning "collisions" occur at a rate α_0 per unit time with each Voronoi neighbor. In the small α_0 limit, binary interactions dominate and take place with a rate $\alpha \approx n_2 \alpha_0$, where n_2 is the typical number of neighbors. In such collisions θ is changed to $\theta' = \Psi(\theta, \theta_n) + \eta$ where θ_n is the heading of the chosen neighbor and the noise η is also drawn, for simplicity, from $P_\sigma(\eta)$. Isotropy is assumed, namely $\Psi(\theta_1 + \phi, \theta_2 + \phi) = \Psi(\theta_1, \theta_2) + \phi[2\pi]$. For the case of ferromagnetic alignment treated in detail below, $\Psi(\theta_1, \theta_2) \equiv \arg(e^{i\theta_1} + e^{i\theta_2})$. Simulations of our stochastic rule indicate that it shares the same collective properties as the system studied in Ref. [23] (not shown).

The evolution of the one-particle phase-space distribution $f(\mathbf{r}, \theta, t)$ (defined over some suitable coarse-grained scales) is governed by the Boltzmann equation

$$\partial_t f(\mathbf{r}, \theta, t) + v_0 \mathbf{e}(\theta) \cdot \nabla f(\mathbf{r}, \theta, t) = I_{\rm diff}[f] + I_{\rm coll}[f], \quad (1)$$

where $\mathbf{e}(\theta)$ is the unit vector along θ. The self-diffusion integral is

$$I_{\rm diff}[f] = -\lambda f(\theta) + \lambda \int_{-\pi}^{\pi} d\theta' \int_{-\infty}^{\infty} d\eta P_\sigma(\eta) \times \delta_{2\pi}(\theta' - \theta + \eta) f(\theta'), \quad (2)$$

where $\delta_{2\pi}$ is a generalized Dirac delta function imposing that the argument is equal to zero modulo 2π. In the small rate limit, orientations are decorrelated between collisions ("molecular chaos hypothesis"), and one can write

$$I_{\rm coll}[f] = -\alpha f(\theta) + \frac{\alpha}{\rho(\mathbf{r}, t)} \int_{-\pi}^{\pi} d\theta_1 \int_{-\pi}^{\pi} d\theta_2 \times \int_{-\infty}^{\infty} d\eta P_\sigma(\eta) f(\theta_1) f(\theta_2) \times \delta_{2\pi}(\Psi(\theta_1, \theta_2) - \theta + \eta). \quad (3)$$

The main difference with the metric case treated in Ref. [12] is the "collision kernel," which is independent from relative angles and inversely proportional to the local density

$$\rho(\mathbf{r}, t) = \int_{-\pi}^{\pi} f(\mathbf{r}, \theta, t) d\theta. \quad (4)$$

Note that, in agreement with the basic properties of models with metric-free interactions, Eq. (1), together with the definitions of Eqs. (2)–(4), is left unchanged by an arbitrary normalization of f (and thus of ρ) and thus does not depend on the global density $\rho_0 = N/L^2$. Furthermore, a rescaling of time and space allows us to set $\lambda = v_0 = 1$, a normalization we adopt in the following.

Equations for the hydrodynamic fields are obtained by expanding $f(\mathbf{r}, \theta, t)$ in Fourier series, yielding the Fourier modes $\hat{f}_k(\mathbf{r}, t) = \int_{-\pi}^{\pi} d\theta f(\mathbf{r}, \theta, t) e^{ik\theta}$, where $\hat{f}_k$ and $\hat{f}_{-k}$ are complex conjugates, $\hat{f}_0 = \rho$, and the real and imaginary parts of $\hat{f}_1$ are the components of the momentum vector $\mathbf{w} = \rho \mathbf{P}$ with $\mathbf{P}$ the polar order parameter field. Using these Fourier modes, the Boltzmann equation Eq. (1) yields an infinite hierarchy:

$$\partial_t \hat{f}_k + \frac{1}{2}(\nabla \hat{f}_{k-1} + \nabla^* \hat{f}_{k+1}) = (\hat{P}_k - 1 - \alpha)\hat{f}_k + \frac{\alpha}{\rho} \hat{P}_k \sum_{q=-\infty}^{\infty} J_{kq} \hat{f}_q \hat{f}_{k-q}, \quad (5)$$

where the complex operators $\nabla = \partial_x + i\partial_y$ and $\nabla^* = \partial_x - i\partial_y$ have been used, the binary collision rate α is now expressed in the rescaled units, $\hat{P}_k = \int_{-\infty}^{\infty} d\eta P_\sigma(\eta) e^{ik\eta}$ is the Fourier transform of P_σ, and J_{kq} is an integral depending on the alignment rule Ψ. Below, we specialize to the case of ferromagnetic alignment, for which

$$J_{kq} = \frac{1}{2\pi} \int_{-\pi}^{\pi} d\theta \cos[(q - k/2)\theta]. \quad (6)$$

For $k = 0$ the rhs of Eq. (5) vanishes and one recovers the continuity equation

$$\partial_t \rho + \nabla \cdot \mathbf{w} = 0. \quad (7)$$

To truncate and close this hierarchy, we assume the following scaling structure, valid near onset of polar order, assuming, in a Ginzburg-Landau-like approach, small and slow variations of fields

$$\rho - \rho_0 \sim \epsilon, \quad \hat{f}_k \sim \epsilon^{|k|}, \quad \nabla \sim \epsilon, \quad \partial_t \sim \epsilon. \quad (8)$$

Note that the scaling of space and time is in line with the propagative structure of our system [26]. The lowest order yielding nontrivial, well-behaved equations is ϵ^3: keeping only terms up to this order, equations for $\hat{f}_{k>2}$ identically vanish, while $\hat{f}_2$, being slaved to $\hat{f}_1$, allows us to close the $\hat{f}_1$ equation which reads, in terms of the momentum field $\mathbf{w}$:

$$\partial_t \mathbf{w} + \gamma(\mathbf{w}\cdot\nabla)\mathbf{w} = -\frac{1}{2}\nabla\rho + \frac{\kappa}{2}\nabla\mathbf{w}^2 + (\mu - \xi\mathbf{w}^2)\mathbf{w} + \nu\nabla^2\mathbf{w} - \kappa(\nabla\cdot\mathbf{w})\mathbf{w}. \quad (9)$$

Apart from some higher order terms we have discarded here, this equation has the same form as the one derived in Ref. [12] for metric interactions, but with different transport coefficients:

$$\mu = \left(\frac{4\alpha}{\pi} + 1\right)\hat{P}_1 - (1+\alpha), \qquad \nu = [4(\alpha + 1 - \hat{P}_2)]^{-1},$$
$$\gamma = \nu\frac{4\alpha}{\rho}\left[\hat{P}_2 - \frac{2}{3\pi}\hat{P}_1\right], \qquad \kappa = \nu\frac{4\alpha}{\rho}\left[\hat{P}_2 + \frac{2}{3\pi}\hat{P}_1\right],$$
$$\xi = \nu\left[\frac{4\alpha}{\rho}\right]^2\frac{1}{3\pi}\hat{P}_1\hat{P}_2. \quad (10)$$

Note first that, contrary to the metric case, the coefficient μ of the linear term does *not* depend on the local density ρ; coefficients of the nonlinear terms depend on density to compensate the density dependence of $\mathbf{w}$. Note further that ν, κ, and ξ are positive since $0 < \hat{P}_k < 1$, so that, in particular, the nonlinear cubic term is always stabilizing. For an easier discussion, we consider now the Gaussian distribution $P_\sigma(\eta) = \frac{1}{\sigma\sqrt{2\pi}}\exp[-\frac{\eta^2}{2\sigma^2}]$ for which $\hat{P}_k = \exp[-k^2\sigma^2/2]$. Then μ is negative for large σ (where the trivial $\mathbf{w} = 0$ solution is stable with respect to linear perturbations), and changes sign for σ_c defined by [27]

$$\sigma_c^2 = 2\ln\left(\frac{1 + 4\alpha/\pi}{1+\alpha}\right). \quad (11)$$

For $\sigma < \sigma_c$, the nontrivial homogeneous solution $\rho = \rho_0$, $\mathbf{w} = \mathbf{w}_1 \equiv \mathbf{e}\sqrt{\mu/\xi}$ (where $\mathbf{e}$ is an arbitrary unit vector) exists and is stable to homogeneous perturbations.

We now focus on the linear stability of $\mathbf{w}_1$ with respect to an arbitrary wave vector $\mathbf{q}$. Because we want to discuss differences between the metric and metric-free cases later, we keep a formal ρ dependence of the linear transport coefficient. Linearization around $\mathbf{w}_1$ yields

$$\partial_t\delta\rho = -\nabla\cdot\delta\mathbf{w}$$
$$\partial_t\delta\mathbf{w} = -\gamma(\mathbf{w}_1\cdot\nabla)\delta\mathbf{w} - \tfrac{1}{2}\nabla\delta\rho + \nu\nabla^2\delta\mathbf{w} + \kappa\nabla(\mathbf{w}_1\cdot\delta\mathbf{w}) - \kappa\mathbf{w}_1(\nabla\cdot\delta\mathbf{w}) - 2\xi\mathbf{w}_1(\mathbf{w}_1\cdot\delta\mathbf{w}) + (\mu' - \xi'\mathbf{w}_1^2)\mathbf{w}_1\delta\rho, \quad (12)$$

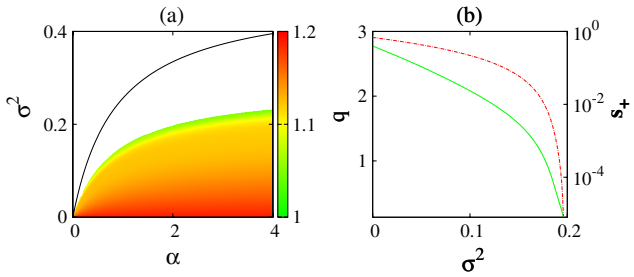

FIG. 1 (color online). Continuous theory for self-propelled particles aligning ferromagnetically [Eqs. (7) and (9) with the coefficients of Eq. (10), Gaussian noise]. (a) Phase diagram in the (α, σ^2) plane. The solid line marks the order-disorder transition. The homogeneous ordered solution $\mathbf{w}_1$ exists below this line and is linearly stable above the colored linear instability region. The color (or gray) scale (in radians) indicates the most unstable wave vector direction ϕ. (b) Modulus q of the most unstable wave vector (green full line) and the real part of its corresponding eigenvalue s_+ (dashed red line) as a function of σ^2 at $\alpha = 2$.

where primes indicate derivation with respect to ρ. Using the ansatz $(\delta\rho(\mathbf{r},t), \delta\mathbf{w}(\mathbf{r},t)) = \exp(st + i\mathbf{q}\cdot\mathbf{r})(\delta\rho_\mathbf{q}, \delta\mathbf{w}_\mathbf{q})$ allows us to recast Eq. (12) as an eigenvalue problem for s.

We have solved numerically this cubic problem for the metric-free case using the coefficients of Eq. (10) and Gaussian noise in the full (α, σ) parameter plane. The resulting stability diagram, presented in Fig. 1, shows that, contrary to the metric case, the homogeneous ordered phase is stable near onset. As in the metric case [28], there exists an instability region to oblique wave vectors of large modulus rather far from the transition line. Given that microscopic simulations show no sign of similar instabilities, we believe that the existence of this region, situated away from the validity domain of our approximations, is an artifact of our truncation ansatz.

At the nonlinear level, we performed numerical simulations [29] of Eq. (9) (again with the coefficients of Eq. (10) and Gaussian noise) starting from initial conditions with large variations of both ρ and $\mathbf{w}$. With parameters α and σ^2 in the ordered stable region of Fig. 1, we always observed relaxation towards the linearly stable homogeneous solution $\mathbf{w}_1$, albeit after typically long transients. Starting in the unstable region, the solution blows up in finite time, signaling that indeed our equation is ill behaved when considered too far away from onset.

The stabilization of the near-threshold region by metric-free interactions can be directly traced back to the absence of ρ dependence of μ, in agreement with remarks in Refs. [12,30] where the long-wavelength instability of $\mathbf{w}_1$ was linked to $\mu' > 0$. In the long-wavelength limit $q = |\mathbf{q}| \ll 1$, the eigenvalue problem can be solved analytically with relative ease. The growth rate s is the solution of the cubic equation

$$s^3 + \beta_2 s^2 + \beta_1 s + \beta_0 = 0, \quad (13)$$

where the coefficients, to lowest orders in q, are given by

$$\beta_2 = 2\mu + 2iq\sqrt{\frac{\mu}{\xi}}\gamma\cos\phi + 2q^2\nu$$
$$\beta_1 = iq\sqrt{\frac{\mu}{\xi}}\cos\phi\left[2\gamma\mu + \left(\mu' - \mu\frac{\xi'}{\xi}\right)\right] + q^2\left[2\mu\nu + \frac{1}{2} - \frac{\mu}{\xi}(\gamma^2\cos^2\phi + \kappa^2\sin^2\phi)\right]$$
$$\beta_0 = \mu q^2\left[\left(\frac{\mu\xi'}{\xi^2} - \frac{\mu'}{\xi}\right)(\gamma\cos^2\phi + \kappa\sin^2\phi) + \sin^2\phi\right] + iq^3\sqrt{\frac{\mu}{\xi}}\cos\phi\left[\left(\mu' - \mu\frac{\xi'}{\xi}\right)\nu + \frac{\gamma}{2}\right] \quad (14)$$

and ϕ is the angle between $\mathbf{q}$ and $\mathbf{w}_1$ (which has been chosen parallel to the abscissa). Near threshold, where our truncation is legitimate and $\mu \sim \epsilon^2$, two eigenvalues are always stable and linear stability is controlled by the dominant solution real part

$$s_+ \approx \frac{q^2\cos^2\phi}{8\mu}\left[\frac{(\mu')^2}{\mu\xi} - h(\phi)\right] + \mathcal{O}\left(\frac{q^2\mu'}{\mu}\right) \quad (15)$$

with $h(0) = 2$ and $h(\phi) = 1$ otherwise [31]. This expression immediately shows that $s_+ < 0$ in the metric-free case where $\mu' = 0$, confirming the stability of the homogeneous ordered solution $\mathbf{w}_1$. This stabilizing effect can be ultimately traced back to the (negative) pressure term $-\nabla\rho$ appearing in Eq. (9). Conversely, in the metric case for which $\mu \sim 0^+$ near threshold, s_+ is always positive, yielding the generic long-wavelength instability leading to density segregation in metric models.

These results rest on the independence of the linear coefficient μ on ρ, a direct consequence of the fact that the interaction rate per particle in topological models is fixed only by geometrical constraints and does not grow with local density. This property actually holds for any metric-free system: all the linear coefficients μ_k appearing in the equations for $\hat{f}_k$ read

$$\mu_k = \hat{P}_k - 1 - \alpha + \alpha\hat{P}_k(J_{kk} + J_{k0}) \quad (16)$$

and are thus independent of ρ. Therefore, the lack of near-threshold spontaneous segregation extends to the other known classes of "dry" active matter [32]: we have in particular worked out the case of polar particles with nematic alignment ("self-propelled rods") for which $\Psi(\theta_1, \theta_2) = \arg(e^{i\theta_1} + \mathrm{sign}[\cos(\theta_1 - \theta_2)]e^{i\theta_2})$. While full details will be given in Ref. [33], we only sketch here the salient points. Let us first recall that with nematic alignment, the metric model studied at the microscopic level in [9] shows global nematic order. In a large region of parameter space bordering onset, order is segregated to a high-density stationary band oriented along it. We have studied numerically the metric-free version of that Vicsek-style model with Voronoi neighbors. As for its ferromagnetic counterpart, no segregation in bands is observed anymore, and the transition to nematic order is then continuous, as testified by finite-size scaling results (Fig. 2).

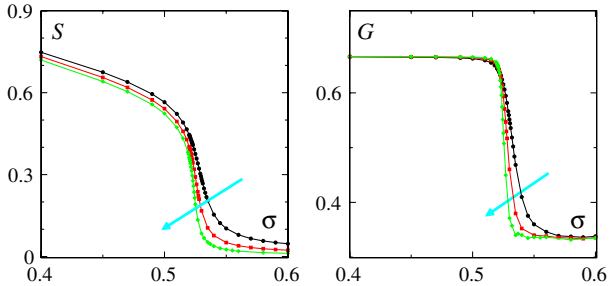

FIG. 2 (color online). Vicsek-style model with nematic alignment and topological neighbors, where $N = L^2$ particles move at a speed $v_0 = \frac{1}{2}$ on a $L \times L$ torus. Headings and positions are updated at discrete time steps according to $\theta_j^{t+1} = \arg[\sum_{k\sim j}\mathrm{sgn}[\cos(\theta_k^t - \theta_j^t)]e^{i\theta_k^t} + n_j^t\sigma\xi_j^t]$ and $\mathbf{r}_j^{t+1} = \mathbf{r}_j^t + v_0\mathbf{e}(\theta_j^{t+1})$, where $\mathbf{e}(\theta)$ is the unit vector along θ, the sum is over the n_j^t Voronoi neighbors of particle j (including j itself), and ξ_j^t is a random unit vector in the complex plane. Nematic order parameter $S = \langle\varphi(t)\rangle_t$ (with $\varphi(t) = |\frac{1}{N}\sum_k e^{i2\theta_k^t}|$) (a) and its Binder cumulant [36] $G = 1 - \langle\varphi(t)^4\rangle_t/(3\langle\varphi(t)^2\rangle_t^2)$ (b) vs σ for $L = 32, 64, 128$ (the arrows indicate increasing sizes). The noncrossing S curves and the absence of minima in the Binder curves all point to a continuous transition. Accurate estimates of its critical exponents will be provided elsewhere.

These properties are well captured, both in the metric and metric-free case, by a controlled hydrodynamic approach of the type presented here, which we only sketch below [33]. The nematic symmetry of the problem requires us to consider three hydrodynamic fields [15], corresponding to the modes $k = 0, 1, 2$ in Eq. (5), with $\hat{f}_2$ coding for the nematic tensor field $\rho\mathbf{Q}$. We have performed the analysis of the 5×5 linear problem expressing the stability of the homogeneous nematically ordered solution ($\mathbf{w} = 0$, $\rho\mathbf{Q} = \mathrm{const}$) appearing at onset in both the metric and nonmetric cases [33]. Whereas the metric case shows a long-wavelength, transversal instability of the homogeneous ordered solution near onset, this solution is linearly stable in the metric-free case. Again, this difference can be traced back to the ρ dependence of the linear coefficients μ_k. At the nonlinear level, simulations indicate that the homogeneous ordered solution is a global attractor in the metric-free case.

Our analysis can also be extended to diffusive active matter such as the driven granular rods model ("active nematics") studied in Refs. [10,11] which, for metric interactions, also shows near-threshold phase segregation [10,34]. Simulations of the metric-free microscopic version (with Voronoi neighbors) show no such segregation. In a kinetic approach, because active nematic particles move by nonequilibrium diffusive currents rather than by ballistic motion, the Boltzmann equation has to be replaced by a more general master equation. But it is nevertheless possible to derive a continuous theory which, in the metric-free case, yields a homogeneous ordered phase stable near onset for essentially the same reasons as in the cases presented above [35].

In conclusion, simple, Vicsek-style, models of active matter where self-propelled particles interact with

neighbors defined via nonmetric rules (e.g., Voronoi neighbors) are amenable, like their "metric" counterparts, to the construction of continuous hydrodynamic theories well controlled near onset. The relatively simple framework of Vicsek-style models offers a two-dimensional parameter plane which can be studied entirely. More complicated microscopic starting points, for instance where positional diffusion would also be considered, inevitably raise the dimensionality of parameter space. We have shown here that nonmetric theories differ essentially from metric ones in the independence of their linear coefficients μ_k on the local density, a property directly linked to the fact that the collision rate per particle is constant in metric-free systems. We have shown further that the homogeneous ordered phase is linearly stable near onset for metric-free systems, in contrast with the long-wavelength instability present in metric cases.

We finally discuss the relevance (say in the renormalization-group sense) of metric-free interactions in deciding active matter universality classes. Our work has shown that the deterministic continuous theories of metric-free active matter systems are formally equivalent to those of their metric counterparts, except for the density dependence of the linear coefficients. In the polar case, our hydrodynamic equations thus share the same structure as the Toner and Tu equations [3]. This could be taken as an indication that the homogeneous, ordered, fluctuating phase observed in the Vicsek model with Voronoi neighbors does *not* differ from the Toner-Tu phase of its metric counterpart, in disagreement with the slight numerical discrepancies between the two cases reported in Ref. [23] about the scaling exponent of the anomalously strong density fluctuations. This calls for more extensive microscopic simulations assessing finite-size effects, but also for incorporating effective noise terms, properly derived in both cases, and for studying the resulting field theories, a task left for future work.

We are grateful to I. Giardina, M. C. Marchetti, J. Prost, and J. Toner for enlightening discussions. This work was initiated in the lively atmosphere of the Max Planck Institute for the Physics of Complex Systems in Dresden, Germany, within the Advanced Study Group 2011/2012: Statistical Physics of Collective Motion. F. G. acknowledges support by Grant IIT-Seed Artswarm.

[1] S. Ramaswamy, Annu. Rev. Condens. Matter Phys. **1**, 323 (2010).
[2] T. Vicsek, A. Czirok, E. Ben-Jacob, I. Cohen, and O. Shochet, Phys. Rev. Lett. **75**, 1226 (1995).
[3] J. Toner and Y. Tu, Phys. Rev. Lett. **75**, 4326 (1995); Phys. Rev. E **58**, 4828 (1998); J. Toner, Phys. Rev. Lett. **108**, 088102 (2012).
[4] J. Toner, Y. Tu, and S. Ramaswamy, Ann. Phys. (Berlin) **318**, 170 (2005); P. Romanczuk *et al.*, Eur. Phys. J. Special Topics, **202**, 1 (2012).
[5] D. J. Sumpter, *Collective Animal Behavior* (Princeton University Press, Princeton, NJ, 2010); J. Buhl, D. J. T. Sumpter, I. D. Couzin, J. J. Hale, E. Despland, E. R. Miller, and S. J. Simpson, Science **312**, 1402 (2006).
[6] H. P. Zhang, A. Beer, L. Florin, and H. L. Swinney, Proc. Natl. Acad. Sci. U.S.A. **107**, 13 626 (2010).
[7] J. K. Parrish, S. V. Viscido, and D. Grünbaum, Biol. Bull. **202**, 296 (2002), and references therein.
[8] G. Grégoire and H. Chaté, Phys. Rev. Lett. **92**, 025702 (2004); H. Chaté, F. Ginelli, G. Gregoire, and F. Raynaud, Phys. Rev. E **77**, 046113 (2008).
[9] F. Ginelli, F. Peruani, M. Bär, and H. Chaté, Phys. Rev. Lett. **104**, 184502 (2010).
[10] H. Chaté, F. Ginelli, and R. Montagne, Phys. Rev. Lett. **96**, 180602 (2006).
[11] S. Ramaswamy, R. A. Simha, and J. Toner, Europhys. Lett. **62**, 196 (2003); S. Mishra and S. Ramaswamy, Phys. Rev. Lett. **97**, 090602 (2006).
[12] E. Bertin, M. Droz, and G. Grégoire, Phys. Rev. E **74**, 022101 (2006); J. Phys. A **42**, 445001 (2009).
[13] T. Ihle, Phys. Rev. E **83**, 030901 (2011).
[14] T. B. Liverpool and M. C. Marchetti, Phys. Rev. Lett. **90**, 138102 (2003); A. Ahmadi, M. C. Marchetti, and T. B. Liverpool, Phys. Rev. E **74**, 061913 (2006).
[15] A. Baskaran and M. C. Marchetti, Phys. Rev. Lett. **101**, 268101 (2008); Phys. Rev. E **77**, 011920 (2008).
[16] V. Narayan, S. Ramaswamy, and N. Menon, Science **317**, 105 (2007).
[17] J. Deseigne, O. Dauchot, and H. Chaté, Phys. Rev. Lett. **105**, 098001 (2010).
[18] V. Schaller, C. Weber, C. Semmrich, E. Frey, and A. R. Bausch, Nature (London) **467**, 73 (2010).
[19] Y. Sumino, K. H. Nagai, Y. Shitaka, D. Tanaka, K. Yoshikawa, H. Chaté, and K. Oiwa, Nature (London) **483**, 448 (2012).
[20] Ballerini *et al.*, Proc. Natl. Acad. Sci. U.S.A. **105**, 1232 (2008).
[21] M. Moussaïd, D. Helbing, and G. Theraulaz, Proc. Natl. Acad. Sci. U.S.A. **108**, 6884 (2011).
[22] J. Gautrais *et al.*, PLoS Comput. Biol. (to be published).
[23] F. Ginelli and H. Chaté, Phys. Rev. Lett. **105**, 168103 (2010).
[24] *Mathematical Methods in Kinetic Theory*, edited by C. Cercignani (Plenum, New York, 1990), 2nd ed., and references therein.
[25] F. Rieke, D. Warland, R. de Ruyter van Steveninck, and W. Bialek, *Spikes: Exploring the Neural Code* (MIT, Cambridge, MA, 1997).
[26] The diffusive ansatz ($\nabla \sim \epsilon$, $\partial_t \sim \epsilon^2$) should be preferred in problems dominated by positional diffusion such as mixtures of filaments, molecular motors, and crosslinking proteins. See I. S. Aranson, and L. S. Tsimring, Phys. Rev. E **71**, 050901(R) (2005); Phys. Rev. E **74**, 031915 (2006); F. Ziebert, I. S. Aranson, and L. S. Tsimring, New J. Phys. **9**, 421 (2007).
[27] While we are considering the small interaction rate limit, α is not necessarily smaller than 1 in the units chosen, for which $v_0 = \lambda = 1$.
[28] In the metric case, this region of instability was overlooked in Ref. [12].

[29] We used a pseudospectral code with Euler time stepping ($\Delta t = 0.01$), with at least 256×256 Fourier modes on square domains of linear size $L = 64$ and antialiasing truncation.

[30] A. Gopinath, M. F. Hagan, M. C. Marchetti, and A. Baskaran, Phys. Rev. E **85**, 061903 (2012).

[31] For $\phi = \pm\pi/2$, one has to resort to higher orders, and then finds $s_+ \approx q^2(-(\mu'/\mu)\kappa\xi + 2\kappa^2\xi - 4\nu\xi^2 + \kappa\xi')/(8\xi^2)$. This quantity is always negative for the coefficients of Eq. (10).

[32] Here we only discuss "dry" systems, where active particles move over a passive background which acts as a momentum sink so that total momentum is not conserved and hydrodynamic long range interactions are ruled out.

[33] A. Peshkov *et al.*, arXiv:1207.5751.

[34] X. Shi and Y. Ma, arXiv:1011.5408.

[35] F. Ginelli *et al.* (to be published).

[36] K. Binder, Rep. Prog. Phys. **60**, 487 (1997).

6.3 CONCLUSION

In the metric-free model, the coefficient α of the linear term is independent of the value of the local density. Thus only chaotic non-homogenous solutions are possible with this set of equations. Moreover no chaotic solutions were observed in simulation of these equations, confirming the microscopic results of the second order phase transition. This leaves almost nothing to study in this equation in it present form. Some additional properties, like giant density fluctuations, could be measured if Langevin type equations could be derived for this model.

But the work presented in this chapter is still important in the fact that it has shown that it is possible to derive equations for the case when interactions are not-metric, contrary to the classical Boltzmann approach.

BIBLIOGRAPHY

[1] I.S. Aranson and L.S. Tsimring. Model of coarsening and vortex formation in vibrated granular rods. *PRE*, 67(2):021305, 2003. (Cited on page 11.)

[2] I.S. Aranson and L.S. Tsimring. Pattern formation of microtubules and motors: Inelastic interaction of polar rods. *Physical Review E*, 71(5 AR 050901), 2005. (Cited on page 11.)

[3] I.S. Aranson and L.S. Tsimring. Theory of self-assembly of microtubules and motors. *PRE*, 74(3):031915, 2006. (Cited on page 11.)

[4] T. Balch and R.C. Arkin. Behavior-based formation control for multirobot teams. *Ieee Transactions on Robotics and Automation*, 14(6):926–939, 1998. (Cited on page 3.)

[5] M. Ballerini, N. Cabibbo, R. Candelier, A. Cavagna, E. Cisbani, I. Giardina, V. Lecomte, A. Orlandi, G. Parisi, A. Procaccini, M. Viale, and V. Zdravkovic. Interaction ruling animal collective behavior depends on topological rather than metric distance: Evidence from a field study. *Proceedings of the National Academy of Sciences*, 105(4):1232–1237, 2008. (Cited on page 147.)

[6] A. Baskaran and M.C. Marchetti. Hydrodynamics of self-propelled hard rods. *PRE*, 77(1):011920, 2008. (Cited on pages 10 and 24.)

[7] A. Baskaran and M.C. Marchetti. Self-regulation in self-propelled nematic fluids. *European Physical Journal E*, 35(9):95, 2012. (Cited on page 136.)

[8] E. Bertin, M. Droz, and G. Grégoire. Boltzmann and hydrodynamic description for self-propelled particles. *Physical Review E*, 74(2 AR 022101), 2006. (Cited on pages 9 and 36.)

[9] E. Bertin, M. Droz, and G. Grégoire. Hydrodynamic equations for self-propelled particles: microscopic derivation and stability analysis. *Journal of Physics A-mathematical and Theoretical*, 42(44):445001, 2009. (Cited on pages 9, 43, and 48.)

[10] D.L. Blair, T. Neicu, and A. Kudrolli. Vortices in vibrated granular rods. *PRE*, 67(3):031303, 2003. (Cited on page 130.)

[11] J.P. Boyd. *Chebyshev and Fourier spectral methods*. Dover Publications, 2001. (Cited on page 57.)

[12] J. Buhl, D. Sumpter, I.D. Couzin, J.J. Hale, E. Despland, E.R. Miller, and S.J. Simpson. From disorder to order in marching locusts. *Science*, 312(5778):1402–1406, 2006. (Cited on page 3.)

[13] A. Cavagna, A. Cimarelli, I. Giardina, G. Parisi, R. Santagati, F. Stefanini, and M. Viale. Scale-free correlations in starling flocks. *Proceedings of the National Academy of Sciences of the United States of America*, 107(26):11865–11870, 2010. (Cited on page 3.)

[14] L.-Y. Chen, N. Goldenfeld, and Y. Oono. Renormalization group and singular perturbations: Multiple scales, boundary layers, and reductive perturbation theory. *Physical Review E*, 54(1):376–394, 1996. (Cited on page 54.)

[15] L.H. Cisneros, R. Cortez, C. Dombrowski, R.E. Goldstein, and J.O. Kessler. Fluid dynamics of self-propelled microorganisms, from individuals to concentrated populations. *Experiments in Fluids*, 43(5):737–753, 2007. (Cited on page 4.)

[16] D.S. Dean. Langevin equation for the density of a system of interacting langevin processes. *Journal of Physics A-mathematical and General*, 29(24):L613–L617, 1996. (Cited on page 26.)

[17] J. Gautrais, C. Jost, M. Soria, A. Campo, S. Motsch, R. Fournier, S. Blanco, and G. Theraulaz. Analyzing fish movement as a persistent turning walker. *Journal of Mathematical Biology*, 58(3):429–445, 2009. (Cited on page 3.)

[18] F. Ginelli and H. Chaté. Relevance of metric-free interactions in flocking phenomena. *Physical Review Letters*, 105(16):168103, 2010. (Cited on pages 4, 9, 20, and 147.)

[19] F. Ginelli, F. Peruani, M. Bar, and H. Chaté. Large-scale collective properties of self-propelled rods. *Physical Review Letters*, 104(18):184502, 2010. (Cited on pages xiii, xiv, 4, 9, 20, 75, and 76.)

[20] L. Giomi, M.J. Bowick, X. Ma, and M.C. Marchetti. Defect annihilation and proliferation in active nematics. *PRL*, 110(22):228101, 2013. (Cited on page 130.)

[21] A. Gopinath, M.F. Hagan, M.C. Marchetti, and A. Baskaran. Dynamical self-regulation in self-propelled particle flows. *Physical Review E*, 85(6 AR 061903), 2012. (Cited on page 10.)

[22] Y. Hatwalne, S. Ramaswamy, M. Rao, and R.A. Simha. Rheology of active-particle suspensions. *Physical Review Letters*, 92(11):118101, 2004. (Cited on page 4.)

[23] T. Ihle. Kinetic theory of flocking: Derivation of hydrodynamic equations. *Physical Review E*, 83(3 AR 030901), 2011. (Cited on page 9.)

[24] T. Ihle. Invasion-wave induced first-order phase transition in systems of active particles. *eprint arXiv:1304.0149*, 2013. (Cited on page 10.)

[25] C. Lanczos. *Linear differential operators*. Van Nostrand, 1961. (Cited on pages 91 and 133.)

[26] L.D. Landau. *Collected papers of L.D. Landau. Edited and with an introduction by D. ter Haar*. Oxford, New York, Pergamon Press, 1965. (Cited on pages 24 and 25.)

[27] N.D. Mermin and H. Wagner. Absence of ferromagnetism or antiferromagnetism in one- or two-dimensional isotropic heisenberg models. *PRL*, 17(22):1133–1136, 1966. (Cited on page 5.)

[28] S. Mishra, A. Baskaran, and M.C. Marchetti. Fluctuations and pattern formation in self-propelled particles. *PRE*, 81(6):061916, 2010. (Cited on page 10.)

[29] M. Moussaid, D. Helbing, and G. Theraulaz. How simple rules determine pedestrian behavior and crowd disasters. *Proceedings of the National Academy of Sciences of the United States of America*, 108(17):6884–6888, 2011. (Cited on page 3.)

[30] S. Ramaswamy, R.A. Simha, and J. Toner. Active nematics on a substrate: Giant number fluctuations and long-time tails. *Europhysics Letters*, 62(2):196–202, 2003. (Cited on page 99.)

[31] P. Romanczuk and L. Schimansky-Geier. Mean-field theory of collective motion due to velocity alignment. *Ecological Complexity*, 10:83–92, 2012. (Cited on page 11.)

[32] V. Schaller, C. Weber, C. Semmrich, E. Frey, and A.R. Bausch. Polar patterns of driven filaments. *Nature*, 467(7311):73–77, 2010. (Cited on pages 3 and 35.)

[33] A. Sokolov and I.S. Aranson. Reduction of viscosity in suspension of swimming bacteria. *Physical Review Letters*, 103(14):148101, 2009. (Cited on pages 3 and 4.)

[34] A. Sokolov, R.E. Goldstein, F.I. Feldchtein, and I.S. Aranson. Enhanced mixing and spatial instability in concentrated bacterial suspensions. *Physical Review E*, 80(3):031903, 2009. (Cited on page 4.)

[35] J. Toner and Y.H. Tu. Long-range order in a 2-dimensional dynamical xy model - how birds fly together. *Physical Review Letters*, 75(23):4326–4329, 1995. (Cited on pages 5, 9, and 26.)

[36] J. Toner, Y.H. Tu, and S. Ramaswamy. Hydrodynamics and phases of flocks. *Annals of Physics*, 318(1):170–244, 2005. (Cited on pages 8, 9, and 75.)

[37] Y. Tu, J. Toner, and M. Ulm. Sound waves and the absence of galilean invariance in flocks. *PRL*, 80(21):4819–4822, 1998. (Cited on pages 7 and 35.)

[38] A.E. Turgut, H. Celikkanat, F. Gokce, and E. Sahin. Self-organized flocking in mobile robot swarms. *Swarm Intelligence*, 2(2-4):97–120, 2008. (Cited on page 3.)

[39] T. Vicsek, A. Czirok, E. Benjacob, I. Cohen, and O. Shochet. Novel type of phase-transition in a system of self-driven particles. *Physical Review Letters*, 75(6):1226–1229, 1995. (Cited on pages 3, 4, and 33.)

Part V

CONCLUSIONS

7 SUMMARY

I have introduced a systematic method to derive coarse-grained hydrodynamic equations of collective motion from microscopical Vicsek type models. This approach that I call Boltzmann-Ginzburg-Landau method is based on the original method of Bertin-Droz-Grégoire. Going beyond the original publication, I have introduced a precise set of rules for the closure of the Fourier series of the Boltzmann equation. Contrary to many other methods presented in the introduction, this approach allows to obtain equations that have the two following important properties:

1. All terms in our equations are balanced according to our scaling ansatz;
2. The dependence of all coefficients on microscopic parameters is known explicitly

Applying this approach to different types of Vicsek like models I have found that we obtain equations that can faithfully reproduce the qualitative properties of the underlying models; the different observed phases and the nature of the phase transitions.

For the polar model, we obtained equations that reproduced the three phases observed in the microscopic model; the disordered phase, the band phase and a homogeneous ordered phase. The transition from the disordered to the band phase is discontinuous presenting a hysteresis phenomenon like in the microscopic model.

For the mixed polar-nematic model, our equations presented the four different phases observed in the microscopic simulations; the disordered phase, the chaotic phase, the band phase and a homogenous ordered phase. I have also found that the band phase is itself chaotic, which was later confirmed by new microscopic simulations.

Equation obtained for the nematic model does not provide the same image that the one provided by the microscopical model. Our equations show the four phases identical to the mixed polar-nematic case. However we cannot neglect that the study at large system sizes will prove that the quasi-stable band phases will not completely vanish, leaving the same image that the one offered by the microscopical models. We have also found the formation of nematic defects that were not yet reported in the microscopical models.

Finally, the metric-free polar equations are faithfully reproducing the behavior of the microscopical model, i.e. a continuous transition from the disordered to the homogenous ordered phase.

8 PERSPECTIVES

8.1 FURTHER STUDIES OF THE CURRENT EQUATIONS

They are still many unanswered questions regarding the equations that I have obtained.

First for the polar model we must find a justification of the pseudo-fourth order truncation of the equations which seems to be more correct in reproducing the soliton behavior than the pure third order truncation. Second, a full study of the obtained soliton solutions and of their stability is needed to completely set the nature of the order-disorder transition. Finally better simulations in 2d are needed to prove or exclude the possibility of other structures than the 1d solitons currently observed in simulations.

For the polar-nematic model, we must better study the chaotic and the unstable band phase to be able to prove that these two phases are different in the thermodynamic limit. Secondly as in the case of the pure nematic model, it will be interesting to see if nematic defects can be obtained with these equations.

In the case of the nematic model, the problems are essentially the same as in the case of the polar-nematic model, we investigate the difference between the chaotic and the unstable band phase. In sum, we must prove that the two models, the polar-nematic one and the pure nematic one, are different as is suggested by microscopical simulations. It is possible that they are in fact asymptotically identical. We must also find a way to stabilize the nematic defects in order to study them precisely.

8.2 DERIVATION OF THE LANGEVIN EQUATIONS

Going beyond the current form of equations, it is necessary to derive the multiplicative noise terms for each of our models. This will allow to perform a renormalization group analysis as was done by Toner and Tu. These terms will allow to further investigate the nature of the order-disorder transition in our equations, confirming or corroborating the results already obtained. This goal is the most important as of today, but is still completely unexplored.

BIBLIOGRAPHY

[1] I.S. Aranson and L.S. Tsimring. Model of coarsening and vortex formation in vibrated granular rods. *PRE*, 67(2):021305, 2003. (Cited on page 11.)

[2] I.S. Aranson and L.S. Tsimring. Pattern formation of microtubules and motors: Inelastic interaction of polar rods. *Physical Review E*, 71(5 AR 050901), 2005. (Cited on page 11.)

[3] I.S. Aranson and L.S. Tsimring. Theory of self-assembly of microtubules and motors. *PRE*, 74(3):031915, 2006. (Cited on page 11.)

[4] T. Balch and R.C. Arkin. Behavior-based formation control for multirobot teams. *Ieee Transactions on Robotics and Automation*, 14(6):926–939, 1998. (Cited on page 3.)

[5] M. Ballerini, N. Cabibbo, R. Candelier, A. Cavagna, E. Cisbani, I. Giardina, V. Lecomte, A. Orlandi, G. Parisi, A. Procaccini, M. Viale, and V. Zdravkovic. Interaction ruling animal collective behavior depends on topological rather than metric distance: Evidence from a field study. *Proceedings of the National Academy of Sciences*, 105(4):1232–1237, 2008. (Cited on page 147.)

[6] A. Baskaran and M.C. Marchetti. Hydrodynamics of self-propelled hard rods. *PRE*, 77(1):011920, 2008. (Cited on pages 10 and 24.)

[7] A. Baskaran and M.C. Marchetti. Self-regulation in self-propelled nematic fluids. *European Physical Journal E*, 35(9):95, 2012. (Cited on page 136.)

[8] E. Bertin, M. Droz, and G. Grégoire. Boltzmann and hydrodynamic description for self-propelled particles. *Physical Review E*, 74(2 AR 022101), 2006. (Cited on pages 9 and 36.)

[9] E. Bertin, M. Droz, and G. Grégoire. Hydrodynamic equations for self-propelled particles: microscopic derivation and stability analysis. *Journal of Physics A-mathematical and Theoretical*, 42(44):445001, 2009. (Cited on pages 9, 43, and 48.)

[10] D.L. Blair, T. Neicu, and A. Kudrolli. Vortices in vibrated granular rods. *PRE*, 67(3):031303, 2003. (Cited on page 130.)

[11] J.P. Boyd. *Chebyshev and Fourier spectral methods*. Dover Publications, 2001. (Cited on page 57.)

[12] J. Buhl, D. Sumpter, I.D. Couzin, J.J. Hale, E. Despland, E.R. Miller, and S.J. Simpson. From disorder to order in marching locusts. *Science*, 312(5778):1402–1406, 2006. (Cited on page 3.)

[13] A. Cavagna, A. Cimarelli, I. Giardina, G. Parisi, R. Santagati, F. Stefanini, and M. Viale. Scale-free correlations in starling flocks. *Proceedings of the National Academy of Sciences of the United States of America*, 107(26):11865–11870, 2010. (Cited on page 3.)

[14] L.-Y. Chen, N. Goldenfeld, and Y. Oono. Renormalization group and singular perturbations: Multiple scales, boundary layers, and reductive perturbation theory. *Physical Review E*, 54(1):376–394, 1996. (Cited on page 54.)

[15] L.H. Cisneros, R. Cortez, C. Dombrowski, R.E. Goldstein, and J.O. Kessler. Fluid dynamics of self-propelled microorganisms, from individuals to concentrated populations. *Experiments in Fluids*, 43(5):737–753, 2007. (Cited on page 4.)

[16] D.S. Dean. Langevin equation for the density of a system of interacting langevin processes. *Journal of Physics A-mathematical and General*, 29(24):L613–L617, 1996. (Cited on page 26.)

[17] J. Gautrais, C. Jost, M. Soria, A. Campo, S. Motsch, R. Fournier, S. Blanco, and G. Theraulaz. Analyzing fish movement as a persistent turning walker. *Journal of Mathematical Biology*, 58(3):429–445, 2009. (Cited on page 3.)

[18] F. Ginelli and H. Chaté. Relevance of metric-free interactions in flocking phenomena. *Physical Review Letters*, 105(16):168103, 2010. (Cited on pages 4, 9, 20, and 147.)

[19] F. Ginelli, F. Peruani, M. Bar, and H. Chaté. Large-scale collective properties of self-propelled rods. *Physical Review Letters*, 104(18):184502, 2010. (Cited on pages xiii, xiv, 4, 9, 20, 75, and 76.)

[20] L. Giomi, M.J. Bowick, X. Ma, and M.C. Marchetti. Defect annihilation and proliferation in active nematics. *PRL*, 110(22):228101, 2013. (Cited on page 130.)

[21] A. Gopinath, M.F. Hagan, M.C. Marchetti, and A. Baskaran. Dynamical self-regulation in self-propelled particle flows. *Physical Review E*, 85(6 AR 061903), 2012. (Cited on page 10.)

[22] Y. Hatwalne, S. Ramaswamy, M. Rao, and R.A. Simha. Rheology of active-particle suspensions. *Physical Review Letters*, 92(11):118101, 2004. (Cited on page 4.)

[23] T. Ihle. Kinetic theory of flocking: Derivation of hydrodynamic equations. *Physical Review E*, 83(3 AR 030901), 2011. (Cited on page 9.)

[24] T. Ihle. Invasion-wave induced first-order phase transition in systems of active particles. *eprint arXiv:1304.0149*, 2013. (Cited on page 10.)

[25] C. Lanczos. *Linear differential operators*. Van Nostrand, 1961. (Cited on pages 91 and 133.)

[26] L.D. Landau. *Collected papers of L.D. Landau. Edited and with an introduction by D. ter Haar*. Oxford, New York, Pergamon Press, 1965. (Cited on pages 24 and 25.)

[27] N.D. Mermin and H. Wagner. Absence of ferromagnetism or antiferromagnetism in one- or two-dimensional isotropic heisenberg models. *PRL*, 17(22):1133–1136, 1966. (Cited on page 5.)

[28] S. Mishra, A. Baskaran, and M.C. Marchetti. Fluctuations and pattern formation in self-propelled particles. *PRE*, 81(6):061916, 2010. (Cited on page 10.)

[29] M. Moussaid, D. Helbing, and G. Theraulaz. How simple rules determine pedestrian behavior and crowd disasters. *Proceedings of the National Academy of Sciences of the United States of America*, 108(17):6884–6888, 2011. (Cited on page 3.)

[30] S. Ramaswamy, R.A. Simha, and J. Toner. Active nematics on a substrate: Giant number fluctuations and long-time tails. *Europhysics Letters*, 62(2):196–202, 2003. (Cited on page 99.)

[31] P. Romanczuk and L. Schimansky-Geier. Mean-field theory of collective motion due to velocity alignment. *Ecological Complexity*, 10:83–92, 2012. (Cited on page 11.)

[32] V. Schaller, C. Weber, C. Semmrich, E. Frey, and A.R. Bausch. Polar patterns of driven filaments. *Nature*, 467(7311):73–77, 2010. (Cited on pages 3 and 35.)

[33] A. Sokolov and I.S. Aranson. Reduction of viscosity in suspension of swimming bacteria. *Physical Review Letters*, 103(14):148101, 2009. (Cited on pages 3 and 4.)

[34] A. Sokolov, R.E. Goldstein, F.I. Feldchtein, and I.S. Aranson. Enhanced mixing and spatial instability in concentrated bacterial suspensions. *Physical Review E*, 80(3):031903, 2009. (Cited on page 4.)

[35] J. Toner and Y.H. Tu. Long-range order in a 2-dimensional dynamical xy model - how birds fly together. *Physical Review Letters*, 75(23):4326–4329, 1995. (Cited on pages 5, 9, and 26.)

[36] J. Toner, Y.H. Tu, and S. Ramaswamy. Hydrodynamics and phases of flocks. *Annals of Physics*, 318(1):170–244, 2005. (Cited on pages 8, 9, and 75.)

[37] Y. Tu, J. Toner, and M. Ulm. Sound waves and the absence of galilean invariance in flocks. *PRL*, 80(21):4819–4822, 1998. (Cited on pages 7 and 35.)

[38] A.E. Turgut, H. Celikkanat, F. Gokce, and E. Sahin. Self-organized flocking in mobile robot swarms. *Swarm Intelligence*, 2(2-4):97–120, 2008. (Cited on page 3.)

[39] T. Vicsek, A. Czirok, E. Benjacob, I. Cohen, and O. Shochet. Novel type of phase-transition in a system of self-driven particles. *Physical Review Letters*, 75(6):1226–1229, 1995. (Cited on pages 3, 4, and 33.)

COLOPHON

This document was typeset using the typographical look-and-feel `classicthesis` developed by André Miede. The style was inspired by Robert Bringhurst's seminal book on typography *"The Elements of Typographic Style"*. `classicthesis` is available for both LaTeX and LyX:

http://code.google.com/p/classicthesis/

Happy users of `classicthesis` usually send a real postcard to the author, a collection of postcards received so far is featured at:

http://postcards.miede.de/

Final Version as of December 19, 2013 (`classicthesis`).